

REACTION RATES IN FAST NUCLEAR REACTORS

A Thesis submitted for the award of
the degree of Doctor of Philosophy of
the University of London

by

RAKESH CHAWLA, M.Sc. (London), D.I.C., B.Sc. (Hons. School)

Nuclear Power Section
Department of Mechanical Engineering
Imperial College of Science and Technology

June, 1970

ABSTRACT

The importance of reaction rate assessments in the physics studies of fast reactors is discussed. It is seen that, in order to meet the stringent target accuracy requirements, new techniques of measurement are necessary for investigating the systematic errors of existing methods.

Absolute techniques for the determination of U-238 capture (C_8) and Pu-239 fission (F_9) rates have been developed and applied for lattice - (C_8/F_9) measurements in zero-energy fast assemblies. This new approach is shown to be potentially more accurate than the earlier-established R.C.R. technique which relies on comparisons with thermal-column irradiations. With the parallel use of both methods, the $\pm 1\%$ accuracy requirement for the reaction rate ratio has been met in several fast-reactor test regions.

(C_8/F_9) measurements in 25% PuO₂/UO₂ and 16% PuO₂/UO₂ materials have been made possible, for the first time, by appropriate application of high-resolution Ge(Li) detectors. Any systematic errors that might arise from the simple use of UO₂ foils in mixed-oxide fuelled assemblies have thus been eliminated.

The experimental results obtained are compared with theoretical predictions made using current methods and data. It is concluded that, with the present improvement in the systematic accuracy of (C_8/F_9) measurements in fast reactors, the validity and value of such comparisons have been considerably enhanced.

ACKNOWLEDGEMENTS

The author wishes to express his deeply felt gratitude to Dr. C. B. Besant and Professor P. J. Grant of the Nuclear Power Section, Imperial College, and to Dr. C. G. Campbell and Dr. J. E. Sanders of the Fast Reactor Physics Division, A.E.E. Winfrith, for their constant guidance, generous encouragement and valuable advice.

Sincere thanks are due to many people at Winfrith - in particular, to Mr. C. F. George for help in some of the experimental work, to Mr. D. Wardleworth for useful discussions on the theoretical methods, to Mr. W. D. Curren for organising the chemistry effort and providing the plutonium-handling facilities, to Mr. G. R. Jamieson for the engineering support, to Mr. F. J. Linden for the electronics services, and to Miss F. Lamb who typed this thesis.

The author gratefully acknowledges the general backing of both the Imperial College and the United Kingdom Atomic Energy Authority, under the joint auspices of whom this research has been carried out.

CONTENTS

	<u>Page</u>
Title	1
Abstract	2
Acknowledgements	3
Contents	4
List of Figures and Plates	7
List of Tables	10
Chapter 1 - Introduction	12
1.1 The Role of Integral Reactor Physics Experiments in Fast Reactor Design	12
1.2 Target Accuracies for Reaction Rates	13
1.3 The Present Work	14
Chapter 2 - Theoretical Methods	16
2.1 The Lattice Cell Calculation	16
2.2 The Treatment of Resonance Shielding in MURAL	19
2.3 The Cross-section Data	22
2.4 Some Assessment Studies of the Accuracy of MURAL for ZEBRA Lattice Calculations	24
2.5 The Reactor Calculation	26
Chapter 3 - The ZEBRA Reactor and Earlier Established Reaction Rate Techniques	31
3.1 The Reactor	31
3.2 The ZEBRA Core 8 Series	33
3.3 Earlier Established Reaction Rate Techniques	39
3.3.1 Measurement of U-238 Capture Rates	39
3.3.2 Fission Rate Measurements	42
3.3.3 Application of Techniques in ZEBRA	44
Chapter 4 - Absolute Measurements of U-238 Capture and Pu-239 Fission Rates	47
4.1 Absolute U-238 Capture Measurement	48
4.1.1 Theoretical Description of the Present Technique	50
4.1.2 Experimental Procedure	54
4.1.3 Investigation of Possible Systematic Errors	61
4.2 Absolute Pu-239 Fission Measurement	65
4.2.1 Elimination of the Gross Systematic Errors	65
4.2.2 Low-geometry α -Assay of the Chamber Deposits	69
4.2.3 Measuring Procedure	73
4.3 Measurements in ZEBRA Core 8C	76

	<u>Page</u>
Chapter 5 - Preliminary Work with the Ge(Li) Detector System	79
5.1 General Considerations for Mixed-oxide Measurements	79
5.2 Physical Properties of the Present Ge(Li) Detectors	81
5.3 The Automatic Foil-Changer and the Coincidence System	85
5.4 Some Experimental Results	94
5.4.1 Qualitative Work	94
5.4.2 A Fission-Product Correction Factor Measurement	95
5.4.3 Ge(Li) Singles for Absolute U-238 Capture Measurements	99
5.4.4 U-238 Capture Ratio Using Nat. U Foils	101
5.4.5 Counting of Pu-containing Samples	102
Chapter 6 - Absolute U-238 Capture Rate Determination Using Thick Oxide Foils	108
6.1 The Method	109
6.2 Feasibility Measurement in ZEBRA Core 8E	113
6.2.1 Experimental Procedure	113
6.2.2 Results Obtained in Core 8E	119
Chapter 7 - Measurements and Assessments in the Mixed-Oxide Cores ZEBRA 8F and 8G	125
7.1 Techniques Employed and Types of Measurements Made	125
7.2 Fission-product Correction Measurements	128
7.3 Measurements in Core 8F	133
7.3.1 UO ₂ -plate Measurements	133
7.3.2 25% PuO ₂ /UO ₂ -plate Measurements	137
7.4 Measurements in the 8G Plate Core	142
7.5 Measurements in the 8G Pin Core, 8G2	149
Chapter 8 - Discussion of Results and Conclusions	154
8.1 Comparison of Absolute and R.C.R. Techniques	154
8.2 Assessment of Mixed-oxide Measurements	156
8.3 Comparison between Experiment and Theory	159
References	161
Appendix A.1 - An Appraisal of the Numerical Approximations in MURAL	165
A1.1 Effect of Varying the Number of Regions	165
A1.2 The Numerical Integration Approximation	167

	<u>Page</u>
Appendix A.2 - Investigation of Backing Effects in Thin-deposit Absolute U-238 Capture Measurements	171
A2.1 Neutron-scattering Effect in the Backing	171
A2.2 Backing-activation Effect	174

LIST OF FIGURES AND PLATES

		<u>Page</u>
Fig. 1	The ZEBRA Reactor	32
Fig. 2	A ZEBRA Fuel Element	34
Fig. 3	Core Plan of the ZEBRA Core 8 Assemblies	36
Fig. 4	Lattice Cell Structure for the Core 8 Test Regions	37
Fig. 5	MURAL-calculated Cell-averaged Broad-group Spectra for the ZEBRA 8A, 8B and 8C Test Regions	38
Fig. 6	Loading of Foils for Reaction Rate Measurements in ZEBRA Plates	45
Fig. 7	Decay Schemes for Am-243, U-239 and Np-239	49
Fig. 8	α -Spectra of the Am-243 and Natural Uranium Deposits	56
Fig. 9	The Special Loading Plate for the Uranium Deposits	57
Fig. 10	ZEBRA Parallel Plate Fission Chamber	66
Fig. 11	Comparison of Pulse-height Spectra Obtained with Old and New ZEBRA Fission Chambers	68
Fig. 12	The Low-geometry α -counter	70
Fig. 13	Block-diagram of Fission-product Counting Electronics	74
Fig. 14	Response to a 0.02 μ c (Am-243 : Np-239) Source of (a) Ge(Li) Detector A and (b) a 2 in x 2 in NaI(Tl) Crystal	83
Fig. 15	Response to a Th-228 (Tl-208) Source of (a) Ge(Li) Detector A and (b) Initially-supplied Ge(Li) Detector B	86
Fig. 16	Foil-changing Machine for the Ge(Li) Detectors	88
Fig. 17	Some of the Foil Holders Used	91
Fig. 18	Block-diagram of the Ge(Li) Coincidence System	92
Fig. 19	Singles and Coincidence Ge(Li) Spectra of Depleted and 37% Enriched U-metal Foils ~20 hrs. after an Epithermal Flux Irradiation	96

		<u>Page</u>
Fig. 20	$Q_5(t)$ Curves	98
Fig. 21	(a) Ge(Li) and (b) NaI(Tl) Singles Spectra of 0.02 μc (Am-243 : Np-239) Source Sandwiched Between Two 1.5 mgm Pu Foils	103
Fig. 22	Ge(Li) Coincidence Spectra of the Sandwiched Source	104
Fig. 23	Ge(Li) Singles Spectra of Liquid Pu-samples Before and After Am-241 Separation	106
Fig. 24	Loading Plate for Core 8E Feasibility Measurement	116
Fig. 25	Ge(Li) Spectra of 8E-irradiated UO_2 Foil and Am-243-doped UO_2 Source-foil	118
Fig. 26	"Modified" Self-absorption Curves for UO_2 Foil and Source-foils	121
Fig. 27	Block-diagram of Additional Electronics for Simultaneous 278 keV Singles Counting	129
Fig. 28	Ge(Li) 102-108 keV Coincidence Counting $Q_9(t)$ Results	131
Fig. 29	$[278 \pm \frac{1}{2}(\text{F.W.H.M.})]$ keV Singles Counting $Q_9(t)$ Results for Ge(Li) Detector A	132
Fig. 30	Loading Plate for Thin-deposit Measurements in Cores 8F and 8G	135
Fig. 31	Ge(Li) Spectra of (a) Unirradiated 25% PuO_2/UO_2 Foil and (b) Am-243-doped 25% PuO_2/UO_2 Source-foil	139
Fig. 32	Direct Comparisons of Np-239 Activities of 25% PuO_2/UO_2 and UO_2 foils Irradiated in Core 8F Mixed-oxide Plates	143
Fig. 33	"Modified" Self-absorption Curves for 25% PuO_2/UO_2 Foils and Source-foils Used in 8G Plate Core Measurements	145
Fig. 34	Ge(Li) Spectra of (a) 16% PuO_2/UO_2 Foil ~25hrs. after Irradiation in 8G2 and (b) Am-243-doped 16% PuO_2/UO_2 Source-foil	151
Fig. 35	"Modified" Self-absorption Curves for 16% PuO_2/UO_2 Foils and Source-foils Used in 8G Pin Core Measurements	152

	<u>Page</u>	
Fig. A1.1	Multi-region Representations of the ZEBRA 8A Cell	166
Fig. A2.1	NaI(Tl) Spectra of Steel- and Aluminium-backed Deposits ~22hrs. after Irradiation in ZEBRA 8C	177
Fig. A2.2	Ge(Li) Spectra of Steel- and Aluminium-backed Deposits ~22 hrs. after Irradiation in ZEBRA 8C	178
Fig. A2.3	Percentage Coincidence Activities from Bare Backings after 2 hr.-irradiation in ZEBRA 8C	179
Plate 1	General View of the α and γ -X-ray Counting Electronics	59
Plate 2	The Ge(Li) Detector Assemblies and Foil- changing Machine	90

LIST OF TABLES

		<u>Page</u>
Table 1	Neutron Balance in a Typical Fast Reactor	13
Table 2	Results of Analyses of the Am-243 Used	54
Table 3	Systematic Accuracy of the Absolute U-238 Capture Measurement	64
Table 4	Comparison of Geometries for Absolute α -counting	72
Table 5	Errors in the Absolute Pu-239 Fission Measurement	75
Table 6	Results obtained in ZEBRA Core 8C	77
Table 7	Comparison of Errors in 8C Measurements of (C_8/F_9)	77
Table 8	Absolute U-238 Capture Rate Measurements in ZEBRA 8D	100
Table 9	Lattice-to-Thermal U-238 Capture Ratio in 8D	101
Table 10	Results from a Preliminary Pu-counting Experiment	105
Table 11	γ -factor Values for UO_2 Source-foils used in Core 8E	114
Table 12	"Modified" Self-absorption Factors for Core 8E Measurement	120
Table 13	(C_8/F_9) Results for Core 8E	123
Table 14	(C_8/F_9) Results for the 8F UO_2 Plates	137
Table 15	(C_8/F_9) Results for the 8F 25% PuO_2/UO_2 Plate	141
Table 16	Direct Comparisons of the Np-239 Activities of PuO_2/UO_2 and UO_2 Foils in Cores 8F and 8G2	142
Table 17	Results of Absolute Measurements in the 8G Plate Core	146
Table 18	(C_8/F_9) Results for the 8G Plate Core	147
Table 19	Errors in the Various Techniques Developed for U-238 Capture Measurements in 25% PuO_2/UO_2 Material	148

		<u>Page</u>
Table 20	(C_8/F_9) Results for the 8G Pin Core	150
Table 21	Comparison of Absolute Thin-deposit and R.C.R. (C_8/F_9) Results	155
Table 22	Summarised Comparison of Mixed-oxide (C_8/F_9) Results	158
Table 23	Comparison between Experimental and Theoretical (C_8/F_9) Values	159
Table A1.1	ZEBRA 8A - Variation of the Number of Regions in MURAL	167
Table A1.2	ZEBRA 8A - Variation of the Numerical Integration Approximation for the Collision Probabilities in MURAL	168
Table A1.3	ZEBRA 8A - Fine Structure Variation with Numerical Approximations in MURAL	169
Table A2.1	Effect of Steel-backing Activation in Core 8B	176

CHAPTER 1

INTRODUCTION

1.1 THE ROLE OF INTEGRAL REACTOR PHYSICS EXPERIMENTS IN FAST REACTOR DESIGN

The important neutron reactions in fast reactor systems are not confined, as in thermal reactors, to particular regions of the neutron energy spectrum. In order to accurately predict the balance of neutron events in a fast reactor, therefore, it is necessary to perform calculations using very many energy groups and to have available for this purpose a reliable set of nuclear cross-section data covering a very wide range of neutron energies.

In the absence of a sufficiently accurate and comprehensive set of differential nuclear data, it becomes essential to check the theoretical predictions experimentally, i.e. by integral measurements in zero-power assemblies. These are essentially of two types. The first, the "mock-up" experiment, is used for simulating, in a zero-power system, the actual geometry and material composition of a particular power reactor as closely as possible. This provides a direct check on the prediction of the key performance parameters of the reactor system under study, and empirical factors can, where necessary, be deduced to correct the calculated values. However, the theoretical representation of the complicated geometry of "mock-up" experiments is invariably imperfect. In view of the resulting uncertainty in the exact causes of failure of the theoretical predictions, these experiments are of little use in identifying errors in the nuclear data.

"Bench-mark" assemblies constitute the second type of integral experiments used in fast reactor studies. These are geometrically simple assemblies for which errors due to calculational approximations are small and which therefore focus attention on uncertainties in the nuclear data. From the analysis of a series of such clean-geometry integral experiments,

covering a sufficiently wide range of neutron energy spectra, it becomes possible to derive an adjusted nuclear data set which will predict the important parameters of fast reactor performance with sufficient accuracy.

Work along these lines has been going on in ZEBRA (Zero Energy Breeder Reactor Assembly), at the U.K. Atomic Energy Establishment, Winfrith. The main limitation, in the overall procedure of using the integral measurements for nuclear data adjustment, has been identified as arising from the possible presence of unsuspected systematic errors in the experimental measurements themselves, particularly in the case of those measurements for which the demanded accuracy is high.

1.2 TARGET ACCURACIES FOR REACTION RATES

The major single parameter determining the neutron balance in a U-Pu fast reactor system is the reaction rate ratio of neutron capture in U-238 relative to fission in Pu-239. This can be seen from Table 1 which gives a simplified balance of neutron events for a typical fast power reactor, the normalisation being to unit neutron production.

TABLE 1. NEUTRON BALANCE IN A TYPICAL FAST REACTOR

Nuclide	Fission	Non-fissile Capture
U-235	0.013	0.004
U-238	0.040	0.397
Pu-239	0.260	0.078
Pu-240	0.012	0.011
Pu-241	0.015	0.002
Steel, Na, O	-	0.098
Total	0.340	0.590
Leakage + Control = 0.070		

Current target accuracies for fast reactor prediction are standard deviations of 1% for the reactivity and 3% for the breeding ratio. Assuming then that the experimental error in any one reaction rate should contribute not more than 0.3% and 1.0% to these parameters respectively, it follows from Table 1 that the accuracy requirement for the determination of the ratio of U-238 capture to Pu-239 fission, ($C_{8/P9}$), is the most stringent one, viz. $\sim 1\%$. The corresponding figures for the other important reaction rates are 2% for U-238 fission and 3% for U-235 fission (relative to fission in Pu-239).

1.3 THE PRESENT WORK

In order to meet the stringent target accuracies for the experimental determination of reaction rates in fast reactor assemblies, particularly that for ($C_{8/P9}$), it is essential to establish that the measuring techniques are free from systematic errors. It is only then that valid and unambiguous comparisons between theory and experiment can be made. The main aim of the present work has been to achieve this by developing new, independent techniques for measuring U-238 capture and Pu-239 fission rates in ZEBRA "bench-mark" assemblies and by comparing the results with values obtained from both theory and earlier-established experimental methods.

All recently published experimental results for the ratio of U-238 capture relative to Pu-239 or U-235 fission in reactor lattices have been obtained by comparison of the lattice ratio with that in a thermal column, where the individual cross-sections for the two reactions are known to an accuracy of about $\pm 1\%$. In order to eliminate this inherent systematic error on the thermal cross-section values used and thereby achieve a higher potential accuracy of measurement, techniques for the absolute measurement of U-238 capture and Pu-239 fission rates in the reactor assembly itself

have been developed for ZEBRA. As a result, direct determination of the reaction rate ratio, without recourse to any comparisons with thermal irradiations, has been made possible.

Secondly, the use of mixed-oxide fuel, containing as much as 25% by weight of plutonium, has to date posed serious problems in the measurement of U-238 capture rates in fast reactor lattices. γ -, X-ray counting techniques, using thallium-activated sodium iodide scintillation detectors, have been well established in the past for measuring radiations from the decay of U-239 or Np-239, in depleted and natural uranium fuels. However, for PuO_2/UO_2 material, these techniques using NaI (Tl) counters have been found to be inadequate because of the very large backgrounds, arising from Pu natural-activity and fission-product radiations, which swamp the observed U-239 and Np-239 counts. U-238 capture measurements in mixed-oxide cores have so far had to be carried out using natural UO_2 foils, introducing possible errors due to (a) the increased number density of U-238, and (b) the absence of mutual shielding of U-238 and Pu-239 resonances, within the foil. In view of the increasing importance of mixed-oxide experiments in fast reactor studies, it has become necessary to eliminate these possible systematic errors by carrying out U-238 capture measurements using foils of exactly the same material composition as the mixed-oxide fuel itself. This has been achieved in the current work through the setting up of a twin lithium-drifted germanium detector system, with both detectors having resolutions of better than 2 kev. at 100 kev. (cf. ~15 kev. for a NaI (Tl) counter). The availability of this superior energy resolution has enabled adequate discrimination of the various γ - and X-rays. By using specially developed absolute and thermal-comparison techniques for the measurements, unambiguous comparisons between experiment and theory have been made possible in mixed-oxide assemblies containing 25% and 16% PuO_2/UO_2 fuel.

CHAPTER 2

THEORETICAL METHODS

2.1 THE LATTICE CELL CALCULATION

The calculation of primary interest in the theoretical analysis of fast "bench-mark" assemblies, of the type presently studied in ZEBRA, is the infinite lattice cell calculation for a central, zero-leakage ($k_{\infty} \sim 1$) test region. Although the actual physical situation in the reactor is that of a finite test region surrounded radially and axially by a U-235 fuelled driver zone and a natural uranium blanket (Chapter 3), effects due to the interaction of the different regions are of secondary importance at the centre of the test lattice where the experimental measurements are conducted. As such, calculations made to estimate correction factors for these effects (Section 2.5) can only be regarded as subsidiary.

The heterogeneity of a typical ZEBRA test-region cell, constructed from plates, has to be accepted from the outset in the lattice calculation. With the dimensions of the cell regions being of the same order of magnitude as the neutron mean free path, the diffusion approximation of the Boltzmann transport equation is inadequate and a solution for the flux may be sought using say the P_n (spherical harmonics) or the Carlson S_n approximation (Ref. 1). The former method is exceedingly complex for multi-region problems where the variation of neutron cross-sections with energy has to be taken into account in detail. The S_n approximation is more suitable as a numerical method for use on computers, but for slab-geometry calculations it has been shown by Meneghetti (Ref. 2) to fare poorly when the cell has a very fine structure - this being due to the complicated spatial dependence of the angular flux in such cases.

A more suitable alternative approach which provides a description of the neutronics phenomena without direct recourse to the Boltzmann

integrodifferential equation is the collision probability method, based on representing the neutron transport in the lattice cell in terms of first-collision probabilities (Ref. 3). Integral, rather than differential, statements of the neutron conservation are used, thereby permitting the use of a relatively coarse spatial mesh. The main disadvantage of the method is that it postulates isotropic scattering. However, where this assumption is valid, one is able to write an integral equation in terms of the scalar flux instead of the angular flux and, as the former is a much smoother function, this procedure overcomes the failings of the S_n method.

An important feature of collision probability methods is that the transport and collision-mechanics parts of the problem are completely dissociated, so that the form of the basic integral transport equations is not dependent on the type of geometry. This means that a computer code used for the numerical solution of these equations can be applied to any system, whatever its geometry, provided that a method of calculating the appropriate first-collision probabilities is made available as a subroutine in the programme.

The basic equations of the collision probability method may be formulated in a simple manner by considering monoenergetic neutrons of which there is a source $S(\bar{r}_1)$ at \bar{r}_1 . If there are no collisions, the flux $\phi(\bar{r})$ at \bar{r} is given by

$$\phi(\bar{r}) = \frac{S(\bar{r}_1)}{4\pi |\bar{r} - \bar{r}_1|^2}$$

If there is removal from this energy, the flux will be reduced by a

factor of $\left[e^{-\int_{\bar{r}_1}^{\bar{r}} \Sigma_t(\bar{r}_1) d\bar{r}_1} \right]$ where Σ_t is the total removal macroscopic cross-section, and one obtains the total flux at \bar{r} as the sum of all such contributions, i.e.,

$$\phi(\bar{r}) = \frac{1}{4\pi} \int \left\{ S(\bar{r}^1) \cdot \frac{e^{-\int_{\bar{r}^1}^{\bar{r}} \Sigma_t(\bar{r}_1) d\bar{r}_1}}{|\bar{r} - \bar{r}^1|^2} \right\} \cdot dV(\bar{r}^1) \dots\dots\dots(2.1)$$

This is the integral equation which may be written in an alternative form as

$$\Sigma_t(\bar{r}) \cdot \phi(\bar{r}) = \int_{\text{Volume}} \{ P(\bar{r}^1 \rightarrow \bar{r}) \cdot S(\bar{r}^1) \} \cdot dV(\bar{r}^1) \dots\dots\dots(2.2)$$

Here
$$P(\bar{r}^1 \rightarrow \bar{r}) = \Sigma_t(\bar{r}) \cdot \frac{e^{-\int_{\bar{r}^1}^{\bar{r}} \Sigma_t(\bar{r}_1) d\bar{r}_1}}{4\pi |\bar{r} - \bar{r}^1|^2} \dots\dots\dots(2.3)$$

and is defined as the probability that a neutron which made a collision at \bar{r}^1 will make its next collision at \bar{r} . From this, the reciprocity relation follows, viz.,

$$\Sigma_t(\bar{r}^1) \cdot P(\bar{r}^1 \rightarrow \bar{r}) = \Sigma_t(\bar{r}) \cdot P(\bar{r} \rightarrow \bar{r}^1) \dots\dots\dots(2.4)$$

For solution of the problem using a computer, the system under consideration is divided into a number of regions within each of which the various nuclear properties are averaged. One may then consider the finite-difference form of Equations (2.2) and (2.4), viz.,

$$V_j \Sigma_{tj} \phi_j = \text{Sum}_i \{ V_i P_{ij} S_i \} \dots\dots\dots(2.5)$$

and
$$V_j \Sigma_{tj} P_{ji} = V_i \Sigma_{ti} P_{ij} \dots\dots\dots(2.6)$$

where the subscripts i and j refer to different regions. It can be seen, from Equation (2.5), that the flux in region j is obtained directly in terms of the neutron sources in the regions i, the macroscopic cross-sections, the region volumes and the various collision probabilities.

The collision probability method, as outlined briefly above, forms the basis for the computer programme MURAL (Ref. 4), developed at Winfrith for multi-region fast reactor cell calculations. Over 2000 neutron energy groups of equal lethargy width are used for the description of the neutron energy spectrum between 0.414 eV and 10 MeV, and the

programme can accommodate up to 20 regions on the IBM 7030 computer (which has a 96 K word fast store). To simplify the editing of the fine group flux solution, a 37-group broad group representation of the neutron spectrum is used as well.

The first stage of an infinite-lattice cell calculation using MURAL is the computation of the fission source distribution from broad group data and the iteration for the effective multiplication factor (k-option). The fine group fluxes in region j are calculated next, using Equation (2.5), from the sources in the regions i . The anisotropic source is not computed in MURAL, and the isotropic source, S , is assumed as consisting of (1) S_F , the fission neutron source, (2) S_{EL} , the elastic scattering source for isotopes other than hydrogen, (3) S_H , the hydrogen elastic scattering source, (4) S_{IN} , the inelastic scattering source and (5) S_B , the broad group scattering source.

After calculating the fine group spectrum for the different regions of the lattice cell, MURAL performs a broad group editing of the output data. Broad group macroscopic cross-sections for each region of the cell, and for the cell itself, are obtained from the fine group constants by simple flux weighting. From the condensed cross-sections, the reactivity k , the fission source distribution and the flux distribution in the different regions are recomputed. It is these recomputed values which are finally used to yield the relative reaction rates for the various isotopes in the different regions of the cell.

2.2 THE TREATMENT OF RESONANCE SHIELDING IN MURAL

The fine group structure of MURAL, though adequate for the detailed description of neutron interactions with the lighter nuclei over a wide range of energies, does not provide groups narrow enough to represent the heavy-element resonances individually. The absorption resonances

in uranium and plutonium isotopes above about 100 eV are of the utmost importance when dealing with fast reactors and a resonance shielding prescription within fine groups has therefore been incorporated in MURAL for their detailed treatment (Ref. 5). This essentially consists of within-group histogram tabulations which, at lower energies, represent real resonances but which at higher energies signify pseudo-resonances chosen to reproduce the resonance shielding to an acceptable accuracy. The shielded fine group cross-section is calculated by weighting each tabulation with the reciprocal of the total cross-section obtained by assuming that all other isotopes in the medium have their average total cross-section constant throughout the group.

That this procedure is a plausible approximation to the shielding may be easily shown from the following arguments. The true effective cross-section in group g for reaction x of isotope k is

$$\sigma_{xkg} = \frac{\int \sigma_{xk}(E) \phi(E) dE}{\int \phi(E) dE} \dots\dots\dots(2.7)$$

where the energy integration is over group g . Assuming for a homogeneous medium that $\phi(E) = S(E)/\Sigma_t(E)$ (P_1 approximation)..... (2.8)

where S is the neutron source and Σ_t is the total macroscopic cross-section, one obtains

$$\sigma_{xkg} \approx \frac{\int \{\sigma_{xk}(E) S(E) dE/\Sigma_t(E)\}}{\int \{S(E)dE/\Sigma_t(E)\}} \dots\dots\dots(2.9)$$

For a narrow group (such as those of MURAL) the variation of the source with energy is small and one may normalise to $S(E) \approx 1$. Further, if the fluctuations of the total cross-sections of other isotopes are uncorrelated with those of isotope k , little error is introduced by replacing $\Sigma_t(E)$ by $\{N_k \sigma_{tk}(E) + \sum_{l \neq k} N_l \bar{\sigma}_{tlg}\}$ where N_l and $\bar{\sigma}_{tlg}$ are the number density and mean total cross-section of isotope l respectively.

Thus, from Equation (2.9),

$$\sigma_{xkg} \approx \frac{\int \{ \sigma_{xk}(E) dE / (\sigma_{exk} + \sigma_{tk}(E)) \}}{\int \{ dE / (\sigma_{exk} + \sigma_{tk}(E)) \}} \dots\dots\dots(2.10)$$

where $\sigma_{exk} = \frac{\text{Sum}}{1/k} N_{1l} \bar{\sigma}_{tlg} / N_k$.

It is seen that by using a histogram representation of $\sigma_{xk}(E)$ and $\sigma_{tk}(E)$ in the integrals of Equation (2.10), one obtains the resonance shielding prescription described earlier.

The arguments used so far for a homogeneous medium can be easily extended to the multi-region case. Here, using the basic collision probability equation (2.5), the flux in region j may be written as

$$\phi_j(E) = \frac{\text{Sum}_i \{ V_i P_{ij}(E) S_i(E) \}}{V_j \Sigma_{tj}(E)} \dots\dots\dots(2.11)$$

From the reciprocity relation (2.6),

$$V_j \Sigma_{tj}(E) = V_i \Sigma_{ti}(E) P_{ij}(E) / P_{ji}(E) \dots\dots\dots(2.12)$$

which when substituted into (2.11) gives

$$\phi_j(E) = \frac{\text{Sum}_i \{ S_i(E) P_{ji}(E) / \Sigma_{ti} \}}{\dots\dots\dots} \dots\dots\dots(2.13)$$

Assuming, as before, that S_i is constant within a group, one obtains the effective cross-section in group g and region j for reaction x of isotope k as

$$\begin{aligned} \sigma_{xkgj} &= \int_g \sigma_{xk}(E) \phi_j(E) dE / \int_g \phi_j(E) dE \\ &= \frac{\text{Sum}_i \{ S_i \int \sigma_{xk}(E) P_{ji}(E) dE / \Sigma_{ti}(E) \}}{\text{Sum}_i \{ S_i \int P_{ji}(E) dE / \Sigma_{ti}(E) \}} \dots\dots\dots(2.14) \end{aligned}$$

Again, it is assumed that all average total cross-sections, except that of isotope k, are constant within the group, i.e.

$$\begin{aligned} \Sigma_{ti}(E) &= N_{ki} \sigma_{tk}(E) + \frac{\text{Sum}}{1/k} N_{li} \bar{\sigma}_{tlg} \\ &= N_{ki} \{ \sigma_{exki} + \sigma_{tk}(E) \} \dots\dots\dots(2.15) \end{aligned}$$

where N_{li} is the number density of isotope l in region i . Making this approximation for $\Sigma_{ti}(E)$ and assuming that in a proportion w_m of the group g

$$\sigma_{xk} = \bar{\sigma}_x (1 + \xi_{xm}) \dots\dots\dots(2.16)$$

(histogram representation of the cross-sections)

one obtains

$$\sigma_{xkgj} = \frac{\sum_i \left[\frac{S_i}{N_{ki}} \sum_m \left\{ \frac{w_m P_{jim} \bar{\sigma}_x (1 + \xi_{xm})}{\sigma_{exi} + \bar{\sigma}_t (1 + \xi_{tm})} \right\} \right]}{\sum_i \left[\frac{S_i}{N_{ki}} \sum_m \left\{ \frac{w_m P_{jim}}{\sigma_{exi} + \bar{\sigma}_t (1 + \xi_{tm})} \right\} \right]} \dots\dots\dots(2.17)$$

where the suffices k and g have been dropped on the right hand side and where P_{jim} is the collision probability calculated using the total cross-section $N_{ki} \{ \sigma_{exi} + \bar{\sigma}_t (1 + \xi_{tm}) \}$ in region i .

It is clear that for the evaluation of the shielded cross-sections from Equation (2.17), M collision probability matrices - one for each of the M points in the histogram representation for the isotope - are required, in addition to the matrix P_{ij} . Although, in particular cases, simplifying assumptions may be made (Ref. 5) to obviate this need, such simplifications are not found to be generally valid (see Appendix A2.1).

2.3. THE CROSS-SECTION DATA

The cross-section data library used by MURAL contains data in essentially three forms, viz.

- (a) Broad group data with 37 groups covering the range from thermal energies to 15 MeV.
- (b) Fine group data with 2176 groups of lethargy width $1/128$ covering the range 0.414 eV to 10 MeV (this range being covered in half-unit lethargy steps by groups 2 to 35 of the broad group set).

and

- (c) Histogram tabulations of resonance structure within fine groups.

Cross-sections for the principal isotopes - H, B-10, C, O, Na, Al, Cr, Fe, Ni, U-235, U-238, Pu-239 and Pu-240 - are represented in fine group form, except for elastic scattering in B-10, inelastic scattering to the continuum and (n, 2n) data, which are in broad group form. For additional isotopes - B-11, N, Si, Ca, Mn, Cu, Ga, Ta, Au, U-234, U-236, Pu-241, Pu-242 and fission products - broad group cross-sections alone are used.

The current fine group data set for MURAL is FGL4, derived from cross-sections tabulated in the U.K. Nuclear Data Library (Ref. 6) using the group averaging programme GALAXY (Ref. 7). The fine group elastic scattering matrices were computed from GALAXY but for certain fine groups only. The fractions scattered from fine groups g to g^1 , $f(g, g^1)$, were obtained by interpolation for the intermediate groups, this approach being adopted to reduce computing time. Fine group inelastic cross-sections for discrete levels were calculated from GALAXY as well, but the fine group intervals, m to n , through which the inelastically scattered neutrons are distributed, were computed separately.

The U-235, U-238, Pu-239 and Pu-240 resonance data below 25 keV were obtained from tabular cross-section values which had been generated from resonance parameters using the GENEX code (Ref. 8). These cross-sections, which are tabulated at some 125,000 energy points between thermal energies and 25 keV, were processed using the GENDEL programme (Ref. 5) which calculates fine-group shielded cross-sections for a range of background cross-sections and then fits these to a histogram representation within each fine group (Section 2.2). The standard data in FGL4 is a two-point histogram fit. The accuracy of this approximation for the resonance shielding in the FGL4 data has been examined (Ref. 5) by comparing a few one and two region MURAL calculations with values obtained using the slowing down routine SDR (Refs. 8 and 9), which calculates cell spectra at all points of a GENEX tabulation using

collision probability methods. Although slight differences were observed in the results, these were not considered serious enough to warrant revision of the MURAL shielding prescription for resonances below 25 keV.

At energies above 25 keV, a code called REGA has been used to generate the appropriate resonance parameters, but the within-group fitting procedure for the shielded cross-sections is essentially the same as below 25 keV.

Further details of the organisation of the MURAL library are given in Ref. 4. A summary of the important sources of the cross-section data for the principal isotopes in the FGL4 set has been presented in Ref. 10. This latter paper also deals with the methods being used at Winfrith for the adjustment of the differential cross-section values - on the basis of comparisons between theoretical predictions and integral measurements in ZEBRA test regions.

2.4 SOME ASSESSMENT STUDIES OF THE ACCURACY OF MURAL FOR ZEBRA LATTICE CALCULATIONS

In using results from the analysis of a series of "bench-mark" assemblies to derive a more accurate nuclear data set, an important assumption has to be made, viz., that negligible calculational errors are introduced due to the various approximations in the theoretical methods themselves. A few assessment studies of the accuracy of MURAL for ZEBRA lattice calculations were made by the present author to examine how well in fact the code meets this "negligible error" requirement. The results are summarised in this section.

The approximations made in MURAL may be divided into two categories - theoretical and numerical. The former are basic simplifications inherent in the theoretical model used and examples of these are (i) the use of

collision probabilities, which are calculated on the basis of isotropic scattering; (ii) the simple representation of resonances for obtaining resonance shielding factors; and (iii) the homogenisation of the fuel element sheath in the lattice cell representation.

Attempts to investigate approximation (i) would entail direct comparisons with theoretical methods which solve the differential transport equation for the angular flux. Difficulties regarding the use of these methods for ZEBRA calculations, as indicated in Section 2.1, are considerable and as such approximation (i) could not be properly assessed.

An examination of the resonance shielding approximation in MURAL has already been made, as mentioned earlier, by Macdougall and Rowlands (Ref. 5) who have compared one and two region MURAL calculations with results obtained using the SDR code. An attempt was made to extend the MURAL-SDR comparison to an actual ZEBRA lattice calculation. This was done for a four-region ZEBRA Core 8A cell (Chapter 3) and differences of the order of a percent in the reaction rate ratios were obtained. However, it was realized that this comparison was probably misleading in that other basic differences in the two codes (such as the much simpler representation of elastic scattering cross-sections for the light elements in SDR and the fact that it ignores inelastic scattering sources) may have swamped the resonance treatment effects.

Approximation (iii) follows from the one-dimensional nature of the present MURAL treatment of the ZEBRA test regions. Although an exact calculation of the sheath heterogeneity effects would require a three-dimensional collision probability subroutine in MURAL, a few simple one-dimensional representations can be used to give some indication of the overall effects on the reaction rate ratios. This was done for three different 9-region calculations for the Core 8A cell in which the fuel

element sheath was (a) homogenised into the various regions of the cell, (b) treated as a separate region in the middle of the natural uranium and (c) treated as a separate region in the middle of the plutonium plate. (The overall cell composition was conserved in each case by appropriate adjustment, where necessary, of number densities and volumes.) A comparison of the results from these calculations showed that neither uranium-sheath, nor plutonium-sheath, heterogeneity effects were important, the differences in every cell-averaged reaction rate ratio being less than 0.2% between the three cases.

The other type of approximations made in MURAL consists of those in the numerical analysis. These approximations are made solely to limit the computational time required for solving a particular case, and they differ from the theoretical simplifications in that the degree of approximation can be reduced (at the expense of the computer job time) to approach the correct solution in the limit. The two chief numerical approximations are (a) the cell representation in terms of a finite number of regions and (b) the calculation of the collision probabilities by numerical integration using Gaussian quadrature with a finite number of points. Both these effects were investigated in detail for ZEBRA Core 8A lattice calculations and the results are presented in Appendix A.1. In brief, it was found that the effects on the reaction rates of increasing the number of regions in the 8A cell beyond 8 were < 0.1%, i.e. insignificant, and that the use of 7-point Gaussian quadrature for calculating the collision probabilities was quite adequate.

2.5 THE REACTOR CALCULATION

The only serious objection against the use of the "raw" results from a MURAL cell calculation, for direct comparison with experimental

measurements in a ZEBRA test region, is that such results ignore effects due to the finite size of the test region and its interaction with the other reactor zones. The method adopted for taking these effects into account essentially involves reactor calculations in a simplified geometry (usually spherical), in which the three reactor regions - test, driver and blanket - are represented in their true volumes and with cell-averaged broad group data generated from MURAL lattice calculations. The code used for the reactor calculations is the diffusion theory programme SCRAMBLE (Ref. 11). The procedure for deriving correction factors from these calculations, for modifying the infinite lattice MURAL results for the test region, is due to Wardleworth (Ref. 12).

For the spherical model of the reactor (S), SCRAMBLE solves the multigroup diffusion equation

$$- D \nabla^2 \Phi + A \Phi = (F/k) \Phi \dots\dots\dots(2.18)$$

where D is the diffusion coefficient vector, A is the absorption and scattering matrix, F is the fission source ($F = \chi \nu \Sigma_f$), and k is the effective multiplication factor for the system. It is seen that criticality is achieved by actually adjusting the fission source (dividing F by k) everywhere in the reactor.

For the infinite lattice calculation (IL), the equation solved is

$$A \Phi = (F/k_\infty) \Phi \dots\dots\dots(2.19)$$

there being no spatial dependence and criticality being achieved here by dividing the fission source by the infinite multiplication factor, k_∞ . The vector Φ is, of course, the infinite lattice spectrum.

Although it would seem that Equation (2.19) defines the infinite multiplication factor for the data used in the spherical calculation, this is not really true because the fission source has been modified by the k-effective value for the reactor. In fact, the "k-infinity", k_∞^1 ,

for this modified data is defined by

$$A\Phi = \left(\frac{F}{k k_{\infty}^1}\right) \Phi \dots\dots\dots(2.20)$$

i.e., $k_{\infty}^1 = \frac{k_{\infty}}{k} \dots\dots\dots(2.21)$

It is easily seen that the infinite lattice spectrum, Φ , is itself unaffected by this modification of the fission source by the scalar quantity k .

If k -infinity for the test region is exactly unity, it is obvious that the asymptotic spectrum for the centre of the region will simply be the infinite lattice spectrum. However, as in practice k -infinity differs from unity, one has to consider the general case where the asymptotic spectrum is not Φ but the fundamental mode (FM) spectrum, Ψ , defined by

$$B^2 D\Psi + A\Psi = (F/k)\Psi \dots\dots\dots(2.22)$$

where k is fixed as the computed k -effective for the reactor calculation and criticality is achieved by adjusting B^2 , the scalar buckling. Clearly, for the special case when k -infinity is unity and $B^2 = 0$, one has $\Psi = \Phi$.

From the above considerations, it is easily seen that there are two quite distinct reasons why the correction factors (IL/S), relating the infinite lattice reaction rate ratios to those at the centre of the spherical reactor model, are not unity. These are (i) that in the finite reactor, the central spectrum is not the asymptotic spectrum for the central region (purely because of the size of the region) and (ii) that this asymptotic spectrum, being the fundamental mode spectrum, is not the infinite lattice spectrum (except when k -infinity is unity).

The effects of finite central-region size and region mismatch are represented by the (FM/S) factors, which from Equations (2.18) and (2.22) are independent of k -infinity. However, for the correction factors of interest, viz. the (IL/S) factors, the dependence on the actual

k-infinity value for the central test region is quite significant. This is a consequence of reason (ii) and the fact that it is k-infinity which determines how different the FM and the IL spectra are. It follows therefore that the experimental value of k-infinity for the test region must be used to determine the proper ($\frac{IL}{S}$) correction factors.

The full procedure for determining the correct ($\frac{IL}{S}$) factors may be summarised as follows. Three sets of data are produced, viz. the broad group MURAL output data (condensed over the infinite lattice spectrum and cell-homogenised), and two other sets of data identical to the first except that F in each group is divided by some arbitrary factor (e.g., 0.96 or 0.98) in each case. As mentioned earlier, these three sets of data will correspond to exactly the same IL-values for the reaction rate ratios because the infinite lattice spectrum is unaffected when the fission source is divided by a constant factor in all groups. However, the modified "k-infinity", or k_{∞}^1 , values for the three data sets will obviously be different, and it follows that the S-values - calculated using these three sets in the same spherical model of the reactor - will be different as well. One thus obtains values of the ($\frac{IL}{S}$) factors as functions of k-infinity. From these plots and from the experimental k-infinity value for the test region (Ref. 13), the appropriate correction factors can be decided upon.

The chief possible sources of error in the methods outlined in this section, for determining the correction factors to be applied to the MURAL infinite-lattice reaction rate ratios, are:

- (i) the use of spherical instead of cylindrical geometry;
- (ii) the effect of data uncertainties, particularly those for the transport cross-sections which determine the interaction between

the different regions;

and

(iii) the error in the experimental value of k-infinity.

Studies have been made (Ref. 14) for each of these effects in ZEBRA Cores 8B, 8C and 8E, and it has been estimated that the net uncertainties, in the applied (I_L/S) correction factors, contribute errors of typically $< \frac{1}{2}\%$ in the predicted central reaction rate ratios. In 8B, for example, the (I_L/S) factors applied to the reaction rate ratios ($C8/F9$), ($F8/F9$) and ($F5/F9$) were (1.009 ± 0.003) , (0.994 ± 0.007) and (1.007 ± 0.002) , respectively.

CHAPTER 3

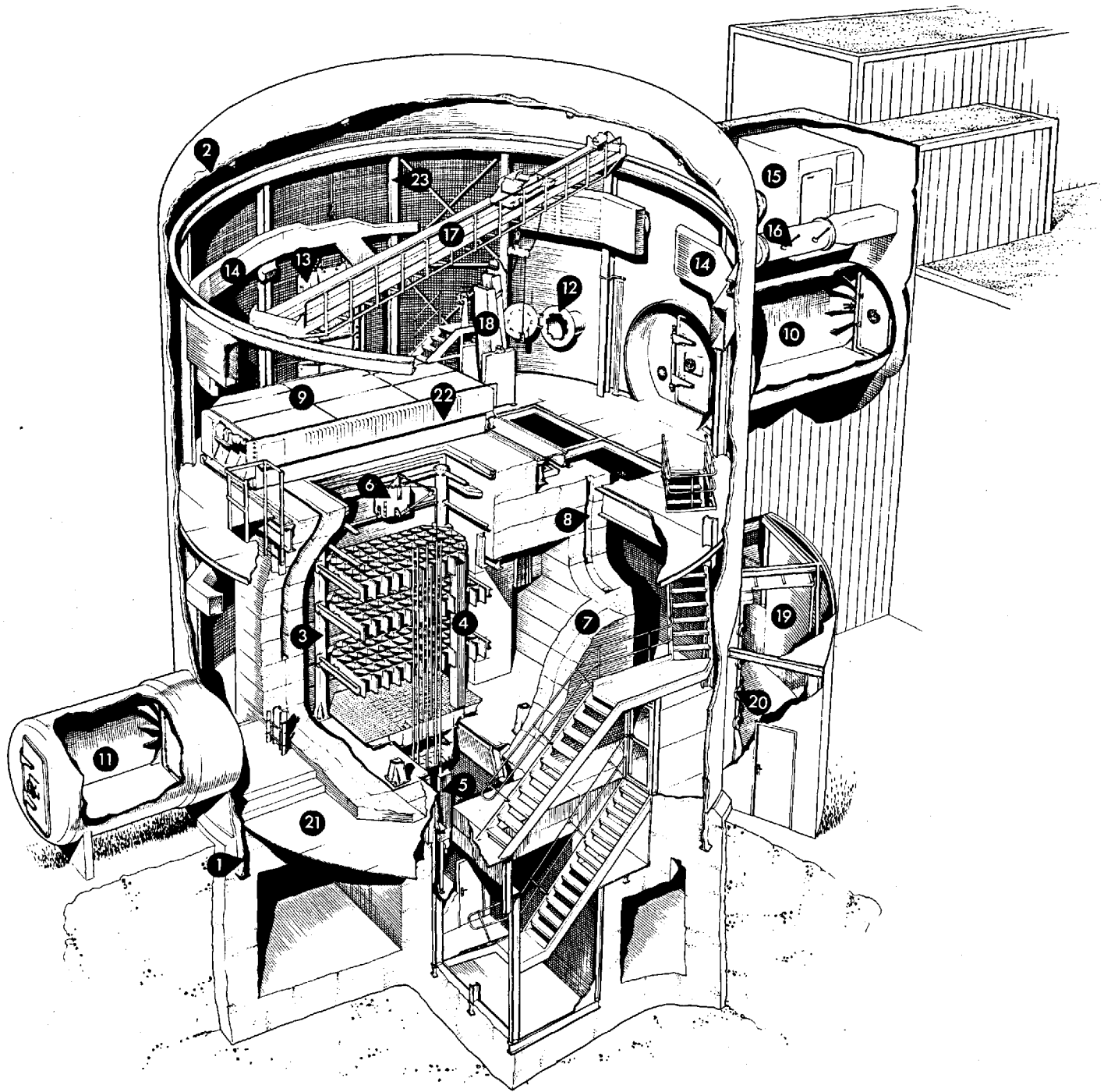
THE ZEBRA REACTOR AND EARLIER ESTABLISHED REACTION RATE TECHNIQUES

3.1 THE REACTOR

The ZEBRA reactor (Ref. 15) was built at Winfrith in 1962 to meet the then growing need for a versatile zero-power assembly which could be used for both "mock-up" and "bench-mark" studies of fast reactor systems. The size of the reactor - approximately a three metre cube - is sufficient to contain the largest systems envisaged for both these types of experiments. A general view of ZEBRA is shown in Fig. 1.

The reactor core itself is assembled over a pit on a rigid steel base plate, 3 m. square, which supports the fuel elements. These consist of stainless steel tubes, 0.76 mm. wall-thickness, 51 mm. square and just under 3 m. long. At the bottom of each element is a stainless steel spigot which locates in a hole in the base plate. The fuel elements are laterally restrained by three steel lattice plates. These are on a square pitch of 27.1 cm., so that the elements are supported in groups of 25.

The versatility of the reactor is realised through the fact that the various core materials are in the form of plates, the majority of which are 51 mm. square and multiples of 1.6 mm. thick. The fuel elements are filled with these plates which are stacked horizontally, one above the other, in an order determined by the basic cell structure of the particular assembly being studied. The ZEBRA inventory contains a large variety of these plates, e.g. plates of steel-clad Pu (5% and 10% Pu-240), steel-clad 25% PuO₂/UO₂, enriched uranium (37.5% and 93% U-235), natural uranium, steel-clad UO₂, stainless steel, boron, graphite, and steel-clad sodium. (In addition, some fuel is also available in the form of 10 mm. diameter pellets which can be used in pins for special calandria studies at the centre of the assembly, e.g. Doppler experiments



KEY:

- 1. STEEL CONTAINMENT VESSEL
- 2. CONTAINMENT VESSEL INSULATION
- 3. REACTOR STRUCTURE
- 4. FUEL ELEMENTS
- 5. CONTROL ROD MECHANISM
- 6. SHUT-OFF ROD MECHANISM
- 7. BIOLOGICAL SHIELD
- 8. FUEL ELEMENT STORAGE CHAMBER

- 9. BIOLOGICAL SHIELD DOOR
- 10. PERSONNEL AIRLOCK
- 11. EMERGENCY AIRLOCK
- 12. FUEL ELEMENT TRANSIT AIRLOCK
- 13. ACCESS DOOR (SHOWN IN RAISED POSITION)
- 14. HEATING AND VENTILATION SYSTEM
- 15. FILTER CHAMBER

- 16. SHUT-OFF VALVES
- 17. 2 TON CIRCULAR TRACK CRANE
- 18. FUEL ELEMENT TURNOVER DEVICE
- 19. CABLE ROOM
- 20. CABLE ENTRIES
- 21. MEMBRANE FLOOR
- 22. REMOVABLE CONCRETE BLOCKS
- 23. CRANE SUPPORT STRUCTURE

FIG. I. THE ZEBRA REACTOR

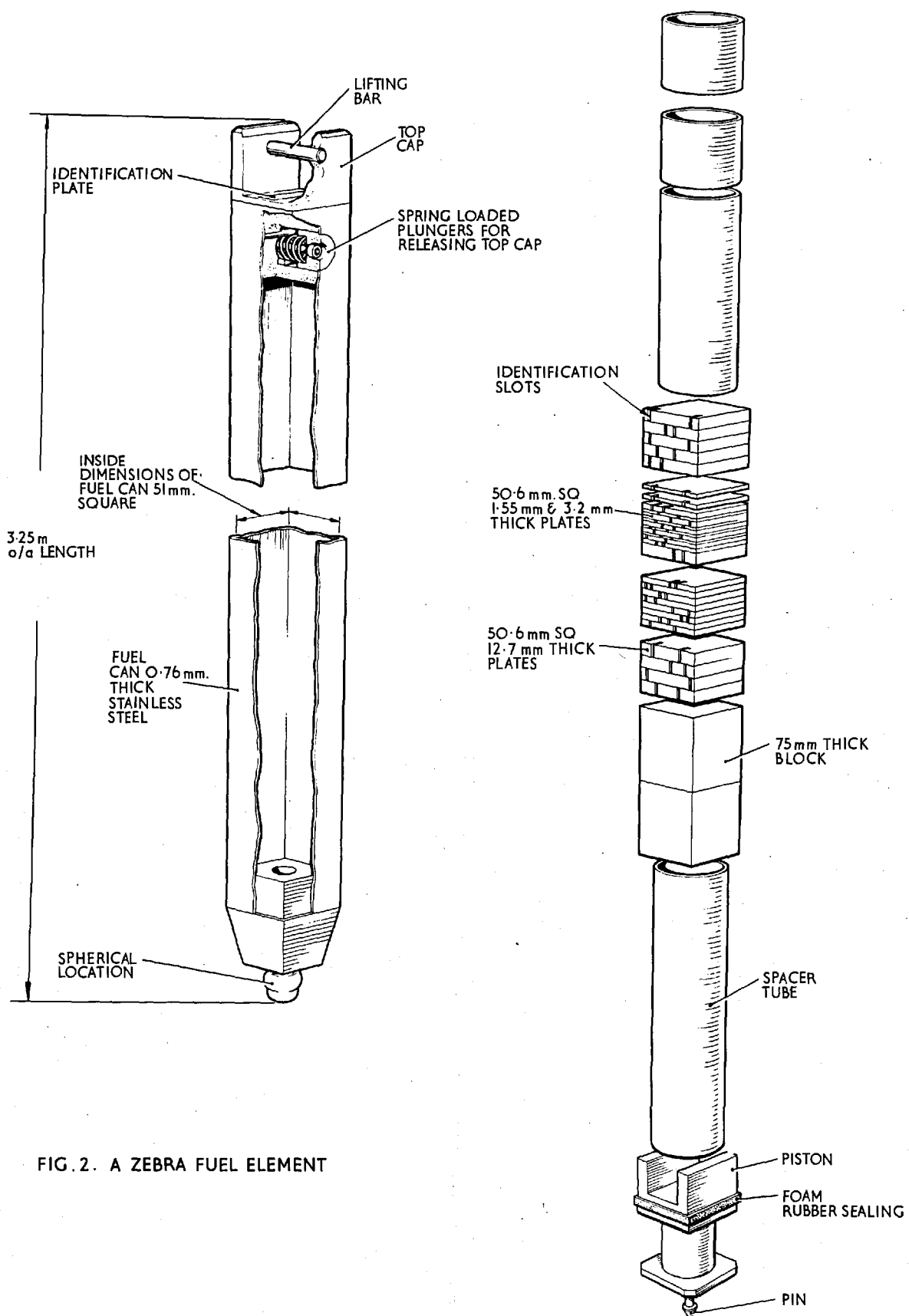
and pin-plate heterogeneity studies.) A typical ZEBRA fuel element and its contents are shown in Fig. 2.

The general lay-out of the reactor in its building is given in Fig. 1. A 1 m.-thick concrete shield closely surrounds the reactor on three sides, while on the fourth side the shielding is spaced 2 m. away from the reactor to allow access to the side of the core. Above the reactor are two concrete doors which can be rolled back to allow access to the top for the loading and unloading of the fuel elements. In the closed position, there is a gap between the doors of about 10 cm. This is generally filled by a row of concrete blocks, the removal of one or more of which allows access to the reactor during operation for experimental purposes (e.g. the insertion of fission chambers). The reactor and its concrete shield are contained in a cylindrical steel vessel about 11.3 m. in diameter and 12.8 m. high, and this is connected via airlocks to an ancillary block of buildings which house the control room, the fuel element assembly room, a fissile material store, various service facilities, etc.

ZEBRA is normally controlled by nine control rods, variable in position and composition and controlling a total of about 5% in reactivity. The control and instrumentation of the reactor has several safety features incorporated into its design, and these ensure that any abnormal condition in the reactor causes an immediate shut-down.

3.2 THE ZEBRA CORE 8 SERIES

The present work has been mainly carried out in the ZEBRA Core 8 series of "bench-mark" assemblies. These were planned as a first stage in a programme of well-defined integral experiments which would provide the basis for a systematic adjustment of the differential nuclear data used in fast reactor calculations (Refs. 10 and 13).



A core plan of the Core 8 assemblies is shown in Fig. 3. The central, plutonium-fuelled, zero-leakage test region is 64 cm. in effective diameter and about 60 cm. high. This is surrounded by the U-235 fuelled driver zone, about 8 cm. wide and itself enclosed in the 30 cm. thick natural uranium blanket. The nine control rods are located in the driver and contain a comparable amount of fuel to the surrounding driver elements.

Fig. 4 gives the lattice cell structures for the seven test regions that have been investigated, viz. those for Assemblies 8A, 8B, 8C, 8D, 8E, 8F, and 8G.

Core 8A was a soft spectrum system designed to study events in the keV region. Core 8B, a second simple Pu-U-C system, had a much harder spectrum. Core 8C had a spectrum intermediate between the first two assemblies and was primarily designed to provide integral data on stainless steel, an important constituent of current fast reactor designs. Fig. 5 shows MURAL calculated broad-group spectra for the 8A, 8B and 8C test regions, and indicates how wide a range of fast reactor spectra can be investigated in studies of this type.

Core 8D was the first of two test regions designed to study the effects of sodium in a neutron spectrum typical of a power reactor such as the Prototype Fast Reactor. Core 8E was the second assembly for the study of sodium, being a harder spectrum version of 8D with carbon removed from the cell.

Cores 8F and 8G were the two mixed-oxide assemblies in the series. The 8F test region had a similar spectrum to that for Core 8A but, being a much more homogeneous system than this earlier assembly, it provided a useful check on the application of the calculational methods and data to lattices in which heterogeneity effects are much less pronounced. The second mixed-oxide test region, 8G, was designed to extend this invest-

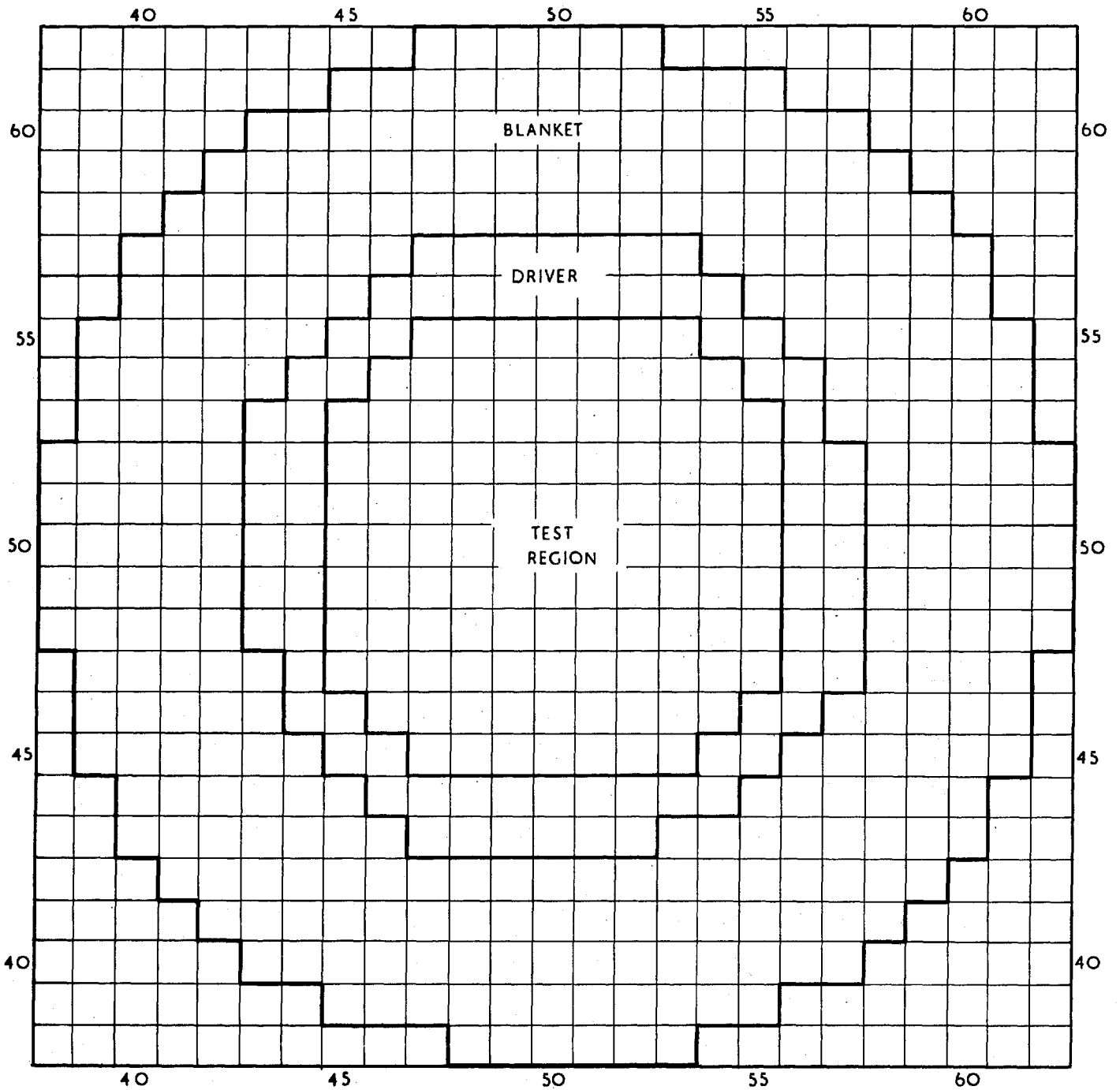
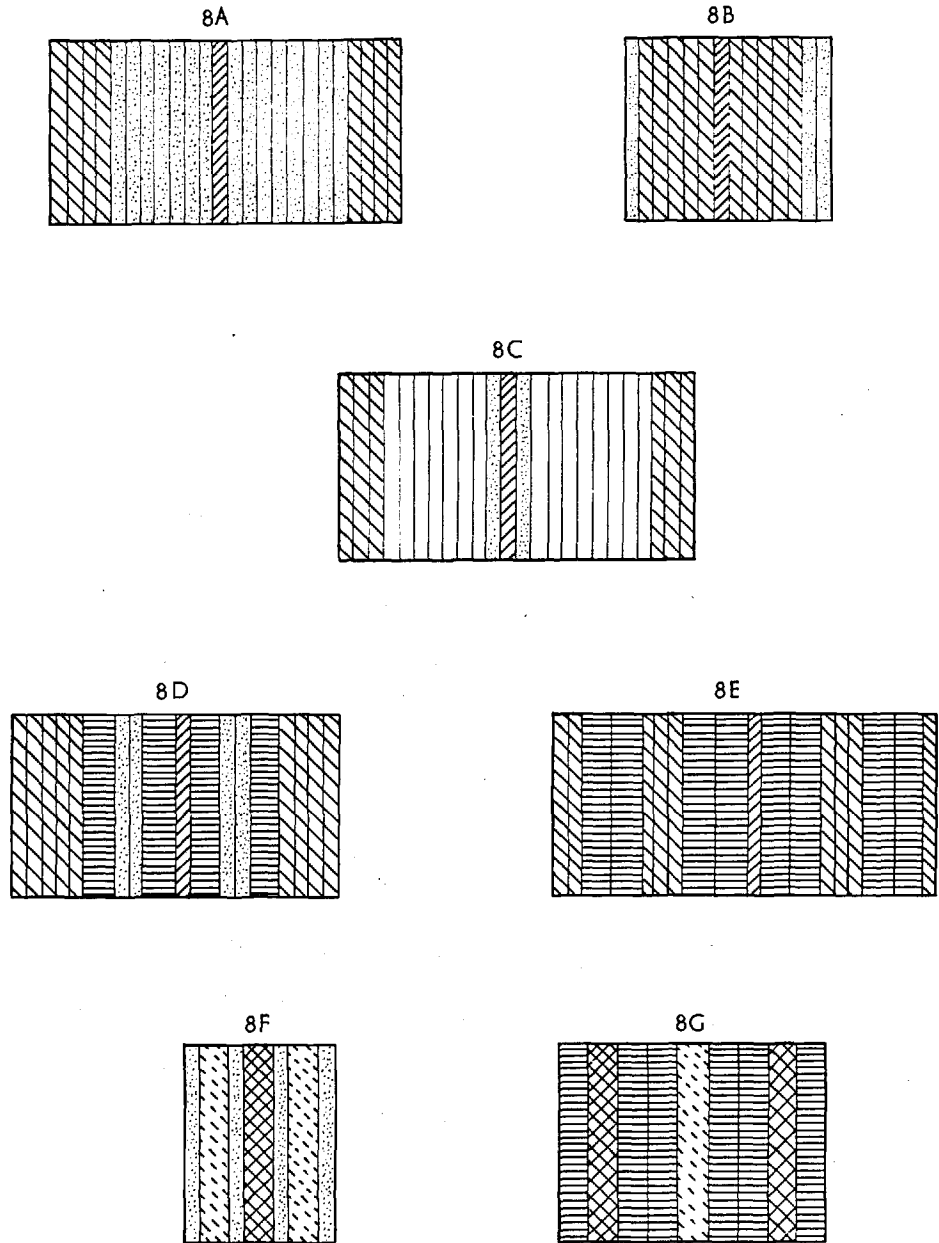



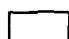
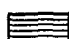

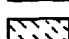

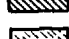


FIG.3. CORE PLAN OF THE ZEBRA CORE 8 ASSEMBLIES



KEY:

-  STAINLESS STEEL CANNED Pu, 3.2 mm. THICK
-  NATURAL U, 3.2 mm. THICK
-  GRAPHITE, 3.2 mm. THICK
-  STAINLESS STEEL, 3.2 mm THICK
-  STAINLESS STEEL CANNED Na, 6.3 mm. THICK
-  STAINLESS STEEL CANNED 25% PuO₂/UO₂, 6.3 mm THICK
-  STAINLESS STEEL CANNED UO₂, 6.3 mm THICK
-  93% U235, 1.6 mm THICK
-  37.5% U235, 3.2 mm. THICK

DRIVER CELL

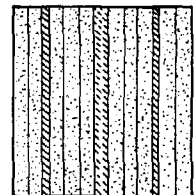


FIG. 4. LATTICE CELL STRUCTURES FOR THE CORE 8 TEST REGIONS

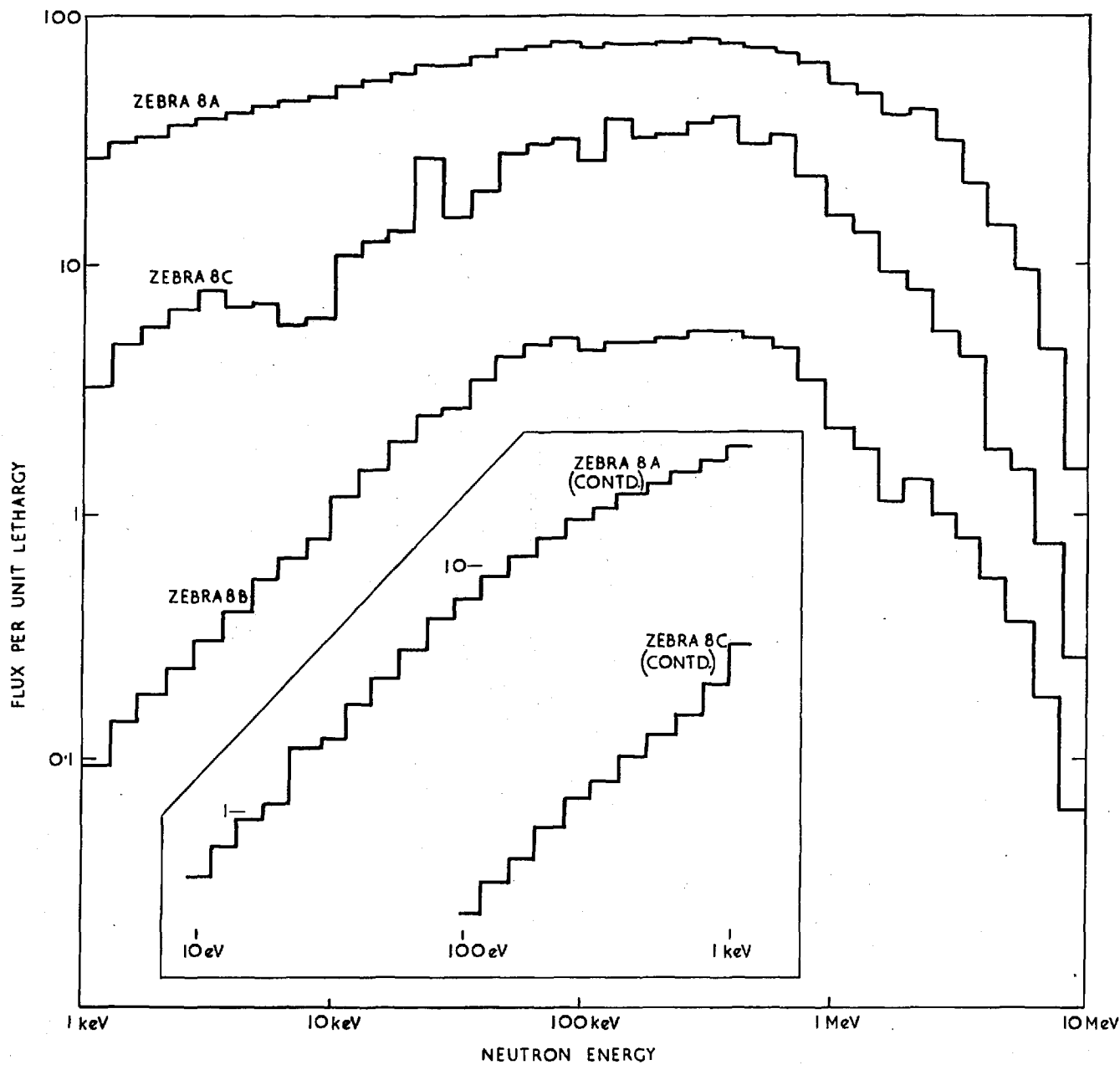


FIG. 5. MURAL-CALCULATED CELL-AVERAGED BROAD-GROUP SPECTRA FOR THE ZEBRA 8A, 8B AND 8C TEST REGIONS

igation to sodium-containing, oxide-fuelled lattices, and further, to provide a comparison of pin and plate heterogeneity effects. (The latter objective was realised in a second part of the experiment by replacing a central portion of the 8G test region by a pin-fuelled sodium calandria of similar composition.)

3.3 EARLIER ESTABLISHED REACTION RATE TECHNIQUES

This section summarises the techniques that were developed in earlier work - on ZEBRA and elsewhere - for the integral measurement of the important reaction rates in low-power reactor assemblies.

3.3.1 MEASUREMENT OF U-238 CAPTURE RATES

The initial conversion ratio, I.C.R., defined as the number of fissile atoms produced (i.e., Pu-239 from capture in U-238) per fissile atom destroyed (U-235 or Pu-239) in fresh fuel, has always been the most important parameter in determining the fuel economy of power reactors - whether thermal or fast (Ref. 16). For a simple uranium fuelled system, it may be written as

$$\text{I.C.R.} = \left(\frac{\sum_{a8} \sigma}{\sum_{a5} \sigma} \right)_M + \eta_5 \epsilon (1 - p) + \eta_5 \cdot \left(\frac{\sigma_{c8}}{\sigma_{f8}} \right)_E \cdot (\epsilon - 1) \dots \dots \dots (3.1)$$

where the two-group (Maxwellian and Epithermal) treatment and nomenclature of Grant have been used (Ref. 17). The earliest methods of determining the I.C.R. for thermal reactor systems involved the measurement of the so-called cadmium ratio of U-238 captures in the fuel (Ref. 18) from which the resonance escape probability, p , could be calculated. Apart from slight systematic errors due to spectrum perturbations by the cadmium, this method was satisfactory for highly thermalised systems in which resonance capture in U-238 was < 20% of the total captures. However, for the more common, undermoderated thermal lattices, the cadmium-ratio

approach proved rather inadequate due to the large uncertainties in the determination of the factor $(1 - p)$.

A number of new techniques were developed which eliminated the use of cadmium by determining the modified conversion ratio (M.C.R.), as proposed by Campbell and Carter (Ref. 19), viz.

$$\text{M.C.R.} = \left(\frac{\text{U-238 capture rate}}{\text{U-235 or Pu-239 fission rate}} \right)_{\text{lattice}} \dots\dots(3.2)$$

This gave

$$\text{I.C.R.} = \text{M.C.R.} \times \frac{(1 + \alpha)_{\text{thermal}}}{(1 + \alpha)_{\text{lattice}}} \dots\dots\dots(3.3)$$

where α is the capture-to-fission cross-section ratio for the reference nuclide, U-235 or Pu-239.

With both the numerator and the denominator in Equation (3.2) being directly measurable quantities in a relative sense, the R.C.R., or relative conversion ratio, approach was developed in which the measurements made in the lattice are related to equivalent ones made simultaneously in the well-thermalised reference spectrum of a graphite thermal column. Thus,

$$\text{R.C.R.} = \frac{(\text{U-238 capture})_{\text{lattice}}}{(\text{U-238 capture})_{\text{thermal}}} \div \frac{(\text{U-235 or Pu-239 fission})_{\text{lattice}}}{(\text{U-235 or Pu-239 fission})_{\text{thermal}}} \dots\dots\dots(3.4)$$

so that

$$\text{M.C.R.} = (\text{R.C.R.}) \times \left(\frac{\sigma_{c8}}{\sigma_f} \right) \dots\dots\dots(3.5)$$

where σ_{c8} is the known thermal cross-section for U-238 capture and σ_f is that for fission in the reference nuclide, U-235 or Pu-239.

For the determination of the relative U-238 capture rate, several techniques have been used by various earlier workers for

counting the radiations from either U-239 or Np-239, the β -, γ -decaying products of U-238 capture.

Singles NaI scintillation counting of the 75 keV γ -ray from U-239 decay has been applied by Davey (Ref. 20) to measurements in depleted uranium fuel. Though the technique is a simple one to use, it cannot be easily extended to measurements in slightly enriched fuels because the fission-product correction becomes too large. Another disadvantage is the relatively short U-239 half-life of 23.5 min.

By far the most popular and well-established technique for relative U-238 capture measurements in natural and slightly enriched uranium has been the NaI γ -X-ray coincidence counting of Np-239 which has a 2.35 day half-life. In the β -decay of Np-239 to Pu-239, a number of γ -rays are emitted of which the more prominent ones are the 106, 210, 228 and 278 keV γ 's. The latter three are highly converted, giving rise to mainly the Pu $K\alpha$ X-rays, of 99.5 and 104 keV, and these appear in coincidence with the 106 keV γ . By setting up a NaI coincidence system in which each channel is gated at (105 ± 10) keV, the effective coincidence counting efficiency is doubled and adequately high count-rates can be obtained from irradiated foils. This method was first applied to R.C.R. measurements in natural uranium fuel by Tunnicliffe, et al. (Ref. 21), and later developed at Winfrith by Brown and Skillings (Ref. 22) for measurements in slightly enriched ($\sim 1.2\%$ U-235) uranium fuels. More recently Besant, et al. (Ref. 23) have refined the technique further and have made experimental checks on a number of points, e.g. the determination of fission-product corrections for the observed coincidence rates, the measurement of the positional sensitivity of the NaI detectors, the appraisal of

self-absorption and foil-edge effects, and the assessment of experimental flux perturbations.

Another technique for Np-239 counting is the β - γ coincidence technique. For adequate fission-product discrimination in this case, however, delayed-coincidence methods have to be applied using the fact that the excited Pu-239 state following about half the Np-239 decays has the comparatively long half-life of 0.19 μ sec. In view of the resulting necessity for a fast ($\sim 10^{-8}$ sec.) coincidence system and other specialised electronic equipment, this technique has found little practical application.

In a second category of techniques for relative U-238 capture measurements, are those which rely on the chemical separation of Np-239, or less commonly U-239, from the irradiated samples to provide adequate discrimination against fission-product backgrounds. The most promising of these has been the one developed by Barnett, et al. (Ref. 24), which is based on the use of Np-237 as an α -tracer for determining the efficiency of the Np-239 extraction process in any given case. Successful comparisons between the physical and chemical techniques have been reported in Ref. 23 for measurements in natural and up to about 2% enriched uranium fuels.

3.3.2 FISSION RATE MEASUREMENTS

The determination of the lattice-to-thermal fission rate ratio is relatively straightforward and essentially involves integral fission-product γ counting of fuel-enrichment foils irradiated simultaneously in the reactor and in the thermal column. A threshold of 1.28 MeV, set using a Na-22 reference source, is usually employed. This setting adequately eliminates any radiations from the U-238 capture products and further, as it lies on a

relatively flat portion of the integral fission-product γ spectrum, the effects of electronic gain instabilities are minimal. The detailed procedures adopted by various workers are outlined in the earlier-mentioned references on R.C.R. measurements. The various corrections that have to be applied to the observed fission-product γ count-rate ratio are also described, e.g. effects due to dead-time losses, pulse pile-up, natural-activity backgrounds, feed-through from other irradiated foils, experimental flux perturbations, fission-product decay, fast fission in U-238 and - for Pu foils - fission in Pu-240 and Pu-241.

An implicit assumption in the method summarised above for determining the lattice-to-thermal fission ratio is that the relation, between the fission-product γ count-rate (at a given time, t , after irradiation) and the true fission rate, is the same in the reactor as it is in the thermal column. For a given nuclide, this is generally valid in thermal reactor lattices. In fast assemblies such as ZEBRA, however, the variation in fission-product yields between the lattice spectrum and the thermal-column spectrum is usually serious enough to necessitate a calibration experiment in which the fission-product γ count-rate ratio is related explicitly to the true fission ratio. The procedure has been described by George (Ref. 25) and involves the use of a reference fission chamber, the lattice-to-thermal count-rate ratio of which is related to the γ count-rate ratio obtained from foils in dummy chambers.

This calibration procedure is, in a sense, similar to the general one used - in both thermal and fast systems - to determine lattice ratios of the true fission rates for different pairs of isotopes. This general method involves the determination of the so-called $P(t)$ factor, which, for two isotopes a and b , is given

by

$$P(t) = \frac{\left[\frac{F_a}{F_b} \right]_{\text{true}}}{\left[\frac{F_a^L(t)}{F_b^L(t)} \right]_{\gamma}} \dots\dots\dots(3.6)$$

where the numerator represents the true lattice fission rate ratio for the two isotopes, and the denominator is the lattice fission-product γ count-rate ratio at time t after irradiation. Techniques for determining $P(t)$ and relative lattice fission rates have been outlined in detail by Brown and Skillings (Ref. 26).

3.3.3 APPLICATION OF TECHNIQUES IN ZEBRA

A brief summary of the experimental techniques used in the early ZEBRA Core 8 assemblies has been presented by Sanders, et al. (Ref. 13). In applying the earlier established reaction rate techniques to these "bench-mark" fast reactor assemblies, the most important precaution has been identified as the need for minimizing flux and spectral perturbations by the measuring devices themselves. As far as possible, all reaction rate measurements are made using foils embedded in the respective plates as shown in Fig. 6. (The aluminium guard foils shown are used for the fission rate measurements only.)

For U-238 capture rate measurements, the standard thermal-column comparison (R.C.R.) method has been applied using the γ -X-ray NaI coincidence technique for Np-239 counting. Natural uranium foils, 6.3 x 3.2 x .08 mm., are located in natural uranium plates for the lattice irradiation, while depleted uranium foils of similar dimensions (and hence having similar γ -X-ray self-absorption properties) are embedded in a graphite rotator in the thermal column of the source reactor NESTOR (Ref. 27). The fission-

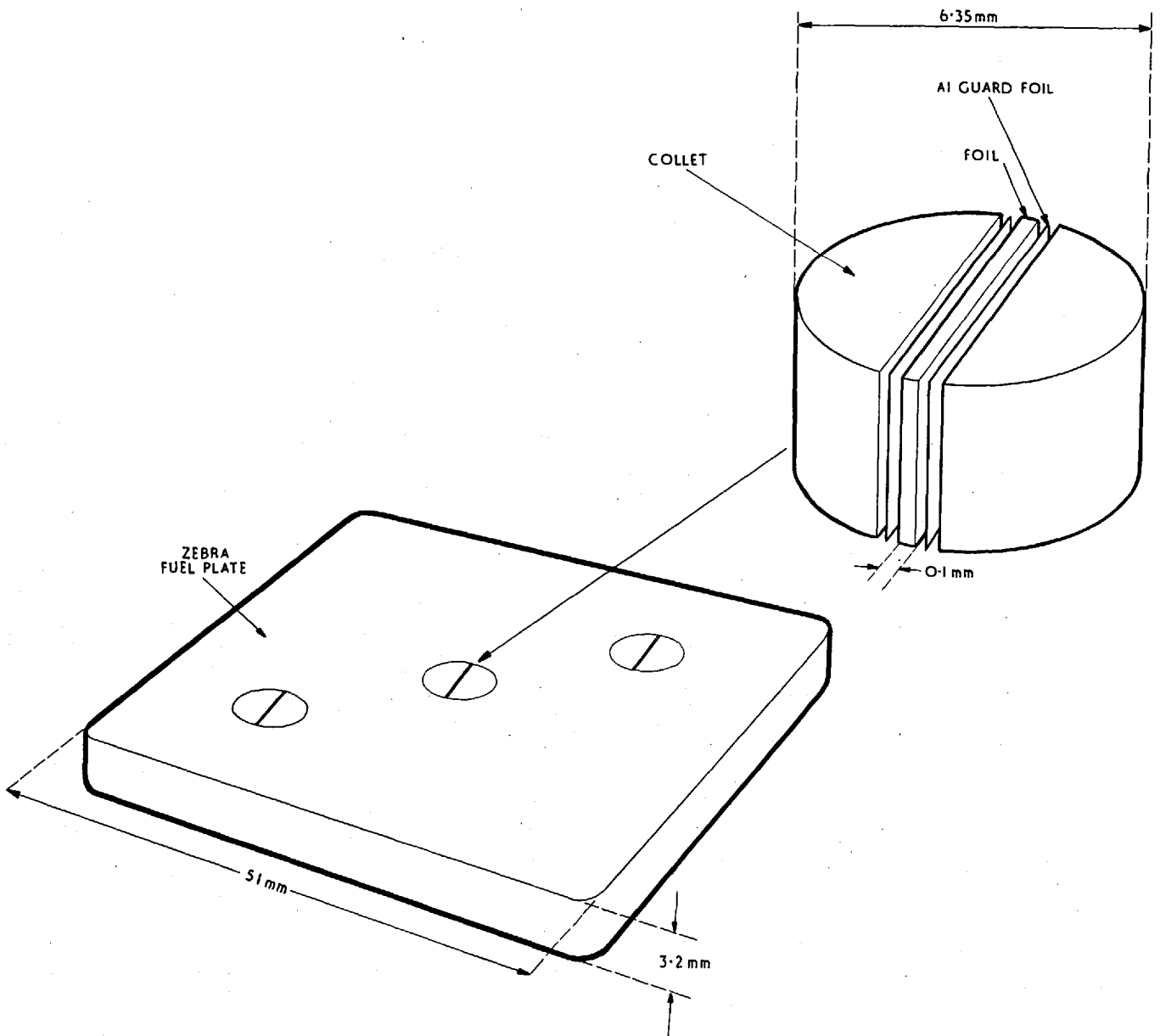


FIG.6. LOADING OF FOILS FOR REACTION RATE MEASUREMENTS IN ZEBRA PLATES

product corrections to the observed coincidences are negligibly small ($< 0.2\%$), because of the high capture-to-fission ratio in ZEBRA and the high depletion of the thermal-column foils.

The reference fission rate used in the measurements is that of Pu-239 as it is the most predominant one. The lattice-to-thermal Pu-239 fission ratio is determined using activation foils embedded in graphite (alongside the U-238 capture foils in the thermal column) and in fuel plates in ZEBRA. As already indicated in Section 3.3.2., a subsidiary calibration experiment, using a reference fission chamber, has to be made to obtain the relation between the relative fission-product γ -activity and the true fission ratio.

The standard techniques for measuring lattice fission rate ratios for different isotopes in ZEBRA are very similar to the ones employed in thermal reactor lattices (Section 3.3.2.). Fission product γ -activity ratios for the different fissile isotopes are determined by irradiating nickel-coated foils in fuel plates, each foil containing a particular isotope to a high degree of purity. These γ -activity ratios are then related to the true fission ratios via the $P(t)$ factors, determined using calibrated fission chambers and dummy chambers containing foils. A recent development has been the application of solid state track recorder techniques for fission rate ratio measurements in the Core 8 assemblies (Ref. 28). The various advantages of this method have not yet, however, been fully exploited.

CHAPTER 4

ABSOLUTE MEASUREMENTS OF U-238 CAPTURE AND PU-239 FISSION RATES

As stated earlier, meaningful comparisons between theory and experiment can only be achieved when the possible presence of any significant systematic errors in the experimental measurements can be safely disregarded. It is important, therefore, to establish the truth of this assumption for a particular measurement by using, if possible, a completely independent technique to determine the same parameter.

For integral reaction rate measurements in fast reactor assemblies, this need has been particularly strong as regards the determination of the ratio of the U-238 capture rate relative to the Pu-239 fission rate - $(C8/F9)$ - a parameter for which, as explained earlier, the highest accuracy is desirable. All recently-quoted experimental values for $(C8/F9)$, or $(C8/F5)$, ratios in reactor lattices have been determined by comparing the lattice ratio with that in a thermal column where the cross-sections for the individual reactions are known to an accuracy of $\pm 1\%$ (Section 3.3). This technique, apart from the inherent error on the thermal cross-section values used, suffers from a few other drawbacks. For example, flux perturbation by the foils and fission chambers used in the thermal-column measurements is significant and corrections for this have to be determined and applied. Secondly, for fast reactor experiments in particular, the two neutron spectra involved in the comparison (i.e., in the lattice and in the thermal column) are usually sufficiently different to necessitate certain subsidiary calibrations (e.g., that for taking into account the effect of the variation in fission-product yields on the fission-product γ counting). Finally, the fact that each reaction rate ratio determination entails two sets of irradiations, using in general two different reactors, results in error due to reactor power intercalibrations and other necessary

correlations.

In the present work, techniques for the absolute measurement of U-238 capture and Pu-239 fission rates in the reactor assembly itself have been developed for ZEBRA, and this has enabled direct evaluation of the reaction rate ratio, or M.C.R. - thereby obviating the need for any comparisons with thermal-column irradiations.

4.1 ABSOLUTE U-238 CAPTURE MEASUREMENT

The present method for the absolute determination of U-238 capture rates is based on the fact that both Am-243 and U-239 decay via Np-239 into Pu-239, as shown in Fig. 7 (Ref. 29). The use of a calibrated Am-243 source, for standardising the detector system used in a particular U-238 capture measurement, was first suggested by Cripps and Weale (Ref. 30), and a technique was later developed for measurements in irradiated foils by Seufert and Stegemann (Ref. 31). The method of Seufert and Stegemann, however, suffers from the following possible sources of systematic error:

- (i) The γ -X-ray self-absorption correction for the uranium foils used was greater than 35% causing extrapolation to zero thickness to be inaccurate.
- (ii) The determination of the amount of uranium in the thin deposits (used for obtaining the self-absorption, vs. thickness, curve) was limited in accuracy by the weighings that had to be made.
- (iii) The source geometry, in the γ -X-ray coincidence counting of the irradiated foils and the Am-243 samples, was not consistent since the uranium foils were 100-500 μ thick while the Am-243 sources were thin, evaporated deposits on glass backings.
- (iv) There was a finite uncertainty in the geometry factor and efficiency of the low-geometry α -counter used for the absolute calibration of

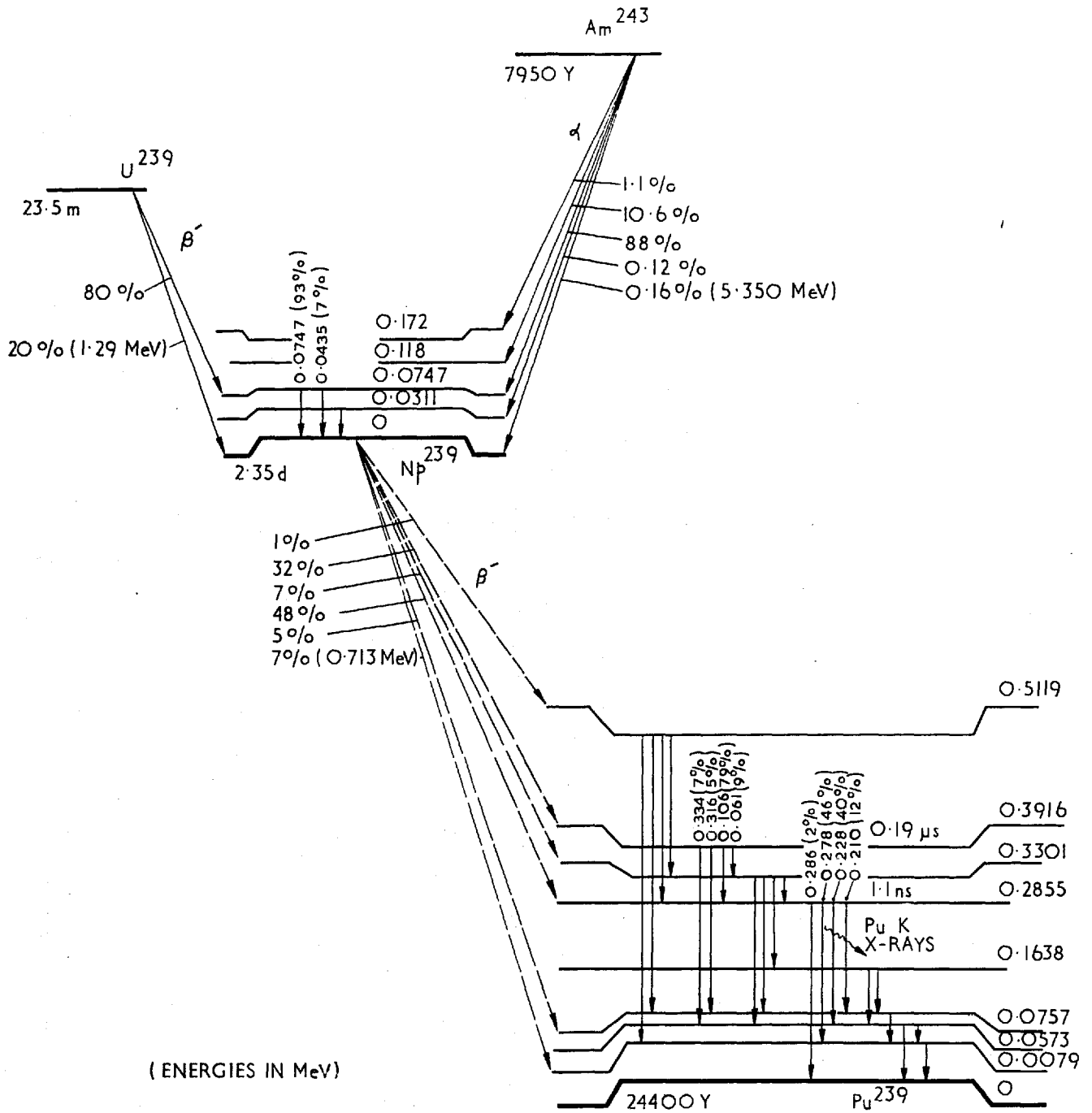


FIG. 7. DECAY SCHEMES FOR AM-243
U-239 AND Np-239

the Am-243 sources.

(v) α -emitting impurities in the Am-243 samples used necessitated large corrections to the measured α count-rates.

The present technique has been aimed at eliminating some of the above mentioned possible sources of error and at reducing the effect of the others to negligible proportions. By using thin uranium deposits and Am-243 sources which were prepared on identical backings and in similar electrolytic cells, consistency in the source geometry was maintained. γ -X-ray self-absorption was only $\sim 0.3\%$ for the uranium deposits and $< 10^{-4}\%$ for the Am-243 sources, so that the error in the applied corrections was negligible. By α -assaying the thin uranium deposits in the same low geometry α -counter as the Am-243 sources, the requirement of explicitly knowing the absolute α -counter efficiency, as well as the need for weighing the uranium deposits, were both eliminated. Lastly, very pure Am-243 was used for preparing the sources and it was estimated that the impurity contribution to the α count-rate was less than 0.1% (Table 2).

4.1.1. THEORETICAL DESCRIPTION OF THE PRESENT TECHNIQUE

The absolute U-238 capture rate, for a uranium deposit irradiated in a reactor lattice, is directly related to the Np-239 activity induced in it and may be written as:

$$\text{Capture Rate/U-238 atom} = [k(t).N_0]^{-1}. \text{ (Induced Np-239 Activity)}$$

.....(4.1)

where N_0 is the number of U-238 atoms in the deposit and $k(t)$ is a proportionality constant. It may easily be shown that $k(t)$ is given by

$$k(t) = \left[\frac{\lambda_{u9}}{\lambda_{u9} - \lambda_{n9}} \cdot \left\{ 1 - \exp(-\lambda_{n9} t_i) \right\} \cdot \exp(-\lambda_{n9} t) \right] - \left[\frac{\lambda_{n9}}{\lambda_{u9} - \lambda_{n9}} \cdot \left\{ 1 - \exp(-\lambda_{u9} t_i) \right\} \cdot \exp(-\lambda_{u9} t) \right] \dots(4.2)$$

λ_{u9} and λ_{n9} being the known U-239 and Np-239 decay constants respectively, t_i being the length of the irradiation, and t the time after the end of the irradiation.

If the earlier described γ -X-ray coincidence technique is used for the Np-239 counting of the irradiated deposit, and if, at time t , $C_u(t)$ is its measured coincidence count-rate (corrected for random and fission-product coincidences, etc.), then Equation (4.1) becomes:

$$\text{Capture Rate/U-238 atom} = \frac{1}{k(t)} \cdot \frac{1}{N_8} \cdot \frac{C_u(t)}{(1-a)\eta} \dots\dots(4.3)$$

where a is the γ -X-ray self-attenuation correction for the thin deposit and η is a calibration factor embodying (a) the various nuclear parameters determining the probability that a Np-239 decay will result in an event capable of yielding a true coincidence in the gated energy regions, and (b) the coincidence geometry, detector efficiencies and various other features characterising the experimental arrangement.

Now, η can be derived using the fact that Am-243 is the long-lived parent (half-life, 7950 years) of Np-239, its short-lived daughter (half-life, 2.35 days). Due to secular equilibrium between the two, the Np-239 activity, A_n , and the Am-243 activity, A_a , in a given Am-243 source are related simply by:

$$A_n = A_a \dots\dots\dots(4.4)$$

If this source is prepared such that its shape and backing are the same as those of the uranium deposit, and if the Np-239 in the source is monitored in exactly the same coincidence arrangement as the irradiated uranium deposit, then it can be seen that the calibration factor η will be the same for the source and the deposit. If C_a is the measured coincidence rate (corrected for random coincidences) from the source, then:

$$C_a = \eta \cdot A_n \cdot (1 - a^1) \dots\dots\dots(4.5)$$

or from Equation (4.4),

$$C_a = \eta \cdot A_a \cdot (1 - a^1) \dots\dots\dots(4.6)$$

a^1 being the γ -X-ray self-absorption correction for the source.

Substituting for η from Equation (4.6) into (4.3), one obtains

$$\text{Capture Rate/U-238 atom} = \frac{1}{k(t)} \cdot \frac{A_a}{N_8} \cdot \frac{C_u(t)}{C_a} \cdot \frac{(1 - a^1)}{(1 - a)} \dots(4.7)$$

The Am-243 activity of the source can be obtained from α -assay in a low-geometry α -counter. If the absolute efficiency of the counter, inclusive of the geometry factor, is ω and if B_a is the measured α count-rate, then A_a is given by

$$A_a = \frac{B_a}{\omega} \dots\dots\dots(4.8)$$

Equation (4.7) now becomes:

$$\text{Capture Rate/U-238 atom} = \frac{1}{k(t)} \cdot \frac{B_a}{\omega} \cdot \frac{1}{N_8} \cdot \frac{C_u(t)}{C_a} \cdot \frac{(1 - a^1)}{(1 - a)} \dots\dots(4.9)$$

For a natural uranium deposit, N_8 is given by:

$$N_8 = 0.9928 N_u \dots\dots\dots(4.10)$$

where N_u is the number of uranium atoms in the deposit. Using λ_u to denote the effective α -decay constant of natural uranium - known to

an accuracy of $\pm 0.2\%$ (Ref. 32) - the α -activity A_u of the natural uranium deposit is given by:

$$A_u = \lambda_u \cdot N_u \dots\dots\dots(4.11)$$

If the natural uranium deposit is α -assayed in exactly the same low-geometry α -counter as the Am-243 source, A_u is obtained as:

$$A_u = \frac{B_u}{\omega} \dots\dots\dots(4.12)$$

where B_u is the measured α count-rate from the deposit and ω is the factor used previously, since the counting system and geometrical arrangement have been preserved.

From Equations (4.10), (4.11) and (4.12), one obtains:

$$N_8 = \frac{0.9928}{\lambda_u} \cdot \frac{B_u}{\omega} \dots\dots\dots(4.13)$$

Finally, substituting for N_8 in (4.9), the absolute U-238 capture rate may be written as:

$$\begin{aligned} \text{Capture Rate/U-238 atom} &= \frac{1}{k(t)} \cdot \frac{\lambda_u}{0.9928} \cdot \frac{B_a}{B_u} \cdot \frac{C_u(t)}{C_a} \cdot \frac{(1 - a^1)}{(1 - a)} \\ &= K(t) \cdot \frac{B_a}{B_u} \cdot \frac{C_u(t)}{C_a} \dots\dots\dots(4.14) \end{aligned}$$

$$\text{where } K(t) = \frac{\lambda_u}{0.9928 k(t)} \cdot \frac{(1 - a^1)}{(1 - a)}$$

K is a parameter known to an accuracy of better than $\pm 0.3\%$ (Table 3), and it therefore follows from Equation (4.14) that the U-238 capture rate is obtained absolutely from two simple relative measurements made with α and γ -X-ray counting systems. Neither absolute calibration of the Am-243 source, nor weighing of the thin uranium deposits, is necessary - the overall accuracy of the result

being limited essentially by counting statistics.

4.1.2 EXPERIMENTAL PROCEDURE

Natural uranium deposits ($0.5 - 1.0 \text{ mgm/cm}^2$ over an area of $\sim 3\frac{1}{2}$ sq. cm.) and thin Am-243 sources (over exactly the same area and about $0.02 \mu\text{c.}$ in strength) were prepared on 27.0 mm. diameter, 0.10 mm. thick aluminium discs. The preparations were carried out by the Chemistry Group at Winfrith using an electrolytic (molecular plating) process (Refs. 33 and 34).

The purity of the prepared samples was confirmed both by mass spectroscopy and α -spectrometry. The Am-243, supplied by A.E.R.E., Harwell, as a nitrate solution, had been originally obtained by ion-exchange extraction from a plutonium "napkin ring" which had been irradiated in the Materials Testing Reactor at Arco, Idaho, for approximately five years, receiving an estimated integrated neutron dose of at least $2.5 \times 10^{22} \text{ n/cm}^2$ during this time (Ref. 35). The results of the analyses made for these Am-243 samples are summarised in Table 2. As for the natural uranium deposits, the mass spectrometric analysis which was carried out established that the relative abundance of the uranium isotopes was correct, viz. 0.0057% U-234, 0.72% U-235 and 99.28% U-238 (Ref. 29).

TABLE 2. RESULTS OF ANALYSES OF THE AM-243 USED

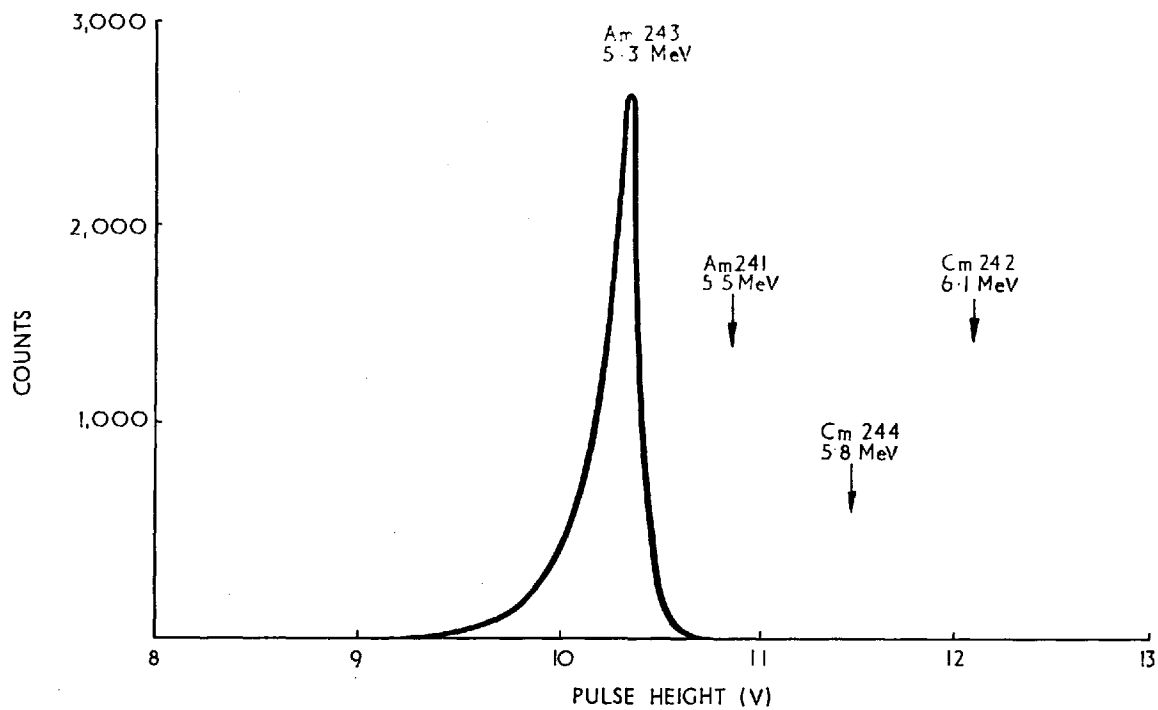
Isotope	Mass Spec. Results (%)	α -Activity Results (%)
Am-243	99.995 ± 0.002	99.94 ± 0.05
Am-241	0.005 ± 0.002	0.04 ± 0.02
Cm-242/244	-	0.02 ± 0.01

Typical α -spectra obtained for the deposits, using a low-geometry

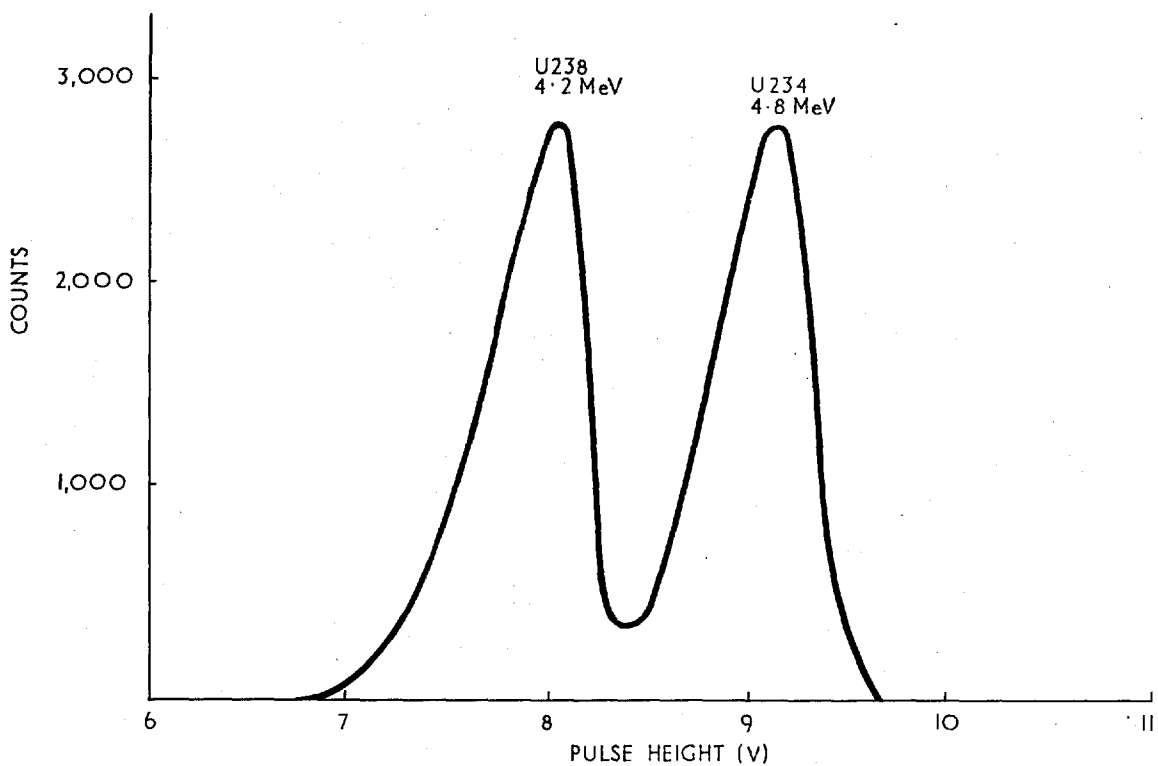
α -counter and a biased multi-channel analyser, are shown in Fig. 8. These spectra confirmed the fact that, though the energy degradation of the α 's in the deposits themselves impaired the observed energy resolution significantly, the effect was small enough to enable undistorted α count-rates to be obtained by simple integral counting above a sufficiently low threshold.

The low-geometry α -counter itself was of standard design (Ref. 36), and geometry factors of between 1 : 150 and 1 : 250 were used. Although this counter was later employed in certain absolute calibrations, where more accurately known geometry factors were used, a discussion of these at this stage would be irrelevant since, as shown in Section 4.1.1, only relative α -counting is necessary in the present technique for absolute U-238 capture measurements. The only important requirement was that the geometries used be repeatable, and this was confirmed experimentally (Section 4.1.3). The detector used in the counter was an E.M.I. Type SB2 surface-barrier silicon diode, with a nominal depletion depth of 0.2 mm. and an operating bias of 25 v. During operation, the counter was evacuated using an Edwards rotary pump and the pressure was maintained at ~ 0.02 torr. The background count-rate for the α -counting was typically 0.2% of the uranium deposit count-rates and 0.03% of the Am-243 deposit counts, and hence negligible error resulted from the background corrections applied. Statistical accuracies of better than $\pm 0.3\%$, in this low-geometry α -counting, were achieved by counting each uranium deposit for 4-5 days and each Am-243 source for about one day.

For loading the uranium deposits into the reactor, special natural uranium plates were made (Fig. 9). Each loading plate consisted of two halves, both of which were 51 mm. square and 1.6 mm.



(a) Am 243 (SHOWING POSITIONS OF POSSIBLE 'IMPURITY PEAKS')



(b) NATURAL URANIUM

FIG. 8 α -SPECTRA OF THE Am-243 AND NATURAL URANIUM DEPOSITS

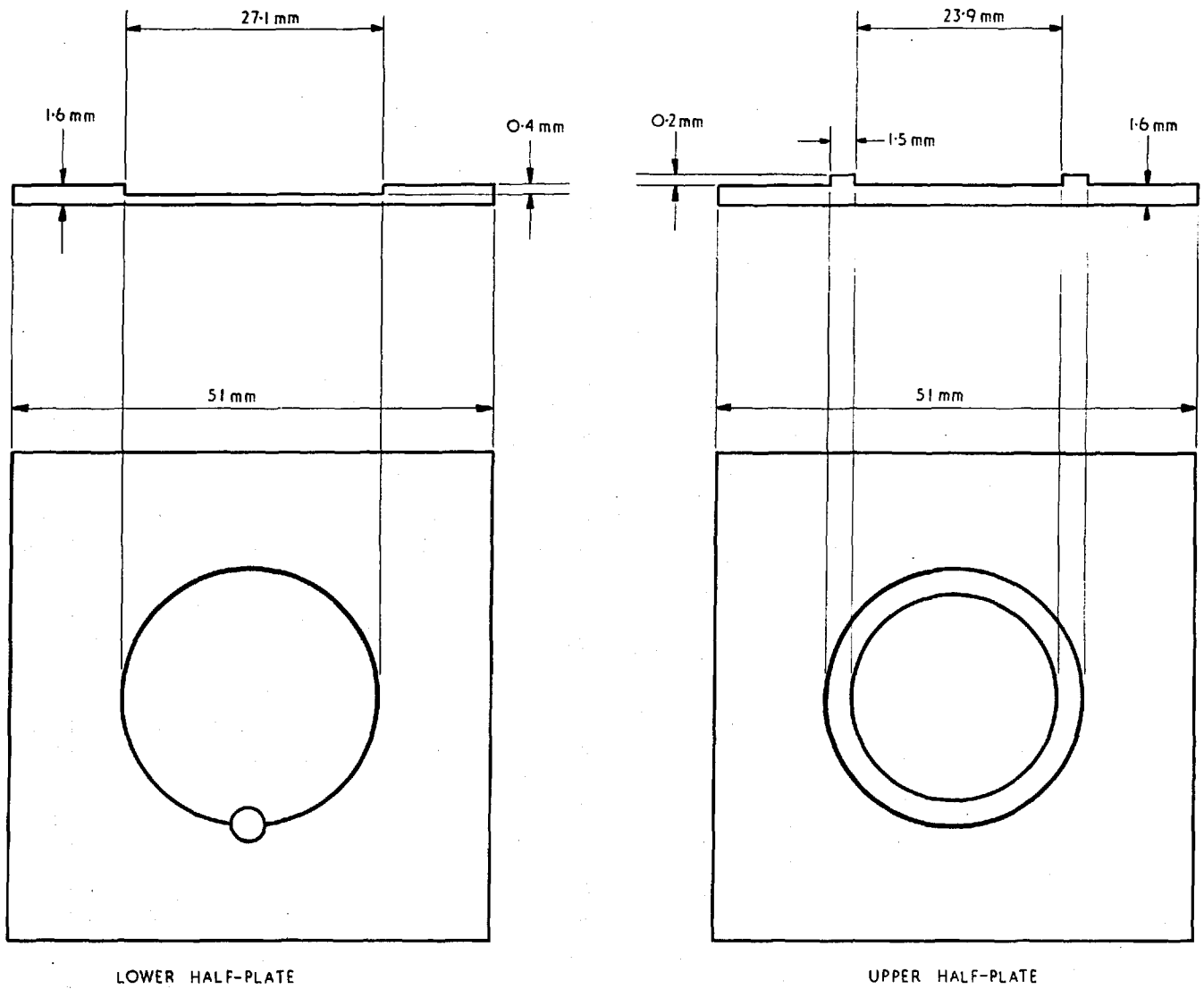
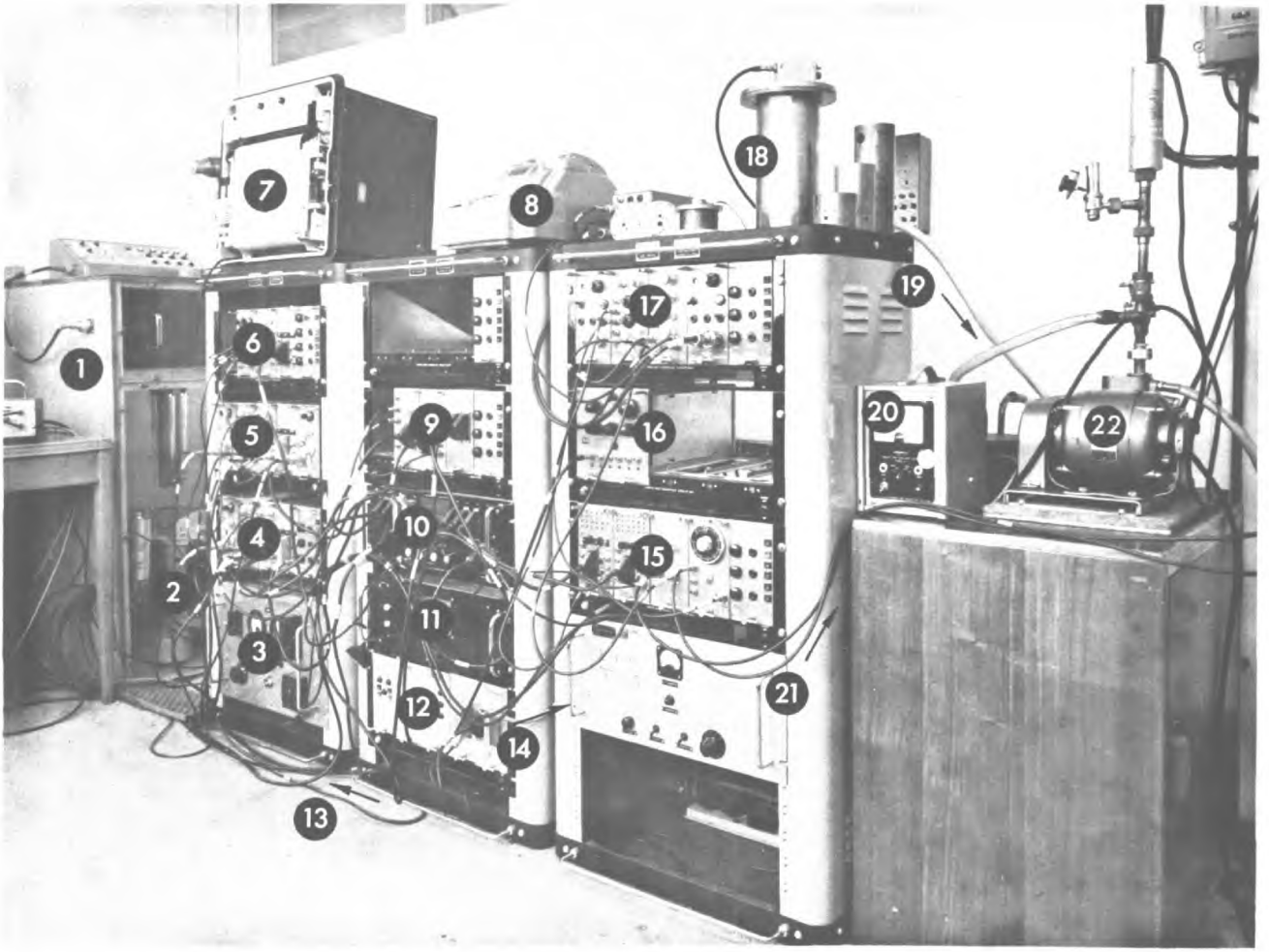


FIG. 9. THE SPECIAL LOADING PLATE FOR THE URANIUM DEPOSITS

thick. One half-plate had a recess for carrying the deposit. The other had a protruding ring, also of uranium, which locked into this cavity and held the deposit in position by pressing against the bare aluminium on the periphery. The deposited surface itself did not touch either half-plate, thereby ensuring that none of it was accidentally scraped off. The protruding ring of the upper half-plate and the staggered positioning of the deposit itself both served to shield it from any neutron streaming effects that might occur along any gap between the two halves. With the deposit loaded and the two half-plates fitted together, the cavity in the middle was less than 0.3 mm. deep and this was shown (from considerations of the U-238 capture fine structure in the various Core 8 cells) to have a negligible perturbing effect. Externally, the loading plate was identical to an ordinary 51 mm. x 51 mm. x 3.2 mm. natural uranium metal ZEBRA plate (Section 3.1) and could therefore be used for measurements in any ZEBRA cell with natural uranium metal in it.

After a 2-4 hour lattice irradiation in ZEBRA (at a nominal maximum power of ~ 100 w.), the natural uranium deposits were counted for the induced Np-239 activity over a period of about $2\frac{1}{2}$ half-lives, between 1200 and 10,000 minutes after irradiation. A general view of the apparatus used in the γ -X-ray coincidence counting of the deposits is shown in Plate 1. The detectors were 2" x 2" NaI(Tl) counters mounted in lead-castles above and below the horizontal turn-table of a Type-1718A automatic foil changer (a.f.c). This was placed inside a temperature-controlled enclosure to minimise electronic gain-shifts. Most of the electronic units used were from the Harwell-2000 series (Ref. 37), each detector channel essentially consisting of a 0045-type pre-amplifier, a 2151-amplifier, and a 2170-single-channel analyser. A Laben multi-



- KEY :
- | | | |
|----------------------------|--------------------------|---|
| 1. TEMP. CONTROL ENCLOSURE | 8. ADDO-X PRINTER | 15. AUXILIARY UNITS FOR LABEN |
| 2. NaI (Tl) a.f.c. | 9. TIMING CONTROL UNITS | 16. PULSE GENERATOR |
| 3. VOLTAGE STABILIZER | 10. a.f.c. CONTROL UNIT | 17. α -COUNTER CHANNEL |
| 4. CHANNEL A | 11. SERIALIZER | 18. α -COUNTER COMPONENTS |
| 5. CHANNEL B | 12. OUTPUT CONTROL UNITS | 19. TO VACUUM PUMP 22 |
| 6. COINCIDENCE UNITS | 13. TO I.B.M. CARD-PUNCH | 20. VACUUM GAUGE |
| 7. SPECTRUM PLOTTER | 14. TO PRINTER | 21. TO LABEN-512
MULTICHANNEL ANALYSER |

PLATE I. GENERAL VIEW OF THE α AND γ -X-RAY COUNTING ELECTRONICS

channel analyser was used for setting up each channel on the 105 keV Np-239 region, with a channel width of $\pm 10\%$; and a coincidence resolving time of 0.2 μ sec. was employed, using a 2071-coincidence-unit in conjunction with a 2185-pulse-shaper and delay-unit. The counting cycle was controlled by a.f.c. control and serializer units and, at the end of each counting interval, the accumulated single-channel and coincidence counts, as well as the time in hundredths of a minute, were fed from 2130-scalers into an Addo-X printer and an I.B.M. card-punch.

To ensure consistency in the experimental conditions, the Am-243 source was counted along with the deposits, the a.f.c. turntable normally having a total of four counting tray positions. As a result, the statistically weighted mean coincidence-rate obtained from the Am-243 source accurately characterised the state of the electronics, geometry, settings, etc., during the common counting period of the source and the irradiated deposits.

A computer programme, CAPABS, was written in the EGTRAN language to analyse the measurements on the KDF9 computer at Winfrith. Briefly, the input data consisted of the α count-rate ratio (B_a/B_u) and its statistical accuracy, a few experimental details (e.g. length of the irradiation, duration of each counting interval, coincidence resolving time, etc.), various slight corrections to be applied (e.g. γ -X-ray self-attenuation, fission-product, natural-activity and other coincidence backgrounds, etc.), and the counting data itself obtained in card form from the I.B.M auto-punch. Equation (4.14) was effectively solved for each point and a statistically weighted mean value of the absolute U-238 capture rate was obtained. A detailed error analysis (Ref. 38) was also carried out and a net r.m.s. percentage error calculated.

4.1.3. INVESTIGATION OF POSSIBLE SYSTEMATIC ERRORS

The 0.10 mm. thick aluminium backings were found to be quite adequate in maintaining the rigidity of the deposits, this being an essential aspect for both the α and γ -X-ray counting. Use of a larger backing thickness or of other material such as steel, however, was found to have two adverse effects. Firstly, the distortion of the neutron spectrum inside the deposit-loaded uranium plate, due to neutron scattering in the backing, became significantly high; and secondly, neutron-activation of the backing itself necessitated a larger correction to the observed γ -X-ray coincidence rate. Both these effects were borne out by absolute U-238 capture measurements that were made in ZEBRA Cores 8A and 8B, using natural uranium deposits and Am-243 sources prepared on 0.50 mm. stainless steel backings (Appendix A.2).

From the investigation of the neutron-scattering effect in the backing, discussed in detail in Appendix A2.1, it was established that the resultant increase in the U-238 capture rate due to the 0.10 mm. aluminium backing was very small indeed. Estimates of $(0.4 \pm 0.2)\%$, $(0.02 \pm 0.01)\%$ and $(0.10 \pm 0.05)\%$ were made for this effect in Cores 8A, 8B and 8C, respectively. It may be mentioned that Core 8A, though it proved very suitable for studying the neutron-scattering effect in the backing, was not a typical fast reactor assembly in that the neutron spectrum in it was very soft (Fig. 5) and heterogeneity effects rather large. As can be seen from the above-quoted estimates, the backing effect is much smaller in other, more typical ZEBRA cores such as 8B and 8C, and it can therefore be safely said that, in general, the error resulting from this backing-effect correction is insignificant.

The other important advantage of using aluminium as the backing

material for the uranium deposits was that the neutron-induced activity in it was very small. An investigation of the effects of steel and aluminium backing activation was carried out in ZEBRA Cores 8B and 8C, and the details are given in Appendix A2.2. In brief, it was found that the slight contribution of the activity induced in the backing, to the observed coincidence rate from an irradiated deposit, was best taken into account by counting, along with the deposit, a simultaneously irradiated bare backing. It was observed that, at about 50 hours after irradiation, the backing contribution to the coincidence rate was typically $<0.5\%$ for the aluminium backing, while it was as much as 4% for the 0.50 mm. steel. With an easily achieved accuracy of about $\pm 10\%$ for the applied correction, it follows that the resultant error for the aluminium is negligible while for the steel it is not.

A less serious disadvantage of using steel was the necessity of applying, to the coincidence count-rate, a correction for any finite variation in backing thickness for the different deposits and sources. This was because of the large γ -X-ray absorption effect ($\sim 12\%$) in the 0.50 mm. steel. Absorption in 0.10 mm. aluminium, on the other hand, is negligible by comparison and this, besides improving the counting statistics, renders differential backing-absorption effects completely insignificant.

An investigation of the other possible systematic errors in the measurement was carried out and this, as discussed below, satisfactorily showed that none of them had any significant effect on the accuracy of the results. The γ -X-ray self-absorption effects in the deposits themselves, for example, were calculated on the basis of theoretical values of the uranium cross-section for 100 keV

γ -X-rays (Ref. 39), and estimates of between 0.2% and 0.6% were obtained for the effects on the coincidence counting. Assuming an accuracy of $\pm 20\%$ in these corrections, the resultant error is clearly negligible. (Attempts to determine the self-absorption effects experimentally, by irradiating natural uranium deposits of different thicknesses under similar conditions and comparing their observed activities, confirmed that the effects being investigated were of the same order as the obtained statistical accuracies, viz. $\sim 0.5\%$.)

Two other small corrections had to be applied to the observed coincidence rates. Firstly, the fission-product coincidence correction for the irradiated natural uranium deposits was estimated as being $(0.2 \pm 0.1)\%$ for most ZEBRA cores - this value being based on previous work carried out at Winfrith with NaI coincidence systems (Ref. 22). The second effect considered was the possible loss by recoil of Np-239 nuclei which are continuously being formed in the Am-243 sources. On the basis of experiments performed with various collectors placed very close to the sources, it was shown that these losses were normally no more than $(0.20 \pm 0.05)\%$, confirming that there was no need for sealing the Am-243 sources and that the error, due to the 0.05% uncertainty in the effect, was negligible.

Sources of error in the γ -X-ray counting, which have been investigated by earlier workers (Refs. 21-23), were shown to be unimportant in the present experimental set-up. Dead-time and pulse pile-up effects for example were unobservable with the low-activity deposits and sources that were counted. With the negligibly small γ -X-ray self-absorption and foil-edge effects, the effective counting geometry was exactly the same for both the irradiated deposits

and the Am-243 sources, the effects of finite radial variation of detector sensitivity being identical in the two cases.

For the determination of the α count-rate ratio, (B_a/B_u), the systematic accuracy was established by (a) using different geometries and different detectors for obtaining this ratio, and (b) counting the uranium deposits both before and after irradiation. In both cases, the repeatability of these measurements was verified by obtaining consistent results within statistical accuracies of better than $\pm 0.3\%$. Another small effect investigated in the α -counting was the possible contamination of the reverse sides of the backings of the various electrodeposits, and this was shown to be negligible in most cases.

Table 3 summarises the various systematic errors in the present technique for absolute U-238 capture measurements.

TABLE 3. SYSTEMATIC ACCURACY OF THE ABSOLUTE U-238 CAPTURE MEASUREMENT

Source of Error	Error (\pm)
1. Effective α -decay constant of natural uranium, λ_u	0.2%
2. Effect of uncertainties in U-239 and Np-239 decay constants on $k(t)$	0.1%
3. Self-absorption of γ -, X-rays	0.1%
4. Neutron-scattering effect in 0.10mm. aluminium backing	0.1%
5. Activation correction for 0.10mm. aluminium backing	0.05%
6. Fission-product correction for irradiated uranium deposit	0.1%
7. Recoil losses of Np-239 from Am-243 source	0.05%
8. Determination of α count-rate ratio	0.2%
9. Effect of possible impurities (Table 2)	0.05%
Total r.m.s. systematic error	< 0.4%

4.2 ABSOLUTE PU-239 FISSION MEASUREMENT

Fission measurements in ZEBRA cavities, using calibrated 2π fission-chambers of the type shown in Fig. 10, have been described by Stevenson and Broomfield (Ref. 40). Although these earlier-made chambers were quite adequate for relative measurements of fission ratios in the reactor, they were found to be unsuitable for the present absolute Pu-239 fission measurements because of the following serious corrections which had to be applied:

- (i) $\sim (2.5 \pm 0.8)\%$ dead-time correction in the reactor instrumentation count-rates for intercalibrating the different reactor powers used for the U-238 capture and Pu-239 fission measurements;
- (ii) $\sim (5.2 \pm 1.6)\%$ correction for fission-product self-absorption in the Pu-239 fission-chamber deposit; and
- (iii) $\sim (2.9 \pm 0.7)\%$ correction for the biased-off low-energy pulses produced in the fission chamber.

There was also finite uncertainty in the collection efficiency and geometry of the collector electrode in the fission chamber.

4.2.1 ELIMINATION OF THE GROSS SYSTEMATIC ERRORS

Two new fission chambers were made with plutonium electrodeposits of ~ 30 and $14 \mu\text{gm}/\text{cm}^2$, over diameter of 28 mm. and 18 mm. respectively, on 38 mm. diameter, 0.13 mm. thick platinum discs. These deposit masses were nearly two orders of magnitude less than those in the earlier ZEBRA chambers, and this enabled absolute fission measurements to be made at the same reactor power as used for the absolute U-238 capture measurement, viz. ~ 100 w. The instrumentation dead-time corrections now being approximately equal in the two cases, there was no resultant error due to (i).

The fission-product self-absorption correction in a deposit of

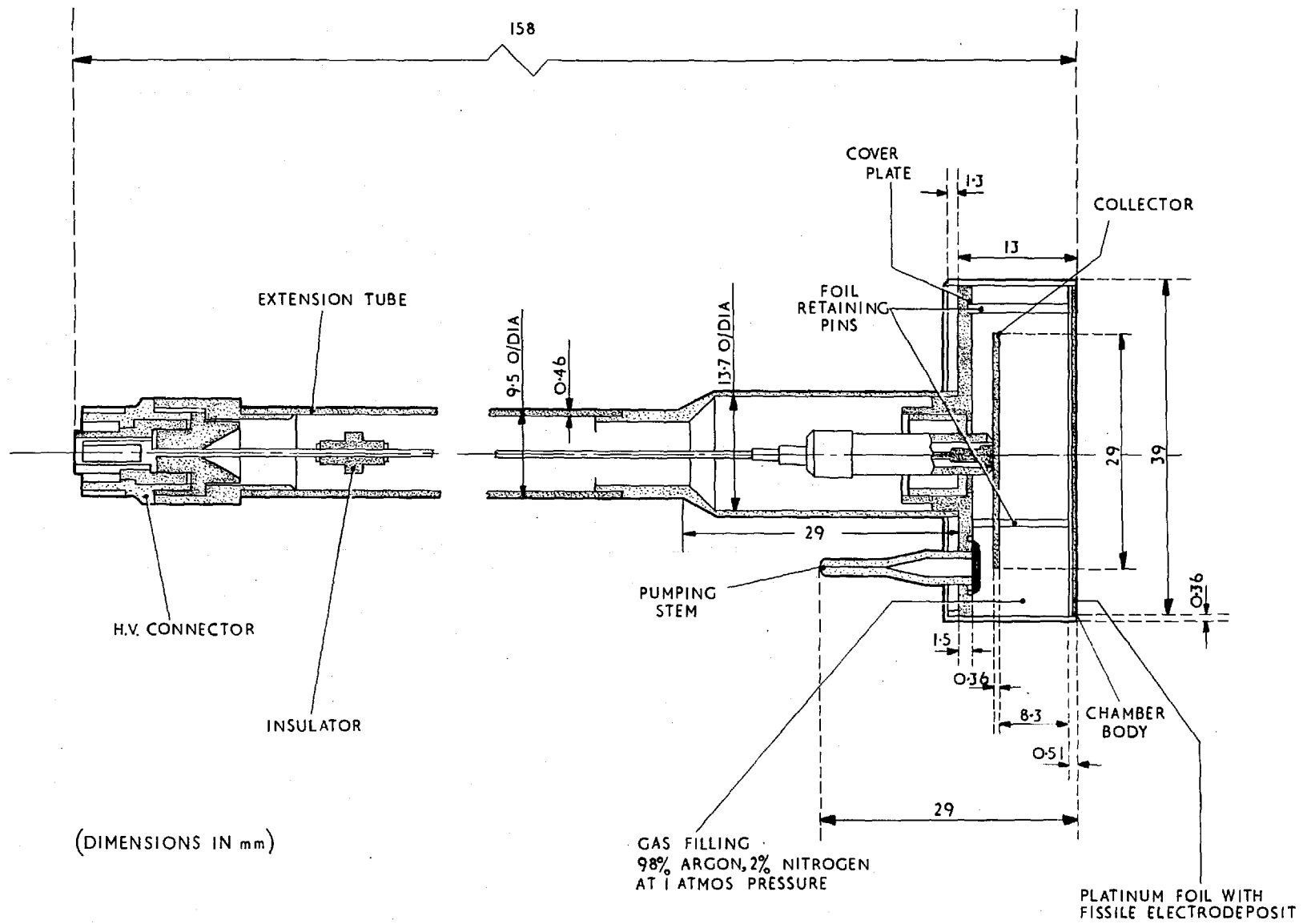


FIG.10. ZEBRA PARALLEL PLATE FISSION CHAMBER

thickness t , with a variation about this value of σ , is given by (Ref. 40):

$$(\sigma^2 + t^2) \cdot (2tR)^{-1}$$

where R is the mean range of the fission fragments in the deposit material. This correction was calculated to be 0.20% for the first new chamber (ZEB-31) and 0.09% for the second (ZEB-32). With an assumed error of $\sim \pm 30\%$ in this correction, the resultant error in the corrected fission rate was insignificant - hence eliminating the effect of (ii).

The pulse-height spectrum of fission fragments in ZEB-32 is compared in Fig. 11 with that obtained using an earlier chamber. Both spectra were obtained for irradiations in ZEBRA Core 8C. The much smaller mass of plutonium in the new chamber caused comparatively negligible α -interference, there being very little pulse pile-up in the low-energy region. Further, the degradation in energy of the fission fragments was far less in the much thinner deposit of the new chamber, and this improved the resolution of the fission-product energy peaks. A comparison of the pulse-height spectra from Chambers ZEB-31 and ZEB-32 revealed that the resolution was better for the latter. This is explained by the smaller area of the deposit in ZEB-32, a feature which reduces the fraction of fission fragments unable to lose their full energy before striking the chamber wall. All the three factors mentioned above contributed to minimising the number of low-energy pulses which had to be biased off. As a result, correction (iii) was only $\sim 0.1\%$ for ZEB-32 and $\sim 0.4\%$ for ZEB-31. Once again, the resulting error was negligible.

The doubt about the collection efficiency and geometry of the collector was cleared by comparing absolute fission-rate results obtained from the different-area deposits in the two new chambers.

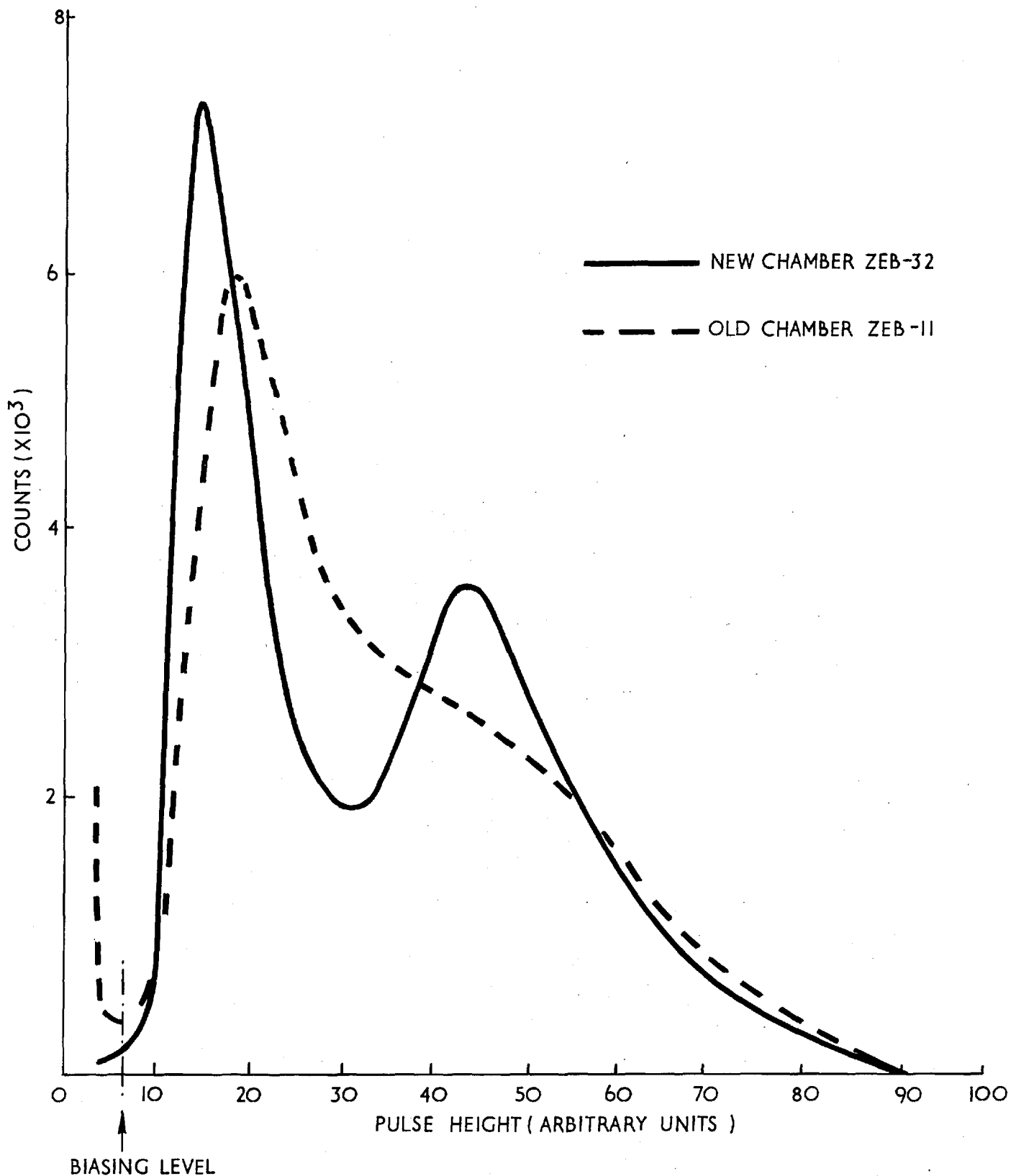


FIG. II COMPARISON OF PULSE-HEIGHT SPECTRA
 OBTAINED WITH OLD AND NEW ZEBRA
 FISSION CHAMBERS.

Within experimental errors of $\pm 0.6\%$, no discrepancy was observed in independent measurements made with the two chambers in the NESTOR thermal column and later in several of the Core 8 assemblies, confirming that the efficiency was the same in the two cases, viz. one corrected count per fission event.

4.2.2 LOW-GEOMETRY α -ASSAY OF THE CHAMBER DEPOSITS

As discussed above, the systematic uncertainties due to the various corrections for the absolute Pu-239 fission chambers, were reduced to negligible proportions. The overall accuracy of the absolute fission measurement was, in fact, limited mainly by the accuracy achieved in the absolute low-geometry α -assay of the chamber deposits. Unlike the simple α -counting requirements of the absolute U-238 capture measurement, where only relative count-rates are needed, the α -assay of the fission chamber deposits has to be carried out with explicitly-known geometry factors. Basic details of the low-geometry counter itself have already been mentioned (Sec. 4.1.2). A cross-sectional diagram is given in Fig. 12. By using various combinations from a range of stop discs and spacing cylinders, a number of well-defined geometries were made available. The crucial physical dimensions, viz. the various x , a and b values, were accurately measured by the Standards Section at Winfrith on two separate occasions, consistent results being obtained well within the demanded precision of $\pm 0.1\%$.

For calculating the geometry factors, G , from the determined dimensions, independent use was made of the solid-angle formulae of Curtis (Ref. 41) and Jaffey (Ref. 42), for a uniform circular source coaxial with a circular aperture. A computer programme, LOGEOM, was written on the basis of these two formulae which are,

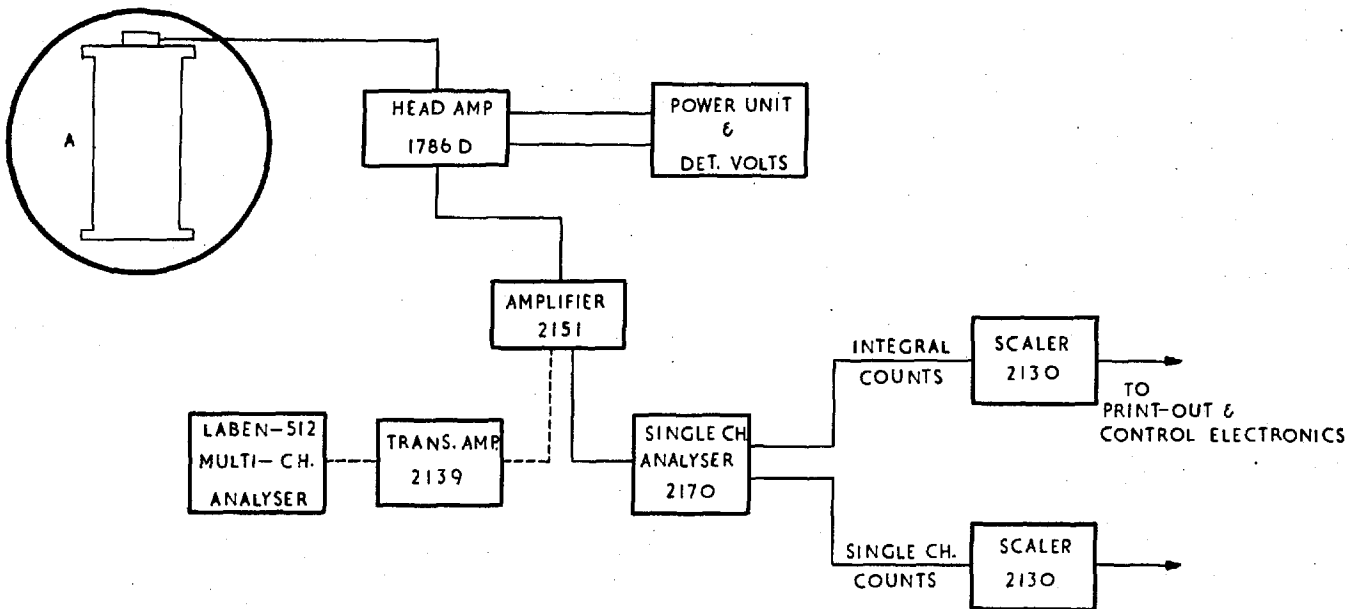
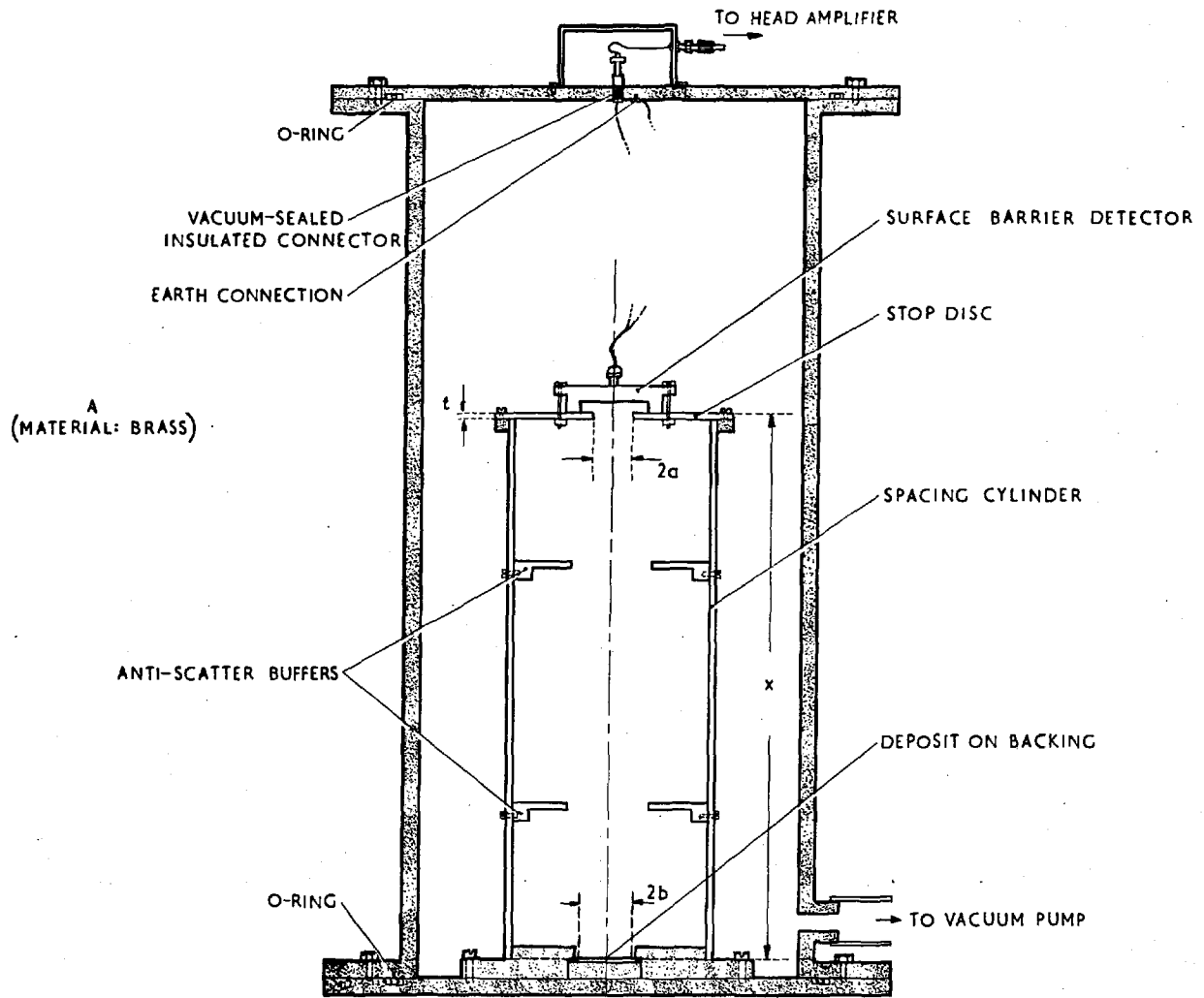


FIG.12. THE LOW-GEOMETRY α - COUNTER

respectively:

$$G = \frac{4x^2}{a^2} \cdot \left[1 - \frac{3}{4x^2} (a^2 + b^2) + \frac{5}{8x^4} (a^4 + b^4 + 3a^2b^2) \right]^{-1}$$

.....(Curtis)

and

$$G = \frac{1}{2} \cdot \left[1 - \frac{x}{(a^2 + x^2)^{\frac{1}{2}}} \right] \cdot \left[1 - \frac{3}{8}b^2 \left\{ \frac{x(x + (a^2 + x^2)^{\frac{1}{2}})}{(a^2 + x^2)^2} \right\} \right]$$

.....(Jaffey)

The agreement between the two calculated factors was found to be better than $\pm 0.1\%$ for G-values >250 . However, there was one experimental feature which neither formula took into account. This was the finite thickness, t , of the stop disc, which can be seen to result in (a) a finite stop-thickness absorption effect which decreases the effective solid angle, and (b) a slight increase in observed counts due to small-angle scattering at the inside "wall" of the aperture. Though, to some extent, the two effects tend to cancel one another, the former is invariably the predominant one and, for intermediate geometries, the resultant loss in counts can be quite serious. It is easily shown that the relative net effect decreases rapidly with increase in x - and a - values, so that for suitably chosen geometries, no corrections need be applied. This can be seen from Table 4 which compares some of the values, for the absolute disintegration rate of a typical plutonium deposit, obtained using different geometry-factors. While the stop-thickness effect is quite evident for the first two geometries, the consistency of the results from the latter three geometries, with their relatively high x - and a - values, is within the statistical errors indicated.

TABLE 4. COMPARISON OF GEOMETRIES FOR ABSOLUTE α -COUNTING

Geometry	y (mm.)	a (mm.)	G ($\times 10^4$)	Abs. disinteg. rate ($\times 10^9 \text{hr}^{-1}$)
1	59.97	1.2357	0.9984	1.699 ± 0.003
2	76.15	1.2357	1.5859	1.711 ± 0.003
3	120.06	2.5336	0.9212	1.760 ± 0.003
4	203.00	1.2357	10.944	1.752 ± 0.006
5	203.15	2.5336	2.607	1.757 ± 0.005
$b=9.169\text{mm.}, t=1.245\text{mm.}, x= y + t$				

Thus, by properly choosing the geometries employed, a systematic accuracy of $\pm 0.5\%$ was easily achieved in the absolute α -counting.

For correcting the observed chamber-deposit α -disintegration rate for the presence of plutonium isotopes other than Pu-239, accurate mass spectrometric analyses of samples of the plutonium were carried out at A.W.R.E., Aldermaston. Values of (0.0555 ± 0.0001), (0.00286 ± 0.00001) and (0.00018 ± 0.00001) were obtained for the atom ratios of Pu-240, Pu-241 and Pu-242 (relative to Pu-239), respectively, the quoted accuracies being confirmed by comparison of the results obtained on four separate occasions. Using the known α -decay constants of the various isotopes (Ref. 29), the required α -activity correction factors (relative to Pu-239) were obtained as ($20.57 \pm 0.06\%$) for Pu-240 and $\sim 0.01\%$ (i.e. negligible) for Pu-241 and Pu-242. Pu-238 could not be detected reliably in the mass spectrometric analysis. However, by quantitative consideration of the α -energy spectra from the deposits, a correction of ($2.05 \pm 0.05\%$) was applied for the 5.5 Mev α peak due to Pu-238 and Am-241 (from Pu-241 β -decay). The net error introduced by the various "other-isotope" corrections

was thus less than $\pm 0.2\%$ (Table 5).

The number of Pu-239 atoms in each deposit was computed from its corrected α -disintegration rate and the known Pu-239 α -decay constant, values of $(4.90 \pm 0.003) \times 10^{17}$ and $(9.55 \pm 0.07) \times 10^{16}$ being finally obtained for the deposits of Chambers ZEB-31 and ZEB-32, respectively.

4.2.3 MEASURING PROCEDURE

Fig. 13 shows a block-diagram of the electronics used, in conjunction with the calibrated chambers, for carrying out the absolute Pu-239 fission measurement. Most of the electronic units were, again, from the Harwell-2000 series. A multi-channel analyser and a pulse-generator were used for setting the threshold on the pulse-height discriminator and, with the earlier-mentioned low corrections for the new chambers, negligible error resulted from this biasing procedure. Counting accuracies of $\pm 0.2\%$ were easily achieved with both ZEB-31 and ZEB-32, and dead-time corrections were estimated as being no greater than $(0.5 \pm 0.2)\%$ in most cases.

In the initial experiments, the absolute fission chamber measurement was carried out in a cavity in the core formed by removing half a fuel-element. With the Core 8 test-regions having near-unity k_{∞} 's, this could be safely assumed as having negligible overall effect on the lattice properties. The reaction rate of interest itself, viz. the absolute Pu-239 fission rate in the Pu-plate of the central cell, was obtained by comparing the fission-product γ -activity of a Pu foil irradiated in the plate to that of a similar foil irradiated simultaneously in a dummy chamber in the cavity, integral γ -counting above 1.28 MeV being applied (Sec. 3.3.2). The correction for self-shielding of the dummy-chamber foil was found

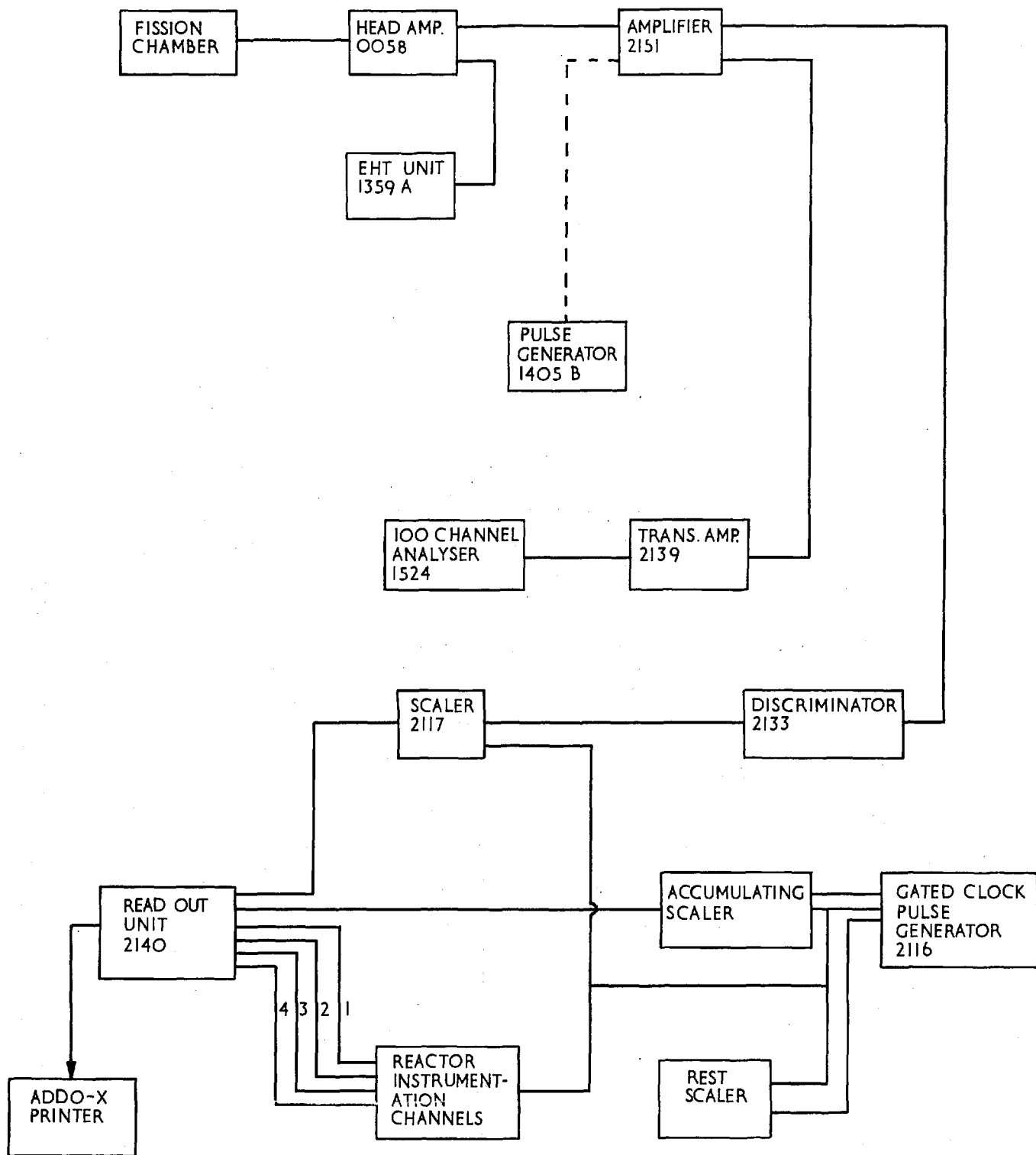


FIG. 13 . BLOCK-DIAGRAM OF FISSION-PRODUCT COUNTING ELECTRONICS

to be negligibly small in most cases, this being established by irradiating foils of different thicknesses in the chamber and comparing their γ -activities.

For some of the measurements made later, viz. in Cores 8E and 8F, it was decided to use the fission chambers in a reference position external to ZEBRA so that the need for a cavity in the test-region, during the plate measurements, could be eliminated. The thermal column of NESTOR was used for the purpose, though it must be stressed that this choice was purely a matter of convenience. The plate-to-chamber fission ratio was obtained as before, by γ -counting of Pu foils, but in this case an additional calibration factor was applied to take into account the different γ -yields in the lattice and in the reference spectra (Sec. 3.3.2).

Both the above described procedures, for determining the absolute Pu-239 fission rate in the Pu-plate from the chamber measurements, were found to yield results with an overall accuracy of about $\pm 0.8\%$. The various error contributions are summarised in Table 5.

TABLE 5. ERRORS IN THE ABSOLUTE PU-239 FISSION MEASUREMENT

Source of Error	Error (\pm)
1. Reactor-power intercalibration correction	0.1%
2. Fission-product self-absorption correction	0.1%
3. Biasing correction	0.1%
4. Effect of 0.1% precision in x, a and b values	0.3%
5. Systematic accuracy in determining effective G-factors	0.4%
6. Other-isotope contributions to α -disintegration rate	0.2%
7. Pu-239 α -decay constant	0.2%
8. Fission-product counting	0.3%
9. Correction for fissions in other isotopes	0.1%
10. Determination of plate-to-chamber fission ratio	0.5%
Total r.m.s. error	$\pm 0.8\%$

4.3 MEASUREMENTS IN ZEBRA CORE 8C

Absolute U-238 capture and Pu-239 fission rate measurements were made in a number of cores, and some of these will be discussed in later chapters. The measurements made in ZEBRA 8C, however, were the first ones to experimentally establish the techniques described in the last two sections, and the results obtained in this core therefore deserve separate mention.

For the absolute U-238 capture measurement, natural uranium deposits were loaded into the central uranium plates of the 8C cell (Fig. 4) at position (50,50) in the reactor lattice (Fig. 3). At the same time, Pu foils were loaded into the central-cell Pu-plate and also inside a dummy fission-chamber positioned in a cavity at (50,52). After a 2-hour irradiation at ~100 w., the deposits and the foils were removed for counting, and the dummy chamber replaced by ZEB-31 and ZEB-32, in turn. The fission-product counting with these chambers was carried out at the same reactor power as used in the main irradiation, negligible error resulting from the finite intercalibration correction applied using the recorded reactor-instrumentation count-rates. A thermal-comparison determination of the central-cell ($C_{8/P9}$) ratio was made at the same time as the absolute measurements and the various results obtained, in two separate sets of measurements, are summarised in Table 6. All the quoted results have been normalised by the use of foils (Ref. 25) to give the central 8C cell-averaged reaction-rate ratio, the theoretically predicted value of which was 0.127. The latter was obtained using the methods described in Chapter 2, viz. by applying a SCRAMBLE-derived correction factor of 1.017 to an infinite-lattice MURAL-FGL4 value of 0.1290.

TABLE 6. RESULTS OBTAINED IN ZEBRA CORE 8C

Expt.	Abs. U-238 Cap. Rate ($\times 10^{-16}$ sec $^{-1}$)	Abs. Pu-239 Fiss. Rate ($\times 10^{-15}$ sec $^{-1}$)	(C_8/F_9) abs. tech.	(C_8/F_9) therm comp.
1	4.22 \pm 0.04	3.28 \pm 0.05	0.129 \pm 0.002	0.126 \pm 0.003
2	5.29 \pm 0.05	4.16 \pm 0.04	0.127 \pm 0.002	0.126 \pm 0.002
$(C_8/F_9)_{\text{theory}} = 0.127$				

Although a detailed discussion would be more appropriate in the final chapter, after all the experimental results have been presented, it may be stated at this stage that the absolute technique did prove to be the more accurate of the two methods used for the (C_8/F_9) determination. This is clearly seen from Table 7 which elaborates on the errors quoted in the 8C results of Table 6.

TABLE 7. COMPARISON OF ERRORS IN 8C MEASUREMENTS OF (C_8/F_9)

Source of Error	Error (\pm)
(a) Absolute Technique	
1. Systematic accuracy of abs. U-238 cap. meas. (Table 3)	0.4%
2. Np-239 γ -X-ray coincidence counting statistics	0.8%
3. Abs. Pu-239 fiss. meas. (Table 5)	0.8%
4. Determination of cell-averaging factors	0.4%
Total error	1.3%
(b) Thermal Comparison Technique (Chapt. 3)	
1. U-238 capture foil ratio	0.8%
2. Pu-239 fission foil ratio	0.5%
3. Flux-perturbation corrections in thermal column	0.5%
4. γ -activity calibration factor	0.6%
5. Determination of cell-averaging factors	0.4%
6. Thermal cross-section ratio	1.1%
Total error	1.7%

The fact - that agreement between the two independent techniques was obtained well within these estimated errors - served to indicate the absence of any unsuspected uncertainties in either method. This was the more important conclusion to be drawn from the 8C measurements, and it was in this light that some of the work presented in the present chapter was published as a paper in the Journal of the British Nuclear Energy Society (Ref. 43).

CHAPTER 5

PRELIMINARY WORK WITH THE Ge(Li) DETECTOR SYSTEM

5.1 GENERAL CONSIDERATIONS FOR MIXED-OXIDE MEASUREMENTS

As mentioned in the opening chapter, one of the foremost requirements for the proper analysis of mixed-oxide assemblies, such as ZEBRA Cores 8F and 8G, is the accurate measurement of U-238 capture rates in PuO_2/UO_2 fuels containing as much as 25% by weight of plutonium. The use of foils of the same material composition as the mixed-oxide fuel itself has, to date, been rendered impossible by the inadequacy of the standard counting systems in effectively discriminating against the very large backgrounds, arising from the Pu natural-activity and fission-product radiations emitted by such irradiated samples. Chemical separation techniques are found to be inapplicable due to (a) difficulties in dissolving and treating sintered Pu-containing foils and (b) the fact that the necessary tracer, Np-237, is already present in the plutonium as one of the products of Pu-241 decay. As a consequence, U-238 capture measurements in mixed-oxide fuels have, in the past, had to be carried out using natural uranium foils embedded in the PuO_2/UO_2 plates (Ref. 44), thereby introducing uninvestigated systematic errors in the experimental assessment of such cores.

The one single feature, which precludes the direct application of any of the physical techniques (Sec. 3.3.1) to U-238 capture measurements in PuO_2/UO_2 material, is the poor resolution of the NaI(Tl) scintillators used for the γ -X-ray counting. In the normally most effective of these methods, viz. that based on the γ -X-ray coincidence counting of the 105 keV Np-239 region, a typical resolution of ~ 15 keV (F.W.H.M.) is the best which can be provided at this energy by the sodium iodide detectors used. This means that - apart from the 106.2 keV Np-239 γ -ray and the coincident 99.5 and 103.7 keV Pu K_{α} X-rays which provide the measure of

the U-238 capture rate - the various K X-rays of uranium (viz. at 94.7, 98.5, 111 and 114.5 keV) are, of necessity, included in the counted regions of both detector channels. It is this inclusion which, in the main, accounts for the two types of swamping backgrounds encountered in the NaI counting of Pu-containing samples. For the very large Pu natural-activity contribution, the predominant mechanism is the production of coincidences between U X-rays following Pu-239 α -decay and simultaneously emitted higher-energy γ -rays which are Compton-scattered into the counted regions. The other effect, i.e. that of fission-product activity, arises mainly as a result of the decay of certain fission products which emit two or more higher-energy γ -rays simultaneously, one of which is scattered into the gated energy region and another of which is absorbed in the uranium of the foil-material to yield a coincident U K X-ray. It follows from the above arguments that what is basically needed is the use of γ -X-ray detectors with sufficiently high resolution in the 100 keV region to effectively separate the various U X-rays from the coincidence-producing 104 and 106 keV Np-239 radiations.

The application of lithium-drifted germanium detectors to problems, in both applied and pure nuclear research, where high γ -ray resolution is an important requirement, has become quite widespread since the first Ge(Li) diode was fabricated in 1962 (Ref. 45). A comparison of the properties of a 7 c.c. planar Ge(Li) detector system, with those of a $1\frac{3}{4}$ " x 2" NaI(Tl) scintillation counter, was made in the present author's M.Sc. dissertation (Ref. 46), and it was shown therein how the superior resolution of the former type of detector greatly simplifies the analyses of γ - γ coincidence experiments. As an initial phase of the present work, the feasibility of applying Ge(Li) detectors to U-238 capture measurements was examined by carrying out R.C.R. measurements at the University of London's CONSORT reactor using the above-mentioned Ge(Li) and NaI systems.

Various techniques, e.g. singles counting of the 75 keV U-239 γ -ray and Np-239 γ -X-ray coincidence counting, were compared (Ref. 47). In brief, the results from the analysis of these early experiments indicated that the most promising approach to the problem of determining U-238 capture rates in PuO₂/UO₂ material was the use of a suitably-designed twin Ge(Li) coincidence system for the γ -X-ray counting of Np-239.

5.2 PHYSICAL PROPERTIES OF THE PRESENT Ge(Li) DETECTORS

In accordance with the arguments presented in the previous section, two planar Ge(Li) detectors were obtained on order from 20th Century Electronics Ltd., Croydon, and a complete coincidence system including a special automatic foil changer was set up at ZEBRA to develop a reliable technique for U-238 capture measurements in the mixed-oxide assemblies, 8F and 8G.

The basic specifications, for each of the two Ge(Li) systems ordered, were:

- (a) a sensitive detector volume of ~ 8 c.c. with a depletion depth of ~ 10 mm.; these dimensions were chosen as the optimum values for meeting the conflicting demands of high detector efficiency and low detector capacitance (i.e., low electronic noise contribution).
- (b) a system resolution of 2 keV, or better, at 100 keV; this was considered adequate for providing the discrimination required and, by current standards (Ref. 48), was not regarded as placing too high a demand on the performance of the diodes and the associated electronics.
- (c) a high geometrical efficiency with the detector mounted vertically within 5 mm. of the outer aluminium casing; the only drawback in using Ge(Li) diodes for coincidence experiments is their

relatively poor intrinsic peak efficiencies compared to those of NaI(Tl) crystals (Ref. 46) but, at 100 keV, this is not too serious a consideration provided the geometrical efficiency of each Ge(Li) detector is as high as possible (viz., ~25%).

- (d) the use of a cold-finger type cryostat, for cooling the detector, instead of the more commonly-applied drip-feed systems; this was aimed at minimising the electronic noise generated as the result of mechanical vibrations caused by the constant boiling of liquid nitrogen in the cryostat (Ref. 49).
- and (e) the use of a cooled-FET pre-amplifier for each system; although the detector noise contribution was recognised as an important limitation to the obtainable system resolution, it was essential to minimise the head-amplifier noise as well (Ref. 50), particularly in view of the fact that the systems were intended mainly for low-energy counting.

The Ge(Li) detectors supplied by 20th Century Electronics to meet these specifications were their Type GL8 with cooled-FET pre-amplifiers Type CE-103 (Ref. 51). The a.c.-coupled CE-103 units were based on a Harwell design for low-noise charge-sensitive pre-amplifiers, and a description of this has been given by Gibbons and Howes (Ref. 48).

Each detector had its copper cold-finger dipping into a 20 l. Union Carbide liquid-nitrogen dewar which was "topped up" twice a week. The vacuum in the cryostats was maintained at $\sim 10^{-7}$ torr using Ferranti ion-pumps (current $< 5 \mu\text{A}$). In addition, a molecular sieve had been fitted in each system to serve as a safeguard against ion-pump failure.

For the first system (A), a detector bias of 775 v. and differentiating-integrating time constants of 1 μs . were found to be the optimum operating conditions, while for the second system (B) the corresponding values were 400 v. and 2 μs . Fig. 14(a) shows the response of Detector A to a 0.02 μc

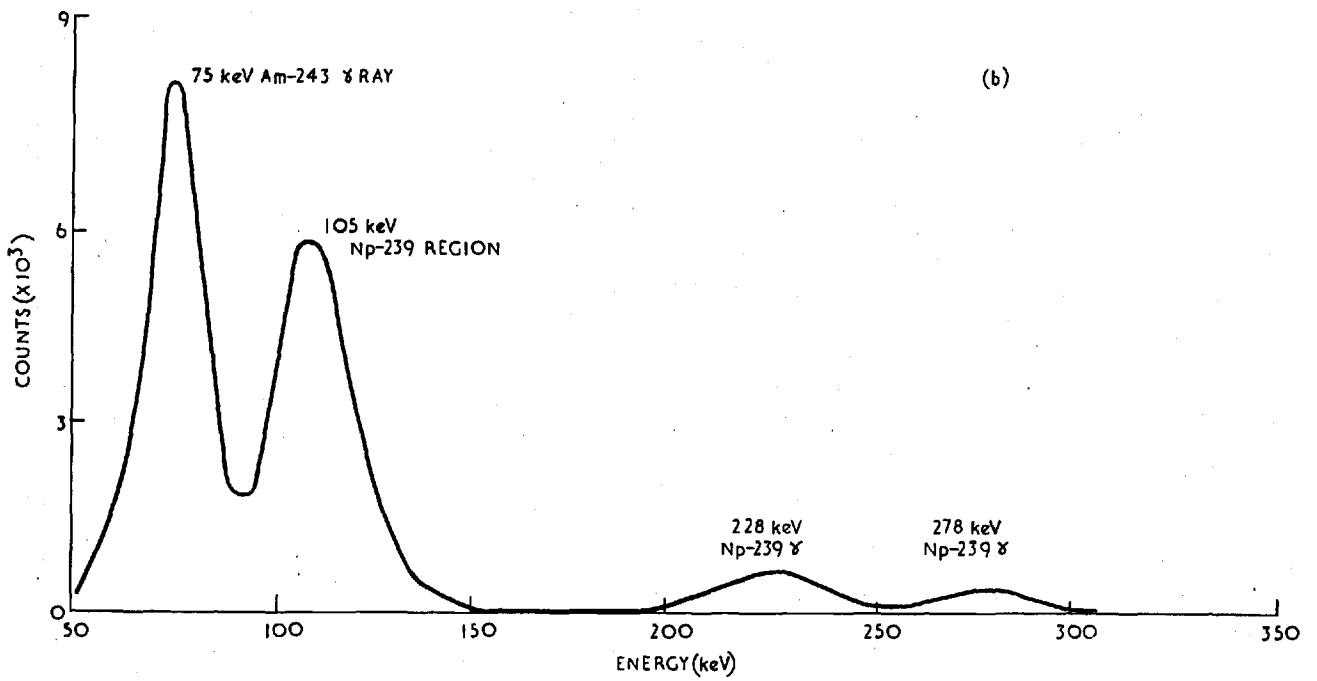
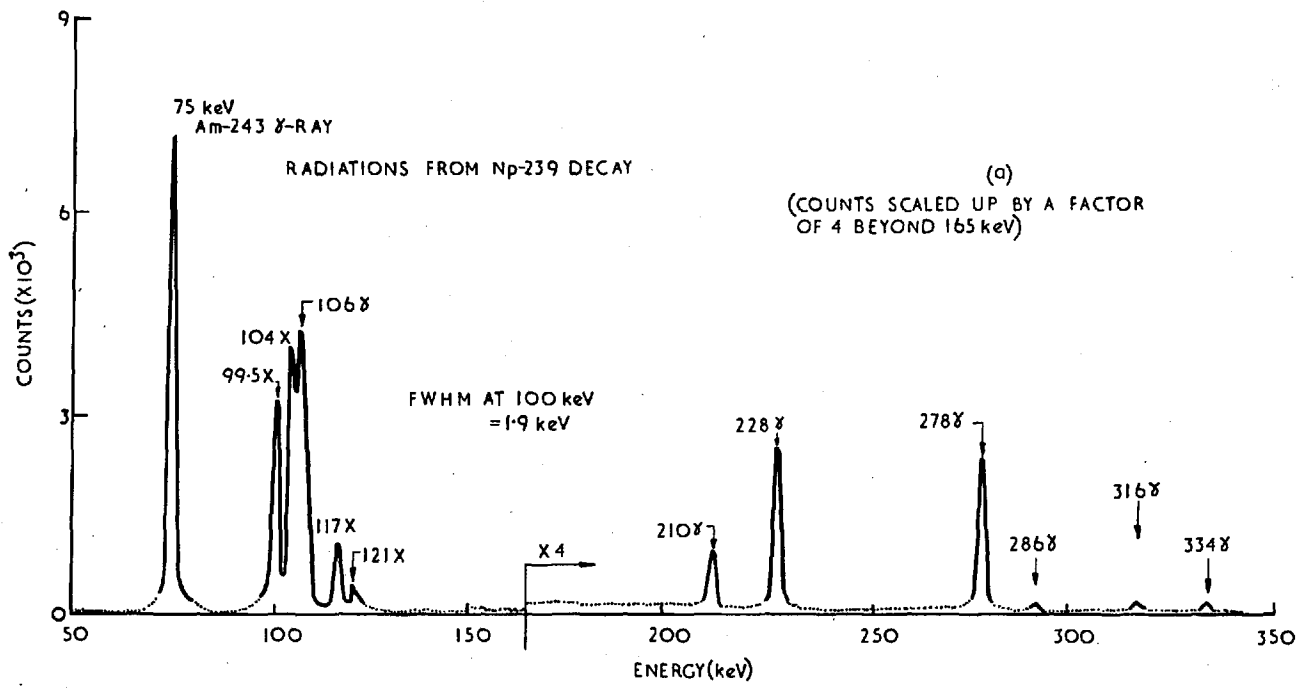


FIG.14. RESPONSE TO A 0.02 μ c (Am-243:Np-239) SOURCE OF
 (a) Ge(Li) DETECTOR A AND
 (b) A 2in X 2in NaI (TI) CRYSTAL

(Am-243:Np-239) source and indicates how effective the system resolution of 1.85 keV was in separating the 99.5 keV X-ray from the 104 keV X-ray and the 106 keV γ -ray of the Np-239 spectrum. Detector B had a similar response with a system resolution of 2.0 keV at 100 keV. For comparison, the response of a 2" x 2" NaI (Tl) crystal to the same source is shown in Fig. 14(b).

The performance of the two Ge(Li) detectors was found to be significantly poorer at higher γ -energies, the resolution being ~ 5 keV for the 1.28 MeV γ -ray of Na-22. This indicated adverse energy-dependent properties of the diodes (viz. trapping, side-surface contamination, incomplete clean-up, etc.). The photopeak to Compton-edge ratio for the 0.66 MeV Cs-137 γ -ray was $\sim 3 : 1$ for both detectors, indicating again that the systems were not as suitable for high-energy work as they obviously were in the 100 keV region.

Using normal single R-C pulse-shaping, the resolution of the detector systems at 100 keV was found to deteriorate markedly at high count-rates but this was more a basic electronics problem than a fault in the detector systems themselves. However, there was another cause of base-line shift which might have been avoided by more careful construction of the cooled pre-amplifier first-stage. This was the high microphony of both systems exemplified by the fact that, with single R-C pulse-shaping, even conversation in the laboratory was picked up and caused observable base-line disturbance. Restoration of the d.c. level by double pulse-shaping was found to reduce both the count-rate and the microphony effects considerably and, in practice, this was achieved by using an external pulse-shaping unit between the pre-amplifier and the main amplifier (Fig. 18).

The other important aspect of detector performance which had to be carefully examined was the photopeak efficiency at 100 keV. For Detector

A, this was estimated, inclusive of the geometry factor, to be of the order of 20% that of a 2" x 2" NaI(Tl) crystal, and hence the system could be considered quite satisfactory for the type of coincidence measurements planned. For the 2.6 MeV γ -ray of Tl-208 (Th-228 source), a photopeak to double-escape peak ratio of 9:10 was obtained with Detector A (Fig. 15), and this indicated a sensitive volume of more than 8 cc. Detector B, however, yielded a corresponding value of 1:6 for the ratio and this, together with the fact that its photopeak efficiency at 100 keV was a factor of ~ 4 down on that of A, confirmed that B's sensitive volume was considerably less than specified.

Subsequently, in time for the main PuO_2/UO_2 measurements, this poor-volume detector was replaced by another Ge(Li) planar diode from 20th Century Electronics. The new detector gave a photopeak to double-escape peak ratio of 7:10 for the 2.6 MeV Tl-208 γ -ray and yielded a 100 keV photopeak efficiency $\sim 60\%$ that of Detector A, both these facts indicating an adequate sensitive volume. The optimum operating conditions for this latter Detector B system were found to be differentiating-integrating time constants of 1 μs and a bias of 700 v. Although the charge collection in the new diode was better than that in the earlier detector (as indicated by the lower optimum time constants), the overall resolution at 100 keV was found to be slightly poorer due to greater leakage current. However, this was not serious and the system was considered quite satisfactory on the whole.

5.3 THE AUTOMATIC FOIL-CHANGER AND THE COINCIDENCE SYSTEM

The basic electronic control units for an automatic foil-changer were already available at ZEBRA - the absolute U-238 capture measurements described in the last chapter having been carried out using these in conjunction with a Type-1718A a.f.c. (Sec. 4.1.2). However, for the

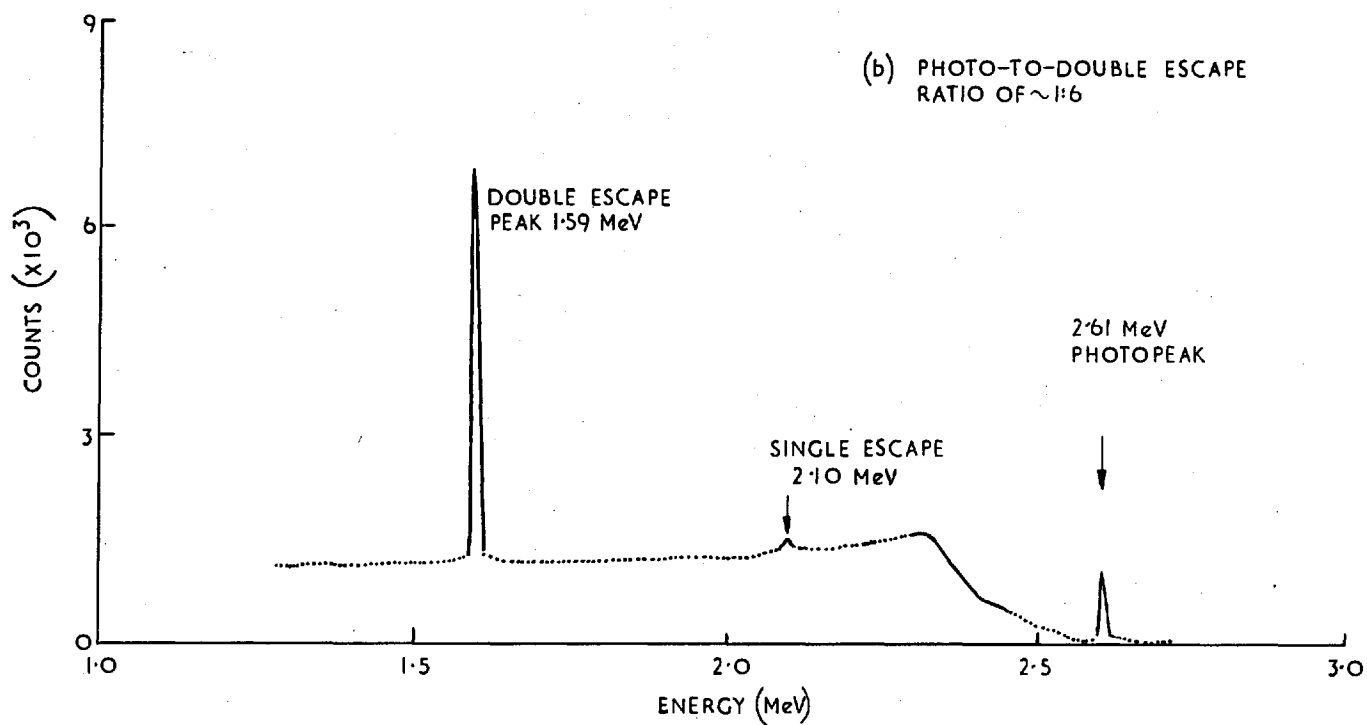
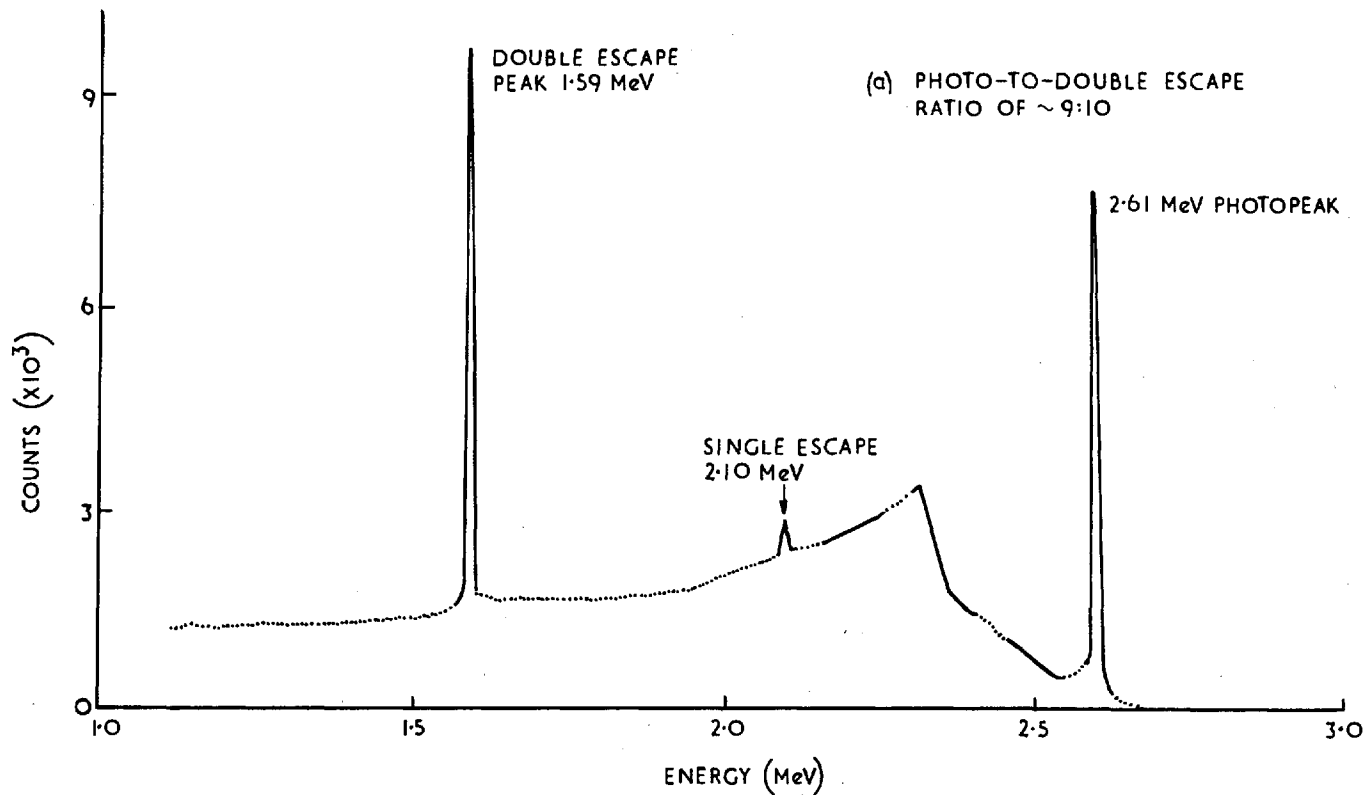


FIG.15. RESPONSE TO A Th-228 (TI-208) SOURCE OF OF (a) Ge(Li) DETECTOR A AND (b) INITIALLY-SUPPLIED Ge(Li) DETECTOR B

Ge(Li) systems, with the diodes mounted in a vertical plane (to achieve symmetry in the coincidence arrangement and also to keep the cold-finger type cryostat design as simple as possible), a new foil-changing machine had to be designed and constructed. The main specifications for this were:

- (a) that it be usable with the existing electronic control units;
 - (b) that the turn-table rotate in a vertical plane;
 - (c) that the separation between the outer casings of the detectors, when in position, be < 10 mm. (to allow as high a geometrical efficiency in the counting as possible);
 - (d) that relative positioning of the detectors be accomplished accurately;
 - (e) that there be ~ 6 cm. of lead shielding around the detectors;
 - (f) that there be six counting positions with a spacing of ~ 20 cm. between consecutive positions;
 - (g) that there be a mechanical means of varying the number of positions to be counted, thus enabling any given number of samples (between one and six) to be automatically counted during a particular measurement;
- and (h) that the foil-holders be such as to accept foils and deposits up to 27 mm. in diameter and that they be spring-loaded into position on the turn-table.

The detailed design and construction of the foil-changing machine were carried out, according to the above specifications, by the Engineering Services Division at Winfrith (Ref. 52). The basic design features are shown in Fig. 16. Essentially, these were (a) an aluminium base plate assembly with two centrally disposed castings and two slideway carriages for the Ge(Li) dewars; and (b) a vertical turntable assembly supported on a robust steel sub-base plate and consisting, in turn, of

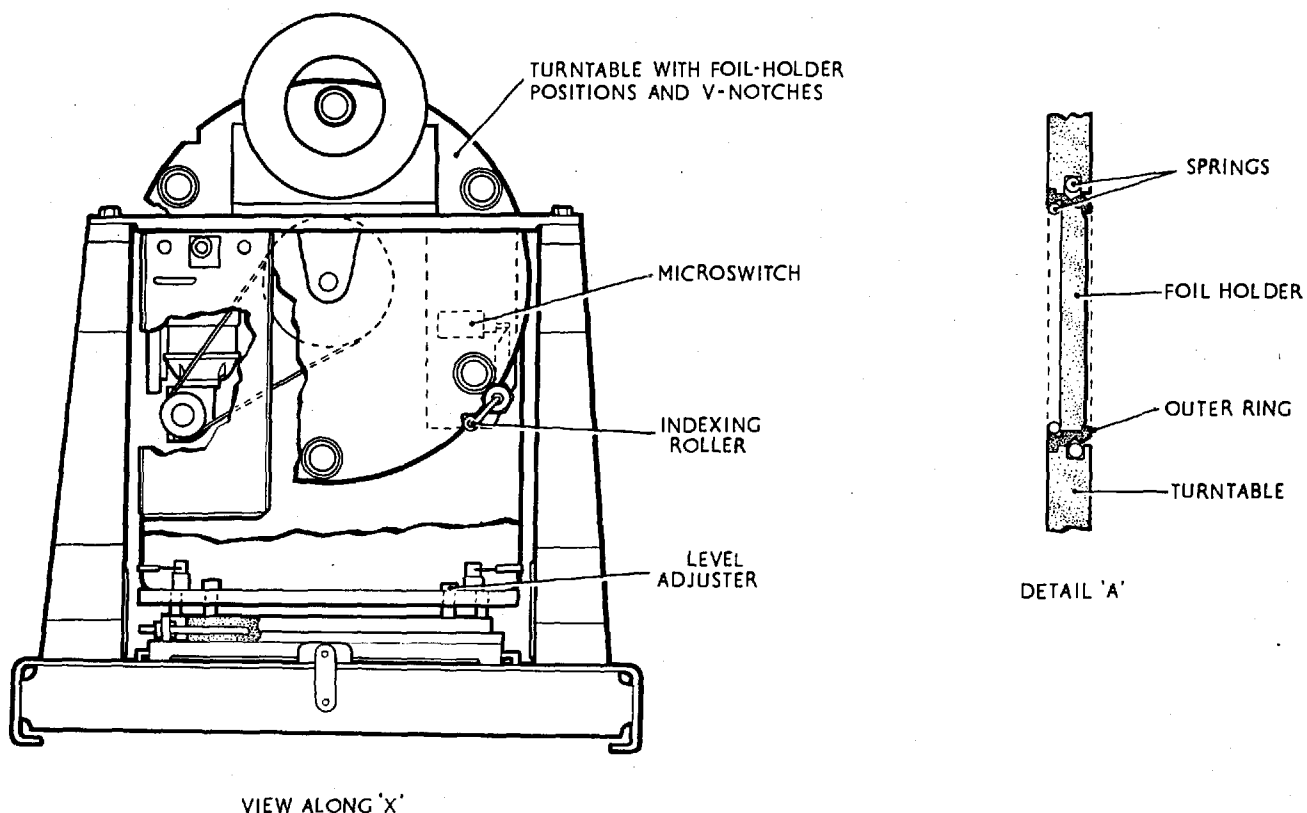
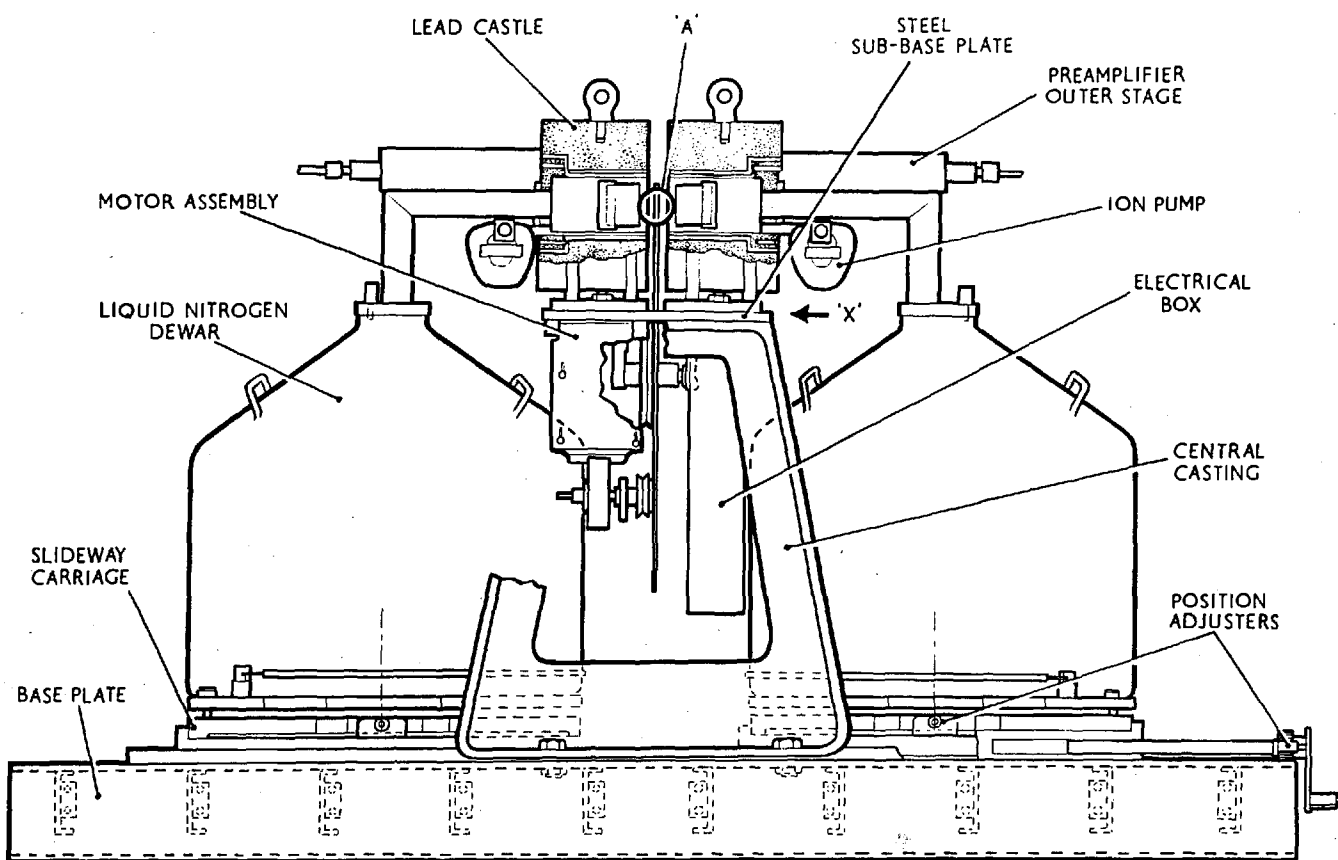


FIG. 16. FOIL-CHANGING MACHINE FOR THE Ge(Li) DETECTORS

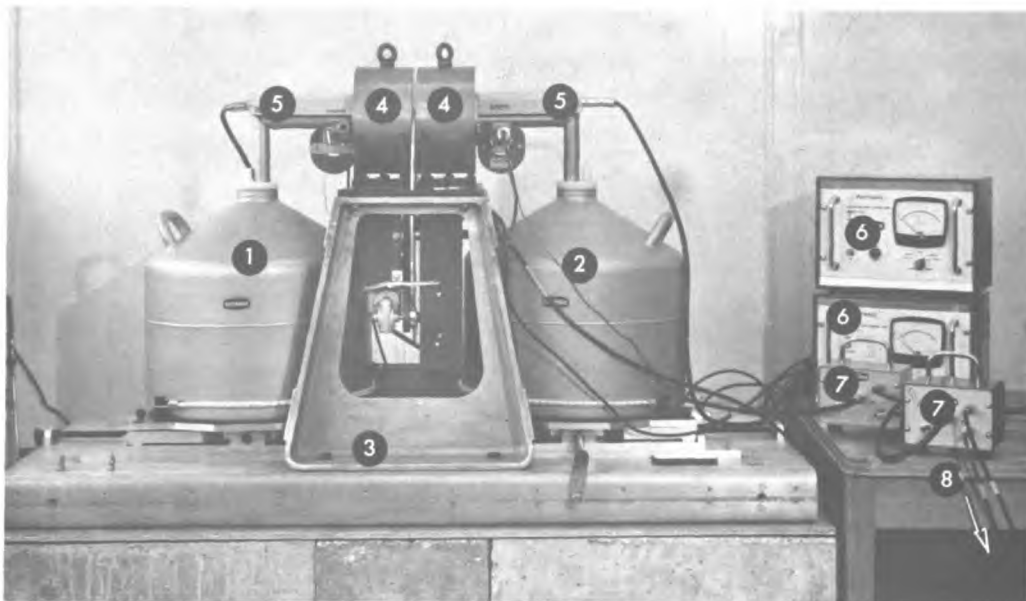
an aluminium turntable carrying six "snap-in" foil-holder positions, a motor-drive unit controlled by an indexing roller and microswitch arrangement, an electrical box linking the a.f.c. to the control electronics, and lead-shield castles for the detectors. Another important aspect of the design was the provision made for the accurate adjustment of vertical height, tilt and horizontal positioning of the Ge(Li) assemblies.

Plate 2(a) shows a general view of the foil-counting machine with the detectors in position. On the right are the ion-pump units and the detector power supplies with the connecting cables going out of the picture to the control and counting electronics.

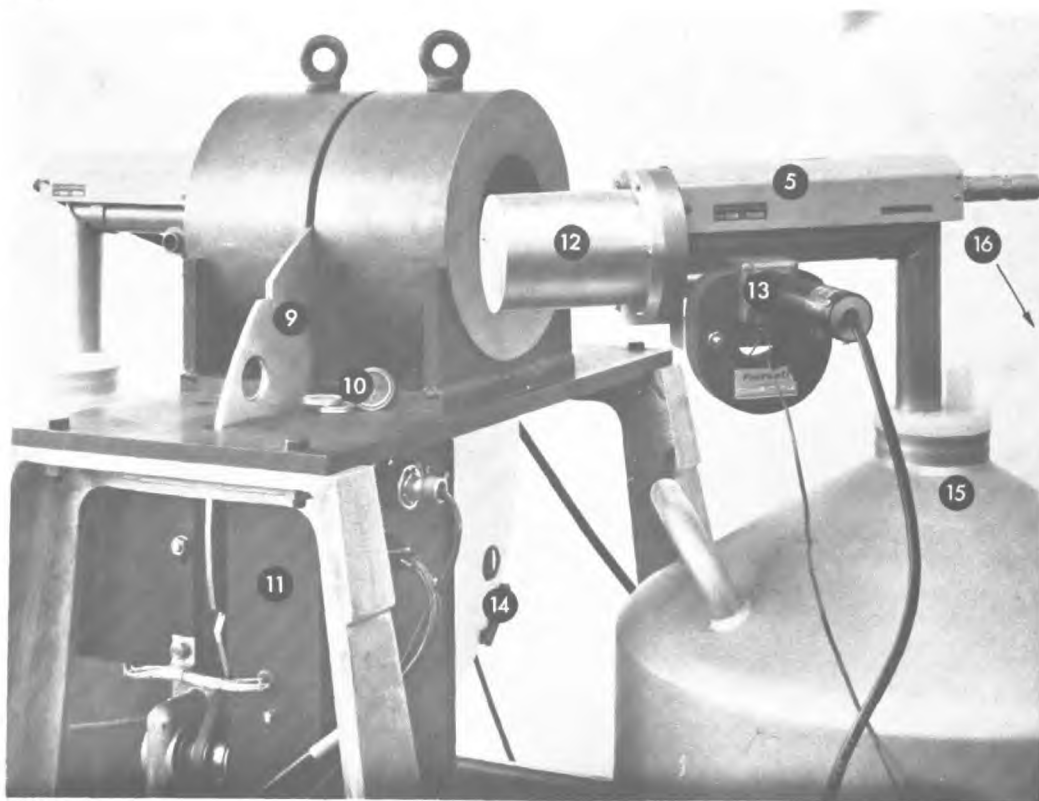
Plate 2(b) gives a more detailed view of the turntable and one of the Ge(Li) detector assemblies. The V-shaped notches in the aluminium wheel could be "filled-up" using specially designed steel V-pieces, and this enabled any unwanted counting-position to be by-passed during each cycle (specification (g) for the foil-changer). Also to be seen in the picture are a few of the foil-holders with their "snap-in" springs. Several types of foil-holders were used in the present work to enable the counting of foils and deposits of various sizes and materials, and some of these are illustrated in Fig. 17. However, the design of the outer ring which carried the foil-holder and which fitted into the turntable was the same for all holder-types. In all cases, the effective thickness of aluminium (i.e., of the foil-holder and the detector window), between the counted sample and each Ge(Li) diode, was quite adequate in eliminating any finite β -activity interference effects in the counting.

A block-diagram of the complete coincidence system is given in Fig. 18. Most of the external electronics was the same as used with the NaI detectors (Sec. 4.1.2. and Plate 1). The Ge(Li) detectors had their own power units with supplies of ± 24 v., while the rest of the equipment

(a)

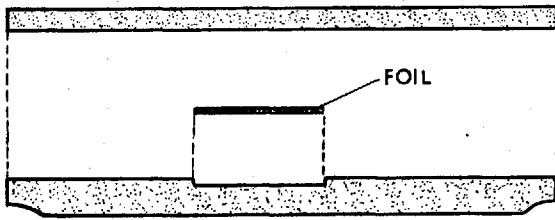
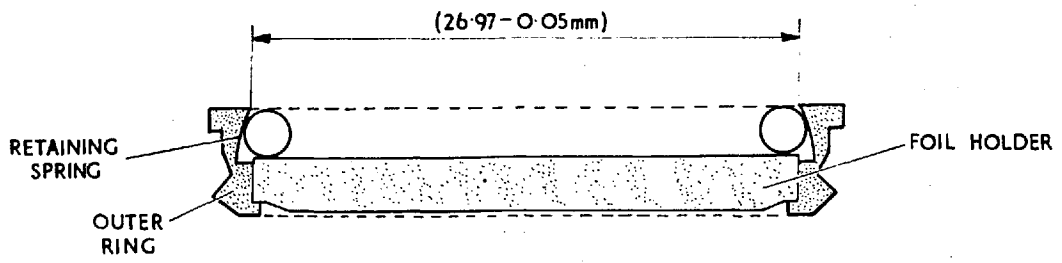


(b)

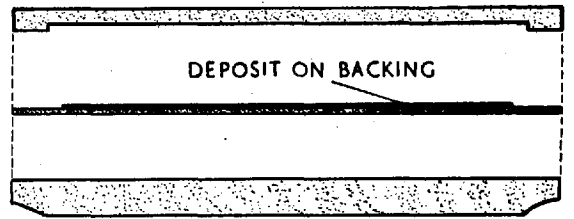


- KEY:
- | | | |
|-----------------------------|--|---------------------------|
| 1. DETECTOR ASSEMBLY A | 7. POWER SUPPLIES AND CONNECTORS | 12. DETECTOR TOP-HAT |
| 2. DETECTOR ASSEMBLY B | 8. TO CONTROL AND COUNTING ELECTRONICS | 13. ION-PUMP HEAD |
| 3. FOIL-CHANGING MACHINE | 9. TURNTABLE | 14. INDEXING ROLLER |
| 4. LEAD CASTLE | 10. FOIL-HOLDERS | 15. LIQUID NITROGEN DEWAR |
| 5. PREAMPLIFIER OUTER STAGE | 11. ELECTRICAL BOX | 16. TO 7 |
| 6. ION-PUMP UNIT | | |

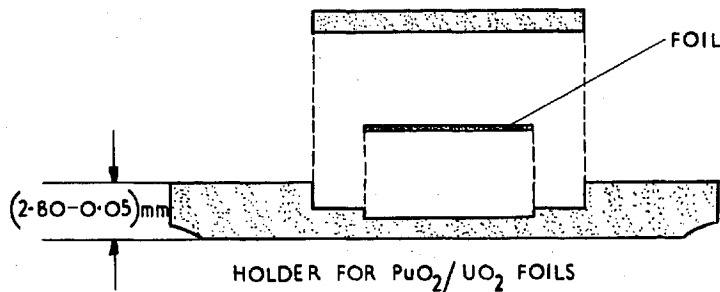
PLATE 2. THE GE (Li) DETECTOR ASSEMBLIES AND FOIL-CHANGING MACHINE



HOLDER FOR NAT U FOILS



HOLDER FOR THIN DEPOSITS



(MATERIAL: ALUMINIUM)

FIG.17 SOME OF THE FOIL HOLDERS USED

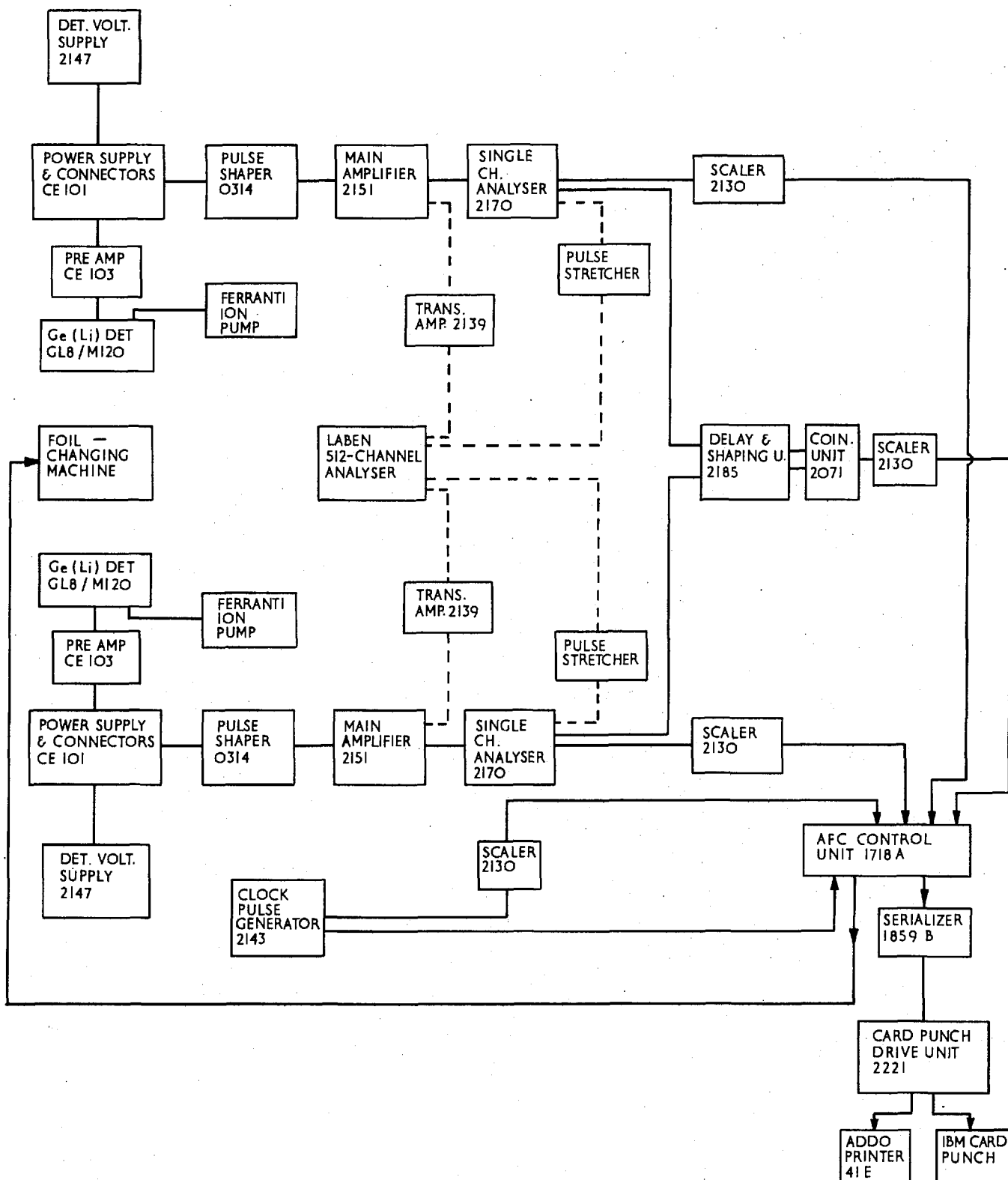


FIG. 18. BLOCK-DIAGRAM OF THE Ge(Li) COINCIDENCE SYSTEM

was run on the standard Harwell-2000 power supplies (Units Type-2015C). The 2151-main amplifiers and 2170-single-channel analysers had been chosen with high stability as an important criterion. The 2071-coincidence unit, in conjunction with the 2185-pulse-shaper and delay unit, could be used for obtaining coincidence resolving times of 20-200 nanosec., thereby causing random-coincidence contributions to be quite small even for Pu-containing foils.

For setting up the individual channels of the 2170's, the Laben 512-channel analyser (with a built-in coincidence unit) was used. The γ -X-ray spectrum was fed into the analyser from each of the main amplifiers, in turn, via a 2139-translation amplifier. By simultaneously feeding the pulses from the single-channel output of the corresponding 2170 into the coincidence input of the Laben, the portion of the spectrum represented by these pulses was set up visually and adjustments could then be made to obtain the required gate. This setting-up procedure was found to be sufficiently accurate for the rather narrow gates that had to be employed. (The built-in coincidence facility of the Laben was also used, in some of the preliminary experiments, for obtaining spectra from one detector in coincidence with a given gate set up on the other.)

The basic control units for the foil-changing machine are included in the block-diagram shown in Fig. 18 and were essentially the same as used for the NaI a.f.c. The motor-drive circuitry, linking the machine to the control electronics, was designed by the Control & Instrumentation Division at Winfrith (Ref. 37) to be directly compatible with the 1718A unit. It was on the latter unit that the duration of each counting-interval and the mode of operation (forward, not forward, etc.) were set up, and as in the NaI counting (Sec. 4.1.2) it also served, in conjunction with the 1859B-serializer unit, to control the output of the accumulated data at the end of each individual interval.

5.4 SOME EXPERIMENTAL RESULTS

When the complete Ge(Li) detector system was ready for use at ZEBRA, a few simple measurements were first made with it to show that its general performance was quite satisfactory. The results of these experiments are discussed in this section.

5.4.1 QUALITATIVE WORK

The stability of the two detector channels was initially established by single-channel counting of the 102-108 keV region of the Np-239 spectrum using a 0.02 μ c Am-243 source (Fig. 14(a)). Consistent counts, within a statistical accuracy of $\pm 0.1\%$, were obtained over a period of ~ 100 hours, the counted region also being visually observed using the Laben and found to remain constant.

In order to qualitatively see the effect of fission-product interference in the Np-239 γ -X-ray counting of fast-spectrum irradiated foils using the Ge(Li) detectors, a magazine of ~ 100 natural uranium plates was loaded into the Nat. U stack in NESTOR Cave A (Ref. 27). Three central plates were loaded with a .04% depleted, a natural and a 37% enriched U-metal foil, respectively. After a 3-hour irradiation, the foils were coincidence-counted with the Ge(Li) detector channels set at 102-108 keV. Experimental decays fitted graphically to the coincidence count-rates, between 20 and 100 hours after irradiation, yielded effective half-lives of 2.39, 2.34 and 2.38 days for the depleted, natural and enriched foils, respectively. The statistical accuracy in the counting was $\sim \pm 1.5\%$ so that all three values seemed to agree, within the experimental errors, with the 2.35 day half-life of Np-239. This indicated how effectively the fission-product interference, even for the 37% enriched foil, could be reduced by eliminating the U X-rays from

the counted regions (Sec. 5.1). Fig. 19 compares singles and coincidence Ge(Li) spectra of the depleted and enriched foils, ~ 20 hours after irradiation, and clearly shows the prominence of the fission-product-excited U X-rays in the enriched-foil spectra - tending to confirm once again the fission-product coincidence-mechanism discussed earlier.

5.4.2 A FISSION-PRODUCT CORRECTION FACTOR MEASUREMENT

Attempts to obtain relative U-238 capture rate values from the three types of uranium-metal foil irradiated in NESTOR Cave A did indicate that the contribution of fission-product coincidences to the observed count-rates was < 5% for the 37% enriched foil. However, in order to obtain a quantitative estimate of the effect of fission-product γ -induced coincidence activity, it would be more appropriate to determine a general correction factor as a function of t, the time after the end of the irradiation, and to standardise the measurement by using some reference neutron spectrum for the irradiation. This approach leads directly to the definition of the so-called Q(t) factor (Ref. 22), viz.:

$$Q_5(t) = \frac{\text{Fission-product coincidences/U-235 atom in thermal column}}{\text{Np-239 coincidences/U-238 atom, corrected for self-absorption}} \dots\dots\dots(5.1)$$

If Pu-239 is the major fissile constituent, as is the case for typical mixed-oxide foils, one would similarly define $Q_9(t)$ - by considering fission-product coincidences per atom of Pu-239, instead of U-235, in Eqn. (5.1). In general, it is easily seen that Q(t) is well-defined for given detector settings, a given length of irradiation and foils of a given thickness and material.

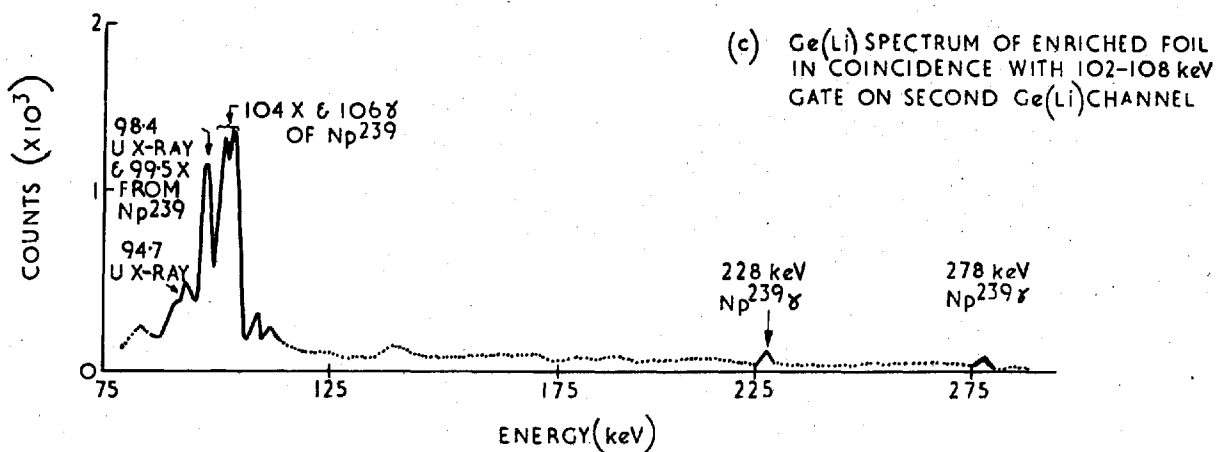
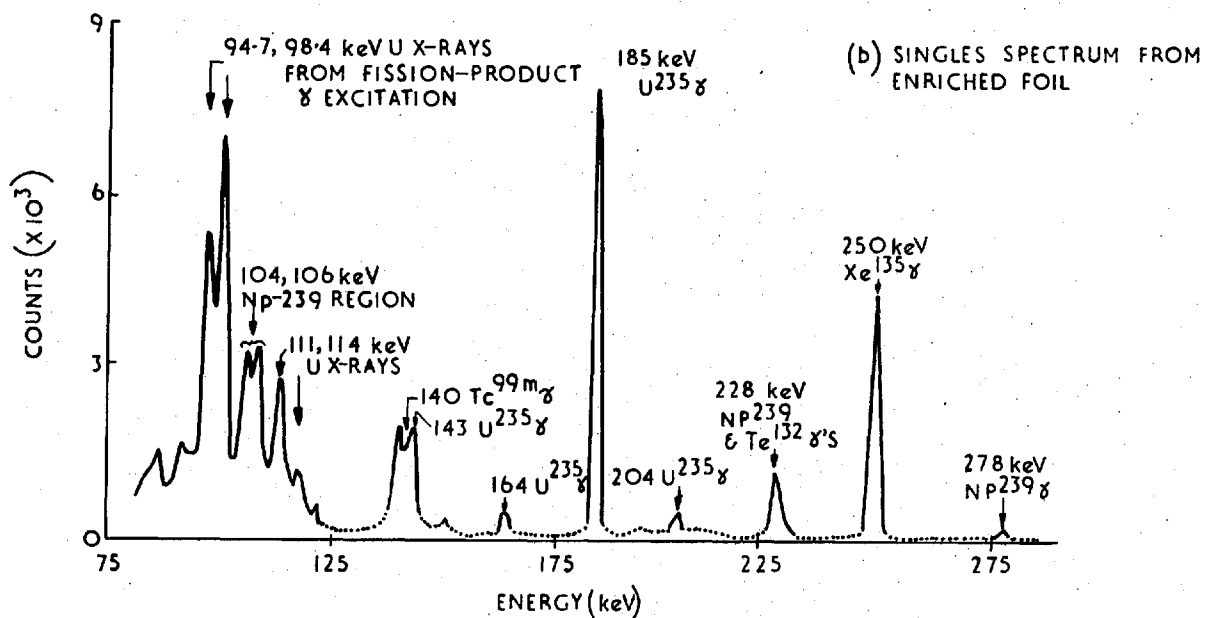
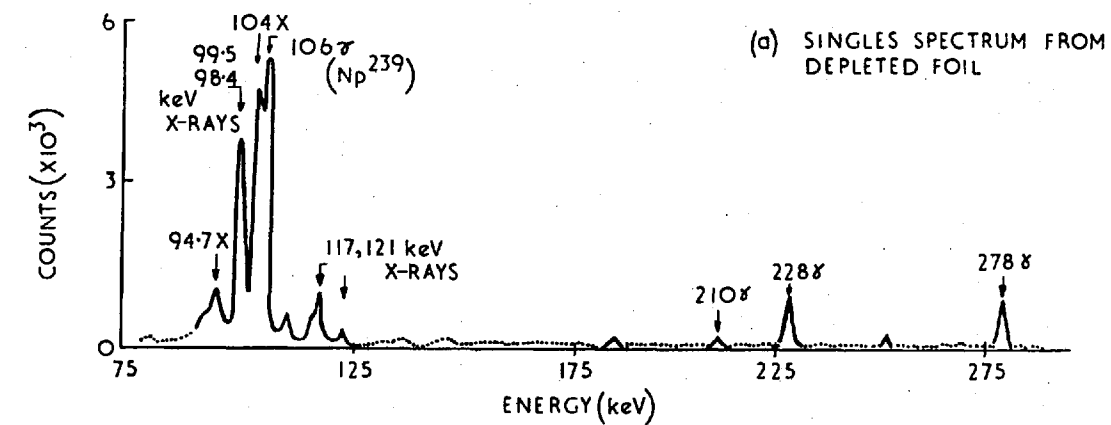


FIG.19. SINGLES & COINCIDENCE Ge(Li) SPECTRA OF DEPLETED & 37% ENRICHED U-METAL FOILS \sim 20HRS AFTER AN EPITHERMAL FLUX IRRADIATION

The measurement of $Q(t)$, as defined above, essentially involves the irradiation of two foils of different enrichments in the reference spectrum of a thermal column. If $C(t)$ is the observed count-rate at time t , N_5 and N_8 are the number of U-235 and U-238 atoms in the foil, a is the γ -X-ray self-absorption factor, f is the relative flux-depression factor for the two foils and if the subscripts n, e denote the lower and higher enriched foil respectively, it can be shown that:

$$Q_5(t) = \frac{C_e(t) \cdot N_{8n} \cdot a_n - C_n(t) \cdot N_{8e} \cdot a_e \cdot f}{C_n(t) \cdot N_{5e} \cdot f - C_e(t) \cdot N_{5n}} \dots\dots\dots(5.2)$$

A 2-hour $Q_5(t)$ measurement was carried out in the NESTOR thermal column for 0.12 mm. thick, 3.2 x 6.3 mm. U-metal foils - the Ge(Li) channel-setting being 102-108 keV for each detector system. The foils used were of natural and 37% enriched U-metal (an accurate mass-spectrometric analysis having been made of the foil materials by the Chemistry Group at Winfrith subsequent to the experiment). The relative flux-depression factor, f , was determined by fission-product γ -counting of the foils 5-15 hours after irradiation (using NaI counters with a threshold of 1.28 Mev) and comparing the measured count-rate ratio with the value expected from the known foil-enrichments. (It was assumed that the presence of the foils in the thermal-column had negligible effect on the U-235 fission to U-238 capture thermal cross-section ration - a valid assumption considering that both reaction are near $-\frac{1}{v}$ at thermal energies).

In order to obtain $Q(t)$ from the Ge(Li) counting data using Eqn. (5.2), as well as to perform a detailed analysis of the systematic and statistical errors in the measurement, a computer programme, QUOTE, was written for the KDF9 at Winfrith. Fig. 20

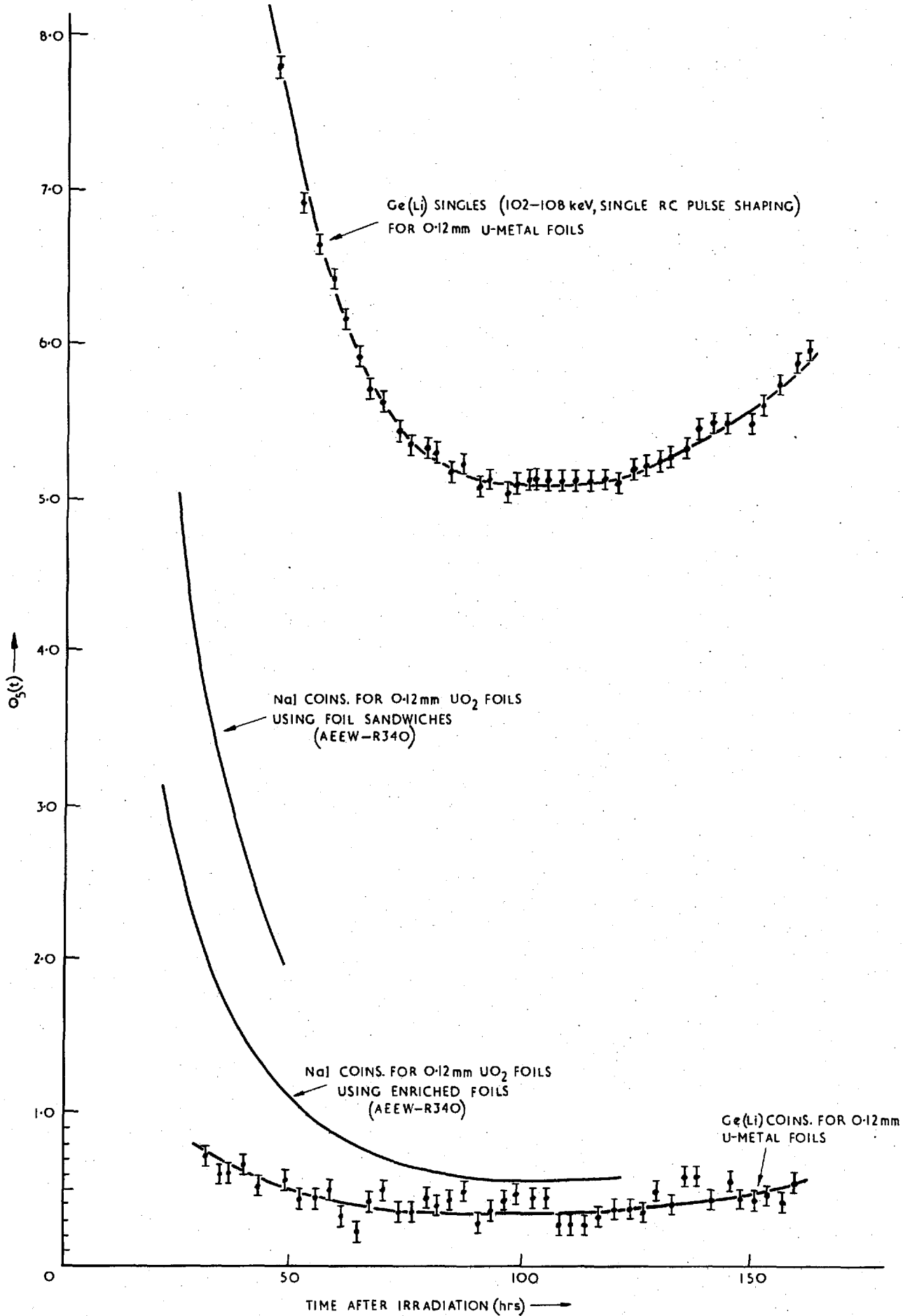


FIG.20. $Q_5(t)$ CURVES

shows the $Q_5(t)$ results obtained from the experiment for coincidence and singles counting of the 102-108 keV region with the Ge(Li) detectors - over a period of $\sim 30-160$ hours after irradiation. Also shown are typical NaI coincidence curves obtained by Brown (Ref. 22). Although these are not directly comparable, the measurements having been made with different foil materials, they do provide some indication of the much greater discrimination achieved with the Ge(Li) detectors.

5.4.3 Ge(Li) SINGLES FOR ABSOLUTE U-238 CAPTURE MEASUREMENTS

In the absolute measurement of (C_8/F_9) ratios, as described in the previous chapter, the most serious single source of error was identified as the relatively poor statistical accuracy of $\sim \pm 0.8\%$ obtained in the NaI γ -X-ray coincidence counting of the ZEBRA-irradiated deposits (Table 7). Although this might have been improved upon by increasing the irradiation time from 2 to 4 hours and by using thicker uranium deposits (up to ~ 3 mgm/cm²), an alternative approach is to substitute NaI coincidence counting by Ge(Li) singles counting of the 102-108 keV Np-239 region. The fission-product correction would be greater for the Ge(Li) singles counting (Fig. 20) but, since it is only $\sim 0.1\%$ for the NaI coincidence counting (Sec. 4.1.3), the resultant loss in accuracy would not be serious. From the $Q_5(t)$ curve of Fig. 20, a typical correction for the Ge(Li) 102-108 keV singles counting is obtained as $\sim (0.5 \pm 0.2)\%$. Although the extrapolation of the 0.12 mm. thick foil $Q(t)$ -values to deposits of ~ 0.5 mgm/cm² thickness is not strictly valid, it is a reasonable approximation within the assumed error, considering that the U X-rays are not included in the counted region and that most of the fission-product counts are due to

Compton-scattered higher-energy γ -rays (with relatively low self-absorption in the uranium). A new uncertainty, however, is the finite contribution of internally-converted Np X-rays to the singles-counting of the Am-243 deposits. This was estimated as only $\sim(0.2 \pm 0.1)\%$ and consequently not considered significant.

In order to study the feasibility of Ge(Li) singles counting of the deposits, a comparison of results obtained using this technique was made with those from the standard NaI coincidence counting - for absolute U-238 capture measurements in ZEBRA Core 8D. Table 8 summarises the results obtained for measurements in two different positions in the central 8D cell (Fig. 4).

TABLE 8. ABSOLUTE U-238 CAPTURE MEASUREMENTS IN ZEBRA 8D ($\times 10^{-16} \text{ sec}^{-1}$)

Deposit - source Combination	Position	NaI Coincidences	Ge(Li) Singles (Ch.A x Ch.B) $^{\frac{1}{2}}$
U7 - A2	1	2.43 ± 0.03	2.43 ± 0.02
U8 - A2	2	2.47 ± 0.03	2.52 ± 0.03

The statistical accuracy was a factor of $\sim 2\frac{1}{2}$ greater for the Ge(Li) singles counting but, since the total available counting time had to be divided between the two different counting methods being compared, the net accuracy was not as high as might have been achieved. However, the agreement between the different values was most promising and did indicate that, under proper conditions, better results could be obtained by Ge(Li) singles counting of the deposits. It may be noted that, by using both Ge(Li) channels for the singles counting and by considering the square root of the product of the two results, any finite error due to non-repeatability of geometry was reduced to negligible proportions.

5.4.4 U-238 CAPTURE RATIO USING NAT. U FOILS

Standard R.C.R. measurements in ZEBRA cores have involved the relative Np-239 counting of natural uranium foils irradiated in the reactor lattice and depleted foils irradiated in the thermal column (Sec. 3.3.3). The need for depleted instead of natural foils in the thermal-column irradiation has arisen from the rather high fission-product coincidence correction that has to be applied for thermal-flux irradiated natural foils, when using NaI detectors for the γ -X-ray counting. In order to confirm that this use of different foil-types in the two irradiations has not been having any unsuspected effect on the experimental R.C.R. values, a comparison of the U-238 capture ratio measurements in ZEBRA Core 8D, following the usual procedure, was made with values obtained using natural uranium foils in both irradiations and coincidence-counting these with the Ge(Li) detectors. Table 9 summarises the results from analysis programmes ANCORA (Ref. 25) and CAPRAT (written by the present author) and shows that satisfactory agreement was obtained. (The flux-depression factors for the thermal-column foils were of the order of $\sim 1\%$ (Refs. 53 and 54), so that the uncertainty in the values used for these factors was considerably less than the statistical errors in the counting.)

TABLE 9. LATTICE-TO-THERMAL U-238 CAPTURE RATIO IN 8D

Position	NaI Coins. (nat. and depl. foils)	Ge(Li) Coins. (both foils nat.)
1	1.43 ± 0.02	1.44 ± 0.02
2	1.44 ± 0.02	1.46 ± 0.02

5.4.5 COUNTING OF PU-CONTAINING SAMPLES

Fig. 21 compares Ge(Li) and NaI spectra of a 0.02 μc (Am-243: Np-239) source sandwiched between Pu-Al alloy foils containing ~ 3 mgm. of Pu. In the Ge(Li) spectrum the photopeaks of the U K X-rays from Pu α -decay are seen to be reasonably well separated from the 102-108 keV Np-239 region, although it should be stated that, in the practical case of a ZEBRA-irradiated 25% PuO₂/UO₂ foil, the relative Pu-activity would be an order of magnitude greater. The value of coincidence counting is illustrated in Fig. 22 which shows the Ge(Li) spectrum of the sandwich, in coincidence with (a) a 100-120 keV gate on a NaI counter and (b) a 102-108 keV gate on the second Ge(Li) channel.

In order to see the effect on the Ge(Li) systems of counting a larger amount of Pu, an 18 mgm. Pu-metal foil was used. It was observed that with single R-C pulse-shaping, the system resolution at 100 keV deteriorated by a factor of ~ 2 . A smaller deterioration was also observed while counting a 15% Pu-U sandwich (containing ~ 6 mgm. Pu) irradiated in NESTOR. This adverse effect was directly attributable to disturbances in the baseline of the pulses due to pile-up at high count rates, and it was found that it could be cured to a considerable degree by using the 0314-pulse shapers (Fig. 18) to restore the baseline.

Another feature of Pu-counting that was given special consideration was the effect of the enormous 60 keV γ -ray peak of Am-241 (from Pu-241 β -decay). The total pulse-duration (after double pulse-shaping) was ~ 10 -20 μsec . for the Ge(Li) systems and, with the 60 keV peak contributing count-rates of the order of several thousand per second, the effects on the counting (of dead-time, pulse pile-up, resolution deterioration, etc.) were quite significant. Considering that Pu-241 has a 13-year half-life and that most of the

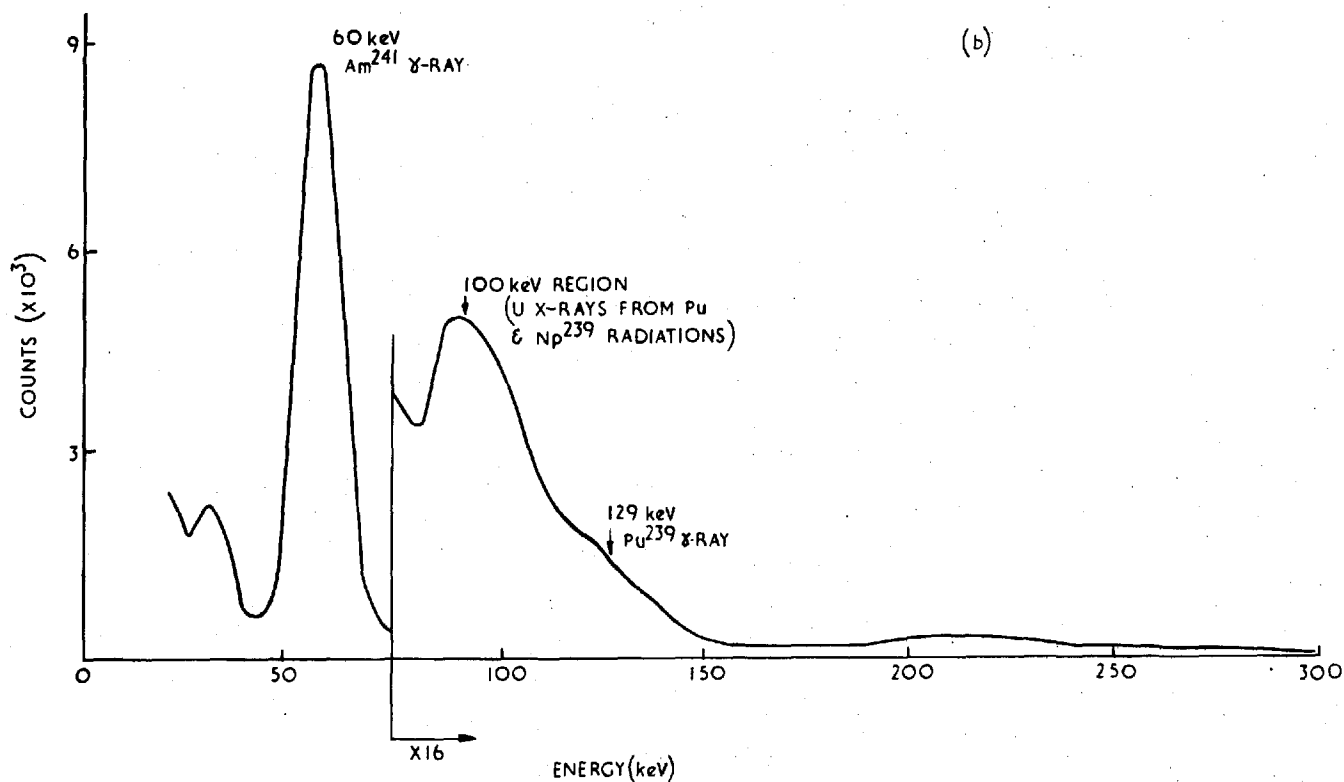
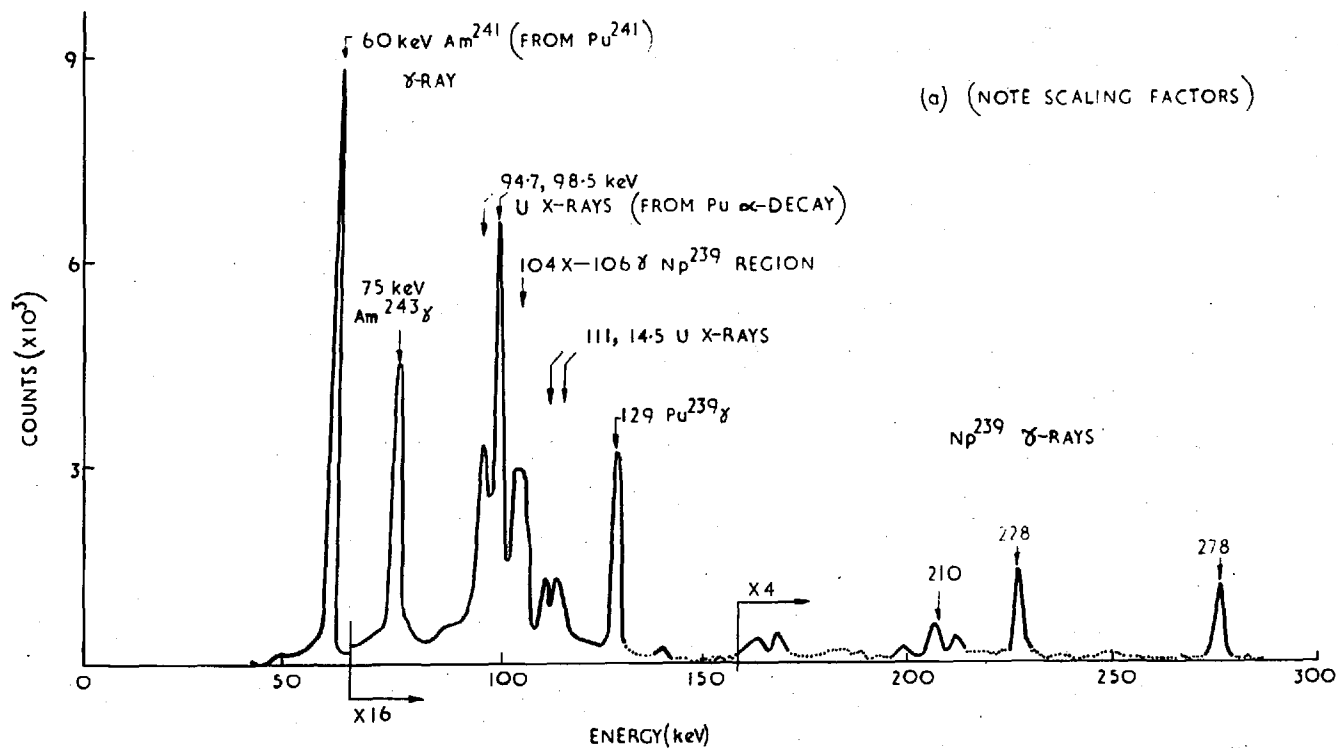


FIG. 21. (a) Ge(Li) AND (b) NaI(Tl) SINGLES SPECTRA OF 0.02 μc (Am^{243} : Np^{239}) SOURCE SANDWICHED BETWEEN TWO 1.5 mgm Pu FOLDS

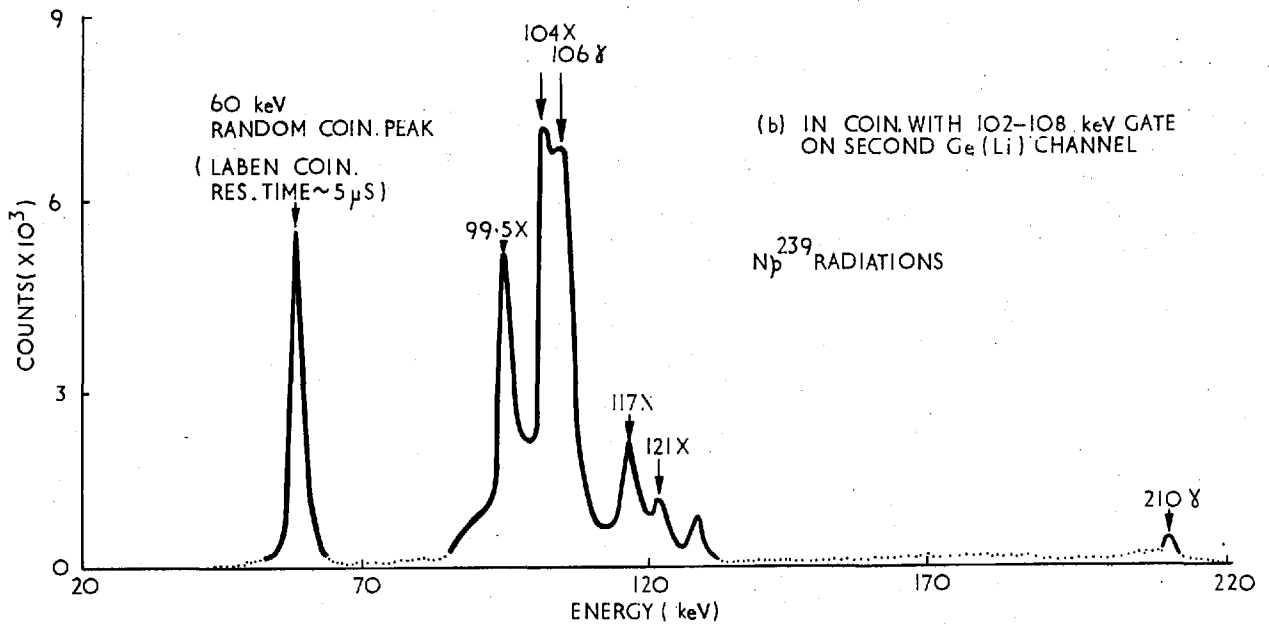
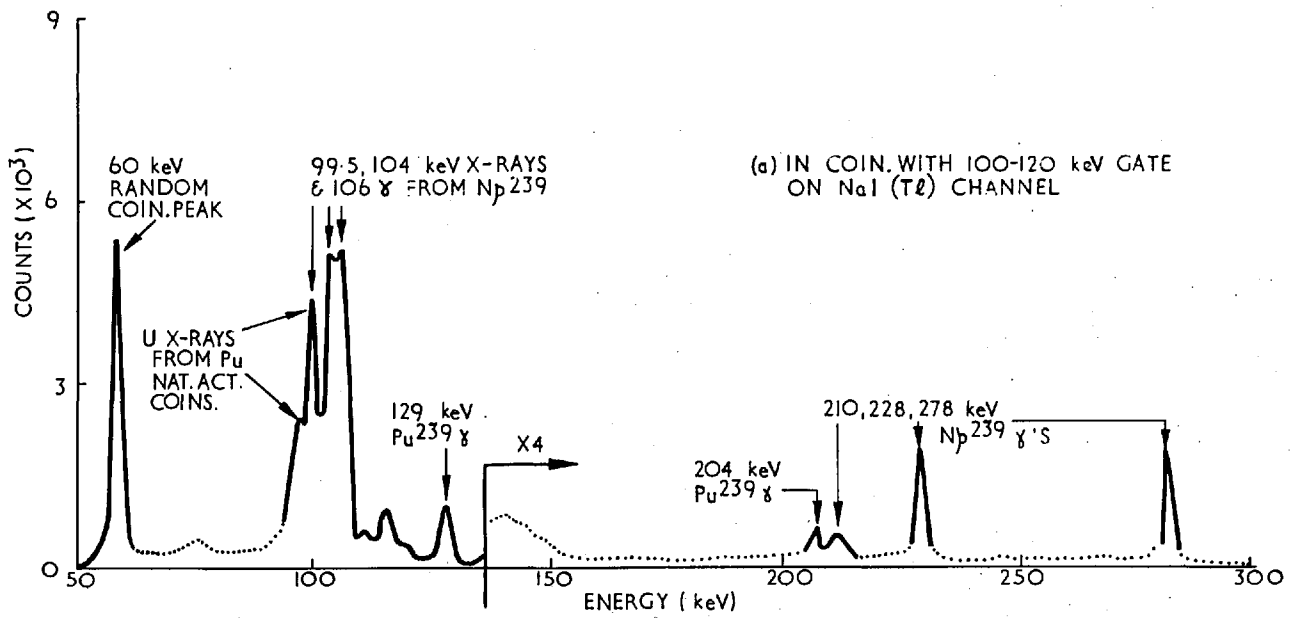


FIG. 22. Ge (Li) COINCIDENCE SPECTRA OF THE SANDWICHED SOURCE

mixed-oxide foils already available had been prepared several years previous to the present work, it was realised that it would be advantageous to use new foils for which the in-grown Am had been initially separated from the Pu by ion-exchange separation. The feasibility of this approach was established by examining the Ge(Li) γ -X-ray spectra of liquid Pu-samples (containing $\sim 1\frac{1}{2}\%$ Pu-241) before and after the Am in them had been separated out by the Chemistry Group at Winfrith (Ref. 55). Fig. 23 compares these spectra and clearly indicates how effective the Am-separation was in simplifying the observed γ -activity.

A few preliminary experiments were performed to study semi-quantitatively the effect which the presence of the 18 mgm. Pu-metal foil had on the coincidence count-rate from a 0.02 μ c (Am-243:Np-239) source, and the results from one of these experiments are given in Table 10.

TABLE 10. RESULTS FROM A PRELIMINARY PU-COUNTING EXPERIMENT

Counted Sample	Gates on Both Ge(Li) Channels	Observed True Coincidence Rate (hr ⁻¹)
18 mgm. Pu foil	96 - 123 keV	5840 \pm 50
(Am:Np) source DX	"	2900 \pm 30
Pu foil + DX	"	8000 \pm 60
18 mgm. Pu foil	102 - 108 keV	150 \pm 10
(Am:Np) source DX	"	1050 \pm 20
Pu foil + DX	"	960 \pm 20

The uncertainties in the observed count-rates were mainly due to

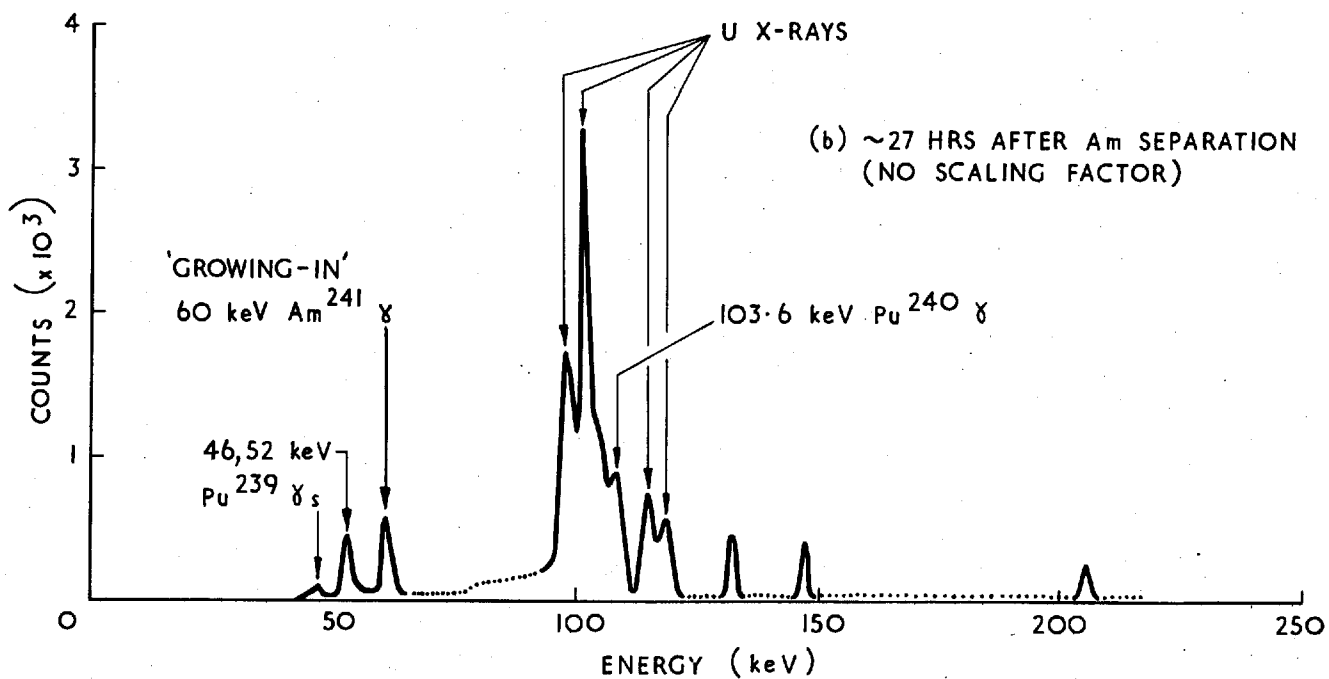
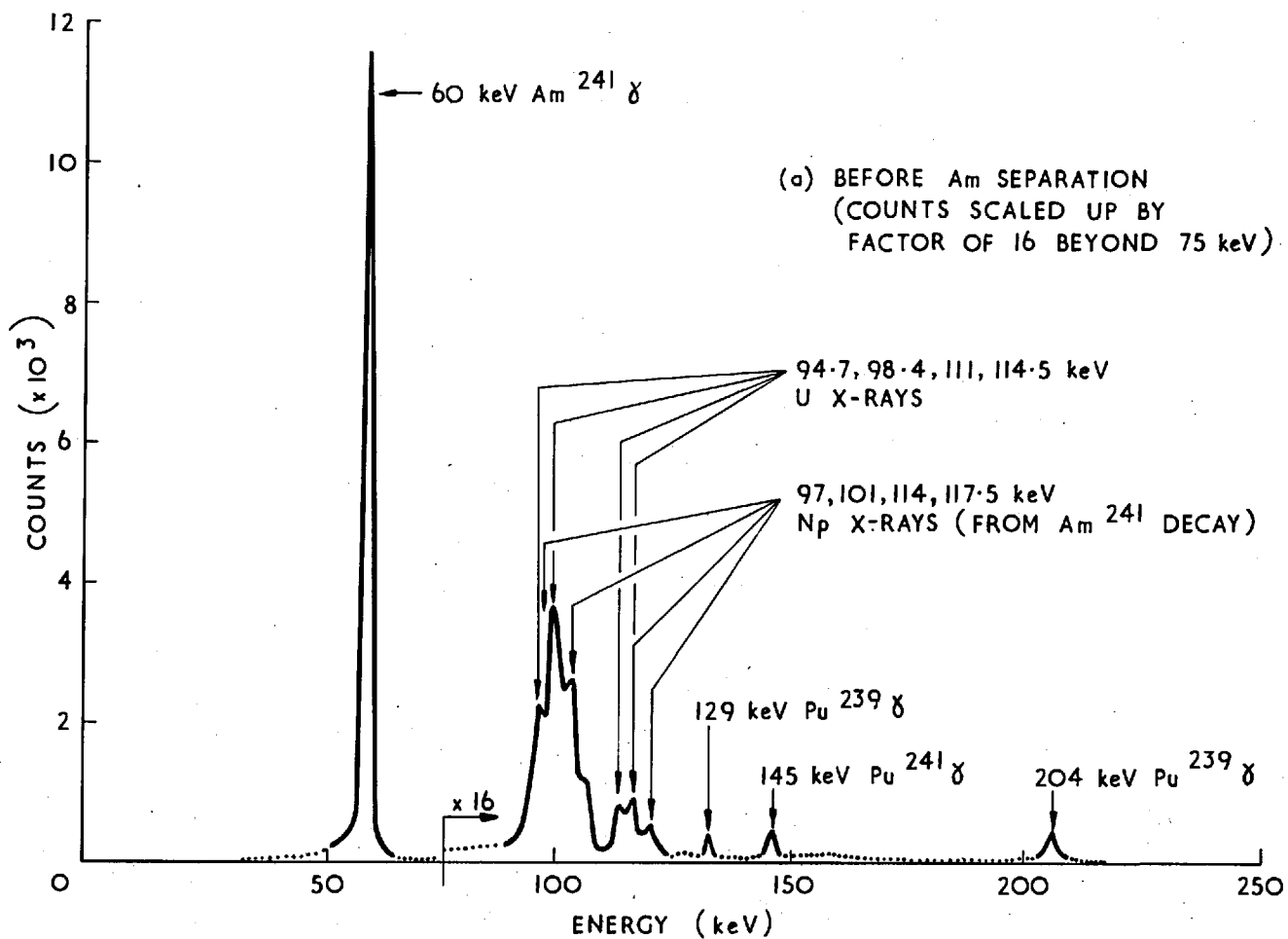


FIG. 23. Ge(Li) SINGLES SPECTRA OF LIQUID Pu-SAMPLES BEFORE AND AFTER Am-241 SEPARATION

doubts regarding the repeatability of the source-geometry. Nevertheless, there did seem to be a definite indication that coincidence counts were "lost" due to the earlier-mentioned high count-rate effects - arising mainly from the large in-grown Am-241 γ -activity of the Pu foil. This was obviously an aspect of the counting which would have to be accurately dealt with in developing a reliable technique for the proposed mixed-oxide measurements.

It can also be seen from Table 10 how, by choosing the Ge(Li) gates as 102-108 keV instead of 96-123 keV, the Pu natural-activity coincidence contribution was reduced by a factor of as high as ~ 40 . On the other hand, the reduction in Np-239 coincidences (due to the elimination of the less important Pu K X-rays) was only by a factor of $\sim 2\frac{1}{2}$.

On the whole, the general performance of the twin Ge(Li) detector system was seen to be quite promising. While the use of a 102-108 keV gate on each channel for coincidence counting seemed to be the most effective means of discriminating against Pu natural-activity and fission-product effects, it was felt that Ge(Li) singles counting of the higher-energy 278 keV γ -ray peak (Fig. 21) might provide a useful alternative approach. However, before either method could be applied with any success, for quantitatively accurate U-238 capture rate measurements in 25% PuO₂/UO₂ foils, it was essential that certain basic points - e.g. the distorting high-count-rate effects in the γ -X-ray counting, the difficulties inherent in extending the standard thermal-comparison R.C.R. technique to mixed-oxide measurements, and the possible development of absolute techniques for solid oxide foils - be given due consideration.

CHAPTER 6

ABSOLUTE U-238 CAPTURE RATE DETERMINATION USING THICK OXIDE FOILS

Although the twin Ge(Li) detector system - as described in the previous chapter - was quite capable of providing the discrimination necessary for measuring the Np-239 γ -X-ray radiations from a ZEBRA-irradiated mixed-oxide foil, one was still left with the serious problem of normalising this measured activity in some way so as to obtain the U-238 capture rate in the lattice relative to the reference reaction rate, viz. that of Pu-239 fission.

The standard R.C.R. approach (Chapter 3), of comparing the activity of the lattice foil with that of a similar foil irradiated in a thermal column, could not be directly applied to the mixed-oxide measurements for several reasons. Firstly, the fission-product correction for the thermally-irradiated mixed-oxide foil would be nearly two orders of magnitude greater than for the lattice foil and hence prove a major source of uncertainty. Secondly, the flux depression caused by the thermal-column mixed-oxide foil would be at least ~ 20 times greater than it is for natural and depleted uranium foils (Sec. 5.4.4). The situation would be worsened by the non $-\frac{1}{v}$ nature of the Pu-239 thermal fission cross-section, and this would have to be taken into account by performing error-introducing subsidiary experiments to obtain the effective thermal reference cross-section ratio.

It was realised that the use of depleted or natural uranium foils for the thermal-column irradiation would overcome the fore-mentioned difficulties, but in this case the γ -X-ray self-absorption properties of the two foil-types being compared would be different and significant error might result from the relative corrections applied. Further, with the natural activities of the two types of foils being so dissimilar, relative corrections for the different count-rate effects might prove embarrassing. In any event,

the basic drawbacks of the thermal-comparison technique for (C_8/F_9) measurements, discussed in Chapter 4, would still be present.

The thin-deposit absolute technique described in Chapter 4, for the determination of U-238 capture rates in natural uranium fuel, could not be directly applied to the ZEBRA mixed-oxide measurements. This was mainly because of the relatively large area of the thin deposits (necessary for obtaining adequate counting statistics) and the fact that, in some cases, the thickness-averaged reaction rate would not be measurable (e.g., across the diameter of a PuO_2/UO_2 pellet in the 8G pin core). However, it was realised that the absolute-technique approach had great potential value for mixed-oxide measurements and that, by developing a new method based on the use of solid oxide foils, one might overcome all the various difficulties discussed earlier, viz. (a) the thermal-column irradiation of a 25% PuO_2/UO_2 foil, (b) the comparison of different foil-types, and (c) the inherent limitations of the thermal-comparison technique. The development of such a method and a feasibility (C_8/F_9) measurement in ZEBRA Core 8E, using 0.13-0.52 mm. thick natural UO_2 foils, are described in this chapter.

6.1 THE METHOD

The two absolute reaction rate measurements involved are, once again, those of U-238 capture and Pu-239 fission.

While the absolute Pu-239 fission rate determination is quite straightforward, the technique remaining basically as described in Sec. 4.2, a new approach has to be adopted for the absolute U-238 capture measurement. Instead of a thin Am-243 deposit being used as the calibrating tool for the Np-239 γ -X-ray counting (Sec. 4.1), what is essentially required is a special mixed-oxide foil of exactly the same material composition and dimensions as the foils used in the mixed-oxide lattice irradiation, but differing in the single respect that it has an accurately

known amount of Am-243 uniformly dispersed in it. It is easily seen that, due to secular equilibrium between parent and daughter, the absolute Np-239 activity, A_s , of such a "source-foil" is equal to the Am-243 activity and is given by:

$$A_s = \frac{m_s}{f_u \cdot M} \cdot N_o \cdot y \quad \dots\dots\dots(6.1)$$

where m_s is the mass of the source-foil in gm., f_u is the fraction of uranium oxide molecules in the mixed-oxide material, M is the effective gm. - molecular weight, N_o is Avogadro's Number, and y is the absolute α -disintegration rate from Am-243 per U atom in the source-foil.

Now, if after irradiation in the lattice, the ordinary mixed-oxide foils are γ -X-ray counted on the Ge(Li) coincidence system along with this special source-foil, the induced Np-239 activity, $A(t)$, in any one of the irradiated foils may be written as:

$$A(t) = \frac{C(t)}{(1-a)} \cdot \frac{(1-a_s)}{C_s} \cdot A_s \quad \dots\dots\dots(6.2)$$

where $C(t)$ is the coincidence rate from the foil (corrected for fission-product, natural-activity and random coincidences) at time t after irradiation, C_s is the coincidence rate (corrected for natural-activity and random coincidences) from the source-foil, and a , a_s are the respective γ -X-ray self-absorption correction factors. This follows from arguments similar to those employed in Sec. 4.1.1.

Thus, using the notation of Eqn. (4.1), one obtains the absolute lattice U-238 capture rate as:

$$\begin{aligned} \text{Capture rate/U-238 atom} &= \frac{1}{k(t)} \cdot \frac{1}{N_8} \cdot A(t) \\ &= \frac{1}{k(t)} \cdot \frac{1}{N_8} \cdot \frac{C(t)}{C_s} \cdot \frac{(1-a_s)}{(1-a)} \cdot A_s \quad \dots\dots\dots(6.3) \end{aligned}$$

N_8 , the number of U-238 atoms in the irradiated mixed-oxide foil, is given by:

$$N_8 = u_8 \cdot N_o \cdot \frac{m_f}{f_u \cdot M} \dots\dots\dots(6.4)$$

where u_8 is the U-238 isotopic fraction of the uranium (e.g. 0.9928 for natural-uranium containing foils), m_f is the mass of the foil, and the other symbols are as defined for the source-foil in Eqn. (6.1).

Substituting for A_s from Eqn. (6.1) and for N_8 from Eqn. (6.4), one obtains the absolute U-238 capture rate from Eqn. (6.3) as:

$$\begin{aligned} \text{Capture rate/U-238 atom} &= \frac{1}{k(t)} \cdot \frac{y}{u_8} \cdot \frac{m_s}{m_f} \cdot \frac{(1 - a_s)}{(1 - a)} \cdot \frac{C(t)}{C_s} \\ &= K^1(t) \cdot \frac{C(t)}{C_s} \dots\dots\dots(6.5) \end{aligned}$$

$$\text{where } K^1(t) = \frac{1}{k(t)} \cdot \frac{y}{u_8} \cdot \frac{m_s}{m_f} \cdot \frac{(1 - a_s)}{(1 - a)}$$

It is easily shown that the limiting factor in the accurate determination of the parameter K^1 is the error in y . $k(t)$ is known to an accuracy of $\pm 0.1\%$ (Sec. 4.1.3), u_8 can be determined with a precision of better than $\pm 0.1\%$ by mass spectroscopy, direct weighings for determining m_f and m_s are easily made accurate to $\sim \pm 0.1\%$ and finally, with the composition and dimensions of the foil and source-foil well matched, a_s and a can be sufficiently similar to render any relative error negligible.

The determination of the quantity y can be carried out in a number of ways. The general procedure for the preparation of the source-foils (e.g., Sec. 6.2) basically involves the use of UO_2 which has been quantitatively doped, in solution, with Am-243. Thus, if W is the weight of Am-243 solution (generally as nitrate) added to g gms. of UO_2 in the doping process, and if an Am-243 deposit is prepared from w gm. of the same Am-243 solution, y is given by:

$$y = \alpha_{Am} \cdot G \cdot \frac{W}{w} \cdot \frac{M^1}{g} \cdot \frac{1}{N_0} \dots\dots\dots(6.6)$$

where α_{Am} is the count-rate from the deposit in a low-geometry α -counter with geometry factor G , and M^1 is the gm-molecular weight of UO_2 (viz., 270).

Alternatively, if an Am-243 deposit is prepared from the Am-243 obtained by quantitative ion-exchange separation (Ref. 33) from m gm. of the doped UO_2 material, one obtains y as:

$$y = \alpha_{Am}^1 \cdot G^1 \cdot \frac{M^1}{m} \cdot \frac{1}{N_0} \dots\dots\dots(6.7)$$

where α_{Am}^1 is the α -count-rate of this deposit with G^1 as the geometry factor.

Still another value of y may be obtained by Am ion-exchange separation from the final doped- UO_2 - undoped- PuO_2 mixtures, but here the analysis may be complicated by the presence of Am-241 in the Pu (Sec. 5.4.5).

The different values of y , obtained as outlined above, will be largely independent in so far as they will have been determined at different stages in the source-foil preparation. Consistency in these values will, therefore, be a useful check on the systematic accuracy of the calibrating procedure. With an established accuracy of better than $\pm 0.5\%$ in the absolute low-geometry α -counting (Sec. 4.2) and with the chemistry involved in the method being relatively straightforward, an overall accuracy of $\sim \pm 0.7\%$ in the determination of y should be attainable. Thus, the net error in the absolute U-238 capture rate, obtained from Eqn. (6.5), will be determined mainly by the statistical and systematic uncertainties in the corrected Ge(Li) γ -X-ray count-rate ratios, $\left[\frac{C(t)}{C_s} \right]$ - and not, as discussed earlier, by the serious inaccuracies inherent in other, simpler normalising procedures.

6.2 FEASIBILITY MEASUREMENT IN ZEBRA CORE 8E

In order to establish the general feasibility of the proposed method before attempting the actual mixed-oxide measurements (Chapter 7), a (C_8/F_9) determination was carried out in ZEBRA Core 8E (Sec. 3.2), using specially-prepared 8.3 mm. diameter, 0.13 - 0.52 mm. thick natural UO_2 foils and Am-243-doped natural UO_2 source-foils of similar dimensions. The experimental procedure used for the measurement is outlined below, and the results are compared with theory as well as with experimental (C_8/F_9) values obtained using the two other independent techniques for measurements in natural uranium fuel, viz. the thermal-comparison method and the thin-deposit absolute technique.

6.2.1 EXPERIMENTAL PROCEDURE

To ensure that the foils and the source-foils were - apart from the Am-243 doping in the case of the latter - of chemically identical materials, the two types were prepared in parallel and processed in similar fashion by the Chemistry Group at Winfrith (Refs. 33 and 55). An appropriate amount of UO_2 powder was first oxidized by ignition, at $\sim 800^\circ C$ for ~ 4 hours, to U_3O_8 which was then cooled, weighed and dissolved in 8N nitric acid. About $80 \mu c.$ of Am-243 (from the same batch as described in Sec. 4.1.2, i.e. having α -impurities $< 0.1\%$) had been obtained from Harwell and this was made to a stock solution of ~ 10 ml. by addition of 2N nitric acid. About a fifth of this solution was added gravimetrically to a known amount of the uranium nitrate solution. Both the doped and undoped uranium nitrate solutions were then evaporated under infra-red lamps and stirred regularly until complete crystallization had taken place. The dried crystals were ignited (at $800^\circ C$ for 4 hours) to yield doped and undoped batches of U_3O_8 , and these were subsequently converted to UO_2 in a reducing furnace. The two separate foil-materials were obtained by grinding the UO_2 to

powder, mixing with an organic binder, granulating, pressing, removing the binder by heating and then sintering at 1600°C. The foils and source-foils were finally obtained by grinding the respective materials to the specified diameter of 8.3 mm. and lapping to thicknesses of 0.13, 0.26, 0.39 and 0.52 mm., the agreement in the final foil masses being well within a few percent for each of these four thicknesses.

The factor y for the source-foils (Sec. 6.1) was firstly determined by preparing two pipetted Am-243 deposits, 1 and 2, on 0.13 mm. thick platinum discs from accurately weighted amounts of the same stock solution as used for the doping. A second, independent value of y was obtained by Am ion-exchange separation from a finished 0.39 mm. source-foil and the preparation of another deposit, 3, characterising the amount of Am-243 in a given mass of UO_2 . Table 11 summarises the results of the low-geometry α -counting of these deposits and gives the y -factor values obtained using Eqn. (6.6) for Deposits 1 and 2, and Eqn. (6.7) for Deposit 3. The agreement between the different values for y is seen to be quite encouraging and indicates the general reliability of the analysis.

TABLE 11. y -FACTOR VALUES FOR UO_2 SOURCE-FOILS USED IN CORE 8E

Am-243 Deposit	α -count rate (hr ⁻¹)	Geometry factor (x10 ⁴)	y -factor (x10 ⁻¹⁷ sec ⁻¹)
1	23320 \pm 40	0.919 \pm 0.005	4.55 \pm 0.04
1	8208 \pm 22	2.605 \pm 0.012	4.55 \pm 0.04
1	1933 \pm 10	10.91 \pm 0.05	4.48 \pm 0.04
2	9138 \pm 20	2.600 \pm 0.012	4.57 \pm 0.04
2	2133 \pm 12	10.88 \pm 0.05	4.47 \pm 0.04
3	150 \pm 1	0.233 \pm 0.002	4.47 \pm 0.06
Mean y -factor = (4.52 \pm 0.04) x 10 ⁻¹⁷ sec ⁻¹			

For irradiation of the ordinary UO_2 foils in the reactor, a special natural U metal plate was used. As shown in Fig. 24, a foil of each of the available four thicknesses was loaded into the plate with the appropriate natural U metal collets. With this arrangement, the Np-239 activity induced in each UO_2 foil could be assumed to characterise the U-238 capture at the centre of the natural U plate - except for the effect of scattering by oxygen atoms in the foil material itself. This effect was estimated as being less than $(0.2 \pm 0.1)\%$ in ZEBRA 8E for the thickest of the foils, from considerations similar to those for the aluminium backing scattering effect in thin-deposit measurements.

After a 4-hour irradiation, the four foils were counted, using 102-108 keV gates on the Ge(Li) coincidence system, together with a 0.13 mm. thick Am-243 doped UO_2 source-foil and an unirradiated ordinary UO_2 foil (for the slight natural activity corrections). In obtaining the true count-rate ratios, $\left[\frac{C(t)}{C_s} \right]$, for Eqn. (6.5), the corrections for random, natural-activity and fission-product induced coincidences, as well as for the slightly different γ -X-ray self-absorption factors for foil and source-foil, were small and relatively simple to apply. However, it was found that the complicating effects associated with gated Ge(Li) counting at high count-rates (Sec. 5.4.5), had also to be taken into account. The activity of the doped source-foils was an order of magnitude greater than for the 8E-irradiated UO_2 foils and this meant that, with the high-geometrical-efficiency positioning of the detectors, the integral count-rates for the source-foils were $>1000 \text{ sec}^{-1}$. Consequently, with the duration of the bipolar pulses entering the single-channel analysers (Fig. 18) being $\sim 10\text{-}20 \mu\text{sec}$, dead-time, pulse pile-up and resolution-deterioration effects could not be ignored.

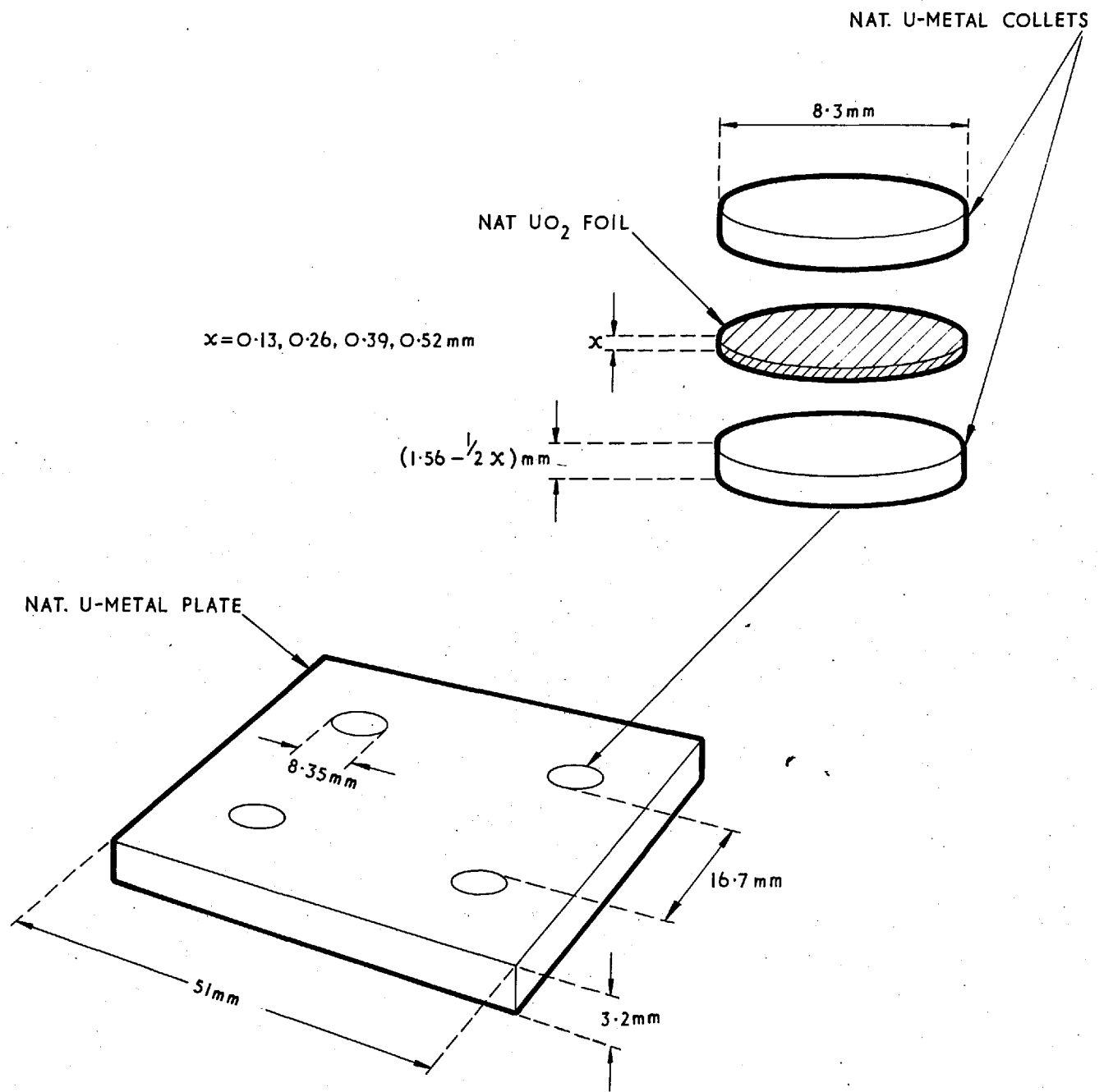


FIG. 24. LOADING PLATE FOR CORE 8E FEASIBILITY MEASUREMENT

It is impossible to apply a general analytical correction to take accurate account of all the three above-mentioned effects. Even in relatively simple activation analyses with Ge(Li) detectors, some kind of practical approach has to be adopted to overcome the difficulties at high count-rates (Ref. 56). In the present case of Np-239 γ -X-ray coincidence counting in the 100 keV region, the problem is further complicated by the fact that the absolute coincidence-counting efficiency is highly dependent on the "effective" gates on the Ge(Li) detectors and can be modified in either direction by pulse pile-up and resolution-deterioration effects. Thus, while the dead-time effect would invariably be negative, these two other effects could be negative or positive, depending on the precise single-channel settings as well as on the nature of the distortion. For example, with the gate set at 102-110 keV, either effect might increase the coincidence-counting efficiency by causing more pulses from the 99.5 keV X-ray photopeak to be included in the channel. On the other hand, loss of pulses from the 106 keV γ -ray peak may be more serious with a slightly different gate setting, and this would result in a decrease in efficiency. Further, both effects depend not only on the integral count-rate, but also on the energy spectrum of the pulses being counted. In the case of irradiated UO₂ foils and doped UO₂ source-foils, for example, the spectra are largely different because of the low uranium natural activity and the consequent prominence of the 75 keV Am-243 γ -ray peak in the source-foil spectrum (Fig. 25). Thus, for a given setting of the single-channel gates, one would expect different count-rate dependence for the effects in the two cases.

Instead of trying to apply some hypothetical correction for each individual count-rate dependent effect, a more practical method was used to yield a relatively accurate estimate of the "lumped", net

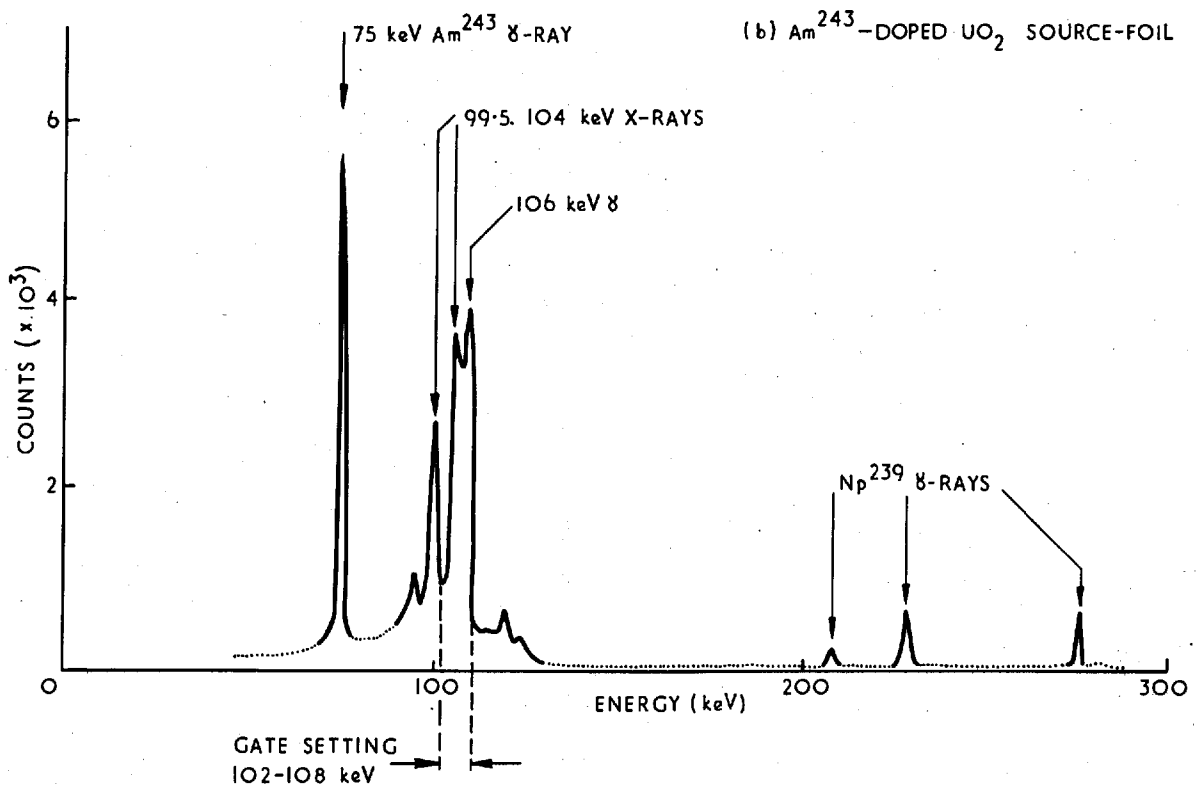
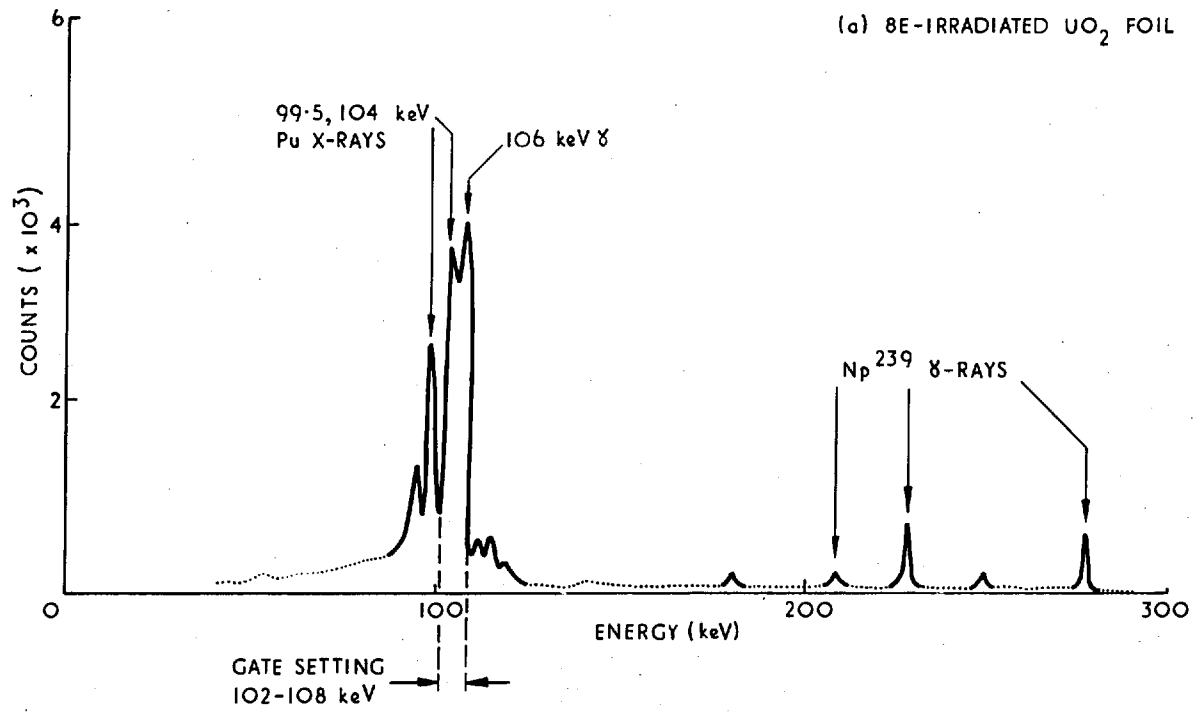


FIG. 25. Ge (Li) SPECTRA OF 8E-IRRADIATED UO_2 FOIL AND Am^{243} -DOPED UO_2 SOURCE-FOIL

effect for both the irradiated foils and the doped source-foils. This essentially involved the use of the Np-239 count-rates, from the four different thicknesses of both foil-types, to experimentally obtain the Np-239 count-rate per unit foil-mass as a function of the foil-mass itself. It may easily be seen that the resulting curves were simply the γ -X-ray self-absorption curves for the irradiated foils and the doped source-foils, modified in each case by the respective dead-time, pulse pile-up and resolution-deterioration effects. Each of these effects, as well as the γ -X-ray self-absorption, would be zero at zero foil-mass, or zero foil-thickness. Hence, by extrapolating and normalising to unity at zero foil-mass, one obtained, for each thickness and each foil-type, "modified" self-absorption factors, a and a_s , which could finally be used to yield the fully-corrected $\left[C(t)/C_s \right]$ ratios.

6.2.2 RESULTS OBTAINED IN CORE 8E

The absolute U-238 capture measurement was made by replacing one of the central natural U plates of the central 8E cell (Fig. 4) by the special loading plate described in the last section. A factor of (1.004 ± 0.002) had been determined by the use of foils (Ref. 25) to convert the measured U-238 capture rate to the average value in the 8E cell, and it is this latter value which will be quoted in the results.

A computer programme, FOILAB, had been written to analyse the experimental data and yield a statistically-weighted mean value of the absolute U-238 capture rate from Eqn. (6.5). Although most of the input data (e.g., the y -factor and its associated error, the length of the irradiation, the coincidence resolving time, the fission-product and natural-activity corrections, etc.) could be fed in directly, the "modified" self-absorption factors

defined in the last section had to be obtained separately before the final results could be computed. To start with, constant a , a_s values were assumed (viz., unity in each case), and FOILAB was used to calculate the relative "observed" Np-239 activities (from both Ge singles and Ge coincidence counting of the 102-108 keV region) for the four different-thickness irradiated UO_2 foils. These different values were normalised to those for the 0.13 mm. thick foil, and then extrapolated to unity at zero foil-mass to yield the "modified" self-absorption curves of Fig. 26. Similar curves for the doped source-foils had been determined earlier by counting the four different-thickness source-foils prior to the irradiation and these curves are also shown. Tables 12(a) and 12(b) summarise the various numerical a , a_s values obtained. (The values quoted for the Ge(Li) singles counting are, in each case, the square root of the product of the individual single-channel values, hence eliminating any finite geometry-effects).

TABLE 12. "MODIFIED" SELF-ABSORPTION FACTORS FOR

(a) THE 8E-IRRADIATED UO_2 FOILS AND (b) THE DOPED UO_2 SOURCE-FOILS

(a)

Irr. Foil	Nom. Thick. (mm)	Mass (mgm)	Rel. 102-108 keV Np-239 Activity			
			Ge Coincidences		Ge Singles	
			Meas.	Extrap. a	Meas.	Extrap. a
-	0.0	0.0	-	1.0	-	1.0
F111	0.13	65.88	1.0	0.830	1.0	0.926
F121	0.26	132.94	0.821	0.681	0.927	0.858
F131	0.39	202.45	0.671	0.557	0.855	0.792
F141	0.52	276.05	0.551	0.457	0.786	0.782

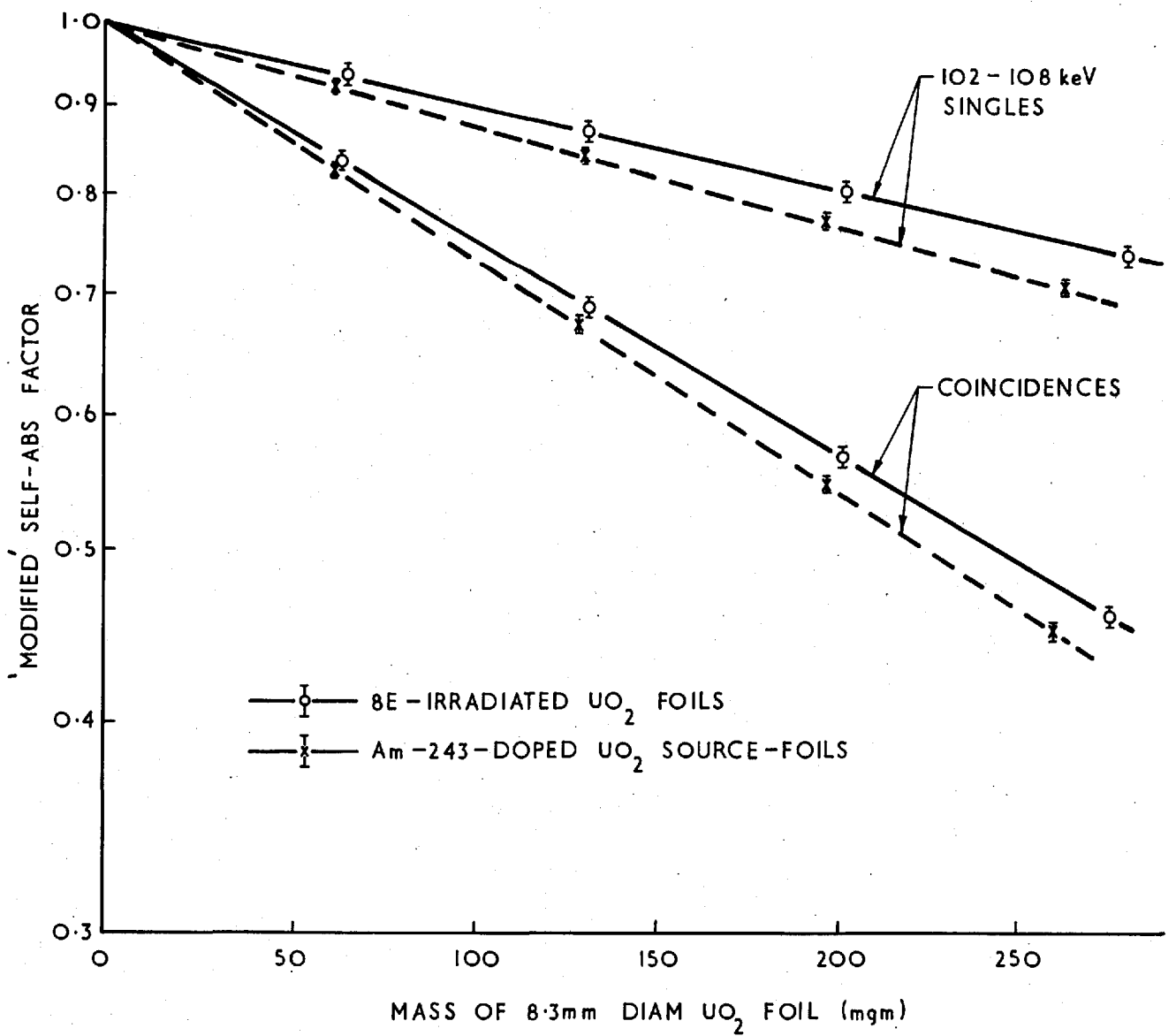


FIG. 26. 'MODIFIED' SELF-ABSORPTION CURVES FOR UO₂ FOILS AND SOURCE-FOILS

(b)

Source-Foil	Nom. Thick. (mm)	Mass (mgm)	Rel. 102-108 keV Np-239 Activity			
			Ge Coincidences		Ge Singles	
			Meas.	Extrap. a_s	Meas.	Extrap. a_s
-	0.0	0.0	-	1.0	-	1.0
S111	0.13	62.87	1.0	0.823	1.0	0.917
S121	0.26	130.49	0.818	0.673	0.913	0.838
S131	0.39	196.52	0.656	0.540	0.829	0.761
S142	0.52	259.67	0.545	0.449	0.767	0.704

Using the appropriate "modified" self-absorption factors from Table 12 and the mean γ -factor value of Table 11, FOILAB finally yielded a value of $(2.00 \pm 0.003) \times 10^{-16} \text{ sec}^{-1}$ for the absolute U-238 capture rate in the central 8E cell, exactly the same value being obtained from both the Ge coincidence and the Ge singles counting data. Though this exact agreement in the results from the two different counting techniques was fortuituous to a certain extent, it did indicate the general validity of the extrapolation procedure used for obtaining the a , a_s values since, as may easily be shown, the "modified" self-absorption curves for Ge singles and Ge coincidences in the 102-108 keV region (Fig. 26) are quite independent of each other.

The absolute Pu-239 fission rate in the central 8E cell, during the same 4-hour irradiation, was determined according to the procedure outlined in Sec. 4.2.3 - i.e., by combining Pu foil measurements, in the Pu plate and in a dummy fission chamber, with measurements made using the absolute Pu-239 fission chambers ZEB-31 and ZEB-32. The value determined was $(1.64 \pm 0.02) \times 10^{-15} \text{ sec}^{-1}$. Using this in conjunction with the FOILAB result for the

absolute U-238 capture rate, the $(C_8/F_9)_{8E}$ ratio was finally obtained as (0.122 ± 0.003) .

An absolute U-238 capture measurement using the thin-deposit technique for natural uranium fuels (Sec. 4.1) was also carried out in ZEBRA 8E, but this was done during a separate 4-hour irradiation together with a separate absolute Pu-239 fission measurement. A value of (0.117 ± 0.002) was obtained for the central 8E (C_8/F_9) ratio from this measurement.

Standard thermal-comparison measurements had been carried out in parallel, during the two 8E irradiations for the absolute reaction-rate experiments, and these yielded a mean $(C_8/F_9)_{8E}$ ratio of (0.117 ± 0.003) (Ref. 25).

The value predicted by theory for the central 8E (C_8/F_9) ratio was 0.120. This had been obtained from the infinite-lattice MURAL-FGL4 value of 0.1271 by applying a correction factor of 1.060, the latter having been derived from reactor calculations made using SCRAMBLE as outlined in Sec. 2.5 (Refs. 12 and 14).

All the various results obtained for $(C_8/F_9)_{8E}$ are summarised in Table 13.

TABLE 13. (C_8/F_9) RESULTS FOR CORE 8E

Experiment			Theory
Abs. Thick-foil Tech.	Abs. Thin-deposit Tech.	Therm. Comp. Tech.	
0.122 ± 0.003	0.117 ± 0.002	0.117 ± 0.003	0.120

The fact, that the experimental results from the three independent techniques used agreed within the estimated errors, was a sufficient indication of the validity of the new thick-foil

absolute method. The simple, practical procedure of exponential extrapolation, adopted for dealing with the Ge(Li) high count-rate problem, seemed to have been quite effective. However, it had to be borne in mind that the high count-rate effects in the present case were of a different nature to what they would be for the absolute mixed-oxide measurements. In the present instance, the considerable differences in integral γ -activity and γ -energy spectrum, between foil and source-foil, were mainly due to the "overdoping" of the latter, as a consequence of which relative corrections of the order of 2% had to be applied for the 0.13 mm. thick foils (Fig. 26). For mixed-oxide measurements, on the other hand, the predominant contribution to the γ -X-ray activity of both the foils and the source-foils would be the natural Pu activity. As this would be exactly the same in the two cases, both the integral count-rates and the overall γ -energy spectrum of the foils and the source-foils would be much more similar to each other than they were in the 8E UO₂ measurement. This would mean that the high count-rate effects, particularly those due to pulse pile-up and resolution deterioration, would be almost the same, hence causing the two "modified" self-absorption curves to nearly overlap and making relative errors in any corrections applied negligibly small.

CHAPTER 7

MEASUREMENTS AND ASSESSMENTS IN THE MIXED-OXIDE CORES ZEBRA 8F AND 8G

7.1 TECHNIQUES EMPLOYED AND TYPES OF MEASUREMENTS MADE

Although the proposed thick-foil absolute U-238 capture technique had been proved feasible by the Core 8E UO₂-foil experiment described in the last chapter, its actual application to mixed-oxide measurements was yet to be fully established. As such, it was decided that a number of different approaches be independently employed for the (^{C8/F9}) measurements in Cores 8F and 8G, so that the results obtained using the various methods could be directly compared and their relative merits properly assessed.

The difficulties inherent in the extension of the standard R.C.R. technique to mixed-oxide measurements were discussed in Chapter 6. While the uncertainties associated with the use of a thermal-column irradiated 25%, or 16%, PuO₂/UO₂ foil were seen to be too great for the direct R.C.R. approach to be practicable, it was mentioned how natural, or depleted, UO₂ foils might be used instead, for the thermal irradiation. In this case, the difficulties would be (a) the different γ -X-ray self-absorption effects, and (b) the different count-rate effects, in the counting of the lattice and thermal-column foils. Both (a) and (b) being zero at zero foil-mass, or zero foil-thickness, one could - by using mixed-oxide and UO₂ foils of different thicknesses - obtain "modified" self-absorption curves for the two foil-types (Sec. 6.2.1) and thence, the corrected lattice-to-thermal count-rate ratios. The accuracy of such an approach would obviously be limited by the magnitude of the relative corrections applied, i.e. by the difference in the slopes of the two "modified" self-absorption curves.

It is easily seen that, from this latter point of view, the Ge(Li)

singles counting of one of the higher-energy Np-239 γ -ray peaks has several advantages over the γ -X-ray coincidence counting of the 102-108 keV region. Firstly, the γ -absorption coefficients in uranium and plutonium are a factor of nearly 2 lower at 250 keV than at 100 keV (Ref. 39). This, coupled with the fact that one would be counting single γ -rays and not coincidence events, would render relative corrections for the different self-absorption effects in the two foil-types a factor of ~ 3 smaller. Further, differences in count-rate effects would be less significant for the higher-energy Np-239 counting. While the effective singles dead-time corrections would be half those for the coincidence counting, effects due to pulse pile-up and resolution deterioration would be inherently smaller at the higher energies because of the much simpler pulse-height distribution (cf. that in the 100 keV region). Finally, statistical errors for the higher-energy singles counting would be about a factor of two less than those for 102-108 keV coincidence measurements.

The obvious drawback in employing the singles-counting approach is that, in general, it is a considerably less effective means of discriminating against Pu natural-activity and fission-product events than is the 102-108 keV γ -X-ray coincidence method (Chapter 5). Thus, the 210 keV Np-239 γ -ray peak cannot be used because of its proximity to the large 208 keV natural-activity peak (due to U-237 from Pu-241 α -decay), while the 228 keV Np-239 γ cannot be employed because there is a high-yield fission-product (Te-132) γ -ray of approximately the same energy.

The 278 keV Np-239 γ -ray, however, was seen as being potentially very useful because it lies in a flat and relatively low count-rate part of the Pu natural-activity (Fig. 21(a)) and fission-product (Fig. 19(b)) γ -ray spectra. Preliminary experiments indicated that the

relative natural-activity corrections, for 278 keV singles and for 102-108 keV coincidence counting, were quantitatively similar but that the fission-product correction would be about an order of magnitude larger for the 278 keV singles counting. However, as the latter correction can be applied more accurately in the case of singles counting (see following Section), the resulting error was not expected to be very much greater.

With all the various considerations in mind, several different types of U-238 capture measurements were made in the mixed-oxide cores. The standard R.C.R. method was applied using 0.13 mm thick UO_2 foils in the UO_2 , as well as in the PuO_2/UO_2 , fuel of the central test-region cells (Ref. 25). The thin-deposit absolute technique, described in Chapter 4, was employed for measurements in the natural UO_2 plates of the 8F and 8G cells (Fig. 4). The mixed-oxide measurements were made using (i) the thick-foil absolute technique of Chapter 6, and (ii) the modified thermal-comparison procedure discussed earlier, i.e. with mixed-oxide foils in the lattice and UO_2 foils in the thermal column. An additional experiment carried out, in both Cores 8F and 8G, was the direct comparison of the Np-239 activities from UO_2 and mixed-oxide foils of different thicknesses after they had been simultaneously irradiated in the mixed-oxide fuel.

As far as possible, both 102-108 keV γ -X-ray coincidence counting and 278 keV singles counting were employed in the Ge(Li) monitoring of the Np-239 radiations so that, for each measurement, two independent results could be obtained and compared. The gate chosen for the singles counting was $[278 \pm \frac{1}{2}(\text{F.W.H.M.})]$ keV for each detector, the F.W.H.M. being ~ 2.2 keV at this energy. This choice of the channel-width was made as a compromise between the discrimination achieved, the statistical

accuracy of the counting and the electronic gain stability. Besides, the simple visual setting up procedure with the Laben analyser (Sec. 5.3) could be applied quite accurately in this case. Fig. 27 shows a block-diagram of the additional electronics used to extend the earlier-described coincidence system (Fig. 18) such that it could monitor the 278 kev singles at the same time as counting the 102-108 kev coincidences. The combined use of both detector channels for the singles counting eliminated any finite geometry-effects, as discussed previously (Secs. 5.4.3 and 6.2.2).

7.2 FISSION-PRODUCT CORRECTION MEASUREMENTS

The determination of $Q(t)$ factors, for standardising the fission-product corrections applied to the observed activity of irradiated foils was described in Sec. 5.4.2. Before accurate quantitative results could be obtained from the mixed-oxide core measurements, it was necessary to ascertain the appropriate $Q_9(t)$ factors for both 102-108 kev coincidences and $[278 \pm \frac{1}{2} \text{ (F.W.H.M.)}]$ kev singles counting.

16% PuO_2/UO_2 , 25% PuO_2/UO_2 and natural UO_2 foils of 0.13, 0.23 and 0.30 mm thicknesses had been prepared for the Core 8F measurements by the Winfrith Chemistry Group (Ref. 55) - initial separation of Am-241 having been effected for the plutonium used (Sec. 5.4.5) - and suitable pairs of these foils were used for the present $Q_9(t)$ measurements. Specially designed graphite holders and a rotator were used for irradiating the foils in the NESTOR thermal column, the measuring and calculational procedure being essentially the same as for the $Q_5(t)$ measurements of Sec. 5.4.2. The determination of the relative flux-depression factor, however, was slightly less accurate in the present case as calibration factors (Ref. 25) had to be used for relating the observed fission-product γ -activity, above 1.28 Mev, to the actual

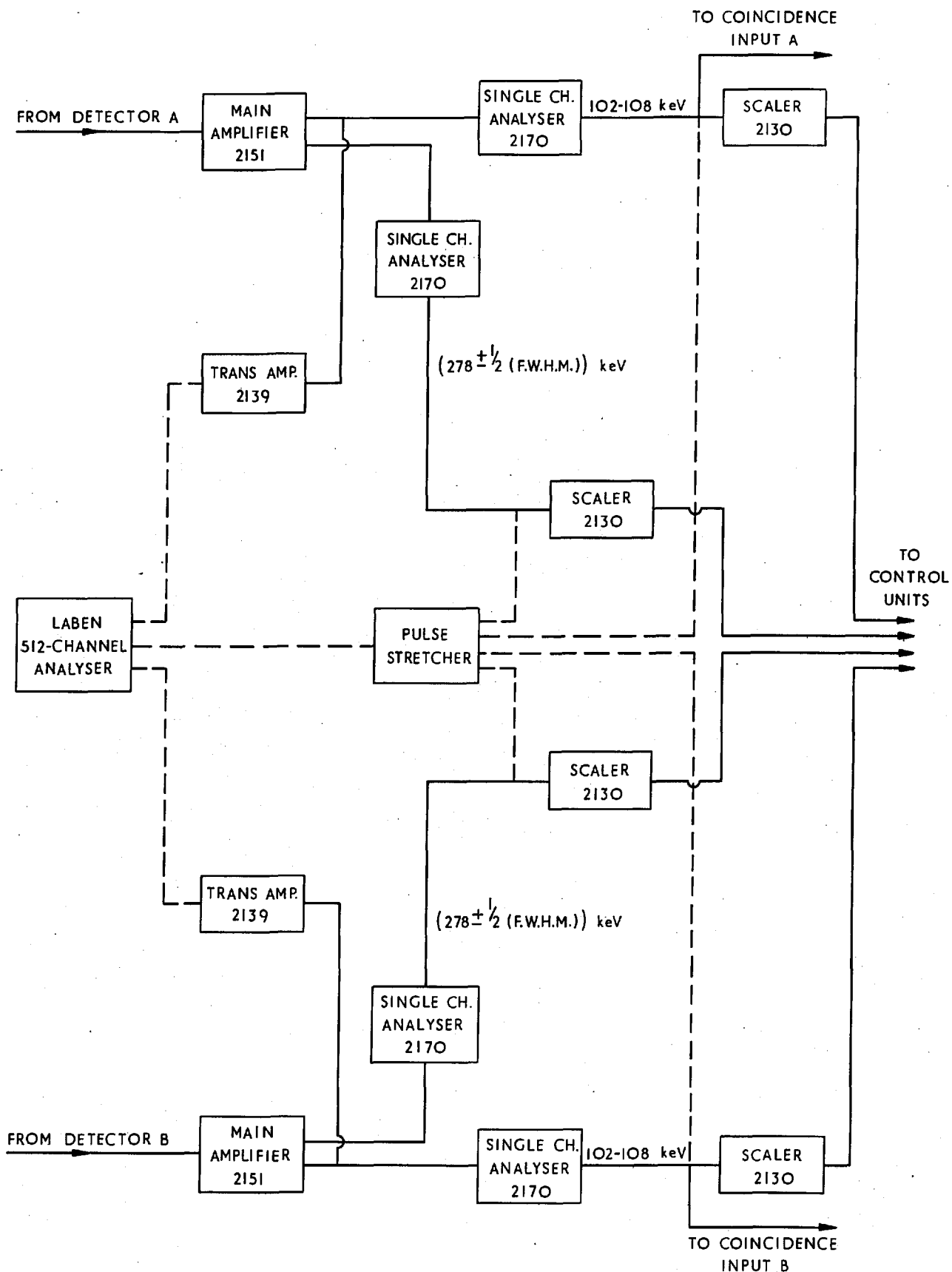


FIG. 27. BLOCK-DIAGRAM OF ADDITIONAL ELECTRONICS FOR SIMULTANEOUS 278 keV SINGLES COUNTING

fission rates in the different isotopes (i.e., Pu-239, Pu-241 and U-235). This was not serious in view of the relatively low overall accuracy sought in the measurements.

Fig. 28 shows 4-hour $Q_9(t)$ results obtained using QUOTE for the 102-108 kev coincidence counting of (a) 0.13 mm thick natural UO_2 and 25% PuO_2/UO_2 foils, (b) 0.23 mm UO_2 and 25% PuO_2/UO_2 foils, and (c) 0.23 mm UO_2 and 16% PuO_2/UO_2 foils. It is seen that, to $\sim \pm 20\%$ accuracy, the $Q_9(t)$ values may be regarded as being independent of the thickness and enrichments of the foils used for the measurements. Thus, one single, averaged curve has been drawn through the various points.

For the $[278 \pm \frac{1}{2}(\text{F.W.H.M.})]$ singles counting, the fission-product correction was recognised as being of a much more simple nature than that for 102-108 kev coincidences since, in this case, the contribution to the observed count rate is mainly via Compton-scattered events and not due to any X-ray excitation in the foil material. The dependence of the correction on the foil thickness could, therefore, be safely ignored except for self-absorption effects. 4-hour $Q_9(t)$ measurements, for the 278 kev singles counting with the two Ge(Li) detectors, were made using 0.23 mm thick UO_2 and 16% PuO_2/UO_2 foils, and the QUOTE results obtained for Detector A are shown in Fig. 29.

In view of the importance of the fission-product correction for the 278 kev singles counting, an independent approach was applied to check the accuracy of the $Q_9(t)$ values. This essentially involved the direct measurement of the fission-product correction, for the mixed-oxide foils irradiated in Cores 8F and 8G, at different times after irradiation. To determine each point, a multi-channel spectrum of the 250-300 kev region was obtained using the Laben, and the 278 kev peak was treated as a Gaussian sitting on a flat background made up of Compton-scatters from (a) higher-energy Np-239 γ -rays (Fig.14), (b) Pu

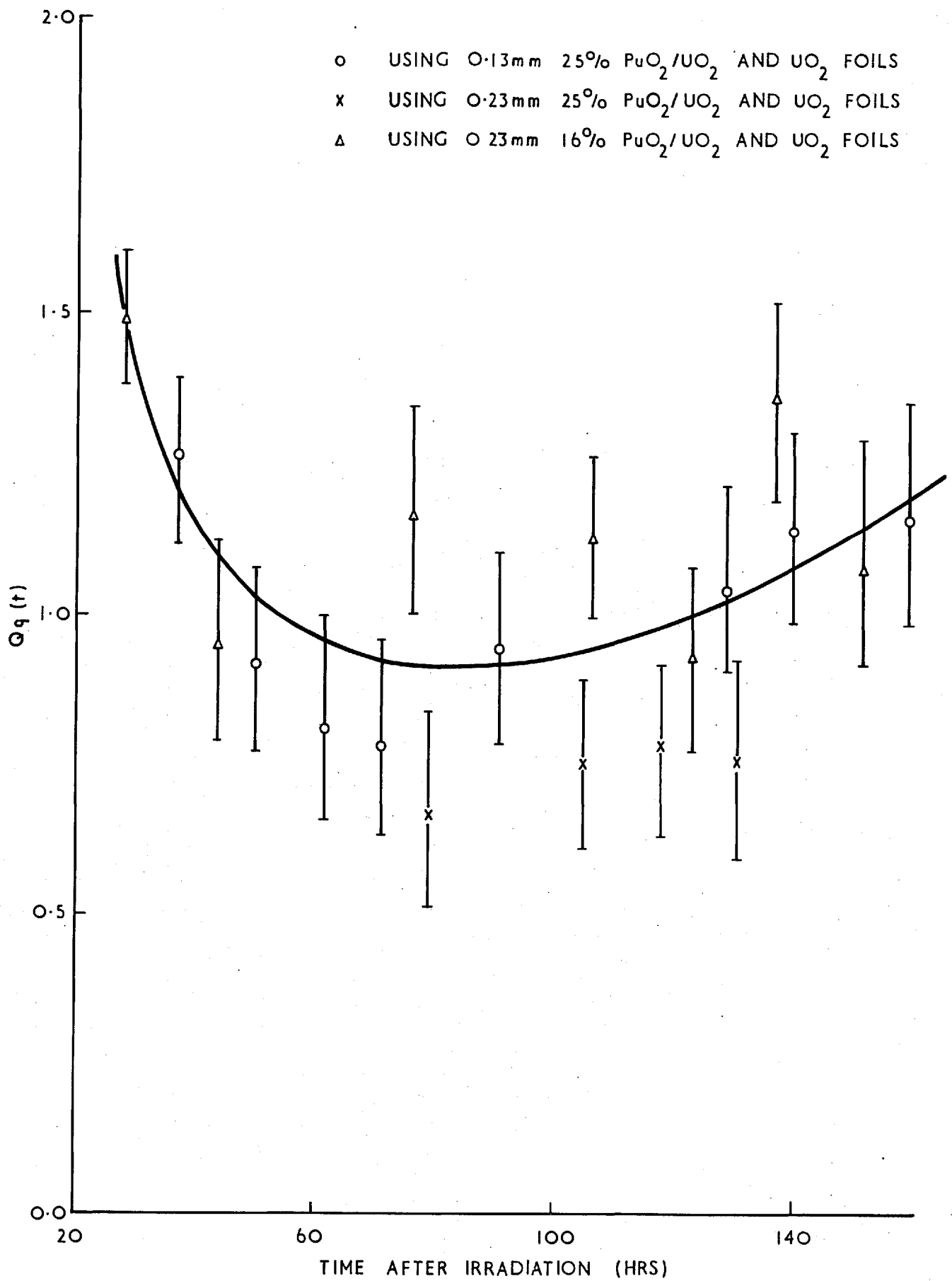


FIG. 28. Ge(Li) 102-108 keV COINCIDENCE COUNTING Qq(t) RESULTS

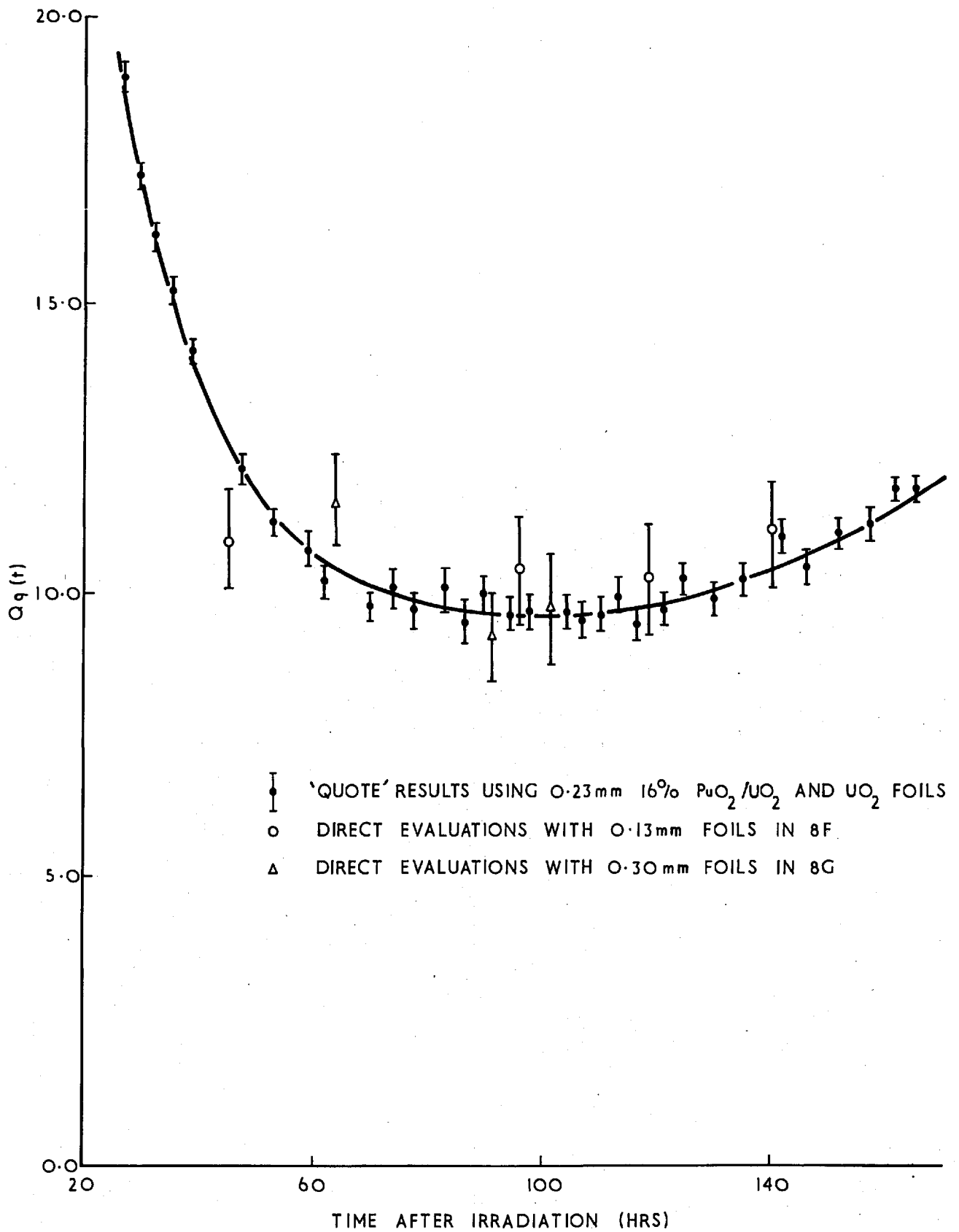


FIG. 29. $(278 \pm \frac{1}{2} \text{ (F.W.H.M)})$ keV SINGLES COUNTING $Q_g(t)$ RESULTS FOR Ge (Li) DETECTOR A

natural-activity γ 's, and (c) fission-product γ 's. Contributions (a) and (b), to the flat background, were estimated within the gated region of interest, viz. $[278 \pm \frac{1}{2}(\text{F.W.H.M.})]$ kev, by quantitative consideration of the spectra from a simple (Am-243 : Np-239) source and an unirradiated mixed-oxide foil, respectively. The fission-product contribution, (c), could then be obtained as a fraction of the Np-239 counts in the gate. Typical values of (a), (b) and (c) expressed as percentages of the total counts, were 1.5, 15.0 and 8.5%, respectively, and an accuracy of $\sim \pm 10\%$ was achieved in each of these direct evaluations of the fission-product correction. $Q_9(t)$ values for Detector A, deduced from some of the directly evaluated points by appropriate normalisation and correction for self-absorption, are shown in Fig. 29 along with the QUOTE results. The general agreement obtained confirmed the absence of any unsuspected error in the fission-product correction measurements, and the error introduced in the U-238 capture results due to this particular correction was estimated as $< \pm 0.5\%$ - for both 102-108 kev coincidences and 278 kev singles counting.

7.3 MEASUREMENTS IN CORE 8F

The (C^8/F_9) measurements made in the central 8F cell (Fig. 4) may be divided into two categories, viz. those for the UO_2 plates and those for the 25% PuO_2/UO_2 plate.

7.3.1 UO_2 -PLATE MEASUREMENTS

The standard R.C.R. technique was applied to the UO_2 -plate measurements as described in Sec. 3.3.3. A factor of (1.018 ± 0.004) was determined to yield the average U-238 capture rate in a UO_2 , or PuO_2/UO_2 , plate from measurements made with centrally-loaded foils and, for the Pu-239 fission ratio measurement, a calibration factor was obtained in the usual manner for relating the integral

fission- γ counting to the true fission ratio (Ref. 25).

In order to check the validity of Ge(Li) [$278 \pm \frac{1}{2}$ (F.W.H.M.)] keV singles γ -counting for U-238 capture measurements, an additional R.C.R. determination, using natural UO₂ foils in both the UO₂ plates and in the thermal column, was made applying this technique. Edge-effects in the Ge(Li) counting of the lattice-irradiated foils (Ref. 22) had been shown to be $< 0.2\%$, and no correction was therefore necessary for these effects. Fission-product corrections of $(5.4 \pm 0.4)\%$ and $(0.8 \pm 0.2)\%$ were applied for the thermal-column and lattice foils respectively, and the flux-depression factors used for the former were $\sim(1.0 \pm 0.3)\%$ (Sec. 5.4.4).

Thin-deposit absolute U-238 capture measurements were made in the 8F cell using special loading plates of the type shown in Fig. 30. The experimental procedure was exactly as described in Sec. 4.1 except that, with the UO₂-plate measurement being made in the central plane of the plate, a factor had to be determined to relate the result to the reaction rate averaged through the thickness of the plate. This was done experimentally using foils and theoretically by performing a 12-region MURAL calculation for the 8F cell. A value of (1.041 ± 0.004) was deduced for the factor. The absolute Pu-239 fission rate in the mixed-oxide plate, during the same 4-hour irradiation, was determined as described in Sec. 4.2.3, i.e. by the combined use of foils and the absolute chambers ZEB-31, 32.

The last type of (^{G8/F9}) measurement carried out for the 8F UO₂ plates was one employing the thick-foil absolute technique of Chapter 6. 6.3 mm x 5.5 mm natural UO₂ foils and Am-243-doped UO₂ source-foils, of 0.13, 0.23 and 0.30 mm thicknesses, had been prepared by the Chemistry Group at Winfrith (Ref. 55) using

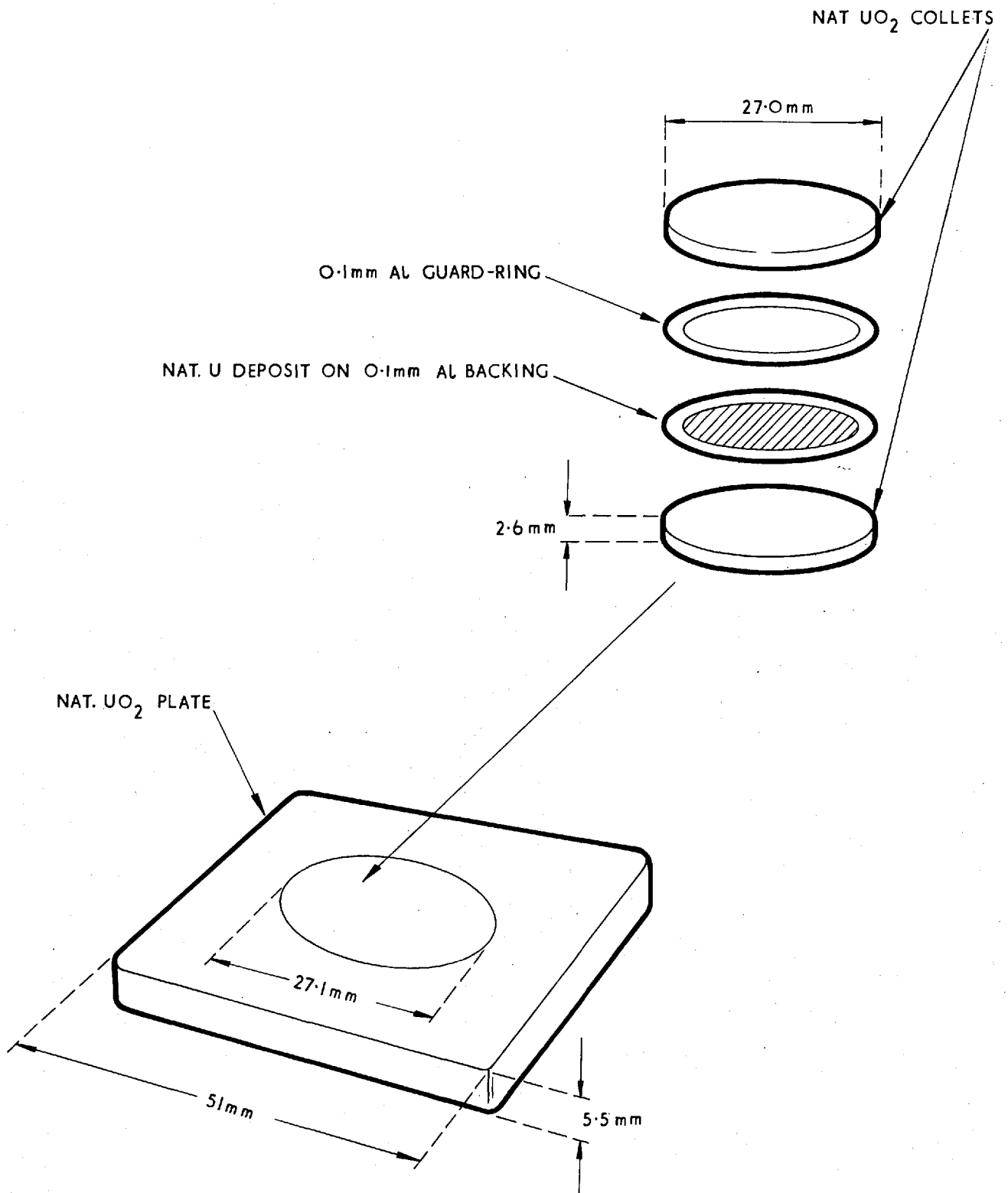


FIG. 30. LOADING PLATE FOR THIN-DEPOSIT MEASUREMENTS IN CORES 8F AND 8G

essentially the same procedure as outlined in Sec. 6.2.1. Care had been taken in this case, however, to keep the Am-243 content of the source-foils down to an appropriate level, and a slightly different approach had been used to obtain the doped UO_2 . As the latter modification involved the initial doping of a smaller quantity of UO_2 , followed by dry-mixing with undoped UO_2 , the chemistry effort was simplified. However, with no quantitative homogeneity tests having been carried out during the mixing process in the present instance, a slight discrepancy was obtained for the finished source-foils, viz. a spread of $\sim 2\%$ in their specific Am-243 content. Although this meant that reliable "modified" self-absorption curves could not be obtained, it was felt that - with the source-foils not being "overdoped" (Sec. 6.2.2) and with 278 kev singles counting being applied (Sec. 7.1) - any relative "modified" self-absorption corrections for foils and source-foils of similar thicknesses could safely be assumed negligible. A mean y-factor value of $(1.08 \pm 0.01) \times 10^{-17} \text{sec}^{-1}$ was determined for the source-foils using the procedures outlined for the Core 8E measurement (Sec. 6.2.1) and, by γ -counting intercalibrations, correction factors for individual source-foils were deduced to $\sim \pm 0.3\%$ accuracy.

The final results obtained for the various 8F UO_2 -plate (C_8/F_9) measurements are given in Table 14, and it can be seen that agreement between the different experimental techniques was within the individual errors.

TABLE 14. (C_8/F_9) RESULTS FOR THE 8F UO_2 PLATES

Technique Applied	Result
R.C.R. (NaI, 95-115 kev coins.)	0.152 ± 0.003
R.C.R. (Ge(Li), 278 kev singles)	0.154 ± 0.003
Thin-deposit absolute	0.156 ± 0.003
Thick-foil absolute	0.155 ± 0.003
Theory	0.147

The theoretical prediction quoted in Table 14 for the 8F UO_2 -plate (C_8/F_9) ratio was obtained by applying a SCRAMBLE-calculated correction factor of 0.988 (Ref. 12) to an infinite-lattice MURAL-FGL4 value of 0.1456, using the methods described in Chapter 2. Another important aspect of the experiment-theory comparison for the 8F U-238 capture measurements was that of heterogeneity effects - Core 8F having been designed primarily as a more-homogeneous version of the soft-spectrum assembly, 8A (Sec. 3.2). A thin-deposit absolute U-238 capture measurement had been carried out in one of the graphite plates of the 8F cell at the same time as in the adjacent UO_2 plate, and a fine-structure ratio of (1.87 ± 0.02) had been obtained relative to the centre of the UO_2 plate. This, when compared with the MURAL-predicted value of 1.72, showed that the theoretical underestimation (by 5-10%) of the U-238 capture heterogeneity in Core 8F was along the same lines as for Core 8A (Appendix A.1).

7.3.2 25% PuO_2/UO_2 -PLATE MEASUREMENTS

The thick-foil absolute technique was applied to a (C_8/F_9) measurement for the 25% PuO_2/UO_2 plate of the 8F cell, using

6.3 mm x 5.5 mm 25% PuO₂/UO₂ foils and source-foils of 0.13, 0.23 and 0.30 mm thicknesses. These had been prepared by the Chemistry Group at the same time as the foils and source-foils used for the 8F UO₂-plate measurement, the same doped UO₂ material having been used in the two cases. The y-factor value was therefore the same for the source-foils, i.e. $(1.08 \pm 0.01) \times 10^{-17} \text{sec}^{-1}$. The plutonium used for the 25% PuO₂/UO₂ mixes was identical to that in the ZEBRA mixed-oxide plates (viz. containing ~10% Pu-240), except for the initial ion-exchange separation of the in-grown Am-241 (Sec. 5.4.5). Fig. 31 shows the Ge(Li) spectra of the finished foils and source-foils, a few weeks after preparation.

The absolute U-238 capture rate determination was made with three 25% PuO₂/UO₂ foils, one of each thickness, loaded with the appropriate collets into a central 25% PuO₂/UO₂ plate. For the $[278 \pm \frac{1}{2}(\text{F.W.H.M.})]$ keV Ge(Li) counting of the irradiated foils and the suitably-matched source-foils, mean natural-activity corrections of 10-15% were applied by including an unirradiated 25% PuO₂/UO₂ reference foil in the counting cycle, the natural activity of this reference having been related to that of each of the other foils prior to the irradiation. An accuracy of better than $\pm 2\%$ was achieved in applying the natural-activity corrections, so that the error contribution to the results was $< \pm 0.3\%$. With the counting being carried out between ~50 and 100 hours after the irradiation, the fission-product correction for the 8F-irradiated 25% PuO₂/UO₂ foils was $(8.5 \pm 0.5)\%$ (Sec. 7.2), and, applying the various corrections and normalising factors, the absolute U-238 capture rate was obtained from FOILAB. An absolute Pu-239 fission measurement, during the same 4-hour irradiation, had been made for the mixed-oxide plate of the adjacent,

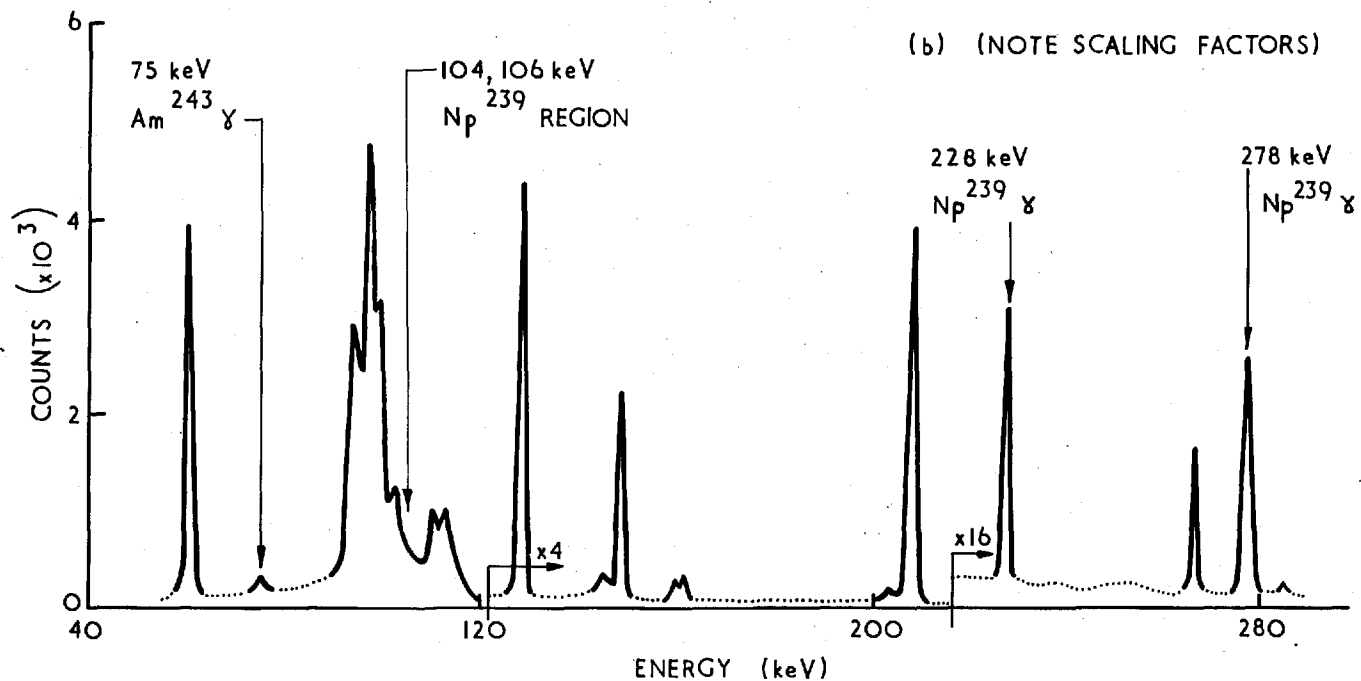
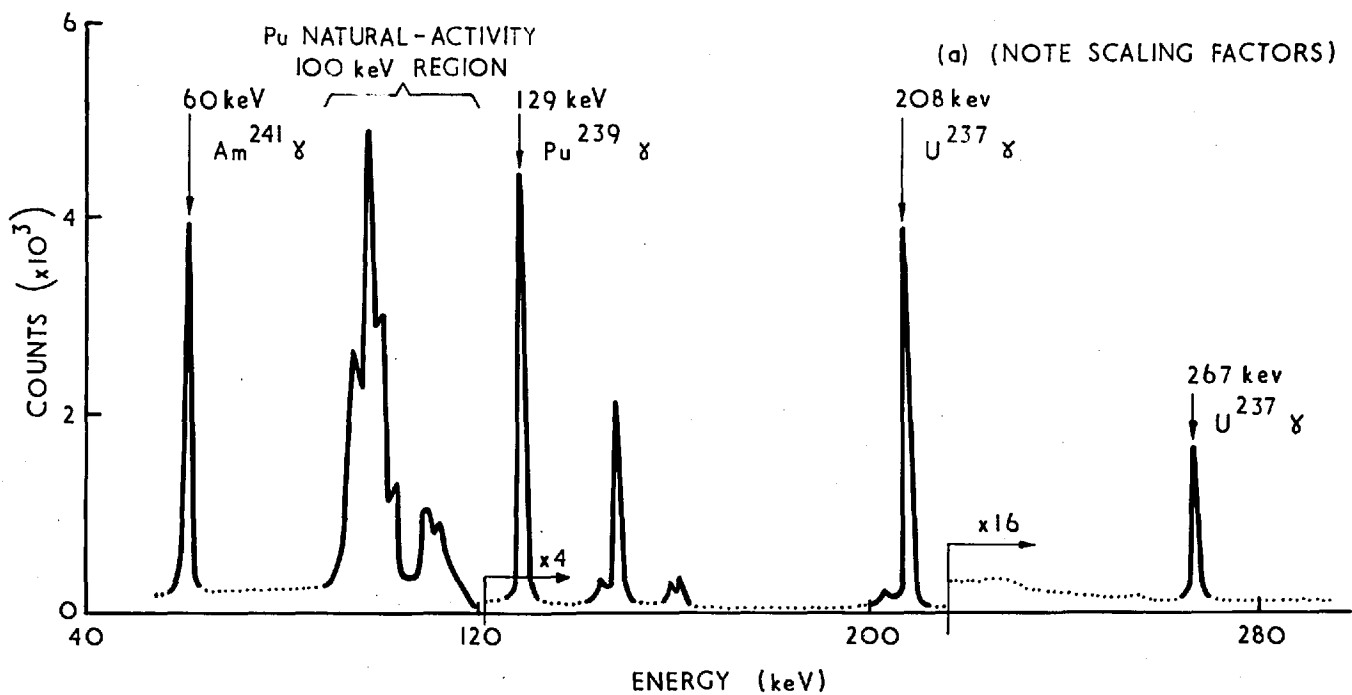


FIG. 31. Ge (Li) SPECTRA OF (a) UNIRRADIATED 25% PuO_2/UO_2 FOIL AND (b) Am-243-DOPED 25% PuO_2/UO_2 SOURCE-FOIL

flux-equivalent cell, thus completing the reaction-rate ratio determination.

The second type of (C_8/F_9) measurement made for the 8F 25% PuO_2/UO_2 plate was one employing the modified thermal-comparison approach outlined in Sec. 7.1. For determining the lattice-to-thermal U-238 capture ratio, 25% PuO_2/UO_2 foils of 0.13, 0.23 and 0.30 mm thicknesses were used in the 8F mixed-oxide plate and natural UO_2 foils of the same three thicknesses were irradiated in the thermal column. $[278 \pm \frac{1}{2}(\text{F.W.H.M.})]$ kev singles counting was applied and "modified" self-absorption curves were obtained for each type of foil. With the relative corrections derived from these curves being typically $\sim (2.0 \pm 0.5)\%$, an accuracy of $\pm 1.0\%$ was achieved in the determination of the U-238 capture ratio.

The standard R.C.R. method was also applied to the mixed-oxide plate measurements, 0.13 mm thick natural UO_2 foils being loaded with 25% PuO_2/UO_2 collets into the plate and depleted UO_2 foils (0.4% U-235) being used in the thermal column. In order to provide some indication of the effect of using ordinary UO_2 foils in the mixed-oxide plate, the lattice foils were irradiated in a pack of three as well as singly.

All the various (C_8/F_9) results for the 8F mixed-oxide plate have been summarised in Table 15. The quoted theoretical value was obtained by applying the SCRAMBLE-calculated (I_{II}/s) factor of 0.988 (Sec. 7.3.1) to the MURAL infinite-lattice prediction of 0.1465.

TABLE 15. $(^{88}/F_9)$ RESULTS FOR THE 8F 25% PuO₂/UO₂ PLATE

Technique Applied	Result
25% PuO ₂ /UO ₂ thick-foil absolute (278 kev singles)	0.156 ± 0.003
Thermal-comparison, 25% PuO ₂ /UO ₂ foils in lattice (278 kev singles)	0.155 ± 0.003
Standard R.C.R., single UO ₂ foil in plate	0.152 ± 0.003
Standard R.C.R., UO ₂ foil from pack of 3 in plate	0.152 ± 0.003
Theory	0.148

The last kind of measurement made in Core 8F was the direct comparison of the Np-239 activities of 25% PuO₂/UO₂ and natural UO₂ foils after a 4-hour irradiation in a 25% PuO₂/UO₂ plate. It was realised that by considering the "modified" self-absorption curves from these two types of foils, one would "lump" - into the self-absorption and count-rate effects (Sec. 6.2.1) of the latter type - an additional factor, viz. the effect of using UO₂ material for measuring the U-238 capture rate in the 25% PuO₂/UO₂ plate. Provided the effect was not large, a simple exponential extrapolation to zero foil-mass, or zero foil-thickness, would not be in serious error and the two "modified" self-absorption curves would extrapolate to the same point, viz. that corresponding to the true U-238 capture rate in the plate.

For the irradiation, three foils of each type (one of each thickness) were loaded into two flux-equivalent 25% PuO₂/UO₂ plates in the centre of the 8F test-region. Both Ge(Li) [278 ± ½(F.W.H.M.)] kev singles γ -counting and 102-108 kev γ -X-ray coincidence counting were employed, the corrections for natural-activity and fission-product effects being applied as described earlier. The correction

for random coincidences in the 102-108 keV γ -X-ray counting was typically $\sim 4\%$ for the mixed-oxide foils and, with the 200 nanosec coincidence resolving time having been determined to ± 10 nanosec, the resulting error due to the applied correction was $< 0.3\%$ in each case. The relative results finally computed from the counting data are shown plotted in Fig. 32, and these do indicate that the "modified" self-absorption curves were determined mainly by self-absorption and count-rate effects.

Similar results were later obtained in the 8G Pin Core (Sec. 7.5) for a comparison between 16% PuO_2/UO_2 and depleted UO_2 foils irradiated in 16% PuO_2/UO_2 fuel. Table 16 summarises the values obtained, in the two cores, for the extrapolated Np-239 activity ratios of the mixed-oxide foils relative to the UO_2 foils.

TABLE 16. DIRECT COMPARISONS OF NP-239 ACTIVITIES OF PuO_2/UO_2 AND UO_2 FOILS IN CORES 8F AND 8G2

Core	Type of Mixed-oxide Fuel	Extrapolated Np-239 Activity Ratio (PuO_2/UO_2 foils rel. to UO_2 foils)	
		278 keV singles	102-108 keV coins.
8F	25% PuO_2/UO_2 Plates	1.009 ± 0.015	1.01 ± 0.02
8G2	16% PuO_2/UO_2 Pins	0.986 ± 0.015	0.98 ± 0.02

7.4 MEASUREMENTS IN THE 8G PLATE CORE

($^{88}\text{F}_9$) measurements in mixed-oxide fuel were of greater importance in Core 8G than in 8F, because the 8G cell contained two 25% PuO_2/UO_2 plates and only one UO_2 plate (Fig. 4).

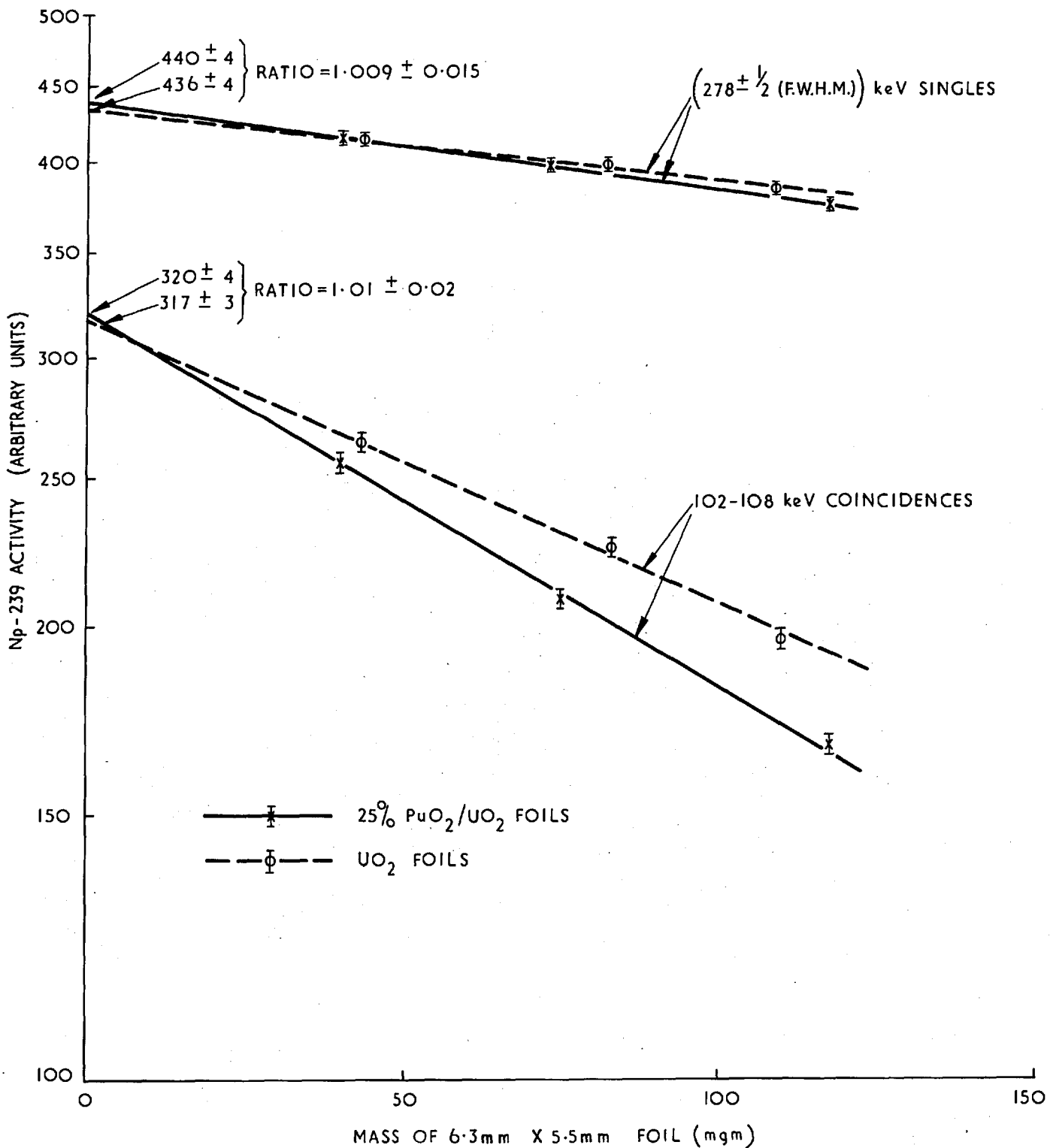


FIG. 32. DIRECT COMPARISONS OF Np-239 ACTIVITIES OF 25% PuO₂/UO₂ AND UO₂ FOILS IRRADIATED IN CORE 8F MIXED-OXIDE PLATES.

In order to eliminate the error due to the source-foil inhomogeneities encountered in the 8F thick-foil absolute measurements (Sec. 7.3), a new set of 25% PuO₂/UO₂ foils and source-foils of 0.18, 0.30 and 0.46 mm thicknesses were prepared by the Chemistry Group (Ref. 55). The same basic procedure was employed except that, in this case, quantitative homogeneity tests - of the doped UO₂ and of the 25% PuO₂/UO₂ mixes - were carried out before the actual foil preparation, to ensure that the variation in the specific Am-243 content of the finished source-foils was <0.5%. The y-factor had been determined for the doped UO₂ using the methods outlined in Sec. 6.1. An additional value was obtained by ion-exchange Am-separation from a few of the finished 25% PuO₂/UO₂ source-foils and the 278 keV γ -counting of the liquid samples obtained - standardisation being done via pure Am-243 liquid samples prepared from pre-calibrated Am-243 electrodeposits (Ref. 33). Agreement between the differently-derived y-factor values was within the individual experimental errors, and a mean of $(2.64 \pm 0.03) \times 10^{-17} \text{sec}^{-1}$ was determined.

Two separate absolute-measurement experiments were carried out in 8G. In each of these, three absolute reaction rate determinations were made - viz. C₈ for one of the central 8G 25% PuO₂/UO₂ plates using the thick-foil absolute technique, C₈ for the central UO₂ plate using the thin-deposit method, and finally F₉ for the second, flux-symmetric mixed-oxide plate.

For the 8G 25% PuO₂/UO₂ thick-foil measurements, both 278 keV singles and 102-108 keV coincidence counting were employed since, with homogeneous foils and source-foils being used, it was possible to obtain reliable "modified" self-absorption curves for intercomparison. These are shown plotted in Fig. 33 and it can be seen that, within the statistical errors of 0.4-0.8%, the curves for the activated foils and

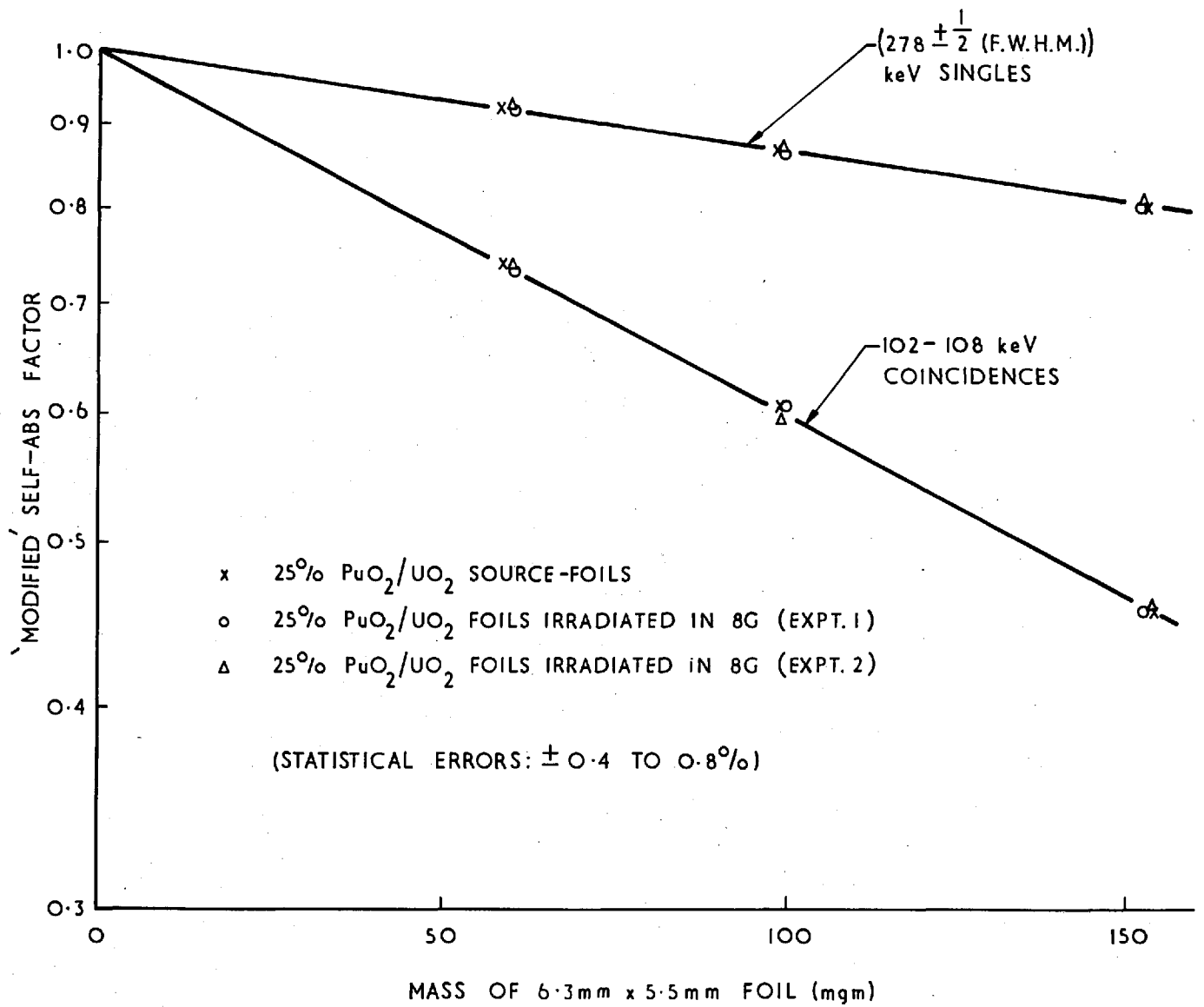


FIG. 33. 'MODIFIED' SELF-ABSORPTION CURVES FOR 25% PuO₂/UO₂ FOILS AND SOURCE-FOILS USED IN 8G PLATE CORE MEASUREMENTS

the doped source-foils coincide exactly, making the error due to any relative corrections applied $< \pm 0.3\%$ - for both the γ -X-ray coincidence counting and the higher-energy γ -singles. (This fully justifies the assumptions made for the Core 8F measurements where reliable "modified" self-absorption curves could not be obtained.)

For the thin-deposit C_8 measurements in the 8G UO_2 plate, the same procedure was used as in Core 8F (Sec. 7.3.1), a factor of (1.020 ± 0.002) having been deduced in the present case (from an 8G 10-region MURAL calculation) to yield the reaction rate averaged through the thickness of the plate.

The determination of the absolute Pu-239 fission rate in each experiment was carried out via chamber measurements in a cavity at position (50,54) in the reactor lattice (Fig. 3), using a mean determined plate-to-cavity ratio of (1.085 ± 0.005) .

The various absolute-measurement results, obtained in the two separate experiments in the 8G Plate Core, are tabulated in Table 17, a normalising factor of (1.008 ± 0.004) having been incorporated (Ref. 25) for yielding the average U-238 capture rate in an 8G UO_2 , or PuO_2/UO_2 , plate from the centrally-made measurements.

TABLE 17. RESULTS OF ABSOLUTE MEASUREMENTS IN THE 8G PLATE CORE

Expt.	Abs. U-238 Capture Rate ($\times 10^{-16} \text{sec}^{-1}$)		Abs. Pu-239 Fiss. Rate ($\times 10^{-15} \text{sec}^{-1}$)	(C_8/F_9)		
	25% PuO_2/UO_2 Plate (Thick-foil abs., Ge(Li)) 102-108 Coins.	UO_2 Plate (Thin-deposit, NaI coins.) 278 Singles		25% PuO_2/UO_2	UO_2	
1	5.45 ± 0.06	5.53 ± 0.06	5.49 ± 0.05	3.63 ± 0.04	0.151 ± 0.003	0.151 ± 0.003
2	5.64 ± 0.06	5.69 ± 0.06	5.63 ± 0.06	3.71 ± 0.04	0.153 ± 0.003	0.152 ± 0.003

For the modified thermal-comparison (C_8/F_9) measurement in the 8G mixed-oxide plates, both [$278 \pm \frac{1}{2}(\text{F.W.H.M.})$] kev singles and 102-108 kev coincidence counting were employed. The error was found to be significantly greater for the latter counting technique because the relative "modified" self-absorption corrections for the two foil-types (i.e. 25% PuO₂/UO₂ and UO₂) were typically $\sim(6 \pm 1)\%$ in this case (cf. $\sim(2.0 \pm 0.5)\%$ for the 278 kev singles).

All the various (C_8/F_9) results obtained for the 8G Plate Core are given in Table 18.

TABLE 18. (C_8/F_9) RESULTS FOR THE 8G PLATE CORE

Technique Applied	Result
<u>(i) 25% PuO₂/UO₂ Plates</u>	
25% PuO ₂ /UO ₂ Thick-foil absolute (102-108 coins.)	0.151 \pm 0.003
" " " " " (278 singles)	0.153 \pm 0.003
Thermal comparison (25% PuO ₂ /UO ₂ , 278 singles)	0.152 \pm 0.003
" " " " " (102-108 coins.)	0.149 \pm 0.004
Standard R.C.R. (single UO ₂ foil in plate)	0.153 \pm 0.003
" " (one of 3 UO ₂ foils in plate)	0.153 \pm 0.003
Theory	0.143
<u>(ii) UO₂ Plate</u>	
Thin-deposit absolute	0.151 \pm 0.002
R.C.R.	0.150 \pm 0.003
Theory	0.141

On the practical basis of the measurements made in the 8F and 8G Plate Cores, a comparison of the errors - for the different techniques developed to determine U-238 capture in 25% PuO₂/UO₂ material - is presented in Table 19.

TABLE 19. ERRORS IN THE VARIOUS TECHNIQUES DEVELOPED FOR U-238 CAPTURE
MEASUREMENTS IN 25% PuO₂/UO₂ MATERIAL

Source of Error	Error (+ %)			
	Thick-foil absolute		Thermal Comparison	
	278 Singles	102-108 coins.	278 Singles	102-108 coins.
1. Natural-activity correction	0.3	0.3	0.3	0.3
2. Fission-product correction	0.5	0.2	0.4	0.2
3. Random coincidences	-	0.3	-	0.3
4. Edge-effects in counting	0.1	0.2	0.1	0.2
5. Counting statistics	0.5	0.8	0.5	0.8
6. Relative "modified" self-abs. correction	0.2	0.3	0.5	1.0
7. Foil weights and compositions	0.3	0.3	0.3	0.3
8. γ -factor determination	1.0	1.0	-	-
9. Thermal cross-sections	-	-	1.1	1.1
10. Thermal-column flux depressions	-	-	0.3	0.3
Total (r.m.s.)	1.3	1.4	1.5	1.8

The theoretical predictions quoted in Table 18 for Core 8G were obtained in a slightly different manner from those for the other Core 8 Assemblies because, unlike the other test regions, that of 8G had a k_{∞} -value considerably greater than unity, viz. ~ 1.3 (Ref. 12). As, in this case, use of the k-option in MURAL (Sec. 2.1) would result in significant distortion of the fission source distribution to produce criticality,

it was realised that an infinite-lattice (IL) calculation with MURAL was not a physically-accurate approach and that it was more appropriate to perform a buckling-search, or fundamental-mode (FM), calculation instead (Ref. 4). Accordingly, the quoted theoretical (C_8/F_9) values, for the 8G core centre, were obtained by applying a SCRAMBLE-derived (F_M/S) factor of 1.026 to the results from an FM MURAL-FGL4 calculation (Ref. 12).

7.5 MEASUREMENTS IN THE 8G PIN CORE, 8G2

Core 8G had been designed primarily to enable a comparison to be made between pin and plate geometries for a sodium-containing, oxide-fuelled, PFR-type lattice (Sec. 3.2). After completing measurements in the Plate Core, a central portion of the test region, approximately a 30 cm. cube, was replaced by a stainless-steel-walled, sodium calandria containing a 15 x 15 array of 16% PuO_2/UO_2 pins (Ref. 25). With the overall composition of this Pin Core, 8G2, being very similar to that of the Plate Core, effects due to spectrum-interaction were minimal and reliable measurements could be made at the core centre.

The loading of foils into the fuel pins for the reaction rate measurements was quite straightforward. Each pin contained five aluminium capsules which in turn held eight 10 mm-diameter, 16% PuO_2/UO_2 pellets of approximately 7 mm thickness. By using foils of exactly the same diameter as the pellets, accurate foil-positioning was easily achieved inside a given capsule, and this could then be loaded into any desired position in the calandria.

For the thick-foil absolute (C_8/F_9) measurement in 8G2, 10 mm-diameter, 16% PuO_2/UO_2 foils and source-foils of 0.18, 0.30 and 0.46 mm thicknesses, were prepared by the Chemistry Group (Ref. 55). The plutonium (~5% Pu-240) and the uranium (depleted, 0.4% U-235) used for the mixes were

identical to those in the fuel pins, except for the initial Am-241 separation from the plutonium. The γ -factor for the source-foils was determined as before (Sec. 7.4), a value of $(2.62 \pm 0.04) \times 10^{-17} \text{sec}^{-1}$ being obtained in the present case.

As in the Plate Core, two separate sets of absolute measurements were made. The γ -X-ray spectra of one of the irradiated 16% PuO₂/UO₂ foils and one of the 16% PuO₂/UO₂ source-foils are compared in Fig. 34. "Modified" self-absorption factors, obtained from the 102-108 kev coincidence and the 278 kev singles counting, are shown plotted in Fig. 35, and these confirm that self-absorption and count-rate effects were identical for the activated foils and the doped source-foils. For the absolute Pu-239 fission measurements, the (50,54) cavity was employed (Sec. 7.4) - a mean pin-to-cavity ratio of (1.115 ± 0.005) having been determined using foils (Ref. 25).

The final, mean results of the 8G2 thick-foil absolute measurements are given in Table 20, along with the (^{C8}/_{F9}) values obtained using the modified thermal-comparison and the standard R.C.R. techniques.

TABLE 20. (^{C8}/_{F9}) RESULTS FOR THE 8G PIN CORE

Technique Applied	Result
16% PuO ₂ /UO ₂ Thick-foil absolute (102-108 coins.)	0.150 \pm 0.003
" " " " (278 singles)	0.151 \pm 0.003
Thermal comparison (16% PuO ₂ /UO ₂ , 278 singles)	0.146 \pm 0.003
" " (" " , 102-108 coins.)	0.146 \pm 0.004
Standard R.C.R. (single UO ₂ foil in pin)	0.149 \pm 0.003
" " (one of 3 UO ₂ foils in pin)	0.149 \pm 0.003
Theory	0.143

The quoted theoretical value for (^{C8}/_{F9}) at the 8G2 core centre was

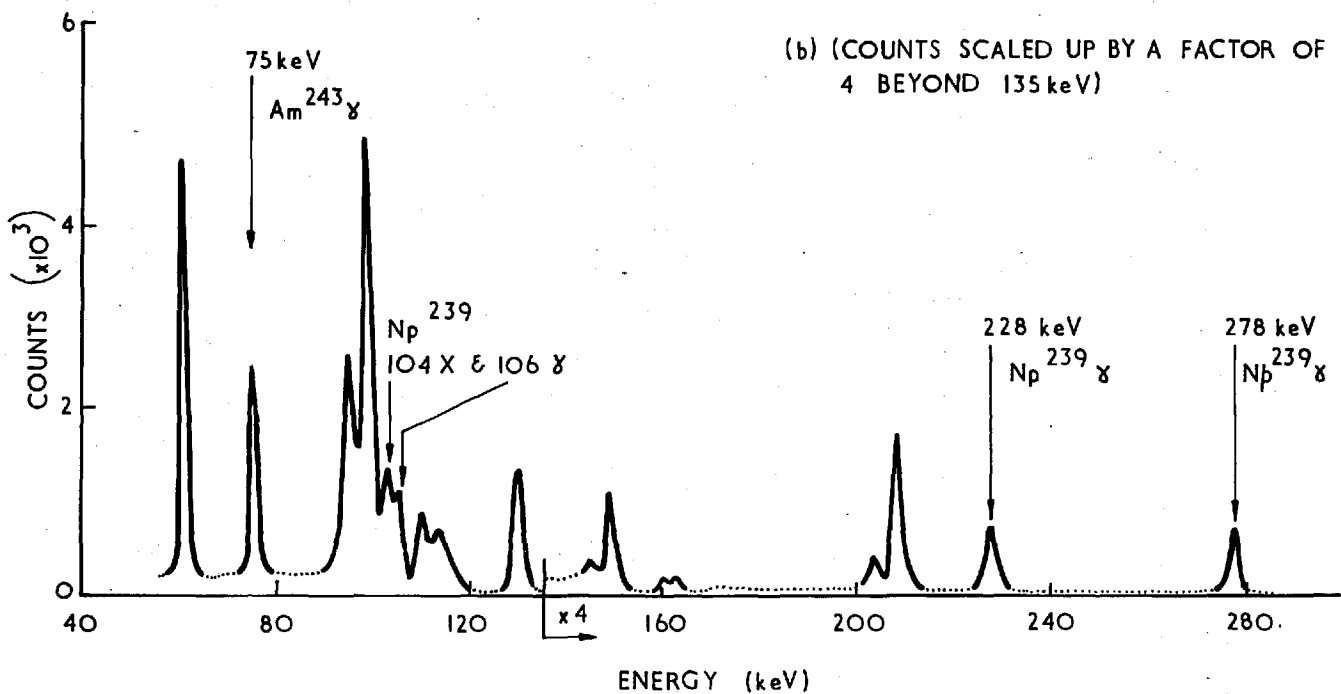
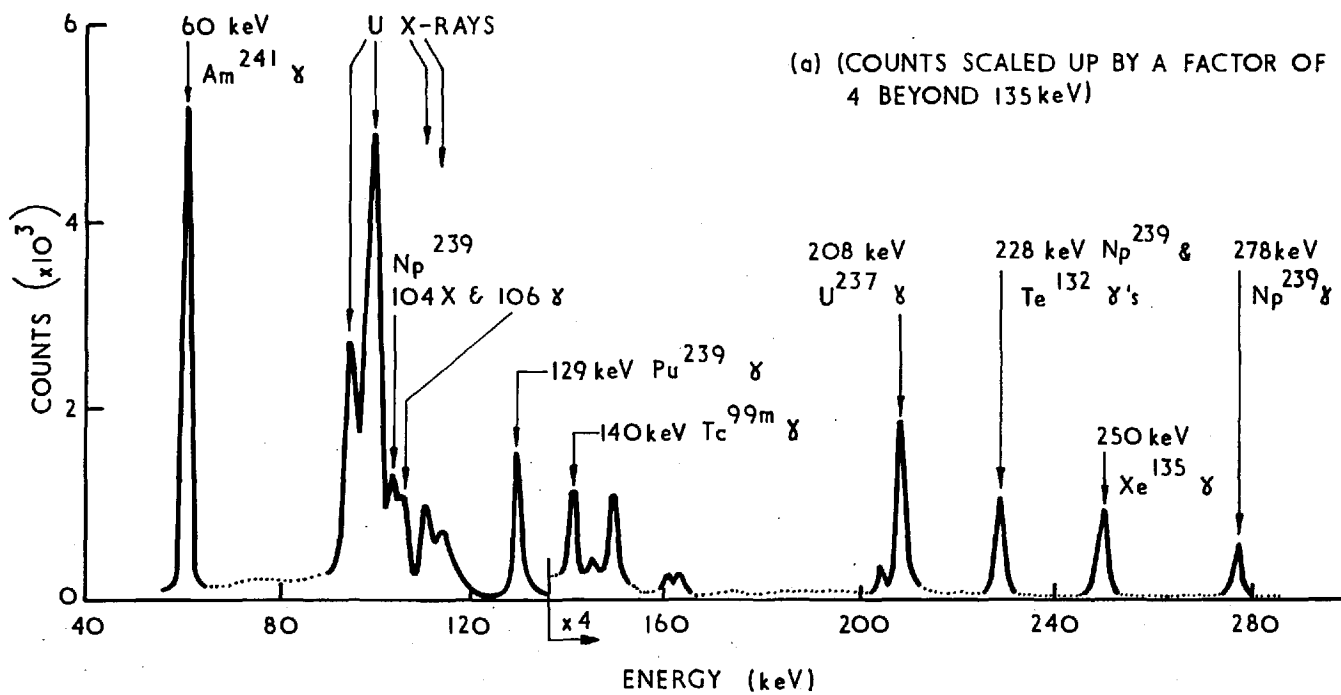


FIG. 34. Ge(Li) SPECTRA OF
 (a) 16% PuO₂/UO₂ FOIL ~ 25 HRS AFTER IRRADIATION IN 8G2 AND
 (b) Am-243-DOPED 16% PuO₂/UO₂ SOURCE-FOIL

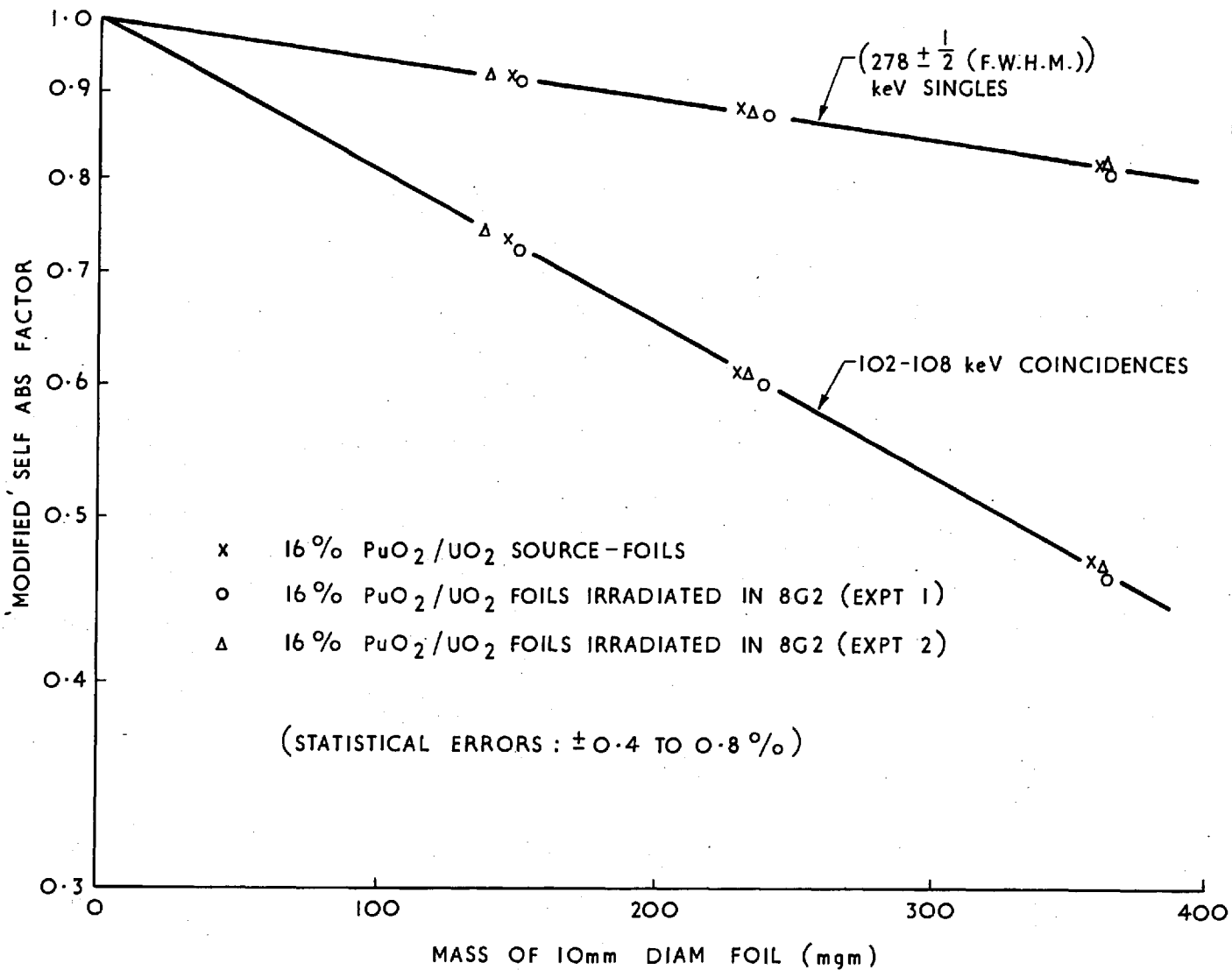


FIG. 35. 'MODIFIED' SELF-ABSORPTION CURVES FOR 16% PuO₂/UO₂ FOILS AND SOURCE-FOILS USED IN 8G PIN CORE MEASUREMENTS

obtained, as for the 8G Plate Core (Sec. 7.4), by applying a SCRAMBLE-calculated (k_{FM}/β) factor (1.027, in the present case) to a MURAL-FGL4 fundamental-mode calculation value. The collision-probability subroutine used in MURAL for the 8G2 calculation was the pin-geometry routine, FLURIG (Ref. 12).

CHAPTER 8

DISCUSSION OF RESULTS AND CONCLUSIONS

It would be appropriate to discuss the various results obtained under three separate headings - viz. (i) the comparison of absolute thin-deposit and R.C.R. techniques for (C_{8/F_9}) measurements in natural uranium, (ii) a general assessment of the experimental approach to mixed-oxide measurements, and (iii) a comparison between experiment and theory for the ZEBRA metal and mixed-oxide "bench-mark" assemblies studied in the course of the present work.

8.1 COMPARISON OF ABSOLUTE AND R.C.R. TECHNIQUES

As discussed in Chapter 4, the absolute thin-deposit technique was developed and applied in order to meet the need for a completely independent method which would improve upon the systematic accuracy of R.C.R.-type (C_{8/F_9}) measurements in fast reactors. A detailed comparison of the errors of the absolute and R.C.R. methods was made in Sec. 4.3 for the ZEBRA Core 8C measurements (Table 7), and it was shown there how the new technique was, in fact, the more accurate of the two (with a net r.m.s. error of $\pm 1.3\%$, cf. $\pm 1.7\%$ for the R.C.R. result). For the comparison of actual (C_{8/F_9}) values derived from the two different methods, it would, of course, be more instructive to consider the results obtained in all the various assemblies for which both types of measurements were made. This has been done in Table 21, using results tabulated earlier - in Tables 6, 13, 14 and 18.

TABLE 21. COMPARISON OF ABSOLUTE THIN-DEPOSIT AND R.C.R. (C_8/F_9)

RESULTS

Core	Abs.			R.C.R.		
	(C_8/F_9)	Error (\pm %)		(C_8/F_9)	Error (\pm %)	
		Rand.	Syst.		Rand.	Syst.
8C	0.128	1.0	0.8	0.126	1.0	1.4
8E	0.117	1.0	0.8	0.117	1.0	1.4
8F	0.156	1.4	0.8	0.152	1.4	1.4
8G	0.151	1.2	0.8	0.150	1.4	1.4
Mean ($Abs./R.C.R.$) Ratio = $1.010 \pm \begin{matrix} (0.012 \text{ (random)}) \\ (0.016 \text{ (systematic)}) \end{matrix}$						

It is seen that the mean ratio of the absolute (C_8/F_9) results, relative to the corresponding R.C.R. - derived values, is obtained as unity within the random error of $\pm 1.2\%$. This confirms the absence of any unsuspected uncertainties in the two methods and further suggests that the combined systematic error of $\pm 1.6\%$ may be too pessimistic. However, one cannot discount the possibility of cancelling errors in the present comparison, and it would be advisable to carry out measurements in a few more assemblies before making any empirical reduction of the currently-estimated, individual systematic errors in either method.

The statistical accuracy achieved in the Np-239 counting of the irradiated uranium deposits was identified as the limiting factor in the accuracy of the absolute U-238 capture measurement (Sec. 5.4.3), the method being free of any error-introducing absolute calibrations. For the absolute Pu-239 fission measurement, on the other hand, the main sources of error were recognised as being of a systematic - rather than

a statistical - nature (Table 5), the limiting factor in this case being the $\pm 0.6\%$ accuracy with which the number of Pu-239 atoms, in the deposits of Chambers ZEB-31, 32, could be absolutely determined (Sec. 4.2.2). In order to render future absolute (C_8/F_9) measurements in ZEBRA independent of this particular systematic uncertainty, it is recommended that new fission chambers - with independently-calibrated Pu-239 deposits of greater isotopic purity - be used. These could be compared with ZEB-31, 32, and an enhancement in the overall systematic accuracy would thence be achieved.

There is little doubt, however, that, with the combined application of absolute and R.C.R. techniques, the target accuracy of $\pm 1\%$ for (C_8/F_9) measurements in simple U-Pu fast reactor assemblies has now become quite readily attainable.

8.2 ASSESSMENT OF MIXED-OXIDE MEASUREMENTS

The present-developed methods for U-238 capture measurements in 25% PuO_2/UO_2 material have made possible the complete elimination of the systematic errors that might arise from the use of UO_2 foils in any given mixed-oxide fast-reactor lattice (Chapter 1).

Although the different techniques employed (Sec. 7.1) were independent to a large extent, the basic feature was common - viz. appropriate application of suitable Ge(Li) detectors to achieve the necessary discrimination of natural-activity and fission product γ -backgrounds (Chapter 5). Another essential characteristic was the initial Am-241 separation effected for the plutonium used in preparing the mixed-oxide foils as, without this step being taken, count-rate effects due to the large in-grown 60 keV γ -activity peak would have been too great to enable accurate measurements to be made (Sec. 5.4.5).

A comparison of the individual errors, in the various mixed-oxide

U-238 capture techniques developed, was provided in Table 19, and it was seen how the thick-foil absolute method was capable of greater accuracy than the modified thermal-comparison technique ($\sim \pm 1.3\%$, cf. $\sim \pm 1.6\%$). This was mainly because, in the latter case, significant relative "modified" self-absorption corrections had to be applied in the comparison of the different foil-types. The systematic accuracy of the thick-foil absolute method was, however, limited by the determination of the y-factor (Sec. 6.1). Several difficulties in the foil, source-foil preparations and calibrations were encountered in the present experiments, e.g. the slight non-homogeneity of the 8F-used mixes (Sec. 7.3), but there is no reason why, in future work, an accuracy better than the quoted $\pm 1.0\%$ for the y-factor (Table 19) should not be attained. All that is needed is more detailed care at each stage of the chemical procedure employed for the preparations. (Greater accuracy in determining the y-factor would, in fact, make the method quite attractive for other types of reaction rate measurements as well, e.g. U-238 capture studies in advanced-reactor particle-fuels, and similar Th-232 capture studies (where Np-237, as the long-lived parent of Pa-233, would replace Am-243).)

The application of two separate Ge(Li) counting techniques for monitoring the Np-239 radiations in the mixed-oxide U-238 capture measurements - viz., 102-108 keV γ -X-ray coincidences and $278 \pm \frac{1}{2}$ (F.W.H.M.) keV γ -ray singles - served to confirm the absence of any unsuspected error in either approach. Although each counting technique had its own merits (e.g., smaller relative "modified" self-absorption corrections for the 278 keV singles, and less fission-product interference for the 102-108 keV coincidences), the use of both methods in parallel (Fig. 27) considerably enhanced the statistical and systematic accuracies of the measurements.

Table 22 summarises the mixed-oxide (C_8/F_9) results obtained using the different experimental techniques in Cores 8F, 8G and 8G2 (Tables 15, 18 and 20, respectively). Since, in each case, the individual values from 278 kev singles and 102-108 kev coincidences agreed within the estimated random errors, only the mean results obtained from the Ge(Li) counting have been considered in the present comparison.

TABLE 22. SUMMARISED COMPARISON OF MIXED-OXIDE (C_8/F_9) RESULTS

Technique	8F	8G	8G2	Error (\pm %)	
				Rand.	Syst.
Mixed-ox. thick-foil abs.	0.156	0.152	0.151	1.2	1.3
Th. comp. (mixed-ox. foils)	0.155	0.151	0.146	1.5	1.4
Std. R.C.R. (UO_2 foils)	0.152	0.153	0.149	1.0	?
Mean Mixed-ox. foil ($\frac{\text{Absolute}}{\text{Th. Comp.}}$) Ratio = $1.015 \pm \begin{cases} 0.012 \text{ (rand.)} \\ 0.019 \text{ (syst.)} \end{cases}$					
Mean ($\frac{\text{Mixed-ox. foil Techs.}}{\text{Std. } UO_2\text{-foil R.C.R.}}$) Ratio = $1.003 \pm 0.010 \text{ (rand.)}$					

It is seen that the U-238 capture results obtained using mixed-oxide foils - via both the thick-foil absolute and the modified thermal comparison techniques - agree well within the quoted random errors with the values derived from the standard-R.C.R., UO_2 -foil measurements. This shows that the effects of using UO_2 foils for the mixed-oxide measurements were not large enough to be discernible in the present study. (Some indication of the smallness of these effects was also provided by the mixed-oxide/ UO_2 -foil direct-comparison experiments in Cores 8F and 8G2 (Table 16), as well as by the use of single and triple-loaded UO_2 foils for the standard R.C.R. measurements.) However,

one cannot generalise too broadly, and it would be proper that in future mixed-oxide assemblies - with possibly different fuel enrichments and heterogeneity effects - at least a few measurements be carried out, using the present-developed mixed-oxide U-238 capture techniques, to ascertain that no systematic errors are being introduced by the simple use of UO_2 foils.

8.3 COMPARISON BETWEEN EXPERIMENT AND THEORY

Table 23 summarises the experimental (mean) and theoretical cell-averaged, core-centre (C_{8/F_9}) values for the various ZEBRA Core 8 test regions studied in the course of the present work (Tables 6, 13, 14, 15, 18 and 20).

TABLE 23. COMPARISON BETWEEN EXPERIMENTAL AND THEORETICAL (C_{8/F_9}) VALUES

Core	Type of Fuel	Expt. (E)	Theory (T)	(T/E)
8C	Pu and U Metal	0.127 ± 0.001	0.127	1.000
8E	Pu and U Metal	0.118 ± 0.001	0.120	1.017
8F	25% PuO_2/UO_2 & UO_2	0.154 ± 0.002	0.147	0.955
8G	25% PuO_2/UO_2 & UO_2	0.152 ± 0.002	0.142	0.934
8G2	16% PuO_2/UO_2 (Pins)	0.149 ± 0.002	0.143	0.960

It is seen that the MURAL-FGL4-SCRAMBLE calculational procedure (Chapter 2) was quite satisfactory for the prediction of the 8C and 8E (C_{8/F_9}) values. The underestimation of the reaction rate ratio by ~5% for Core 8F, however, suggests that the theoretical methods and/or data are inadequate for calculating (C_{8/F_9}) values for assemblies with relatively soft neutron-energy spectra. This trend was observed earlier

(Ref. 13) for ZEBRA Core 8A which, though considerably more heterogeneous than 8F, had a similar neutron spectrum (Sec. 3.2). Another common feature of the U-238 capture rate determinations in Cores 8A and 8F was that, in both cases, the theoretically-predicted fine structure was found to be 5-10% less than experiment (Appendix A.1 and Sec. 7.3.1). These results indicate that in addition to data uncertainties, there may be shortcomings in the MURAL resonance treatment for studies of soft-spectrum systems, and it is recommended, as one possible course of action, that more detailed comparisons be made of MURAL with the SDR code (Sec. 2.4).

The discrepancies between theory and experiment for the (C_8/F_9) values in the 8G Plate and Pin Cores are possibly suggestive of additional systematic effects, e.g. errors in the calculation of the leakage from these assemblies ($k_\infty \sim 1.3$, cf. 1.0 for the other Core 8 test regions). For relative consideration of plate and pin heterogeneities, however, it is sufficient to compare the individual (T/E) values for 8G and 8G2, and these can be seen to agree within the experimental errors.

As regards the adjustment of the differential nuclear data for more accurate fast reactor calculations (Sec. 2.3), the methods developed and applied at Winfrith have been described by Rowlands and Macdougall in Ref. 10. Also reported in this paper are the main cross-section changes recommended, for the FGL4 data set, on the basis of earlier fast-reactor integral experiments. It is expected that the present reaction rate studies in ZEBRA Core 8, with the considerably improved systematic accuracy of the (C_8/F_9) measurements, will provide valuable evidence for further modifications in the differential data, and may possibly suggest slight reappraisal of certain aspects of the theoretical methods themselves.

REFERENCES

- Ref. 1 Tait, J. H.; Neutron Transport Theory; Longmans (1964)
- Ref. 2 Meneghetti, D. and Loomis, M. F.; Calculation of Heterogeneity Effects in ZPR-III Fast Assemblies Using the DSN Programme; ANL-6218 (1960)
- Ref. 3 Beardwood, J. E., Clayton, A. J. and Pull, I. C.; The Solution of the Transport Equation by Collision Probability Methods; ANL-7050, pp. 93-112 (1965)
- Ref. 4 Macdougall, J. D., Ross, R. W. and Rowlands, J. L.; The Calculation of Neutron Spectra and Group-averaged Cross-sections Using the Computer Programmes FRESKO and MURAL; Internal Winfrith Report (1968)
- Ref. 5 Macdougall, J. D. and Rowlands, J. L.; The Calculation of Resonance Shielding Factors in FRESKO and MURAL; Internal Winfrith Report (1968)
- Ref. 6 Norton, D. S.; The U.K.A.E.A. Nuclear Data Library; AEEW-M824 (1968)
- Ref. 7 Bell, V. J., et al; A User's Guide to GALAXY 3; AEEW-R379 (1964)
- Ref. 8 Brissenden, R. J. and Durston, C.; A User's Guide to GENEX, SDR, and Related Computer Codes; AEEW-R622 (1968)
- Ref. 9 Brissenden, R. J. and Durston, C.; The Calculation of Neutron Spectra in the Doppler Region; ANL-7050, pp. 51-76, (1965)
- Ref. 10 Rowlands, J. L. and Macdougall, J. D.; The Use of Integral Measurements to Adjust Cross-sections and Predict Reactor Properties; Proc. of the B.N.E.S. Conference on the Physics of Fast Reactor Design (1969)
- Ref. 11 Green, C., et al.; SCRAMBLE Users' Manual; AEEW-DCG (1968)
- Ref. 12 Wardleworth, D.; Private communication
- Ref. 13 Sanders, J. E., et al.; Measurements of k-infinity, Reaction Rates and Spectra in ZEBRA Plutonium Lattices; Proc. of the B.N.E.S. Conference on the Physics of Fast Reactor Design (1969)
- Ref. 14 Hodgson, C. D.; M.Sc. Project Report, University of Aston (1969)
- Ref. 15 Smith, R. D.; ZEBRA - A Zero-power Fast Reactor; Nucl. Eng., Vol. 7, No. 76, pp. 364-367 (1962)

- Ref. 16 Spinard, B. I., et al.; Reactivity Changes and Reactivity Lifetimes of Fixed-fuel elements in Thermal Reactors; Proc. of International Conference on Peaceful Uses of Atomic Energy, Vol. 5, pp. 125-140 (1955)
- Ref. 17 Grant, P. J.; Elementary Reactor Physics; Pergamon Press (1966)
- Ref. 18 Kouts, H., et al.; Physics of Slightly Enriched, Normal Water Lattices; Proc. of 2nd International Conference on Peaceful Uses of Atomic Energy, Vol. 12, pp. 446-482 (1958)
- Ref. 19 Campbell, C. G. and Carter, M. D.; The Experimental Determination of Conversion Factors and Fast Fission Factors; AERE R/R2397 (1958)
- Ref. 20 Davey, W. G.; The Ratio of U-238 Capture and U-235 Fission Cross-sections in Fast Reactors; Nucl. Sc. & Eng., Vol. 24, pp. 26-41 (1966)
- Ref. 21 Tunnicliffe, P. R., Skillings, D. J. and Chidley, B. G.; A Method for the Accurate Determination of Relative Initial Conversion Ratios; Nucl. Sc. & Eng., Vol. 15, pp. 268-283 (1963)
- Ref. 22 Brown, W. A. V. and Skillings, D. J.; The Measurement of Relative Conversion Ratio in Low Enrichment Oxide Lattices; AEEW-R340 (1964)
- Ref. 23 Besant, C. B., et al.; Measurement of Relative Conversion Ratio and Fast Fission Ratio in Low Enrichment Oxide Lattices; AEEW-R648 (1969)
- Ref. 24 Barnett G. A., et al.; The Separation and Precise Comparative Determination of Np-239 in Irradiated Low-Enrichment Uranium Oxide Foils and Pellets; Reactor Sc. & Tech., Vol. 17, pp. 389-393 (1963)
- Ref. 25 George, C. F.; Private communication
- Ref. 26 Brown, W. A. V. and Skillings, D. J.; Measurement of Fast Fission Ratio; AEEW-R341 (1964)
- Ref. 27 Wilson, D. J.; Private communication
- Ref. 28 Besant, C. B. and Ipson, S. S.; Progress in the Application of Solid-state Track Recorders to Reactor Physics Experiments; AEEW-M881 (1969)
- Ref. 29 Lederer, C. M., et al.; Table of Isotopes (6th Ed.); John Wiley & Sons (1967)
- Ref. 30 Cripps, F. H. and Weale, J. W.; A New Method for the Absolute Counting of Np-239; J. Inorg. Nucl. Chem., Vol. 7, pp. 339-342 (1958)

- Ref. 31 Seufert, H. and Stegemann, D.; A Method for Absolute Determination of U-238 Capture Rates in Fast Zero-Power Reactors; Nucl. Sc. & Eng., Vol. 28, pp. 277-285 (1967)
- Ref. 32 Fleming, E. H. Jr., Ghiorso, A. and Cunningham, B. B.; The specific α -activities of U-234, U-235 and U-236; Phys. Rev., Vol. 88, pp. 642-652 (1952)
- Ref. 33 Barnett, G. A. and Bolton, F. M.; Private communication
- Ref. 34 Parker, W., Bildstein, H. and Getoff, N.; Molecular Plating - The Rapid Preparation of Radioactive Reference Samples; Nucl. Inst. & Methods, Vol. 26, pp. 314-316 (1964)
- Ref. 35 Glover, K. M.; Private communication
- Ref. 36 EURATOM Round Table on High Precision Mass Spectrometry and α -counting; EANDC-53"S" (1965)
- Ref. 37 Linden, F. J.; Private communication
- Ref. 38 Topping, J.; Errors of Observation and Their Treatment (3rd Ed.); Inst. of Phys. & Phys. Soc. (1962)
- Ref. 39 Storm, E., et al.; γ -ray Absorption Coefficients; LA-2237 (1958)
- Ref. 40 Stevenson, J. M. and Broomfield, A. M.; Measurements and Calculations of Ratios of Effective Fission Cross-sections in the Zero-Power Fast Reactor, ZEBRA; AEEW-R526 (1967)
- Ref. 41 Curtis, M. L., et al.; Absolute α -Counting; Nucleonics, Vol. 13, No. 5 (1955)
- Ref. 42 Jaffey, A. H.; Solid Angles Subtended by a Circular Aperture; Rev. Sci. Inst., Vol. 25, pp. 349-354 (1954)
- Ref. 43 Chawla, R. and Besant, C. B.; Absolute Measurements of U-238 Capture and Pu-239 Fission Rates in Fast Reactors; J. of Brit. Nucl. En. Soc., Vol. 9, No. 1, pp. 28-34 (1970)
- Ref. 44 George, C. F., et al.; Experimental Physics Studies of Steam-Cooled Fast Reactor Lattices; AEEW-R560 (1969)
- Ref. 45 Proceedings of the 1966 IAEA Symposium on Ge(Li) Detectors; IAEA, Vienna (1966)
- Ref. 46 Chawla, R.; Determination of the Intrinsic Peak Efficiency of a Ge(Li) Detector, in γ - γ Coincidence with a NaI Scintillation Counter; M.Sc. Dissertation, University of London (1967)
- Ref. 47 Chawla, R; Conversion Ratio Measurements in CONSORT; Paper presented at University Reactor Users' Meeting, 1968

- Ref. 48 Gibbons, P. E. and Howes, J. H.; γ -ray Spectrometer Systems Using Ge(Li) Detectors; AERE-R5703 (1968)
- Ref. 49 Lauber, A., et al.; Special Cryostats for Ge(Li) Detectors; AE-320 (1968)
- Ref. 50 Radeka, V; State of the Art of Low Noise Amplifiers for Semiconductor Radiation Detectors; BNL-12798 (1968)
- Ref. 51 Wilburn, C.; Private communication
- Ref. 52 Jamieson, G. R., Hilton, R. K. and Bridge, P.; Foil Counting Machine; Internal Winfrith Report (1968)
- Ref. 53 Murphy, M. F.; Private communication
- Ref. 54 Hanna, G. C.; The Neutron Flux Perturbation Due to an Absorbing Foil; Nucl. Sc. & Eng., Vol. 15, pp. 325-337 (1963)
- Ref. 55 Curren, W. D. and Boyd, J. V.; Private communication
- Ref. 56 Anders, O. U.; Experiences with the Ge(Li) Detector for High Resolution γ -ray Spectrometry and a Practical Approach to the Pulse Pile-up Problem; Nucl. Inst. & Methods, Vol. 68, pp. 205-208 (1969)

APPENDIX A.1

AN APPRAISAL OF THE NUMERICAL APPROXIMATIONS IN MURAL

As stated in Section 2.4, the two chief numerical approximations made in MURAL are (a) the cell representation in terms of a finite number of regions and (b) the numerical integration approximation for calculating the collision probabilities. The results from the investigation of these two effects for ZEBRA Core 8A lattice calculations are presented below.

A1.1 EFFECT OF VARYING THE NUMBER OF REGIONS

Figure A1.1 shows the 4, 6, 8, 10 and 12 region representations that were made for the ZEBRA 8A cell in order to investigate approximation (a). MURAL is limited to a maximum of 8 regions on the KDF9 computer at Winfrith, but its use can be extended to about 20 regions on the IBM 7030 at Aldermaston. Since the effects being investigated were small, it was important to perform a consistent set of comparisons, and this was done by running all cases on the IBM 7030 using exactly the same programme and library tapes in each case.

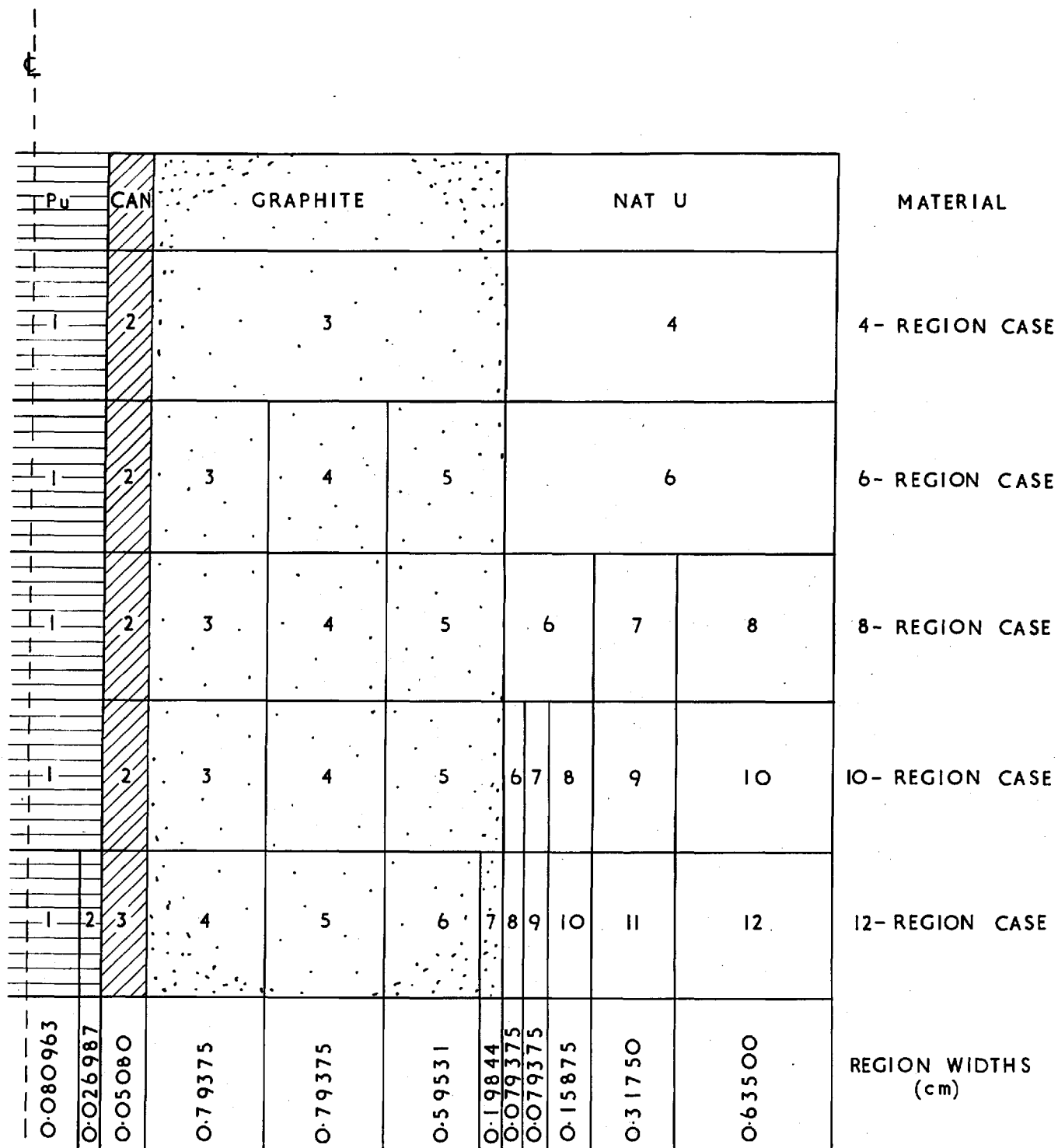


FIG. A1.1. MULTI-REGION REPRESENTATIONS OF THE ZEBRA 8A CELL

TABLE A1.1. ZEBRA 8A - VARIATION OF THE NUMBER OF REGIONS IN MURAL

(SEE FIG. A1.1)

No. of Regions	4	6	8	10	12
Job Time (mins)	12.6	19.6	26.7	34.5	44.0
k_{∞}	0.990704	0.991317	0.992556	0.993002	0.993044
(C_8/F_9)	0.12015	0.11995	0.11956	0.11944	0.11943
(C_9/F_9)	0.41118	0.41064	0.41088	0.41095	0.41079
(F_8/F_9)	0.014291	0.014232	0.014196	0.014188	0.014187
(F_5/F_9)	1.3060	1.3055	1.3051	1.3057	1.3061
(F_0/F_9)	0.18343	0.18442	0.18423	0.18415	0.18412
(F_1/F_9)	1.7717	1.7717	1.7739	1.7747	1.7764

Table A1.1 summarises the k_{∞} -values and the region-averaged reaction rate ratios obtained using the results from the different cases. It can be seen that, although changes of $\sim \frac{1}{2}\%$ are brought about by going from 4 to 8 regions, the effects of increasing the number of regions beyond 8 are $< 0.1\%$, i.e. insignificant.

A1.2 THE NUMERICAL INTEGRATION APPROXIMATION

The method of computing the collision probabilities in the subroutine PROB, for MURAL calculations in slab geometry, is basically that used in the RIPPLE programme (Ref. 12). The integrations are performed numerically using Gaussian quadrature. The current MURAL programme tape includes a 7-point integration routine, but by compiling a separate collision-probability deck the effect of varying the number of points for the integration can be invest-

igated. This was done for the Core 8A 4-region case using 5, 7, 9 and 16-point Gaussian quadrature. (The Gaussian abscissae and weights used were accurate to ten figures in each case). A 7- and 9-point comparison was also made for the 8-region case to show that approximations (a) and (b) are largely independent. The various results are summarised in Table A1.2 and clearly show that the 7-point integration is quite adequate for the calculation

TABLE A1.2. ZEBRA 8A - VARIATION OF THE NUMERICAL INTEGRATION APPROXIMATION FOR THE COLLISION PROBABILITIES IN MURAL

No. of Regions	4				8	
	5	7	9	16	7	9
Job Time (mins)	13.4	12.6	13.7	16.7	26.7	27.6
k_{∞}	0.989444	0.990704	0.990955	0.990869	0.992556	0.992812
(C_8/F_9)	0.12045	0.12015	0.12010	0.12012	0.11956	0.11951
(C_9/F_9)	0.41207	0.41118	0.41102	0.41109	0.41088	0.41071
(F_8/F_9)	0.014333	0.014291	0.014286	0.014290	0.014196	0.014191
(F_5/F_9)	1.3093	1.3060	1.3055	1.3057	1.3051	1.3045
(F_0/F_9)	0.18210	0.18343	0.18369	0.18359	0.18423	0.18449
(F_1/F_9)	1.7736	1.7717	1.7714	1.7716	1.7739	1.7736

The effects of both the numerical approximations, (a) and (b), on the fine structure are shown in Table A1.3. It may be seen that the 8-region, 7-point representation is sufficiently accurate.

TABLE A1.3. ZEBRA 8A - FINE STRUCTURE VARIATION

. WITH NUMERICAL APPROXIMATIONS IN MURAL

(a) U238 CAPTURE

Position (Plate)	8-Region		10-Region	12-Region	Experiment
	7-point	9-point			
Centre of C	4.206	4.205	4.219	4.235	4.55 ± .05*
U 1+8	1.2035	1.2035	1.1996	1.1995	1.248 ± .01
U 2+7	1.0359	1.0359	1.0356	1.0356	1.047 ± .01
U 3+4+5+6	1.0000	1.0000	1.0000	1.0000	1.000

* Value obtained using thin Nat.-U deposits (zero self-shielding)

(b) U238 FISSION

Position (Plate)	8-Region		10-Region	12-Region	Experiment
	7-point	9-point			
Pu	1.7396	1.7452	1.7398	1.7392	1.76 ± .06
Centre of C	1.1968	1.1973	1.1970	1.1972	1.21 ± .03
U 1+8	1.0591	1.0586	1.0591	1.0590	1.054 ± .02
U 2+7	1.0255	1.0254	1.0254	1.0254	1.027 ± .02
U 3+4+5+6	1.0000	1.0000	1.0000	1.0000	1.000

(c) U235 FISSION

Position (Plate)	8-Region		10-Region	12-Region	Experiment
	7-point	9-point			
Pu	1.0294	1.0298	1.0291	1.0294	1.03 ± .01
Centre of C	1.0970	1.0970	1.0968	1.0978	1.14 ± .01
U 1+8	1.0316	1.0316	1.0311	1.0308	1.056 ± .01
U 2+7	1.0122	1.0121	1.0123	1.0123	1.024 ± .01
U 3+4+5+6	1.0000	1.0000	1.0000	1.0000	1.000

The results show that the discrepancies between experiment and theory for the U-238 capture and the U-235 fission fine structure are certainly not due to either numerical approximation, and it is

only the MURAL resonance treatment and the FGL4 data which can be doubted.

All in all, the numerical approximations in MURAL have been shown to be sound. 7-point Gaussian quadrature has been seen to be sufficiently accurate for calculating the collision probabilities. By proper choice of the number and type of regions in the cell representation, negligible error has been shown to result from the finite-number-of-regions approximation.

APPENDIX A.2

INVESTIGATION OF BACKING EFFECTS IN THIN-DEPOSIT

ABSOLUTE U-238 CAPTURE MEASUREMENTS

A2.1 NEUTRON-SCATTERING EFFECT IN THE BACKING

A comparison of (C_8/F_9) measurements was made in ZEBRA Core 8A, using 0.50 mm.-stainless-steel-backed natural uranium deposits for the absolute U-238 capture measurement. The results revealed that the presence of the 0.50 mm. thick stainless steel caused a $(17 \pm 1)\%$ increase in the observed γ -X-ray coincidence activity of deposits irradiated in the centre of the 8A-cells block of natural uranium plates (Fig. 4). That this was in fact due to an increased U-238 capture rate, was deduced from the decay-curves of the irradiated deposits which, after correcting for backing activation (Sec. A2.2), corresponded exactly to the 2.35-day activity of Np-239.

In order to experimentally establish that the effect was simply due to lattice-spectrum perturbations caused by neutron scattering in the steel backing, absolute U-238 capture and Pu-239 fission measurements were carried out in the NESTOR thermal column. Similar steel-backed deposits were used, the absolute U-238 capture measurement being made in a dummy chamber to minimise relative flux-depression corrections. It was found, within an experimental error of $\sim \pm 2\%$, that the obtained (C_8/F_9) ratio agreed reasonably well with the known thermal cross-section ratio, confirming the earlier statement that the Core 8A-observed discrepancy was solely a result of lattice-spectrum perturbation effects.

Theoretically, a simple explanation of the lattice effect is easily obtained if one considers the fact that, though the perturbations in the neutron spectrum due to scattering in the backing are only

slight, they considerably alter the resonance shielding of the U-238 in the deposit. If $\phi_1(E)$ is the neutron flux incident on the block of uranium plates, then, ignoring relaxation effects, the spectrum at the centre of the block, $\phi_0(E)$, may be approximated by

$$\phi_0(E) = \phi_1(E) \cdot \frac{\Sigma_s(E)}{\Sigma_t(E)}$$

where $\Sigma_s(E)$ is the non-resonant scattering cross-section of uranium at energy E and $\Sigma_t(E)$ is the total cross-section. Thus, the flux in the central cavity, housing the deposits, contains large "dips" corresponding to the various resonances. The U-238 capture cross-section averaged over this spectrum, viz. the fully-shielded cross-section, σ_0 , is given by:

$$\sigma_0 = \langle \sigma \rangle \phi_0$$

However, due to the presence of the backing, a fraction f of the neutrons undergo a scattering collision in the steel, and these may be regarded as having been scattered into the normal $\phi_1(E)$ spectrum (assuming that the average energy loss per scattering collision, though much larger than the widths of the resonances, is sufficiently small to have negligible effect on the overall neutron distribution). The U-238 capture cross-section of these scattered neutrons may then be approximated by the infinite dilution cross-section, σ_1 , viz.:

$$\sigma_1 = \langle \sigma \rangle \phi_1$$

If P_c is the average collision probability of the neutrons in the backing, the fraction f may be written simply as $\frac{1}{2}P_c$. Thus, the effective U-238 capture cross-section for the deposit can be approximated as follows:

$$\sigma_{\text{eff}} = \sigma_0 \cdot \left(1 - \frac{1}{2}P_c\right) + \sigma_1 \cdot \left(\frac{1}{2}P_c\right)$$

$$\text{i.e.} \quad \left(\frac{\sigma_{\text{eff}} - \sigma_0}{\sigma_0}\right) = \frac{1}{2} P_c \cdot \left(\frac{\sigma_1 - \sigma_0}{\sigma_0}\right)$$

$$\sim \frac{1}{2} \cdot \left[1 - \left(\frac{1}{1 + 2\Sigma t}\right)\right] \cdot \left(\frac{\sigma_1 - \sigma_0}{\sigma_0}\right) \dots\dots\dots (A)$$

where the Wigner rational approximation has been used for P_c , Σ being the average macroscopic neutron cross-section in the backing and t its thickness.

Equation (A) can be used to give a rather approximate quantitative estimate of the fractional change in the U-238 capture rate due to the presence of the backing. One has for the stainless steel backing in Core 8A, $\Sigma \sim 0.9 \text{ cm}^{-1}$, $t = 0.05 \text{ cm.}$, $\sigma_1 = 0.965 \text{ b.}$ and $\sigma_0 = 0.289 \text{ b.}$ (Ref. 12). Substituting these values into (A), one obtains:

$$\left(\frac{\sigma_{\text{eff}} - \sigma_0}{\sigma_0}\right)_{\text{steel}}^{8A} \sim 9\%$$

Comparing this with the experimental value, it is clear that the derived formula underestimates the effect and that, in general, if Eqn. (A) gives a value of $p\%$, it would be more appropriate to regard $(2p \pm p)\%$ as the correct estimate.

A more sophisticated calculation of the 8A steel-backing effect was sought using the MURAL code. Initial attempts at this calculation failed to produce meaningful results, and the cause of failure was identified as being the use of an invalid approximation to obtain the collision probability matrices $P_{j\text{im}}$ of Eqn. (2.17) in Sec. 2.2. The code was modified by its author (Ref. 5) to eliminate the error-producing simplification, and this enabled successful usage of MURAL for the present case. An estimate of 11% was obtained for the 8A steel-backing effect,

the $(6 \pm 1)\%$ discrepancy with experiment indicating the difficulty of accurate theoretical estimation of this highly spectrum-sensitive effect.

Although the neutron-scattering effect in the 0.50 mm. steel backing was sufficiently large in 8A to enable a reasonably accurate comparison between experimental and theoretical estimates of the effect, it must be stressed that, for the usually-employed 0.10 mm.-aluminium-backed deposits, the effect is scarcely detectable. Substituting $\Sigma \sim 0.09 \text{ cm}^{-1}$ and $t \sim 0.01 \text{ cm.}$ (for the aluminium), one obtains from (A),

$$\left(\frac{\sigma_{\text{eff}} - \sigma_0}{\sigma_0} \right)_{\text{alum.}}^{8A} \sim 0.2\%,$$

or, as suggested above, the estimated effect is $\sim (0.4 \pm 0.2)\%$. For other ZEBRA test regions, the effect is even smaller, e.g. for Cores 8B ($\sigma_1 \sim 0.25 \text{ b.}, \sigma_0 \sim 0.22 \text{ b.}$) and 8C ($\sigma_1 \sim 0.37 \text{ b.}, \sigma_0 \sim 0.25 \text{ b.}$), the corresponding estimates are only $(0.02 \pm 0.01)\%$ and $(0.10 \pm 0.05)\%$, respectively. Attempts were made in Cores 8A and 8C to obtain experimental estimates of the aluminium-backing effects in these cores, by irradiating aluminium-backed deposits with extra bare backings packed alongside. Within the experimental accuracies of $\sim \pm 1\%$, no effects could be detected, tending to confirm the above-quoted theoretical estimates.

A2.2 BACKING-ACTIVATION EFFECT

The finite contribution of activated isotopes in the backing material itself, to the observed count-rate from an irradiated uranium deposit, was borne out by absolute U-238 capture measurements in ZEBRA

Core 8B. These were carried out using the 0.50 mm. steel-backed deposits, no experimental corrections being applied in the counting for the backing-activation effect. The uncorrected results obtained for the various deposit-source combinations used in the counting are given in column (a) of Table A2.1 and these clearly show that, though there is excellent agreement between values derived from the same uranium deposit, there is a constant discrepancy between the results for Deposit U_{S1} and those for Deposit U_{S2}. This is easily understood if one remembers that, for a given deposit, the activation effect, E, is inversely dependent on the uranium-to-steel ratio. As the steel-backing mass was constant (within ~ 1%) for the various deposits, one could write

$$E_i = \frac{k^1}{\alpha_i}$$

where k^1 is a proportionality constant and α_i is the uranium α count-rate from deposit i.

Denoting the effects for the two deposits used in Core 8B by E_{S1} and E_{S2} , respectively, it is easily seen from the above expression for E_i that:

$$E_{S1} = \frac{(E_{S1} - E_{S2}) \cdot \alpha_{S2}}{(\alpha_{S2} - \alpha_{S1})} \quad \text{and} \quad E_{S2} = \frac{(E_{S1} - E_{S2}) \cdot \alpha_{S1}}{(\alpha_{S2} - \alpha_{S1})} \quad \dots\dots(B)$$

From column (a) of Table A2.1, one obtains $(E_{S1} - E_{S2})$ as $(0.072 \pm 0.015) \times 10^{-16}$. Further, from the relative α -counting of the deposits, α_{S1} and α_{S2} were known to be - for a particular geometry - $(593 \pm 2) \text{ hr}^{-1}$ and $(1282 \pm 3) \text{ hr}^{-1}$ respectively.

Substituting these numerical values into (B), the effects for the 8B deposits are obtained as:

$$E_{S1} = (0.134 \pm 0.030) \times 10^{-16} \text{ sec.}^{-1} \quad \text{and}$$

$$E_{S2} = (0.062 \pm 0.015) \times 10^{-16} \text{ sec.}^{-1}$$

Applying these derived corrections, one obtains the results given in column (b) of Table A2.1, the agreement between these corrected values fully justifying the above analysis.

TABLE A2.1. EFFECT OF STEEL-BACKING ACTIVATION IN CORE 8B

Deposit-Source Combination	Abs. U-238 Cap. Rate ($\times 10^{-16} \text{ sec.}^{-1}$)	
	(a) Uncorrected	(b) Corrected
$U_{S1} - A_{S1}$	2.232 ± 0.015	2.10 ± 0.03
$U_{S1} - A_{S2}$	2.210 ± 0.015	2.08 ± 0.03
$U_{S2} - A_{S1}$	2.153 ± 0.015	2.09 ± 0.02
$U_{S2} - A_{S2}$	2.145 ± 0.015	2.08 ± 0.02

A direct comparison of the activation effects for 0.10 mm. aluminium and 0.50 mm. stainless steel backings was made in Core 8C, where absolute U-238 capture measurements were carried out using both types of deposits. NaI(Tl) and Ge(Li) spectra of the radiations from the two types, at ~ 22 hours after irradiation, are compared in Figs. A2.1 and A2.2. In the case of the steel-backing deposit, the 105 keV Np-239 region is seen to be swamped (in the NaI spectrum) by a huge steel-activity peak. This was identified (from the Ge spectrum) as the 140 keV γ -ray of Tc-99m formed by the decay of Mo-99 which, in turn, is produced by the (n, γ) reaction of the Mo-98 in the steel. Although this particular γ -ray distorts the singles spectrum and increases the random coincidence rate, it does not contribute significantly

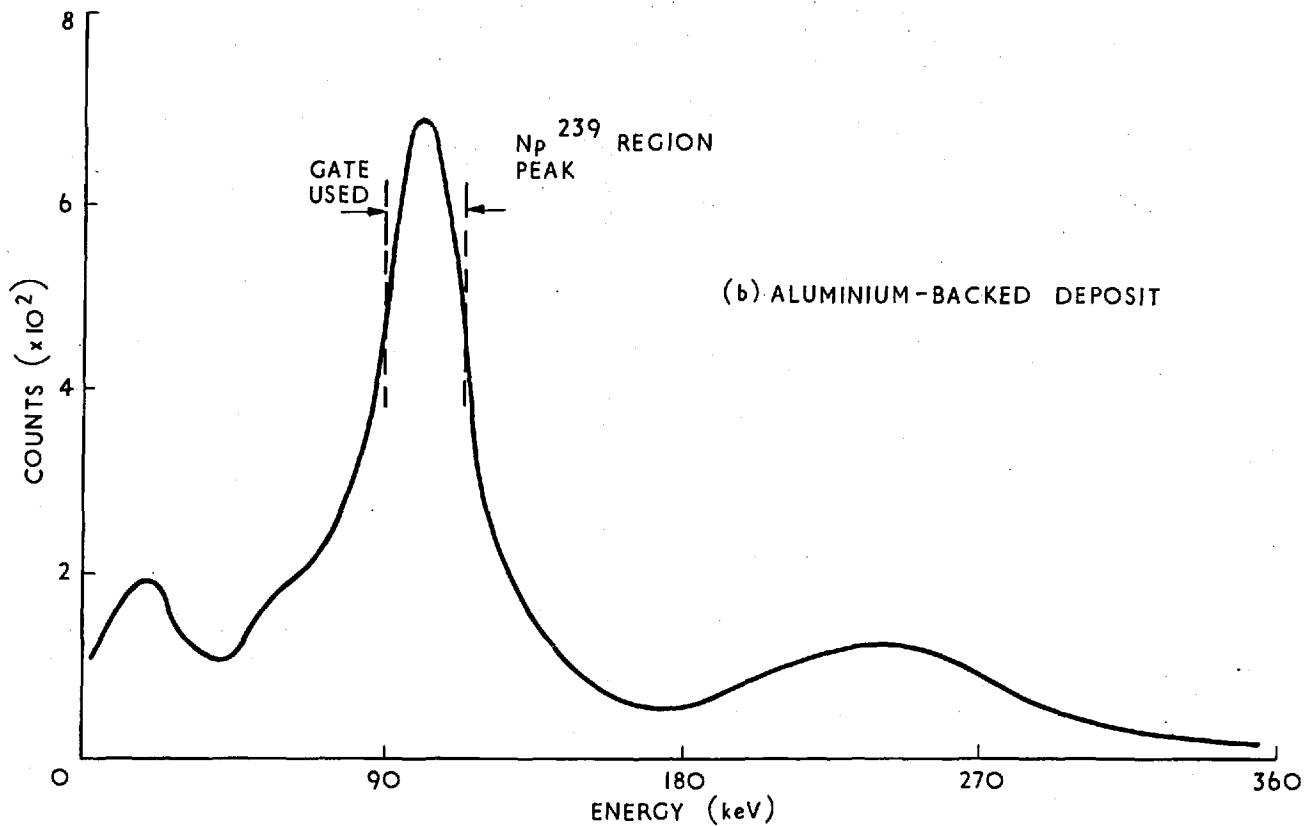
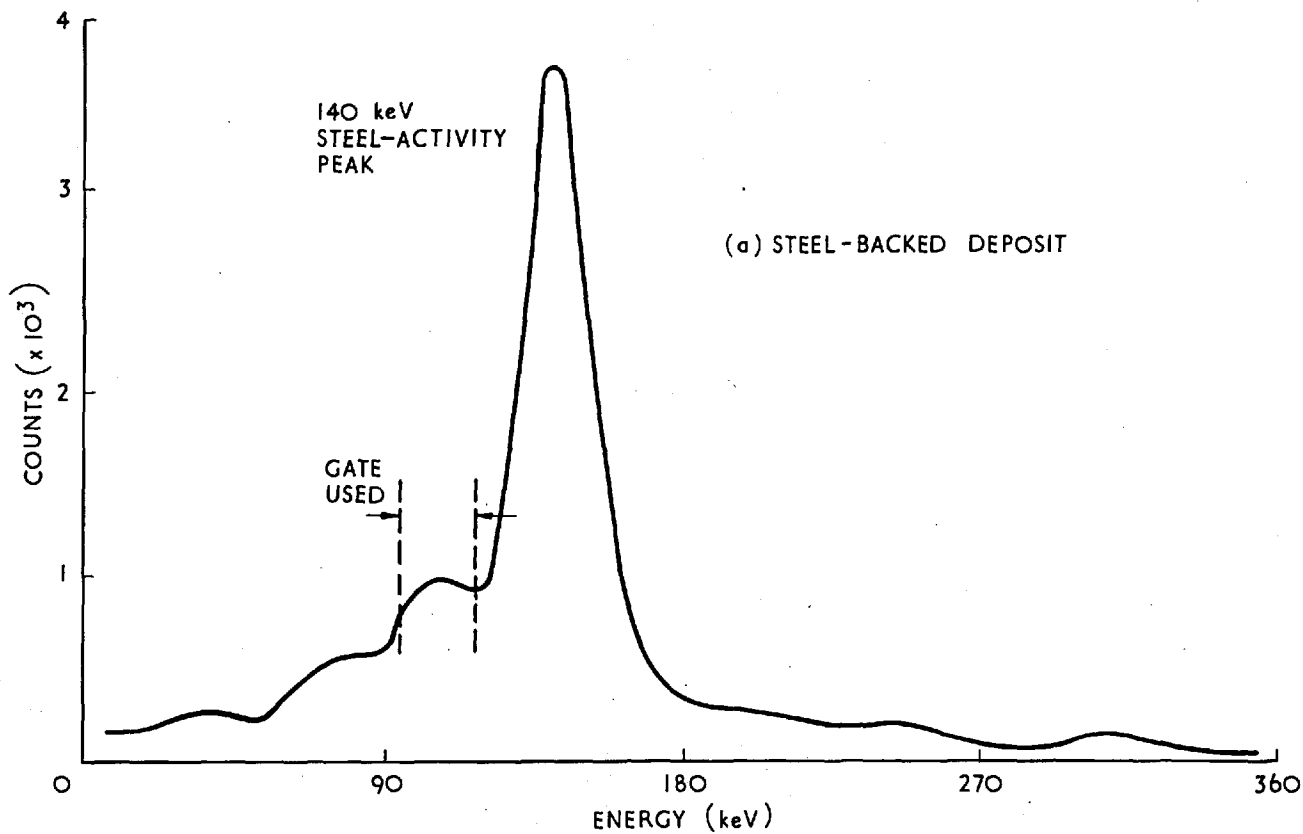


FIG. A2.1. NaI (TL) SPECTRA OF STEEL- & ALUMINIUM-BACKED DEPOSITS
~ 22 HRS AFTER IRRADIATION IN ZEBRA 8C

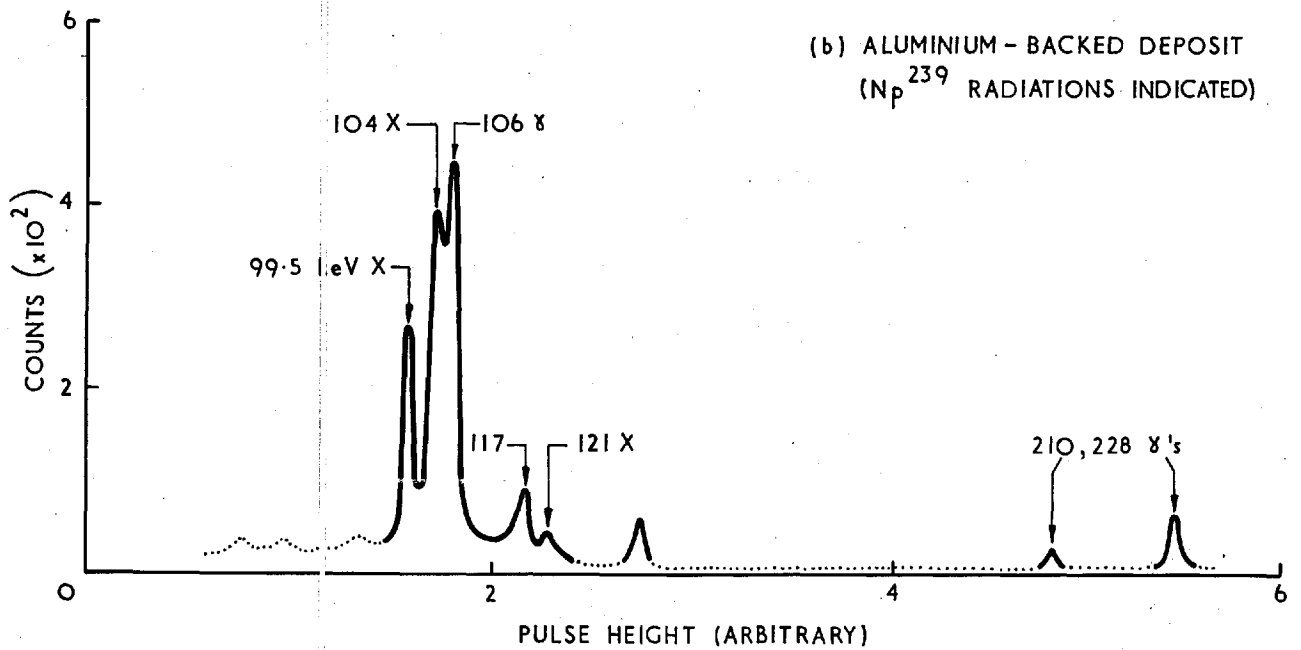
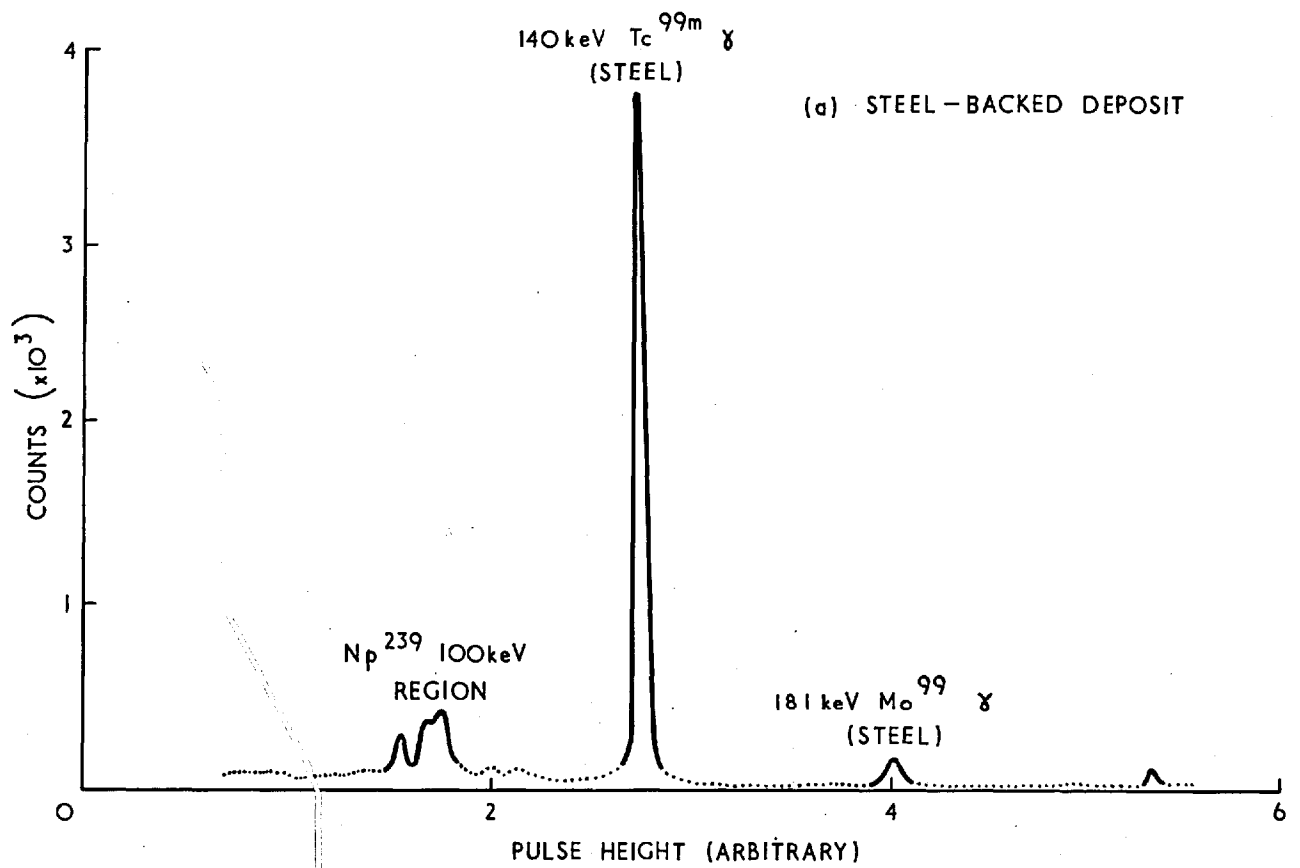


FIG. A2.2. Ge(Li) SPECTRA OF STEEL - & ALUMINIUM-BACKED DEPOSITS
~22HRS AFTER IRRADIATION IN ZEBRA 8C

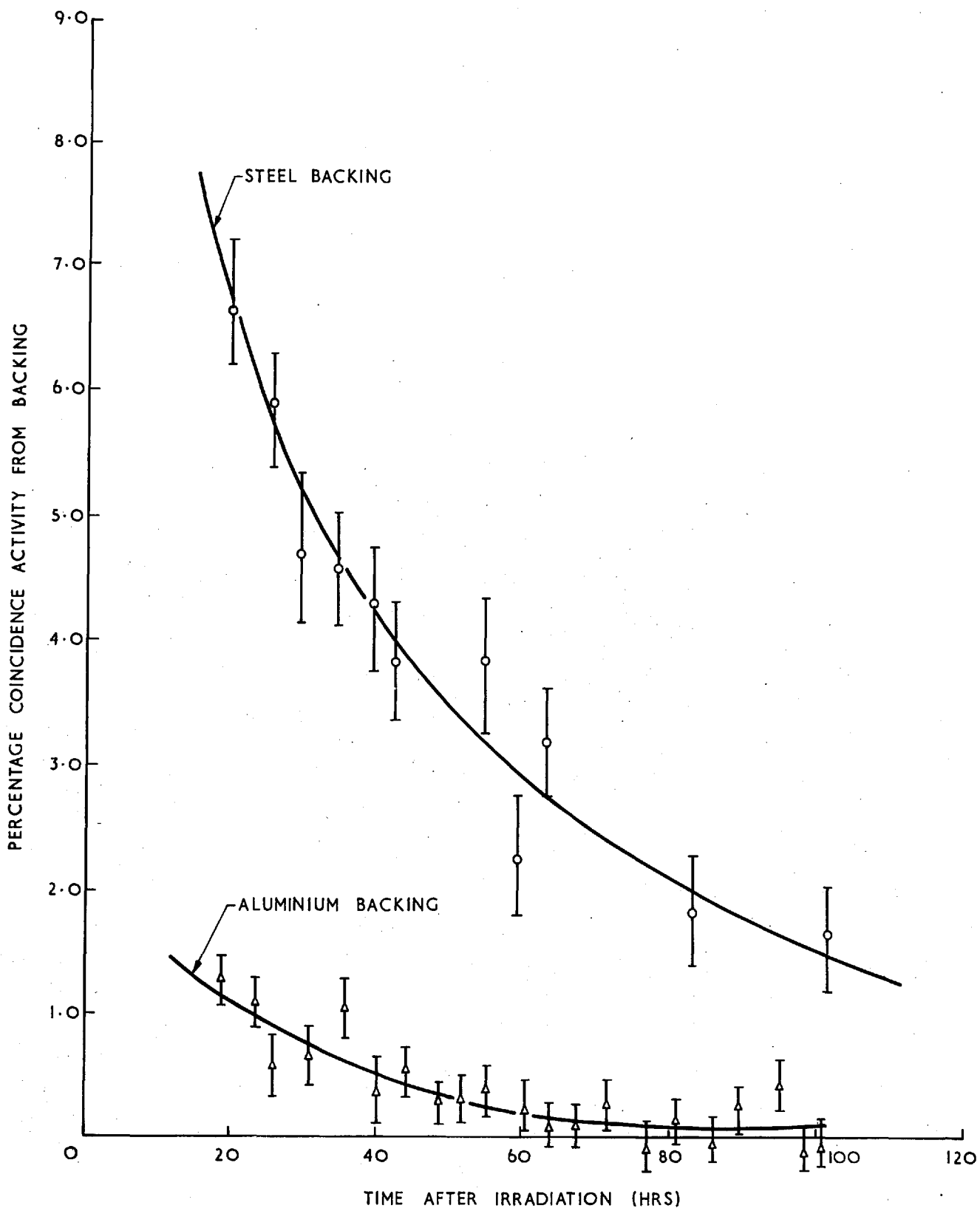


FIG. A2.3. PERCENTAGE COINCIDENCE ACTIVITIES FROM BARE BACKINGS AFTER 2HR-IRRADIATION IN ZEBRA 8C

to the true coincidences. There are, however, other activated isotopes, e.g. Mn-56 from the (n,γ) reaction of Mn-55, which do so by registering coincident Compton-scattered events from higher-energy γ -rays. Fig. A2.3 shows the decay of the spurious coincidences, from irradiated bare steel and aluminium backings, expressed as a percentage of the Np-239 coincidence activity from a typical simultaneously-irradiated uranium deposit. To compare the two curves, one may note the contributions to the true coincidence rate at 50 hours after the end of the irradiation. This is seen to be $\sim 4\%$ for the 0.50 mm. steel, but less than 0.5% for the aluminium backing.

The effect of the aluminium activation is too small to be deduced in the manner used for the steel-backed deposits in 8B, where the steel-activation effect was nearly an order of magnitude greater than the statistical accuracy of the Np-239 counting. However, by irradiating a bare aluminium backing under similar conditions to those for the uranium deposit, and by counting it on the a.f.c. as part of the normal measurement, an accuracy of better than $\pm 10\%$ can be achieved in the estimation of the effect. This then renders the error, due to the applied correction, quite negligible for the aluminium-backed deposits.

Techniques for the absolute determination of ^{238}U capture and ^{239}Pu fission rates in a fast reactor assembly have been developed. The effective reaction rate ratios derived from these absolute measurements have been found to agree within 2% with those obtained using the standard thermal-comparison technique which tends to confirm the absence of any unsuspected systematic error in either method. It is shown that the absolute technique has a greater potential accuracy in the determination of this reaction rate ratio than is possible with the thermal-comparison method.

Absolute measurements of ^{238}U capture and ^{239}Pu fission rates in fast reactors

R. Chawla, MSc, DIC, BSc*

C. B. Besant, PhD, DIC, BSc(Eng)†

INTRODUCTION

The ratio of the neutron capture rate in ^{238}U relative to the fission rate in ^{239}Pu is the major parameter determining the neutron balance in a U-Pu fast reactor system. Studies have shown that, for useful comparisons between theory and experiment, an accuracy of at least $\pm 1\%$ is desirable in the measurement of this reaction-rate ratio in low-power fast reactor assemblies such as ZEBRA.¹

It is also important, wherever possible, to firmly establish the absence of any systematic errors in a particular measurement by using a completely independent technique to determine the same parameter. To date, all experimental results for the ratio of ^{238}U capture relative to ^{239}Pu or ^{235}U fission in reactor lattices have been obtained by comparison of the lattice ratio with that in a thermal column, where the individual cross sections for the two reactions are known to an accuracy of $\pm 1\%$.²⁻⁵ This technique apart from the inherent error on the thermal cross section values used, suffers from a few other drawbacks. For example, self-shielding of the foils and fission chambers used in the thermal measurements is significant and corrections for this have to be applied. Further, the fact that each reaction rate ratio measurement entails two sets of irradiations, using in general two different reactors, results in error due to reactor power intercalibrations and other necessary correlations.

Techniques for the absolute measurement of ^{238}U capture and ^{239}Pu fission rates in the reactor assembly itself have been developed for ZEBRA, and this has enabled direct determination of the reaction-rate ratio without recourse to any comparisons with thermal irradiations.

ABSOLUTE ^{238}U CAPTURE MEASUREMENT

The present technique for the absolute determination of

^{238}U capture rates is a modification of the method described by Seufert and Stegemann.⁶ This method is based on the fact that both ^{243}Am and ^{239}U decay via ^{239}Np into ^{239}Pu and this enables the detector system, used in measuring the ^{238}U captures in an irradiated uranium sample, to be calibrated. The technique as applied by Seufert and Stegemann, however, suffers from the following possible sources of systematic error:

- The gamma-X ray self-absorption correction for the uranium foils used was greater than 35%, causing extrapolation to zero thickness to be inaccurate.
- The method of determining the amount of uranium in the thin deposits (used for obtaining the self-absorption vs. thickness, curve) was limited in accuracy by the weighings that had to be made.
- The source geometry in the gamma-X ray coincidence counting of the uranium foils and the ^{243}Am samples was not consistent, since the uranium foils were 100-500 μ thick while the ^{243}Am sources were thin, evaporated deposits on glass backings.
- There was a finite uncertainty in the geometry factor and absolute efficiency of the low geometry alpha counter used for calibrating the ^{243}Am sources.
- Alpha-emitting impurities in the ^{243}Am samples used necessitated large corrections to the measured alpha count rates.

The present technique has been aimed at eliminating some of the above-mentioned possible sources of systematic error and at reducing the effect of the others to negligible proportions. By using thin uranium deposits and ^{243}Am sources which were prepared on identical backings and in similar electrolytic cells, consistency in the geometry was maintained. Gamma-X ray self-absorption was only $\sim 0.5\%$ for the uranium deposits and $< 10^{-4}\%$ for the ^{243}Am sources. By alpha-assaying the thin uranium deposits in the same low geometry alpha counter as the ^{243}Am sources, the requirement of explicitly knowing the absolute alpha-counter efficiency and the need of weighing the uranium

* Research Student, Imperial College of Science and Technology, University of London, researching under contract with the UKAEA at AEE, Winfrith.

† Lecturer, Imperial College of Science and Technology, University of London.

deposits were both eliminated. Finally, very pure ^{243}Am was used for preparing the sources and it was estimated that the impurity contribution to the alpha count rate was less than 0.1%.

Theoretical description of the present technique

The absolute ^{238}U capture rate, for a uranium deposit irradiated in a reactor lattice, is directly related to the 2.35-day ^{239}Np activity induced in it and may be written as:

$$\text{Capture rate}/^{238}\text{U atom} = (k(t) \cdot N_8)^{-1} \cdot (\text{Induced } ^{239}\text{Np activity}) \quad (1)$$

where N_8 is the number of ^{238}U atoms in the deposit and $k(t)$ is a proportionality constant given by:

$$k(t) = \left[\frac{\lambda_{u9}}{\lambda_{u9} - \lambda_{n9}} \cdot (1 - \exp(-\lambda_{n9}t_1)) \cdot \exp(-\lambda_{n9}t) \right] - \left[\frac{\lambda_{n9}}{\lambda_{u9} - \lambda_{n9}} \cdot (1 - \exp(-\lambda_{u9}t_1)) \cdot \exp(-\lambda_{u9}t) \right] \quad (2)$$

λ_{u9} and λ_{n9} being the known ^{239}U and ^{239}Np decay constants respectively, t_1 being the length of the irradiation and t , the time after the end of the irradiation.

The ^{239}Np activity can be accurately measured by the well established γ -X ray coincidence technique described by Tunnicliffe, *et al.*² If $C_u(t)$ is the measured coincidence count rate from the deposit (corrected for random and fission product coincidences, etc.), then equation (1) becomes:

$$\text{Capture rate}/^{238}\text{U atom} = \frac{1}{k(t)} \cdot \frac{1}{N_8} \cdot \frac{C_u(t)}{(1-a)} \quad (3)$$

where a is the γ -X ray self-attenuation correction for the thin deposit and η is a calibration factor which embodies (a) the various nuclear parameters determining the probability that a ^{239}Np decay will result in an event capable of yielding a true coincidence in the gated energy regions, and (b) the coincidence geometry, detector efficiencies and various other features characterizing the experimental arrangement.

η is derived from the knowledge that ^{243}Am is the long-lived parent (half-life, 7950 years) of ^{239}Np . Due to secular equilibrium between the two, the ^{239}Np activity A_n in the source is related to the ^{243}Am activity A_a by:

$$A_n = A_a \quad (4)$$

If a ^{243}Am source is prepared such that its shape and backing are the same as those of the uranium deposit, and if the ^{239}Np in the source is monitored in exactly the same coincidence arrangement as the irradiated uranium deposit, then it can be seen that the calibration factor η will be the same for the source and the deposit. If C_a is the measured coincidence rate (corrected for random coincidences) from the source, then:

$$C_a = \eta \cdot A_n \cdot (1-a') \quad (5)$$

or from equation (4),

$$C_a = \eta \cdot A_a \cdot (1-a') \quad (6)$$

a' being the γ -X ray self-absorption correction for the source.

Substituting for η from equation (6) into (3), one obtains:

$$\text{Capture rate}/^{238}\text{U atom} = \frac{1}{k(t)} \cdot \frac{A_a}{N_8} \cdot \frac{C_u(t)}{C_a} \cdot \frac{(1-a')}{(1-a)} \quad (7)$$

The ^{243}Am activity A_a of the source can be obtained from an alpha-assay in a low geometry alpha counter. If the absolute efficiency of the counter, inclusive of the geometry factor, is ω and if B_a is the measured alpha count rate, then A_a is given by:

$$A_a = \frac{B_a}{\omega} \quad (8)$$

Equation (7) now becomes

$$\text{Capture rate}/^{238}\text{U atom} = \frac{1}{k(t)} \cdot \frac{B_a}{\omega} \cdot \frac{1}{N_8} \cdot \frac{C_u(t)}{C_a} \cdot \frac{(1-a')}{(1-a)} \quad (9)$$

For a natural uranium deposit, N_8 is given by:

$$N_8 = 0.9928N_u \quad (10)$$

where N_u is the number of uranium atoms in the deposit. If the effective alpha decay constant of natural uranium, known to an accuracy of $\pm 0.2\%$ ⁷ is denoted by λ_u , then the alpha activity A_u of the natural uranium deposit is given by:

$$A_u = \lambda_u \cdot N_u \quad (11)$$

If the natural uranium deposit is alpha-assayed in exactly the same low geometry alpha counter as the ^{243}Am source, A_u is obtained as:

$$A_u = \frac{B_u}{\omega} \quad (12)$$

where B_u is the measured alpha count rate from the deposit and ω is the factor used previously, since the counting system and geometrical arrangement have been preserved.

From equations (10), (11) and (12), one obtains:

$$N_8 = \frac{0.9928}{\lambda_u} \cdot \frac{B_u}{\omega} \quad (13)$$

Finally, substituting for N_8 in (9), the absolute ^{238}U capture rate may be written as:

$$\begin{aligned} \text{Capture rate}/^{238}\text{U atom} &= \frac{1}{k(t)} \cdot \frac{\lambda_u}{0.9928} \cdot \frac{B_a}{B_u} \cdot \frac{C_u(t)}{C_a} \cdot \frac{(1-a')}{(1-a)} \\ &= K(t) \cdot \frac{B_a}{B_u} \cdot \frac{C_u(t)}{C_a} \end{aligned} \quad (14)$$

where

$$K(t) = \frac{\lambda_u}{0.9928k(t)} \cdot \frac{(1-a')}{(1-a)} \quad (15)$$

K is a parameter known to an accuracy better than $\pm 0.3\%$ (Table 1), and therefore it follows from equation (14) that the ^{238}U capture rate is obtained absolutely from two simple relative measurements made with alpha and γ -X ray counting systems. Neither absolute calibration of the ^{243}Am source, nor weighing of the thin uranium deposits, is necessary, the overall accuracy of the result being limited essentially by counting statistics.

Experimental procedure

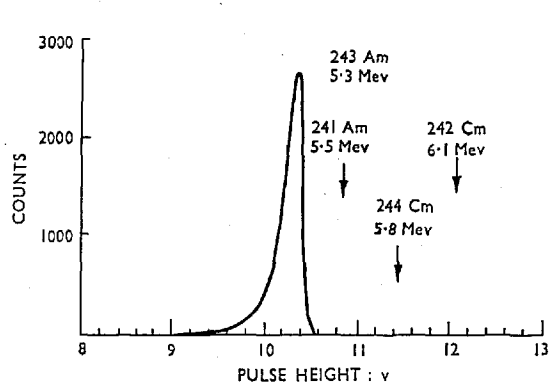
Natural uranium deposits (0.5–1.0 mgm/cm² over an area of $\sim 3\frac{1}{2}$ cm²) and thin ^{243}Am sources (over exactly the same area) were prepared on 27.0 mm dia. 0.10 mm thick aluminium discs by an electrolytic (molecular plating) process.⁸ The purity of the prepared samples was checked both by mass spectroscopy and alpha spectrometry.

Table 1: Potential accuracy of the absolute measurements

Source of error	Error
Absolute ^{238}U capture measurement	
1. Effective alpha decay constant of natural uranium, λ_a	0.2%
2. Effect of uncertainties in ^{239}U and ^{239}Np decay constants on $k(t)$	0.1%
3. Self-absorption of γ -, X-rays	0.1%
4. Effect of 0.10 mm thick aluminium backing	0.2%
5. Fission-product correction to observed ^{239}Np activity	0.1%
6. Recoil losses of ^{239}Np from ^{243}Am source	0.05%
7. ^{239}Np counting statistics	0.4%
8. Determination of alpha count-rate ratio	0.2%
Absolute ^{239}Pu fission measurement	
1. Calibration of the fission chamber deposit	0.5%
2. Fission product counting	0.2%
3. Determination of plate to chamber fission rate ratio	0.3%
Total rms error	0.8%

Fig. 1 shows typical alpha spectra for the deposits obtained using a low geometry alpha counter and a biased multichannel analyser. These spectra confirmed the fact that, though the energy degradation of the alphas in the deposits themselves impaired the observed energy resolution significantly, the effect was small enough to enable undistorted alpha count rates to be obtained by integral counting above a sufficiently low threshold.

The low geometry alpha counter itself was of standard design,⁹ and geometry factors of between 1:150 and 1:250 were used. The detector was a surface-barrier silicon diode with a nominal depletion depth of 0.2 mm and an operating bias of 25 V. During operation, the counter was evacuated using a rotary pump and the pressure was maintained at ~ 0.02 torr. The background count rate for the alpha counting was typically 0.2% of the uranium deposit count rates and 0.03% of the ^{243}Am deposit counts, and hence negligible error resulted from the background corrections applied. Statistical accuracies of better than $\pm 0.3\%$, in this low geometry alpha-counting, were obtained by counting each uranium deposit for 4-5 days and each ^{243}Am source for about one day.

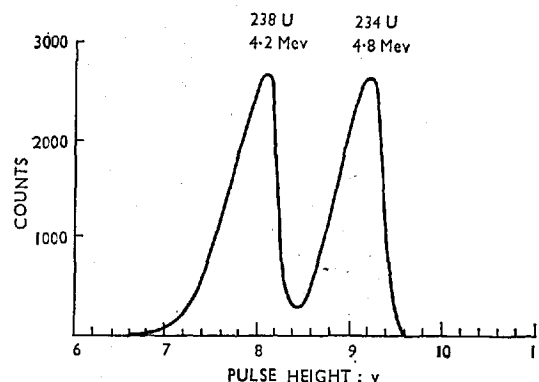


(a) ^{243}Am (Showing positions of possible 'impurity peaks')

For loading the uranium deposits into the reactor, special natural uranium plates were made (Fig. 2). Each loading plate consisted of two halves, both of which were 50.6 mm square and 1.55 mm thick. One half-plate had a recess for carrying the deposit. The other had a protruding ring (also of uranium) which locked into this cavity and held the deposit in position by pressing against the bare aluminium on the periphery. The deposited surface itself did not touch either half-plate, thus ensuring that none of it was accidentally scraped off. The protruding ring of the upper half-plate and the staggered positioning of the deposit itself both served to shield it from any neutron streaming effects that might occur along any gap between the two halves. With the deposit loaded and the two half-plates fitted together, the cavity in the middle was less than 0.3 mm deep and this was assumed to be sufficiently small to have negligible effect. Externally, the loading plate was identical to an ordinary 50.6 mm \times 50.6 mm \times 3.1 mm natural uranium ZEBRA plate¹ and could therefore be used for measurements in any ZEBRA cell.

γ -X ray coincidence counting of the irradiated deposits was carried out between 1200 and 10 000 minutes (i.e., over about $2\frac{1}{2}$ half-lives) after irradiation, using an automatic foil changer and a thermo-regulated NaI(Tl) coincidence system with a coincidence resolving time of 0.2 μsec . The channels were set on the 105 keV ^{239}Np region, with a channel width of $\pm 10\%$. To ensure consistency in the experimental conditions, the ^{243}Am source was counted along with the deposits and a weighted mean of its coincidence rate was obtained, accurately characterizing the state of the electronics, geometry, settings, etc., during the common counting-period.

A computer program, CAPABS, was written to analyse the measurements. The input data consisted of the alpha count rate ratio (B_a/B_u) and its statistical accuracy, a few experimental details (e.g. length of the irradiation, duration of each counting interval, coincidence resolving time, etc.), various corrections to be applied (e.g. γ -X ray self-attenuation, fission product, natural activity and other coincidence backgrounds), and the coincidence measurement data itself obtained in card form from an IBM auto-punch linked to the electronics. Equation (14) was effectively solved for each point, a statistically weighted mean value of the absolute ^{238}U capture rate was obtained and a net rms percentage error calculated.



(b) NATURAL URANIUM

Fig 1 Alpha spectra of the ^{243}Am and natural uranium deposits

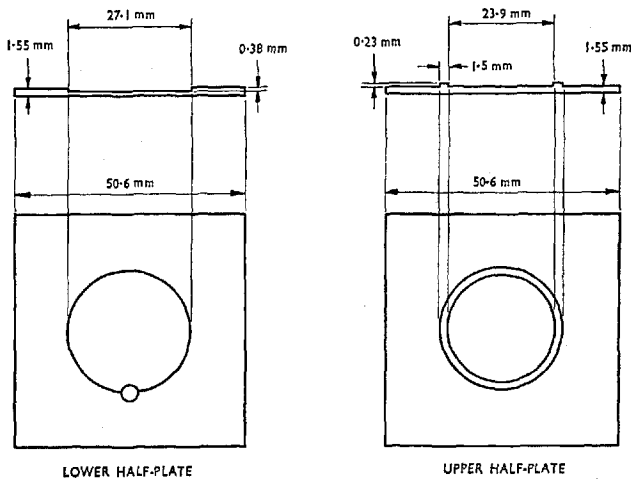


Fig 2 The ZEBRA loading plate for the uranium deposits

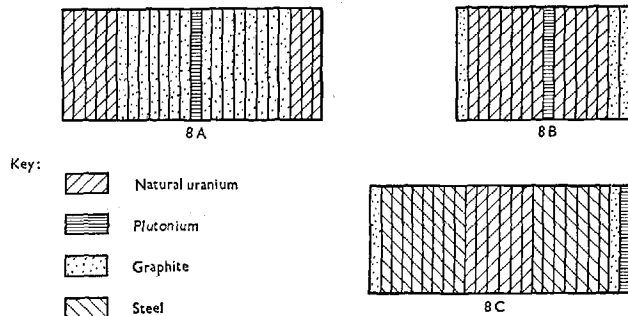


Fig 3 Lattice cells for ZEBRA cores 8A, 8B and 8C

Investigation of possible systematic errors

The 0.10 mm thick aluminium backings were found to be adequate in maintaining the rigidity of the deposits, this being an essential aspect of both the alpha and the γ -X ray counting. Increasing the backing thickness or replacing it by other material such as steel, however, was found to have two adverse effects. First, the distortion of the neutron spectrum inside the uranium plate, due to neutron scattering in the backing, became significant; and secondly, neutron activation of the backing itself necessitated a larger correction to the observed γ -X ray coincidence rates. Both these effects were investigated by preparing a few natural uranium deposits and ^{243}Am sources on 0.50 mm stainless steel backings and using these independently for some absolute ^{238}U capture measurements in ZEBRA cores 8A and 8B (Fig. 3).

From the investigation of the neutron scattering effect in the uranium deposit backing (see Appendix), it was established that the resultant increase in the ^{238}U capture rate due to the 0.10 mm aluminium backing was very small indeed. Estimates of $(0.23 \pm 0.23)\%$, $(0.01 \pm 0.01)\%$ and

$(0.05 \pm 0.05)\%$ were made for this effect in cores 8A, 8B and 8C, respectively. It may be mentioned that core 8A, though very suitable for studying the neutron scattering effect in the backing, is not a typical fast reactor core in that the neutron spectrum is very soft. For other ZEBRA cores, the backing effect is much smaller (e.g. for cores 8B and 8C), and it can safely be said that, in general, the error resulting from the backing effect correction is negligibly small.

The other important advantage of using aluminium as the backing material for the uranium deposits was that the neutron-induced activity in it was very small. The γ -X ray singles spectrum from an irradiated aluminium-backed deposit was observed to show, at ~ 24 hours after irradiation, mainly the ^{239}Np peaks. On the other hand, the singles spectrum from an irradiated steel-backed deposit was severely distorted by a 140 keV γ -ray peak due to Mo-activation in the steel. The contribution of the activity induced in the backing, to the observed coincidence rate from an irradiated deposit, was taken into account in each measurement by counting, along with the deposit, coincidences from a simultaneously-irradiated bare backing. It was observed that, at ~ 50 hours after irradiation, the backing contribution to the coincidence rate was only about 0.5% for the aluminium backing while it was as much as 4% for the 0.50 mm steel. Assuming that the correction can be applied to $\sim \pm 10\%$ accuracy, it is clear that the resultant error for the aluminium is negligible while for the steel it is not.

An investigation of the other possible systematic errors in the measurement was carried out and this, as discussed below, satisfactorily showed that none of them had any significant effect on the accuracy of the results. The γ -X ray self-attenuation effects were calculated⁶ on the basis of theoretical values of the uranium cross section for 100 keV γ -X rays.¹⁰ For the natural uranium deposits used in the present measurements, the self-attenuation correction was estimated as being between 0.3 and 0.7%, and the accuracy of $\sim \pm 20\%$ in these estimates was quite adequate in rendering the resultant error insignificant.

Two other small corrections were applied to the measured deposit coincidence rates. Firstly, the fission product coincidence correction was estimated as being $\sim (0.2 \pm 0.1)\%$ for natural uranium deposits in most ZEBRA cores—this value being based on previous work done at Winfrith with NaI(Tl) coincidence systems.³ The second effect considered was the possible loss by recoil of ^{239}Np nuclei which are continuously being formed in the ^{243}Am sources. On the basis of experiments performed with various collectors placed very close to the sources, it was shown that these losses were no more than $(0.20 \pm 0.05)\%$. This confirmed that there was no need for sealing the ^{243}Am sources, and that the error, due to the 0.05% uncertainty in the effect, was negligible.

The systematic accuracy in the determination of the alpha count rate ratio, (B_a/B_u) , was established by (a) using different geometries and different detectors for obtaining this ratio, and (b) counting the uranium deposits both before and after irradiation. In both cases, the repeatability of these measurements was confirmed by obtaining consistent results within statistical accuracies of better than $\pm 0.4\%$.

Table 1 summarizes the limiting errors of the absolute ^{238}U capture measurement.

ABSOLUTE ^{239}Pu FISSION MEASUREMENT

Absolute fission measurements in ZEBRA using gas-filled fission chambers have been described by Stevenson and Broomfield.¹¹ Though these chambers are quite adequate for relative measurements of fission ratios in the reactor, they were found to be unsuitable for the present absolute ^{239}Pu fission measurements because of the following serious corrections which had to be applied:

- (a) $\sim(2.5 \pm 0.8)\%$ dead-time correction in the instrumentation count-rates for intercalibrating the different reactor powers used for the capture and fission measurements;
- (b) $\sim(5.2 \pm 1.6)\%$ correction for fission product self-absorption in the ^{239}Pu fission-chamber deposit; and
- (c) $\sim(2.9 \pm 0.7)\%$ correction for the biased off low energy pulses produced in the fission chamber. There was also finite uncertainty in the collection efficiency and geometry of the collector electrode in the fission chamber.

Two new fission chambers were made with ^{239}Pu electro-deposits of ~ 30 and $14 \mu\text{g}/\text{cm}^2$, over diameters of ~ 2.85 cm and 1.90 cm respectively, on 3.8 cm dia., 0.13 mm thick platinum discs. These deposit masses were nearly two orders of magnitude less than those in the earlier ZEBRA chambers, and this enabled absolute fission measurements to be made at the same reactor power as the absolute ^{238}U capture measurement, namely ~ 100 W. Since the instrumentation dead-time corrections were approximately equal in the two cases, there was no resultant error due to (a).

The fission product self-absorption correction in a deposit of thickness t , with a variation about this value of σ , is given by:¹¹

$$(\sigma^2 + t^2)(2tR)^{-1} \quad (16)$$

where R is the mean range of the fission fragments in the deposit material. This correction was calculated to be 0.20% for the first new chamber (ZEB-31) and 0.09% for the second (ZEB-32). With an assumed error in this correction of $\sim \pm 30\%$, the resultant error in the observed count rate was insignificant.

The pulse height spectrum of fission fragments in ZEB-32 is compared in Fig. 4 with that of one of the early chambers. Both spectra were obtained for irradiations in core 8C (Fig. 3). The much smaller mass of the plutonium in the new chamber caused comparatively negligible alpha interference, there being very little pulse pile-up in the low energy region. Further, the degradation in energy of the fission fragments was far less in the thin deposit and this improved the resolution of the fission-product energy peaks. A comparison of the pulse height spectra from chambers ZEB-31 and ZEB-32 revealed that the resolution was better for the latter. This is explained by the smaller area of the deposit in the latter, a feature which reduced the fraction of fission fragments unable to lose their full energy before striking the chamber wall. All the three factors described above contributed to minimizing the number of low energy pulses which had to be biased off. As a result, correction (c) was only 0.1% for ZEB-32 and 0.4% for ZEB-31. Once again, the resultant error was negligible.

The doubt about the collection efficiency and geometry of the collector was cleared by comparing the fission rate results obtained for the different area deposits in the two new chambers. No discrepancy was observed.

As discussed above, the errors, due to the various correc-

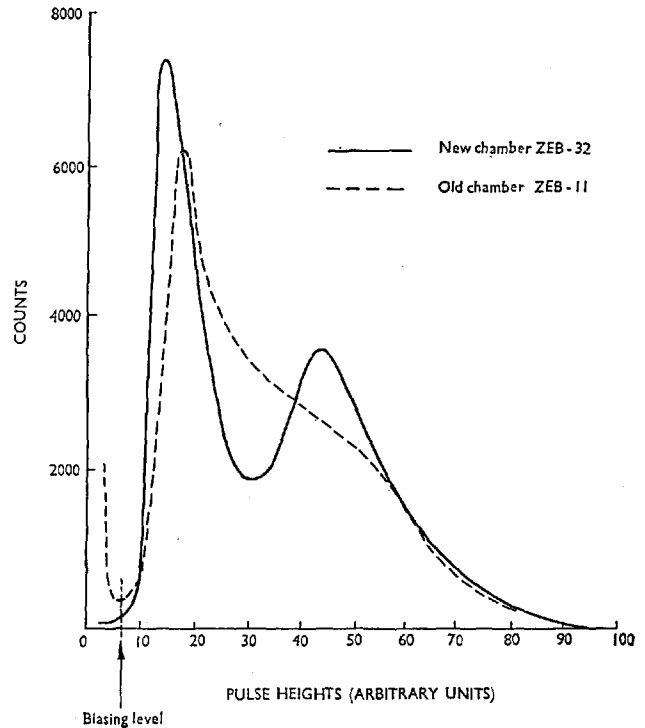


Fig 4 Comparison of pulse height spectra obtained with old and new ZEBRA fission chambers in ZEBRA core 8C

tions for the absolute ^{239}Pu fission chambers, have been reduced to negligible proportions. The overall accuracy of the absolute fission measurement was, in fact, limited mainly by the accuracy obtained in the absolute low-geometry alpha-assay of the ^{239}Pu fission-chamber deposits (Table 1).

It should be noted that the absolute fission chamber measurement was carried out in a cavity in the core formed by removing half a fuel element. However, the reaction rate of interest for theoretical comparison is that in the Pu plate itself. This was obtained by comparing the fission-product gamma activity of a Pu foil in the plate to that of a similar foil in a dummy fission chamber in the cavity, using a NaI(Tl) scintillation counter for integral gamma-counting above a threshold of 1.28 MeV. The correction for self-shielding of the dummy-chamber foil is usually negligibly small but, where significant, it can be determined accurately by irradiating foils of different thicknesses in the chamber. An accuracy of $\pm 0.3\%$ is quite feasible in the determination of the plate-to-chamber fission rate ratio in this way. The possibility of applying solid state track recorders to absolute fission measurements in ZEBRA is being currently investigated. If this method proves successful, it will enable direct absolute measurements to be made in the Pu plate and thereby eliminate the necessity of plate-to-chamber correlation.

RESULTS AND COMPARISON OF TECHNIQUES

Absolute ^{238}U capture and absolute ^{239}Pu fission measurements were carried out in ZEBRA core 8C along with a

thermal-comparison determination of the reaction-rate ratio in the core. For the absolute ^{238}U capture measurement, natural uranium deposits were loaded into the central uranium plates of the 8C cell (Fig. 3) at position (50, 50) in the reactor lattice, while the absolute ^{239}Pu fission measurement was made at position (50, 52). Table 2 summarizes

Table 2: Results obtained in ZEBRA core 8C

Expt.	Abs. ^{238}U cap. rate ($\times 10^{-16} \text{ s}^{-1}$)	Abs. ^{239}Pu fiss. rate ($\times 10^{-15} \text{ s}^{-1}$)	(σ_c^8/σ_f^8) abs. tech.	(σ_c^8/σ_f^8) thermal tech.	(σ_c^8/σ_f^8) theory
1	4.22 ± 0.04	3.28 ± 0.05	0.129 ± 0.002	0.126 ± 0.003	0.127
2	5.29 ± 0.05	4.16 ± 0.04	0.127 ± 0.002	0.126 ± 0.002	0.127

the results obtained in two separate sets of measurements. All the quoted results have been normalized by the use of foils¹² to give the average reaction rate ratio in the 8C cell. The value of this ratio predicted using current calculational methods and nuclear data was 0.127.

CONCLUSIONS AND DISCUSSION

The fact that the results obtained from the absolute and the thermal comparison techniques agree within their assigned errors, in both 8C measurements, indicates the absence of any unsuspected systematic error in either method.

The various advantages of the absolute technique over the thermal-comparison method have been discussed earlier. It only remains to affirm that the former is also capable of the greater accuracy. The errors of $\sim 1\%$ quoted for the absolute ^{238}U capture rates in the 8C measurements were mainly due to the relatively poor statistics obtained in the γ -X ray coincidence counting of the irradiated deposits. Increasing the irradiation time from two to four hours and the use of thicker uranium deposits (up to $\sim 3 \text{ mgm/cm}^2$) would reduce this error to less than 0.5%. The ^{239}Pu counting statistics could be further improved by substituting NaI(Tl) coincidence counting of the deposits by singles counting of the 102-108 keV ^{239}Pu region using a high-resolution Ge(Li) detector. It is concluded that, with the absolute techniques described in this Paper, an overall accuracy of better than $\pm 1\%$ is quite feasible in determining ^{238}U capture-to ^{239}Pu -fission ratios in fast reactors.

ACKNOWLEDGEMENTS

Thanks are due to Dr C. G. Campbell, Professor P. J. Grant and Dr J. E. Sanders for their suggestions and advice, to Mr C. F. George for help in some of the experimental work, to Mr D. Wardleworth for useful theoretical discussions, and to Messrs F. M. Bolton and G. A. Barnett for preparing the various deposits.

APPENDIX: INVESTIGATION OF THE NEUTRON-SCATTERING EFFECT IN THE URANIUM-DEPOSIT BACKING

Measurements in ZEBRA core 8A, which had a very soft neutron spectrum, revealed that the presence of a 0.50 mm

thick stainless steel backing caused a $(17 \pm 1)\%$ increase in the ^{238}U capture rate measured from a uranium deposit. This large effect is easily explained if one considers the fact that, though the perturbations in the neutron spectrum caused by the steel backing are only slight, they considerably alter the resonance shielding of the ^{238}U in the deposit. If $\phi_1(E)$ is the neutron flux incident on the block of uranium plates, the flux at the centre of the block, $\phi_0(E)$, may be approximated by:

$$\phi_0(E) = \phi_1(E) \frac{\Sigma_s(E)}{\Sigma_t(E)} \quad (17)$$

where $\Sigma_s(E)$ is the non-resonant scattering cross section of uranium at energy E and $\Sigma_t(E)$ is the total cross section. Thus the flux in the central cavity, where the deposits are located, contains large 'dips' corresponding to the various resonances. The ^{238}U capture cross section averaged over this spectrum, that is, the fully shielded cross section, σ_0 , is given by:

$$\sigma_0 = \langle \sigma \rangle_{\phi_0} \quad (18)$$

However, due to the presence of the backing, a fraction f of the neutrons undergo a scattering collision in the steel and may be regarded as having been scattered into the normal $\phi_1(E)$ spectrum. The ^{238}U capture cross section of these neutrons is the infinite dilution cross section, σ_1 , given by:

$$\sigma_1 = \langle \sigma \rangle_{\phi_1} \quad (19)$$

If P_0 is the average collision probability of the neutrons in the backing, the fraction f may be written simply as $\frac{1}{2}P_0$. Thus, the effective ^{238}U capture cross section for the deposit can be written as:

$$\sigma_{\text{eff}} = \sigma_0 (1 - \frac{1}{2}P_0) + \sigma_1 (\frac{1}{2}P_0)$$

i.e.

$$\left(\frac{\sigma_{\text{eff}} - \sigma_0}{\sigma_0} \right) = \frac{1}{2}P_0 \cdot \left(\frac{\sigma_1 - \sigma_0}{\sigma_0} \right) \sim \frac{1}{2} \cdot \left[1 - \left(\frac{1}{1 + 2\Sigma_s t} \right) \right] \cdot \left(\frac{\sigma_1 - \sigma_0}{\sigma_0} \right) \quad (20)$$

where the Wigner rational approximation has been used, Σ being the average macroscopic neutron cross section in the backing and t its thickness.

Equation (20) can be used to give an approximate estimate of the fractional change in the ^{238}U capture rate due to the presence of the backing. One has for the stainless steel backing in core 8A, $\Sigma \sim 0.9 \text{ cm}^{-1}$, $t = 0.05 \text{ cm}$, $\sigma_1 = 0.965 \text{ b}$, and $\sigma_0 = 0.289 \text{ b}$. (Wardleworth¹³). Substituting these values into (20), one obtains:

$$\left(\frac{\sigma_{\text{eff}} - \sigma_0}{\sigma_0} \right)_{\text{steel}}^{8A} \sim 9\% \quad (21)$$

Comparing this with the experimental estimate, it is clear that the formula and the cross sections used are not accurate quantitatively and that it would be appropriate to attribute an error to the calculation equal to the calculated effect itself. A more sophisticated calculation of the effect was made using the code MURAL¹⁴ and an almost equally inaccurate value of 11% was obtained, indicating the difficulty of accurately estimating this highly spectrum-sensitive effect.

It must be mentioned that the backing effect in the 8A measurement was grossly exaggerated solely to enable its investigation and the comparison of the experimental dis-

crepancy with a theoretical estimate. For the usual 0.10 mm aluminium backing, the effect is comparatively negligible. Substituting $\Sigma \sim 0.09 \text{ cm}^{-1}$, $t = 0.10 \text{ mm}$ (for the aluminium), one obtains from 20:

$$\left(\frac{\sigma_{\text{eff}} - \sigma_0}{\sigma_0} \right)_{\text{alum.}}^{\text{BA}} \sim (0.23 \pm 0.23)\% \quad (22)$$

For other ZEBRA cores, the effect is even smaller, e.g. for cores 8B ($\sigma_1 = 0.25 \text{ b.}$, $\sigma_0 = 0.22 \text{ b.}$) and 8C ($\sigma_1 = 0.37 \text{ b.}$, $\sigma_0 = 0.25 \text{ b.}$), one obtains the estimates as only $(0.01 \pm 0.01)\%$ and $(0.05 \pm 0.05)\%$ respectively.

REFERENCES

1. SMITH R. D. ZEBRA—A zero-power fast reactor. *Nucl. Engng*, 1962, 7 (Sept.), 364–367
2. TUNNICLIFFE P. R., SKILLINGS D. J. and CHIDLEY B. G. A method for the accurate determination of relative initial conversion ratios. *Nucl. Sci. Engng*, 1963, 15, 268–283
3. BROWN W. A. V. and SKILLINGS D. J. The measurement of relative conversion ratio in low enrichment oxide lattices. AEEW 1964, R 340
4. DAVEY W. G. The ratio of ^{238}U capture and ^{235}U fission cross sections in fast reactors. *Nucl. Sci. Engng*, 1966, 24, 26–41
5. ARNOLD M. J., FOX W. N., GEORGE C. F. and RICHMOND R. Paper presented at IAEA Symposium on fast reactor physics, Karlsruhe, 1967
6. SEUFERT H. and STEGEMANN D. A method for absolute determination of ^{238}U capture rates in fast zero-power reactors. *Nucl. Sci. Engng*, 1967, 28, 277–285
7. FLEMING E. H. JR., GHIORSO A. and CUNNINGHAM B. B. The specific alpha-activities of ^{234}U , ^{235}U and ^{238}U . *Phys. Rev.*, 1952, 88, 642–652
8. PARKER W., BILDSTEIN H. and GETOFF N. Molecular plating—the rapid preparation of radioactive reference samples. *Nucl. Instrum. Meth.*, 1964, 26, 314–316
9. EURATOM round table on high precision mass spectrometry and alpha counting. EANDC—53 S, 1965
10. STORM E., GILBERT E. and ISRAEL H. Gamma-ray absorption coefficients. LA-2237, 1958
11. STEVENSON J. M. and BROOMFIELD A. M. Measurements and calculations of ratios of effective fission cross sections in the zero power fast reactor ZEBRA. AEEW, 1967 R 526
12. GEORGE C. F. Private communication
13. WARDLEWORTH D. Private communication
14. MACDOUGALL J. D. Private communication